RALSTONIA SOLANACEARUM—PLANT INTERACTIONS: PLANT DEFENSE RESPONSES, VIRULENCE MECHANISMS AND SIGNALING PATHWAYS

EDITED BY: Yasufumi Hikichi, Marc Valls and Stephane Genin

PUBLISHED IN: Frontiers in Plant Science and Frontiers in Microbiology

frontiers Research Topics

ISSN 1664-8714
ISBN 978-2-88976-257-6
DOI 10.3389/978-2-88976-257-6

About Frontiers

Frontiers is more than just an open-access publisher of scholarly articles: it is a pioneering approach to the world of academia, radically improving the way scholarly research is managed. The grand vision of Frontiers is a world where all people have an equal opportunity to seek, share and generate knowledge. Frontiers provides immediate and permanent online open access to all its publications, but this alone is not enough to realize our grand goals.

Frontiers Journal Series

The Frontiers Journal Series is a multi-tier and interdisciplinary set of open-access, online journals, promising a paradigm shift from the current review, selection and dissemination processes in academic publishing. All Frontiers journals are driven by researchers for researchers; therefore, they constitute a service to the scholarly community. At the same time, the Frontiers Journal Series operates on a revolutionary invention, the tiered publishing system, initially addressing specific communities of scholars, and gradually climbing up to broader public understanding, thus serving the interests of the lay society, too.

Dedication to Quality

Each Frontiers article is a landmark of the highest quality, thanks to genuinely collaborative interactions between authors and review editors, who include some of the world's best academicians. Research must be certified by peers before entering a stream of knowledge that may eventually reach the public - and shape society; therefore, Frontiers only applies the most rigorous and unbiased reviews.
Frontiers revolutionizes research publishing by freely delivering the most outstanding research, evaluated with no bias from both the academic and social point of view. By applying the most advanced information technologies, Frontiers is catapulting scholarly publishing into a new generation.

What are Frontiers Research Topics?

Frontiers Research Topics are very popular trademarks of the Frontiers Journals Series: they are collections of at least ten articles, all centered on a particular subject. With their unique mix of varied contributions from Original Research to Review Articles, Frontiers Research Topics unify the most influential researchers, the latest key findings and historical advances in a hot research area! Find out more on how to host your own Frontiers Research Topic or contribute to one as an author by contacting the Frontiers Editorial Office: frontiersin.org/about/contact

RALSTONIA SOLANACEARUM–PLANT INTERACTIONS: PLANT DEFENSE RESPONSES, VIRULENCE MECHANISMS AND SIGNALING PATHWAYS

Topic Editors:
Yasufumi Hikichi, Kōchi University, Japan
Marc Valls, University of Barcelona, Spain
Stephane Genin, Institut National de la Recherche Agronomique (INRA), France

Citation: Hikichi, Y., Valls, M., Genin, S., eds. (2022). Ralstonia Solanacearum–Plant Interactions: Plant Defense Responses, Virulence Mechanisms and Signaling Pathways. Lausanne: Frontiers Media SA. doi: 10.3389/978-2-88976-257-6

Table of Contents

04 ***Editorial:*** **Ralstonia solanacearum*–Plant Interactions: Plant Defense Responses, Virulence Mechanisms and Signaling Pathways***
Yasufumi Hikichi, Marc Valls and Stephane Genin

06 ***The Immune Receptor Roq1 Confers Resistance to the Bacterial Pathogens* Xanthomonas*,* Pseudomonas syringae*, and* Ralstonia *in Tomato***
Nicholas C. Thomas, Connor G. Hendrich, Upinder S. Gill, Caitilyn Allen, Samuel F. Hutton and Alex Schultink

16 ***L-Amino Acid Oxidases From Mushrooms Show Antibacterial Activity Against the Phytopathogen* Ralstonia solanacearum**
Jerica Sabotič, Jože Brzin, Jana Erjavec, Tanja Dreo, Magda Tušek Žnidarič, Maja Ravnikar and Janko Kos

34 ***Super-Multiple Deletion Analysis of Type III Effectors in* Ralstonia solanacearum *OE1-1 for Full Virulence Toward Host Plants***
Ni Lei, Li Chen, Akinori Kiba, Yasufumi Hikichi, Yong Zhang and Kouhei Ohnishi

44 ***KatE From the Bacterial Plant Pathogen* Ralstonia solanacearum *Is a Monofunctional Catalase Controlled by HrpG That Plays a Major Role in Bacterial Survival to Hydrogen Peroxide***
María Laura Tondo, Roger de Pedro-Jové, Agustina Vandecaveye, Laura Piskulic, Elena G. Orellano and Marc Valls

56 ***Sound Vibration-Triggered Epigenetic Modulation Induces Plant Root Immunity Against* Ralstonia solanacearum**
Jihye Jung, Seon-Kyu Kim, Sung-Hee Jung, Mi-Jeong Jeong and Choong-Min Ryu

72 **Streptomyces *sp. JCK-6131 Protects Plants Against Bacterial and Fungal Diseases via Two Mechanisms***
Khanh Duy Le, Jeun Kim, Hoa Thi Nguyen, Nan Hee Yu, Ae Ran Park, Chul Won Lee and Jin-Cheol Kim

85 ***Comparative Transcriptome Profiling Reveals Defense-Related Genes Against* Ralstonia solanacearum *Infection in Tobacco***
Xiaoying Pan, Junbiao Chen, Aiguo Yang, Qinghua Yuan, Weicai Zhao, Tingyu Xu, Bowen Chen, Min Ren, Ruimei Geng, Zhaohui Zong, Zhuwen Ma, Zhenrui Huang and Zhenchen Zhang

98 ***Metabolic Profiling of Resistant and Susceptible Tobaccos Response Incited by* Ralstonia pseudosolanacearum *Causing Bacterial Wilt***
Liang Yang, Zhouling Wei, Marc Valls and Wei Ding

109 ***Complete Genome Sequence Analysis of* Ralstonia solanacearum *Strain PeaFJ1 Provides Insights Into Its Strong Virulence in Peanut Plants***
Xiaodan Tan, Xiaoqiu Dai, Ting Chen, Yushuang Wu, Dong Yang, Yixiong Zheng, Huilan Chen, Xiaorong Wan and Yong Yang

frontiers | Frontiers in Plant Science

EDITORIAL
published: 05 May 2022
doi: 10.3389/fpls.2022.890877

Editorial: *Ralstonia solanacearum*–Plant Interactions: Plant Defense Responses, Virulence Mechanisms and Signaling Pathways

Yasufumi Hikichi[1*†], *Marc Valls*[2*†] *and Stephane Genin*[3*†]

[1] Faculty of Agriculture and Marine Science, Kochi University, Kochi, Japan, [2] Genetics Section, Universitat de Barcelona, Catalonia, Spain, [3] LIPME, Université de Toulouse, INRAE, CNRS, Castanet-Tolosan, France

Keywords: ***Ralstonia solanacearum*-plant interactions, plant defense responses, virulence mechanisms, signaling pathways, development of the disease control system**

Editorial on the Research Topic

Ralstonia solanacearum–Plant Interactions: Plant Defense Responses, Virulence Mechanisms and Signaling Pathways

OPEN ACCESS

Edited and reviewed by:
Lucy N. Moleleki,
University of Pretoria, South Africa

***Correspondence:**
Yasufumi Hikichi
yhikichi@kochi-u.ac.jp
Marc Valls
marcvalls@ub.edu
Stephane Genin
Stephane.genin@inra.fr

†These authors have contributed equally to this work

Specialty section:
This article was submitted to Plant Pathogen Interactions, a section of the journal Frontiers in Plant Science

Received: *06 March 2022*
Accepted: *25 March 2022*
Published: *05 May 2022*

Citation:
Hikichi Y, Valls M and Genin S (2022) Editorial: Ralstonia solanacearum–Plant Interactions: Plant Defense Responses, Virulence Mechanisms and Signaling Pathways. Front. Plant Sci. 13:890877. doi: 10.3389/fpls.2022.890877

In the Research Topic *Ralstonia solanacearum–Plant Interactions: Plant Defense Responses, Virulence Mechanisms and Signaling Pathways*, we aimed to collect manuscripts dealing with not only molecular mechanisms of *R. solanacearum* virulence and host responses but also development of the disease control system such as the disease-resistance cultivars and microbial inoculants.

The molecular study of the interaction of strains of the *R. solanacearum* with their host plants has largely focused on solanaceous species, mainly on tomato and to a lesser extent potato. Nevertheless, there are plants of major agronomic interest outside the Solanaceae on which researchers are now seeking to better understand the mechanisms of susceptibility/resistance to bacterial wilt. In their study, Tan et al. make a valuable contribution toward the understanding of the virulence mechanisms of strains pathogenic on legume plants, which have so far been relatively unexplored. By screening more than 100 peanut cultivars, Tan et al. were able to identify two strains that were phylogenetically very close, but differed remarkably in their virulence profile. The article presents the genome analysis of these strains and examines the major differences observed. Several candidate genes to explain the difference in virulence were identified, including regulatory genes, genes contributing to motility and adhesion, and only four type 3 effectors differing in the repertoires of these two strains.

In addition to genomic or transcriptomic comparison studies, more advanced approaches aimed at better quantification of proteins or metabolites are now routinely used. Yang et al. conducted a comparative study to identify differences in metabolite content in tobacco xylem sap during *R. solanacearum* infection, both in susceptible and resistant tobacco cultivars. Interestingly, among the metabolites differentially concentrated, several of them appear to be significantly induced in the susceptible cultivar and not in the resistant one, which opens up interesting avenues for future investigation of how the pathogen induces such metabolic reprogramming in its host.

The article by Pan et al. addresses tobacco gene expression in the highly resistant 4411-3 and the moderately resistant K326 varieties in basal conditions or at three time points after *R. solanacearum* inoculation. This work revealed an unusually large number of genes induced by the pathogen. Previous transcriptomic and functional studies in other plant hosts had shown that cell wall components and plant hormones including auxin and ABA were involved in the responses to *R. solanacearum*. Pan et al. confirmed these results in tobacco, and found that the levels of both hormones are lower in plants showing higher resistance to the disease. The study also identified

response specificities and suggested the involvement of ABC transporters, endocytosis and the metabolism of glutathione and glycerolipids in tobacco resistance against *R. solanacearum*. The study provides a number of candidate genes related to cell wall metabolism, plant hormone and glutathione metabolism whose involvement in *Nicotiana* resistance to *R. solanacearum* deserves to be further studied.

Plant cells under pathogen attack often induce the formation of Reactive-Oxygen Species (ROS) that trigger a signaling cascade, increase cell wall cross-linking, trigger plant defense and act as antimicrobial agents. Plant-associated bacteria use oxidative stress response genes to counter-attack ROS. The work by Tondo et al. characterized an *R. solanacearum* monofunctional heme catalase named KatE, a ROS-scavenging enzyme long considered a key candidate virulence gene. The authors demonstrated that *katE* expression is induced upon hydrogen peroxide treatment and transcriptionally activated by the central virulence regulator HrpG. However, although KatE was shown to be essential for bacterial survival to oxidative stress, it was proven that it does not contribute to *R. solanacearum* virulence or bacterial growth in the plant. This result is surprising, considering that the gene was proposed in a previous study as essential for survival *in planta* and makes us wonder whether oxidizing conditions are important in other environments encountered by *R. solanacearum* during its life cycle such as the phylosphere or the rhizosphere.

More than 100 type III effectors (T3Es) are predicted among different *R. solanacearum* strains, with an average of about 70 T3Es in each strain. Among them, 32 core T3Es are found to be conserved among the RSSC. Highly variable repertoires of T3Es might be responsible for the host range of different *R. solanacearum* strains. Lei et al. created the 42 T3 effector (all 21 T3Es of AWR, GALA, HLK, and SKWP families, 15 core T3Es, and six extended core T3Es) genes-deletion mutant from the strain OE1-1, which are virulent on both tobacco and eggplant plants. The mutant exhibited a significantly reduced colonization in both tobacco and eggplant plants and a significantly reduced virulence on them, demonstrating that all the core and extended core T3Es are nearly crucial for virulence of the strain OE1-1 toward host plants, and the T3Es-free strain will enable primary function of individual T3Es in host cells.

T3Es are common elicitors of intracellular plant immune receptors encoded by nucleotide-binding domain and leucine-rich repeat containing (NLR) genes. T3Es contribute to both virulence on a susceptible host and an immune response on non-host plants, which have the cognate receptor to recognize the T3E. NLR genes typically confer strong, dominant resistance to pathogens that deliver the cognate recognized T3E. The NLR protein Roq1 of *Nicotiana benthamiana* recognizes the T3Es XopQ and HopQ1, which are highly conserved and present in most plant pathogenic strains of *Xanthomonas* and *Pseudomonas syringae*. Furthermore, A homolog of XopQ/HopQ1, RipB, is present in most *Ralstonia* strains. Thomas et al. found that expression of *Roq1* in tomato plants confers immunity to *Xanthomonas*, *P. syringae*, and *Ralstonia* upon recognition of the cognate pathogen T3E, demonstrating the widespread potential of using naturally occurring plant immune receptors to manage diverse and difficult to control pathogen species.

The studies collected in this Research Topic will shed light on a deeper understand of *R. solanacearum*-Plant Interactions and ultimately pave the way to deal with this devastating pathogen and developing sustainable control system on the disease.

AUTHOR CONTRIBUTIONS

All authors listed have made a substantial, direct, and intellectual contribution to the work and approved it for publication.

Conflict of Interest: The authors declare that the research was conducted in the absence of any commercial or financial relationships that could be construed as a potential conflict of interest.

Publisher's Note: All claims expressed in this article are solely those of the authors and do not necessarily represent those of their affiliated organizations, or those of the publisher, the editors and the reviewers. Any product that may be evaluated in this article, or claim that may be made by its manufacturer, is not guaranteed or endorsed by the publisher.

frontiers in Plant Science

ORIGINAL RESEARCH
published: 23 April 2020
doi: 10.3389/fpls.2020.00463

The Immune Receptor Roq1 Confers Resistance to the Bacterial Pathogens *Xanthomonas*, *Pseudomonas syringae*, and *Ralstonia* in Tomato

*Nicholas C. Thomas[1,2], Connor G. Hendrich[3], Upinder S. Gill[4,5], Caitilyn Allen[3], Samuel F. Hutton[4] and Alex Schultink[1,2]**

[1] Fortiphyte Inc., Berkeley, CA, United States, [2] Innovative Genomics Institute, University of California, Berkeley, Berkeley, CA, United States, [3] Department of Plant Pathology, University of Wisconsin–Madison, Madison, WI, United States, [4] IFAS, Gulf Coast Research and Education Center, University of Florida, Wimauma, FL, United States, [5] Department of Plant Pathology, North Dakota State University, Fargo, ND, United States

OPEN ACCESS

Edited by:
Marc Valls,
University of Barcelona, Spain

Reviewed by:
Nemo Peeters,
Institut National de la Recherche Agronomique (INRA), France
Kee Hoon Sohn,
Pohang University of Science and Technology, South Korea
Kouhei Ohnishi,
Kochi University, Japan

***Correspondence:**
Alex Schultink
alex.schultink@fortiphyte.com

Specialty section:
This article was submitted to Plant Microbe Interactions, a section of the journal Frontiers in Plant Science

Received: 24 December 2019
Accepted: 30 March 2020
Published: 23 April 2020

Citation:
Thomas NC, Hendrich CG, Gill US, Allen C, Hutton SF and Schultink A (2020) The Immune Receptor Roq1 Confers Resistance to the Bacterial Pathogens Xanthomonas, Pseudomonas syringae, and Ralstonia in Tomato. Front. Plant Sci. 11:463. doi: 10.3389/fpls.2020.00463

Xanthomonas species, *Pseudomonas syringae* and *Ralstonia* species are bacterial plant pathogens that cause significant yield loss in many crop species. Generating disease-resistant crop varieties can provide a more sustainable solution to control yield loss compared to chemical methods. Plant immune receptors encoded by nucleotide–binding, leucine–rich repeat (NLR) genes typically confer resistance to pathogens that produce a cognate elicitor, often an effector protein secreted by the pathogen to promote virulence. The diverse sequence and presence/absence variation of pathogen effector proteins within and between pathogen species usually limits the utility of a single NLR gene to protecting a plant from a single pathogen species or particular strains. The NLR protein Recognition of XopQ 1 (Roq1) was recently identified from the plant *Nicotiana benthamiana* and mediates perception of the effector proteins XopQ and HopQ1 from *Xanthomonas* and *P. syringae* respectively. Unlike most recognized effectors, alleles of XopQ/HopQ1 are highly conserved and present in most plant pathogenic strains of *Xanthomonas* and *P. syringae*. A homolog of XopQ/HopQ1, named RipB, is present in most *Ralstonia* strains. We found that Roq1 confers immunity to *Xanthomonas*, *P. syringae*, and *Ralstonia* when expressed in tomato. Strong resistance to *Xanthomonas perforans* was observed in three seasons of field trials with both natural and artificial inoculation. The *Roq1* gene can therefore be used to provide safe, economical, and effective control of these pathogens in tomato and other crop species and reduce or eliminate the need for traditional chemical controls.

Keywords: plant immunity, *Ralstonia*, *Xanthomonas*, *Pseudomonas*, tomato

INTRODUCTION

Bacterial pathogens from the species *Pseudomonas syringae* and the genera *Ralstonia* and *Xanthomonas* can infect many different crop species and inflict significant yield losses when environmental conditions favor disease. *Xanthomonas* and *P. syringae* tend to enter plant stem, leaf, or flower tissue through wounds or natural openings, such as stomata or hydathodes, whereas

Ralstonia is soilborne, entering roots through wounds and natural openings before colonizing xylem tissue (Vasse et al., 1995; Gudesblat et al., 2009). Once inside the host these bacteria manipulate host metabolism and suppress plant immunity using multiple strategies, including effector proteins delivered by the type III secretion system (Kay and Bonas, 2009; Peeters et al., 2013; Xin et al., 2018). This enables the pathogens to multiply to high titers while the plant tissue is still alive and showing few or no visual symptoms. Once the bacteria reach high populations, they typically cause necrosis of infected leaf tissue or wilting and eventual death of the plant.

Effective control measures for bacterial pathogens are relatively limited, particularly once plants become infected (Davis et al., 2013). Soil fumigation can reduce *Ralstonia* populations in the soil but this is expensive, potentially hazardous to workers and the environment, and of limited efficacy (Yuliar et al., 2015). Copper sulfate and antibiotics such as streptomycin have been used to control *Xanthomonas* species and *P. syringae* but have adverse environmental impacts and many strains have evolved tolerance to these chemicals (Kennelly et al., 2007; Griffin et al., 2017). Applying chemicals that induce systemic acquired resistance, such as acibenzolar-S-methyl, can provide partial control but increases production cost and can depress crop yields when used repeatedly (de Pontes et al., 2016).

The most effective, economical, and safe way to control bacterial pathogens is to plant crop varieties that are immune to the target pathogen (Jones et al., 2014; Vincelli, 2016). Such immunity is often mediated by plant immune receptor genes. Plants have large families of cell surface and intracellular immune receptor proteins that surveil for the presence of invading pathogens (Zipfel, 2014; Jones et al., 2016). Effector proteins delivered by the bacterial type III secretion system are common elicitors of intracellular plant immune receptors encoded by nucleotide−binding domain and leucine−rich repeat containing (NLR) genes (Li et al., 2015; Jones et al., 2016; Kapos et al., 2019). While effector proteins contribute to virulence on a susceptible host, an immune response is activated in the plant if that plant has the cognate receptor to recognize the effector. NLR genes typically confer strong, dominant resistance to pathogens that deliver the cognate recognized effector protein (Tai et al., 1999; Jones and Dangl, 2006; Boller and He, 2009; Deslandes and Rivas, 2012; Li et al., 2015). Disease-resistant plants can be generated by identifying the appropriate plant immune receptor genes and transferring them into the target crop species (Dangl et al., 2013).

We recently identified the *Nicotiana benthamiana* immune receptor gene named *Recognition of XopQ 1* (*Roq1*), which appears to be restricted to the genus *Nicotiana* and contributes to resistance against *Xanthomonas* spp. and *P. syringae* (Schultink et al., 2017). The Roq1 protein is a Toll/Interleukin−1 Receptor (TIR) NLR immune receptor that mediates recognition of the *Xanthomonas* effector protein XopQ and the homologous effector HopQ1 from *P. syringae*. XopQ is present in most species and strains of *Xanthomonas* (Ryan et al., 2011) and HopQ1 is present in 62% (290 of 467) sequenced putative pathogenic *P. syringae* strains (Dillon et al., 2019). XopQ/HopQ1 has homology to nucleoside hydrolases and has been shown to enhance virulence on susceptible hosts (Ferrante and Scortichini, 2009; Li et al., 2013), possibly by altering cytokinin levels or interfering with the activity of host 14-3-3 proteins (Giska et al., 2013; Li et al., 2013; Hann et al., 2014; Teper et al., 2014). The conservation of XopQ/HopQ1 and their importance in virulence suggests that *Roq1* has widespread potential to confer resistance to these pathogens in diverse crop species. Indeed, transient expression assays demonstrated that *Roq1* can recognize XopQ/HopQ1 alleles from *Xanthomonas* and *P. syringae* pathogens of tomato, pepper, rice, citrus, cassava, brassica, and bean (Schultink et al., 2017). However, it was not known if *Roq1* can confer disease resistance when expressed in a crop plant.

Tomato is one of the most important vegetable crops and is highly susceptible to several bacterial diseases. Bacterial spot, bacterial speck, and bacterial wilt of tomato are caused by *Xanthomonas* species, *P. syringae* pv. *tomato* and *Ralstonia,* respectively. These diseases are difficult to control, especially if the pathogens become established in a field and environmental conditions favor disease (Rivard et al., 2012; Potnis et al., 2015). Tomato breeding germplasm has only limited resistance against these diseases and in some cases linkage drag has complicated introgression of resistance genes from wild relatives (Sharma and Bhattarai, 2019). *Ralstonia* contains a homolog of XopQ/HopQ1 called RipB. Roq1 is able to mediate the perception of RipB (Staskawicz and Schultink, 2019), and silencing *Roq1* in *N. benthamiana* resulted in severe wilting phenotypes upon *Ralstonia* infection (Nakano and Mukaihara, 2019). This suggests that expressing *Roq1* in tomato could also confer resistance to bacterial wilt. Like XopQ/HopQ1 in *Xanthomonas* and *P. syringae*, RipB is highly conserved and is present in approximately 90% of sequenced *Ralstonia* isolates (Sabbagh et al., 2019). Here we present data showing that expression of *Roq1* in tomato confers resistance against *Xanthomonas*, *Pseudomonas*, and *Ralstonia* upon recognition of the cognate pathogen effector.

MATERIALS AND METHODS

Generation of Tomato Expressing Roq1

The Roq1 coding sequence was amplified from *N. benthamiana* cDNA and cloned into the pORE E4 binary plasmid (Coutu et al., 2007). The expression of *Roq1* was driven by the constitutive $P_{ENTCUP2}$ promoter, which was derived from tobacco and has been reported to drive expression in leaf, root, and stem tissue (Malik et al., 2002). *Agrobacterium tumefaciens* co-cultivation was used to transform *Roq1* into the tomato variety Fla. 8000 at the University of Nebraska Plant Transformation Core Research Facility. Transformed plants were selected by resistance to kanamycin, confirmed by genotyping, and selfed to obtain homozygous lines.

Bacterial Leaf Spot and Leaf Speck Disease Assays

Xanthomonas cultures were grown in NYG broth (0.5% peptone, 0.3% yeast extract, 2% glycerol) with rifampicin (100 μg/mL) overnight at 30°C. *P. syringae* cultures were grown in KB broth (1% peptone, 0.15% K_2HPO_4, 1.5% glycerol, 5 mM

$MgSO_4$, pH 7.0) with rifampicin (100 μg/mL) overnight at 28°C. Bacterial cultures were spun down at 5200 *g*, washed once with 10 mM $MgCl_2$, and then diluted to the appropriate infiltration density with 10 mM $MgCl_2$. Leaf tissue of tomato plants (approximately 4 weeks old) was infiltrated with bacterial solution using a needleless syringe. To quantify bacterial growth, leaf punches were homogenized in water, serially diluted and plated on NYG (for *Xanthomonas* spp.) or KB (for *P. syringae*) plates supplemented with 100 μg/mL rifampicin and 50 μg/mL cycloheximide to measure colony forming units. Three biological replicates were performed for each condition and the reported results are representative of at least three independent experiments. *Xanthomonas perforans* strain 4B, *Xanthomonas euvesicatoria* strain 85-10, and *P. syringae* strain DC3000 and the corresponding XopQ/HopQ1 deletion mutants and complemented strains were described previously (Wei et al., 2007; Schwartz et al., 2015; Schultink et al., 2017). The *P. syringae* pv. *tomato* Race 1 strain was isolated from a field of tomatoes with the PTO resistance gene in 1993 in California.

Transient Expression of RipB and XopQ

Alleles of RipB from *Ralstonia* strains GMI1000 and MolK2 (NCBI Genbank accessions CAD13773.2 and WP_003278485) were synthesized and cloned into a *Bsa*I-compatible version of the pORE E4 vector (Coutu et al., 2007). This plasmid was transformed into *A. tumefaciens* strain C58C1. *A. tumefaciens* cultures were grown on a shaker overnight at 30°C in LB broth with rifampicin (100 μg/mL), tetracycline (10 μg/mL), and kanamycin (50 μg/mL). The cells were collected by centrifugation and resuspended in infiltration buffer [10 mM 2-(*N*-morpholino)ethanesulfonic acid, 10 mM $MgCl_2$, pH 5.6], and diluted to an OD_{600} of 0.5 for infiltration into *Nicotiana tabacum* leaf tissue. Each experiment was performed on multiple leaves and multiple plants with the selected images being representative of the observed result.

N. tabacum roq1 Mutant Lines

Nicotiana tabacum roq1 mutant lines were generated by transforming *N. tabacum* with a construct coding for CAS9 and a guide RNA targeting the *Roq1* gene with the sequence GATGATAAGGAGTTAAAGAG. This construct was also used for the generation of *N. benthamiana roq1* mutants published in Qi et al. (2018). Transformed *N. tabacum* plants were generated by *Agrobacterium* co-cultivation and selected for using kanamycin. Transformed plants were genotyped for the presence of mutations at the target site by PCR and Sanger sequencing (**Supplementary Table S1**).

Bacterial Wilt Virulence Assays

Ralstonia virulence on tomato was measured as previously described (Khokhani et al., 2018). Briefly, cells of *Ralstonia* strains GMI1000 and UW551 grown overnight in CPG (0.1% casein hydrolysate, 1% peptone, 0.5% glucose, pH 7.0) at 28°C were collected by centrifugation and diluted to an OD_{600} of 0.1 in water (1×10^8 CFU/mL). 50 mL of this suspension was poured on the soil around 17-day old tomato plants. Disease was rated daily for two weeks on a 0–4 disease index scale, where 0 is no leaves wilted, 1 is 1–25% wilted, 2 is 26–50% wilted, 3 is 51–75% wilted, and 4 is 76–100% wilted. Data represent a total of four biological replicates with 10 plants per replicate. Virulence data were analyzed using repeated measures ANOVA (Khokhani et al., 2018). For petiole infection, the petiole of the first true leaf was cut with a razor blade horizontally approximately 1 cm from the stem. A drop of bacterial solution (2 μL, OD_{600} = 0.001) was pipetted onto the exposed cut petiole surface.

Field Trial Disease Assays

Three field trials were conducted at the University of Florida Gulf Coast Research and Education Center in Balm during the spring seasons of 2018 and 2019 and the fall season of 2018 and under the notification process of the United States Department of Agriculture. Large-fruited, fresh market tomato lines were used in these trials and included the inbred line, Fla. 8000, and nearly isogenic lines containing either *Roq1* (event 316.4) or *Bs2* (Kunwar et al., 2018). The *Roq1* tomato line selected for the field trial was the same line used in the experiments shown in **Figures 1**, **2**, **5**. For each trial, seeds were sown directly into peat-lite soilless media (Speedling, Sun City, FL, United States) in 128-cell trays (38 cm^3 cell size). Transplants were grown in a greenhouse until 5 or 6 weeks, then planted to field beds that had been fumigated and covered with reflective plastic mulch. Field trials were conducted using a randomized complete block design with four blocks and 10-plant plots. Field plants were staked and tied, and irrigation was applied through drip tape beneath the plastic mulch of each bed. A recommended fertilizer and pesticide program were followed throughout the growing season, excluding the use of plant defense inducers, copper, or other bactericides (Freeman et al., 2018). Fruits were harvested from the inner eight plants of each plot at the breaker stage and beyond and graded for marketability according to USDA specifications with block considered a random effect.

Field trials were inoculated with *X. perforans* race T4 (strain mixture of GEV904, GEV917, GEV1001, and GEV1063). Bacterial strains were grown on nutrient agar medium (BBL, Becton Dickinson and Co., Cockeysville, MD, United States) and incubated at 28°C for 24 h. Bacterial cells were removed from the plates and suspended in a 10 mM $MgSO_4$ solution, and the suspension was adjusted to OD_{600} = 0.3, which corresponds to 10^8 CFU/mL. The suspension for each strain was then diluted to 10^6 CFU/mL, mixed in equal volume, and applied along with polyoxyethylene sorbitan monolaurate (Tween 20; 0.05% [vol/vol]) for field inoculation. Field trial plants were inoculated approximately 3 weeks after transplanting.

Bacterial spot disease severity was recorded three to eight weeks after inoculation using the Horsfall-Barratt scale (Horsfall and Barrat, 1945), and ratings were converted to midpoint percentages for statistical analysis. Blocks were considered random effects.

Generation of the *Ralstonia* Δ*ripB* Mutant

An unmarked Δ*ripB* mutant was created using *sacB* selection with the vector pUFR80 (Castañeda et al., 2005). Briefly, the

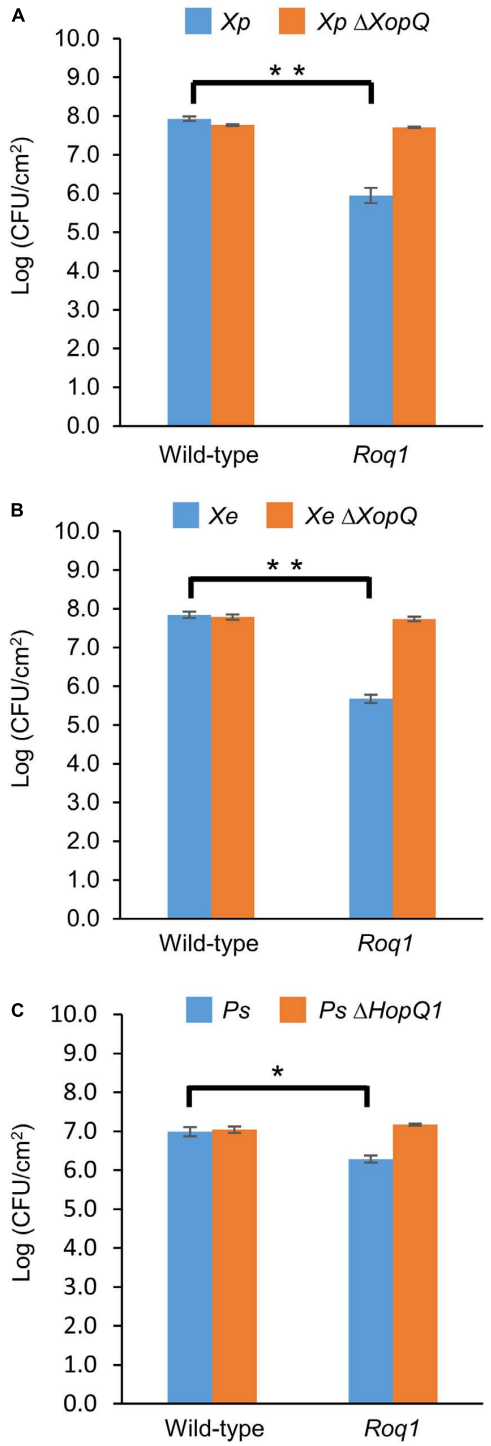

FIGURE 1 | Bacterial growth in tomatoes expressing Roq1. *Xanthomonas perforans* 4B (*Xp*), *Xanthomonas euvesicatoria* 85-10 (*Xe*), and *Pseudomonas syringae* DC3000 (*Ps*) were infiltrated into leaf tissue of wild-type tomato and tomato expressing Roq1 at a low inoculum (OD_{600} = 0.0001 for *Xe* and *Xp*; OD_{600} = 0.00005 for *Ps*). Bacterial abundance was quantified by homogenizing leaf punches and counting colony forming units (CFU) per square centimeter of leaf tissue at 6 days post infiltration for *Xe* and *Xp*; 3 days post infiltration for *Ps*. Error bars indicate standard deviation from three biological replicates. $^{*}p < 0.05$, $^{**}p < 0.01$ by Student's *t*-test.

regions upstream and downstream of *ripB* were amplified using the primers ripBupF/R and ripBdwnF/R (**Supplementary Table S1**). These fragments were inserted into pUFR80 digested with *Hin*dIII and *Eco*RI using Gibson Assembly (Gibson et al., 2009) (New England Biolabs, Ipswitch, MA, United States) and this construct was incorporated into the genome of strain GMI1000 using natural transformation, with successful integrants selected on CPG + kanamycin (Coupat et al., 2008). Plasmid loss was then selected for on CPG plates containing 5% w/v sucrose. Correct deletions were confirmed using PCR and sequencing.

Phylogenetic Analysis of XopQ, HopQ1, and RipB Alleles

RipB alleles were identified by BLAST search of the NCBI protein database. Clustal Omega (Sievers et al., 2011) was used to generate a multiple sequence alignment with XopQ and HopQ1 alleles. To span the diversity of RipB alleles without having many redundant sequences, only a single sequence was retained if there were multiple identical or nearly identical sequences identified. A maximum likelihood tree was generated using PhyML (Guindon et al., 2010). The phylotype calls of the strains were obtained from previously published worked (Liu et al., 2009; Mukaihara and Tamura, 2009; Safni et al., 2014).

RESULTS

Tomatoes Expressing *Roq1* Are Resistant to *Xanthomonas* and *P. syringae*

We generated homozygous tomato plants expressing the *Roq1* gene from *N. benthamiana* and tested them for resistance to *Xanthomonas* and *P. syringae* by measuring bacterial growth *in planta*. Population sizes of wild-type *X. perforans* strain 4B and *X. euvesicatoria* strain 85-10 were approximately 100-fold smaller in tomato expressing *Roq1* compared to wild-type tomato at 6 days post inoculation (**Figure 1**). In contrast, XopQ deletion mutants multiplied equally well in leaves of both wild-type and *Roq1* tomato. Disease symptoms begin as small water-soaked lesions and progress to necrosis of infected tissue. Wild-type *X. perforans* and *X. euvesicatoria* caused severe disease symptoms on wild-type tomato plants but failed to cause visible symptoms on *Roq1* plants (**Figure 2**). The XopQ mutants caused similar disease symptoms on both wild-type and *Roq1* tomato. Similar results were observed for *P. syringae* DC3000, and its HopQ1 mutant (**Figures 1**, **2**) and a Race 1 isolate of *P. syringae* pv. *tomato* (**Supplementary Figure S1**). Tomatoes expressing *Roq1* were resistant to *Xanthomonas* and *Pseudomonas* XopQ/HopQ1 mutants complemented with a wild-type copy of XopQ/HopQ1 (**Supplementary Figure S2**). A second tomato line expressing *Roq1*, derived from an independent transformation event, also showed resistance to wild-type *X. euvesicatoria* and *X. perforans* but not to the XopQ deletion strains (**Supplementary Figure S3**).

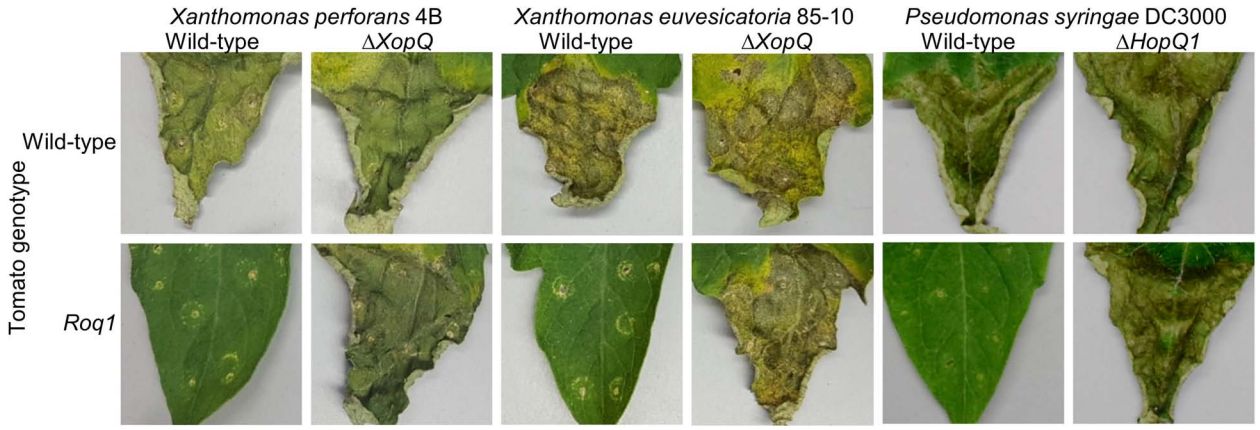

FIGURE 2 | Bacterial disease symptoms on *Roq1* tomato. *Xanthomonas perforans* 4B (*Xp*), *Xanthomonas euvesicatoria* 85-10 (*Xe*), and *Pseudomonas syringae* DC3000 (*Ps*) wild-type and XopQ/HopQ1 knockout strains were infiltrated into tomato leaf tissue at low inoculum and disease symptoms were imaged at 12, 13, and 4 days post infiltration for *Xe*, *Xp*, and *Ps*, respectively. The infiltration was performed using a needleless syringe and circular wounds from the infiltration are visible. The distal part of region of each leaf was infiltrated and the proximal part was left untreated. *Xe* and *Xp* were infiltrated at an OD_{600} of 0.0001 whereas *Ps* was infiltrated at an OD_{600} of 0.00005. The images shown here are representative of at least three independent experiments.

Expression of *Roq1* Confers Resistance to *Xanthomonas perforans* in the Field

To determine if the resistance observed in growth chamber experiments would hold up under commercial tomato production conditions, we tested the ability of *Roq1* tomatoes to resist *X. perforans* infection in the field. *Roq1* tomatoes were grown along with the Fla. 8000 wild-type parent as well as a Fla. 8000 variety expressing the *Bs2* gene from pepper as a resistant control (Kunwar et al., 2018). For each of the three growing seasons, both *Roq1* and the resistant *Bs2* control tomatoes showed significantly lower disease severity than the parental Fla. 8000 variety (**Table 1**) ($p < 0.05$). The total marketable yield of the *Roq1* plants was not significantly different from that of the susceptible parent for any of the three seasons ($p > 0.05$). No obvious difference in growth morphology was observed between *Roq1* and wild-type tomato plants (**Supplementary Figure S4**).

The *Ralstonia* Effector RipB, a Homolog of XopQ/HopQ1, Is Recognized by Roq1

RipB, considered a "core" *Ralstonia* effector, is present in approximately 90% of sequenced strains (Sabbagh et al., 2019) making it an attractive target ligand for engineering crop plants to be resistant to this pathogen. Roq1 perceives diverse alleles of XopQ and HopQ1 and we hypothesized that it can also recognize different alleles of RipB. We constructed a phylogenetic tree using a subset of RipB alleles identified by BLAST search to approximately span the diversity of this effector in *Ralstonia* (**Figure 3**). The *Ralstonia* genus contains many diverse strains that have been divided into four phylotypes based on based on sequence analysis of the internal transcribed spacer region of the 16S–23S rRNA gene (Poussier et al., 2000; Prior and Fegan, 2004; Safni et al., 2014). We selected RipB alleles from *Ralstonia* strains GMI1000 and MolK2, from phylotypes I and II, respectively, for subsequent analysis. These two RipB alleles share 71% amino acid identity with each other and approximately 52% identity with XopQ excluding the divergent N terminus containing the putative type III secretion signal. An alignment of these two RipB proteins with XopQ and HopQ1 is shown in **Supplementary Figure S5**. To test for Roq1-dependent recognition of RipB, we used *Agrobacterium* to transiently express RipB from GMI1000 and Molk2 in leaf tissue of wild-type and *roq1* mutant *N. tabacum*. The *N. tabacum roq1-1* mutant was generated using a CRISPR/CAS9 construct targeting exon 1 of the *Roq1* gene (**Supplementary Figure S6**). Both RipB alleles

TABLE 1 | Field trial results.

Season/Genotype	Disease severity	Marketable yield (kg/ha)
Spring 2018		
Fla. 8000	86 ± 5	54, 655 ± 9, 450
Fla. 8000 Roq1	1 ± 1	52, 656 ± 3, 810
Fla. 8000 Bs2	1 ± 1	66, 270 ± 10, 309
Fall 2018		
Fla. 8000	25 ± 7	19, 576 ± 11, 038
Fla. 8000 Roq1	5 ± 1	18, 538 ± 5, 901
Fla. 8000 Bs2	0 ± 0	33, 770 ± 13, 176
Spring 2019		
Fla. 8000	84 ± 2	73, 009 ± 15, 243
Fla. 8000 Roq1	11 ± 7	92, 837 ± 11, 072
Fla. 8000 Bs2	5 ± 1	80, 516 ± 14, 531

A field trial was conducted in Florida with disease pressure from Xanthomonas perforans. Disease severity presented as percent infected tissue, converted from field ratings that were scored using the Horsfall–Barratt scale. Harvested tomatoes were graded and sized by USDA specifications to calculate the total marketable yield. The values shown are means ± standard deviation from at least four replicate plots of 10 plants each. Tomato plants expressing the Bs2 immune receptor gene were included as a resistant control.

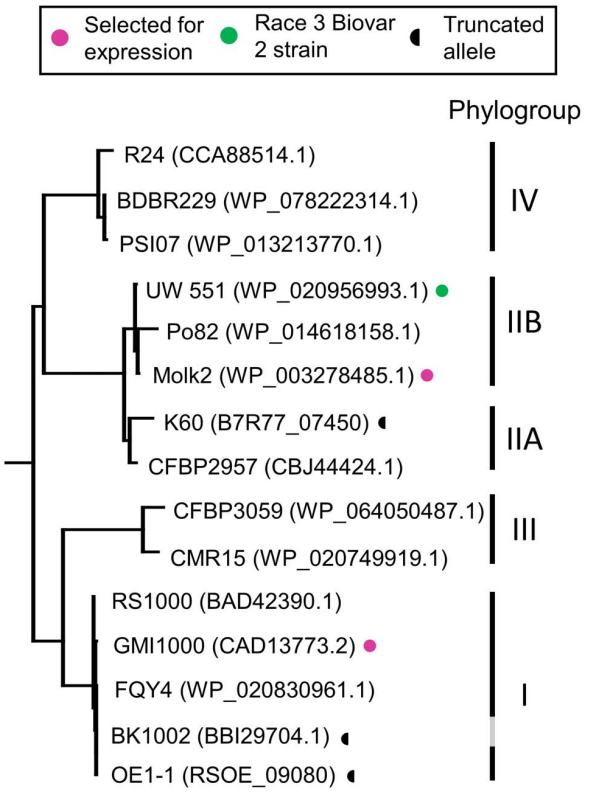

FIGURE 3 | Phylogenetic tree of RipB proteins. RipB alleles from *Ralstonia* strains GMI1000 and MolK2 were cloned for testing in this study and are indicated by magenta dots. Putatively non-functional RipB alleles with C-terminal truncations are marked with a half circle. Strain names are given along with the associated NCBI protein accession or locus tag. Phylotype groups were labeled based on previous publications with the exception of BK1002, for which an assignment was not available. The tree was rooted using XopQ and HopQ1.

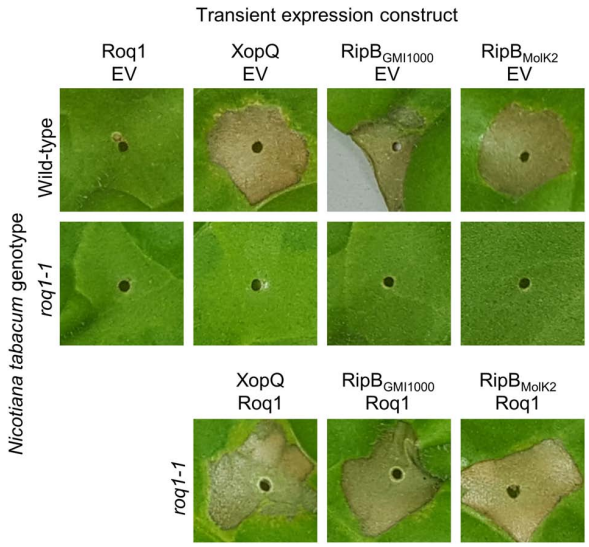

FIGURE 4 | Roq1-dependent recognition of RipB in *Nicotiana tabacum*. *Agrobacterium tumefaciens* was 'used to transiently express XopQ, RipB$_{GMI1000}$ and RipB$_{Molk2}$ along with either Roq1 or an empty vector (EV) control in wild-type *Nicotiana tabacum* and a *roq1* loss of function mutant. The *Agrobacterium* was infiltrated at a total OD$_{600}$ of 0.5 and the leaves were imaged at 3 days post infiltration. The images shown here are representative of three independent experiments.

triggered a strong hypersensitive/cell death response in wild-type *N. tabacum*, indicating immune activation. This response was absent in the *roq1-1* mutant but could be restored by transiently expressing Roq1 along with XopQ, RipB$_{GMI1000}$, or RipB$_{Molk2}$ (**Figure 4**).

Roq1 Tomatoes Are Resistant to *Ralstonia* Containing RipB

Our observation that Roq1 can recognize RipB in leaf transient expression assays suggested that Roq1 can mediate resistance to bacterial wilt caused by *Ralstonia* in tomato. We tested this hypothesis by challenging wild-type and *Roq1*-expressing tomato plants with *Ralstonia* strain GMI1000 using a soil soak inoculation disease assay. Wild-type plants developed severe wilting approximately 7 days after inoculation, whereas *Roq1* tomato plants remained mostly healthy over the 2-week time course (**Figure 5A** and **Supplementary Figure S7**). The *Roq1* tomato plants were susceptible to a deletion mutant lacking RipB (GMI1000 Δ*ripB*). We also challenged plants by introducing bacteria directly to the xylem by placing bacteria on the surface of a cut petiole. Wild-type plants were wilted by eight days whereas *Roq1* plants remained healthy (**Figure 5B**). Tomatoes expressing *Roq1* were also resistant to *Ralstonia* strain UW551, which is a race 3 biovar 2 potato brown rot strain from phylotype II that has a RipB allele (**Figure 3** and **Supplementary Figure S8**).

Distribution of RipB Alleles in *Ralstonia*

To investigate the potential for using *Roq1* to protect plants from *Ralstonia*, we investigated the occurrence of RipB alleles in select strains. **Table 2** lists some *Ralstonia* strains with their known hosts along with their respective phylotype and RipB allele accession information. **Table 2** illustrates that strains lacking putative functional RipB alleles correlate with strains that are virulent on tobacco, which contains a native *Roq1* gene. All strains in **Table 2** except for tobacco pathogenic strains K60, Y45, BK1002, and OE1-1 contain putative full-length and functional RipB alleles. Relative to other RipB alleles, the K60 RipB allele is truncated after residue 437 and missing approximately 65 C-terminal residues and the OE1-1 allele is truncated after residue 417, missing approximately 77 residues based on a published genome sequence (Hayes et al., 2017) (**Supplementary Figure S5**). Y45 does not have a predicted RipB allele based on a draft genome sequence (Li et al., 2011). Published gene models for RipB disagree on which start codon is the correct one, leading some RipB alleles to look like they are missing part of the N terminus or have N-terminal extensions. Analysis of the DNA sequence of diverse RipB alleles showed that out of three possible in-frame start codons, only a single putative start codon is conserved among *Ralstonia* strains from all four

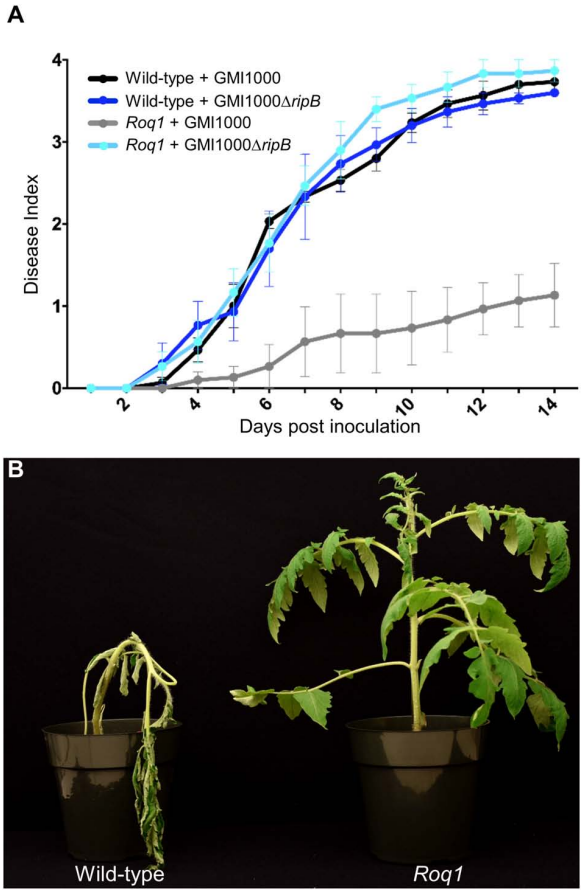

FIGURE 5 | Bacterial Wilt disease development in Roq1 tomatoes. **(A)** Wild-type and *Roq1* tomato plants were infected with wild-type and RipB mutant *Ralstonia* strain GMI1000 by soil soak inoculation. Disease symptoms were monitored over 14 days, with no wilting corresponding to a Disease Index of 0 and complete wilting corresponding to a Disease Index of 4. Error bars indicate standard error from four biological replicates. Disease progression of wild-type *Ralstonia* on tomatoes expressing *Roq1* was significantly lower ($p < 0.05$) than the three other conditions (Friedman test with Dunn's multiple comparisons test). **(B)** Wild-type and *Roq1* tomato plants 8 days after petiole inoculation with approximately 2000 cells of wild-type GMI1000.

phylotypes (**Supplementary Figure S9**), suggesting that this is the true start codon and eliminating the N-terminal discrepancy between different RipB alleles.

DISCUSSION

Roq1 expression in tomato confers strong resistance to *X. perforans*, *X. euvesicatoria*, *and P. syringae* pv. *tomato*. Its effectiveness is dependent on the presence of the recognized effector protein XopQ/HopQ1 (**Figures 1**, **2**). Field trials revealed that tomatoes expressing *Roq1* were less susceptible to *X. perforans* than wild-type tomatoes in conditions approximating commercial production (**Table 1**). *Roq1* conferred a similar level of resistance as the *Bs2*-containing resistant check variety in one season and was slightly weaker in the other two. Bacterial spot caused by *X. perforans* can cause lesions on fruits, making them unsuitable for commercial sale, and also reduce plant productivity by damaging leaf tissue. The onset of fruit lesions requires high disease pressure during a particular phase of fruit development. Environmental conditions did not favor the development of fruit lesions and we did not observe significant fruit lesion formation on any of the genotypes in any of the three seasons. Despite showing a strong reduction in foliar disease symptoms, the *Roq1* line did not have a significantly greater yield than the susceptible parental variety. A possible explanation for this finding is that bacterial spot did not appear to be a major constraint on yield in any of the three seasons. In spring 2018, weather conditions promoted the development of disease only late in the season after much of the yield was already set. Fall 2018 was unseasonably hot and dry for most of the season resulting in low disease pressure and very poor yield for all genotypes. Of the three seasons, spring 2019 had weather conditions expected to be most conducive for observing an impact of bacterial spot on marketable yield with mid-season rain promoting the development of disease symptoms. The average marketable yield for the *Roq1* tomatoes was 27% higher than wild-type in this season, although a relatively small sample size (four replicate plots of 10 plants each) and a large variability of yield between plots resulted in a *p*-value of 0.08 by Student's *t*-test. Notably the yield of the resistant check variety expressing *Bs2* was not significantly higher than the susceptible control in this season, though it was previously reported to give a yield increase of 1.5–11x relative to susceptible varieties under high disease pressure (Horvath et al., 2012). This suggests that bacterial spot was not severe enough to have a strong impact on yield in this season and that *Roq1* may result in an increase in marketable yield under stronger disease pressure.

It was unclear if *Roq1* could confer resistance to *Ralstonia* because it colonizes different tissues than *Xanthomonas* and *P. syringae*. While *Xanthomonas* and *P. syringae* colonize tomato leaf tissue, *Ralstonia* enters through the roots and colonizes xylem vessels. Although the type III secretion system is essential for virulence in *Ralstonia*, it is not clear when and where the pathogen delivers effectors into host cells. It was therefore not clear if *Roq1* would be able to confer resistance to this pathogen in tomato. Here we demonstrated that tomato plants expressing *Roq1* had strong resistance to *Ralstonia* expressing RipB as measured by both soil soak and cut-petiole inoculation assays (**Figure 5**). In addition to conferring resistance to the phylotype I strain GMI1000, *Roq1* also confers resistance to *Ralstonia* race 3 biovar 3 strain UW551, a phylotype II strain that can overcome other known sources of bacterial wilt resistance in tomato (Milling et al., 2011). Some but not all of the *Roq1* tomatoes inoculated with GMI1000 by soil soak were colonized by a moderate or low population of *Ralstonia* (**Supplementary Figure S10**). This observation suggests that Roq1-mediated immune responses may act to both restrict the establishment of vascular colonization and separately reduce bacterial titers if colonization does occur. Activation of immune receptors, including Roq1, is known to induce many defense-associated genes with different putative activities (Sohn et al., 2014; Qi

TABLE 2 | RipB occurrence and host range in *Ralstonia*.

*Ralstonia*strain	Host(s)	Origin	Phylotype	RipB allele	RipB accession
GMI1000	Tomato, Pepper, Arabidopsis	French Guyana	I	Present	CAD13773.2
RS1000	Tomato	Japan	I	Present	BAD42390.1
OE1-1	Tobacco	Japan	I	Truncated	RSOE_09080**
BK1002	Tobacco	Japan	not available	Truncated	BBI29704.1
Y45	Tobacco	China	I	Absent	None
K60	Tomato, Tobacco	United States	IIA	Truncated	B7R77_07450**
CFBP2957	Tomato	Martinique	IIA	Present	CBJ44424.1
Po82	Tomato, Banana, Potato	Mexico	IIB	Present	WP_014618158.1
IPO1609*	Potato	Netherlands	IIB	Present	WP_020956993.1
MolK2	Banana	Philippines	IIB	Present	WP_003278485.1
UW551*	Geranium	Kenya	IIB	Present	WP_020956993.1
CMR15	Tomato	Cameroon	III	Present	WP_020749919.1
PSI07	Tomato	Indonesia	IV	Present	WP_013213770.1
BDB R229	Banana	Indonesia	IV	Present	WP_078222314.1
R24	Clove	Indonesia	IV	Present	CCA88514.1

*The published host range of select Ralstonia strains is listed along with the identified RipB allele. Truncated indicates that the identified allele is missing conserved residues at the C terminus and is putatively non-functional. * Indicates a race 3 biovar 2 strain. ** Indicates NCBI locus tag from genome accession CP009764.1 for strain OE1-1 and genome NCTK01000001.1 for strain K60.*

et al., 2018), presumably acting to inhibit pathogen virulence by distinct mechanisms. The observation that Roq1 inhibits both colonization establishment and population growth suggests that at least two independent downstream defense responses mediate the observed resistance phenotype.

The *Roq1* tomatoes were susceptible to a *Ralstonia* mutant lacking *RipB*, indicating that the resistance depends on the interaction between RipB and Roq1. This is consistent with the observation that several naturally occurring *Ralstonia* strains that can infect tobacco have a truncated or are missing the RipB effector (**Table 2**) (Nakano and Mukaihara, 2019), suggesting that losing RipB can allow the pathogen to overcome the native *Roq1* gene present in *N. tabacum*. Tobacco-infecting strains K60 and OE1-1 contain independently truncated RipB alleles (**Figure 3** and **Supplementary Figure S5**) and there have likely been multiple independent gene loss events which enable strains to evade Roq1-mediated resistance. Similarly, HopQ1 has been lost in strains of *P. syringae* that can infect tobacco (Denny, 2006; Ferrante and Scortichini, 2009; Li et al., 2011). This suggests that this effector is not essential for virulence in all circumstances and it would therefore be prudent to deploy *Roq1* in combination with other disease resistance traits to avoid resistance breakdown due to pathogens losing XopQ/HopQ1/RipB. Although minor foliar symptoms were observed on the *Roq1* tomatoes, particularly in spring 2019 (**Table 1**), we do not believe this was due to a naturally occurring XopQ mutant arising during the trial. Instead, we think that these low disease scores may have been the result of fungal diseases, which can cause foliar symptoms that look similar to bacterial spot, or by the *Roq1* tomatoes supporting a low level of bacterial growth.

No other known NLR immune receptor confers resistance against such a broad range of bacterial pathogenic genera as Roq1. Effectors that are recognized by NLR proteins act as avirulence factors and are under strong evolutionary pressure to diversify or be lost to evade immune activation. Therefore the effector repertoires of pathogens are often quite diverse, with relatively few "core" effectors conserved within a species and even fewer shared between different genera (Grant et al., 2006). Effectors recognized by plant NLRs are typically narrowly conserved within a single bacterial genus (Kapos et al., 2019). One such effector is AvrBs2, recognized by the *Bs2* receptor from pepper, which is present in many *Xanthomonas* strains but is absent from *P. syringae* and *Ralstonia*. In contrast, XopQ/HopQ1/RipB is highly conserved in most *Xanthomonas*, *P. syringae*, and *Ralstonia* strains that cause disease in crop plants including kiwi (*P. syringae* pv. *actinidae*), banana (*Ralstonia* and *X. campestris* pv. *musacearum*), stone fruit (*P. syringae*), pepper (*X. euvesicatoria*), citrus (*X. citri*), strawberry (*X. fragariae*), brassica (*X. campestris*), rice (*X. oryzae*), potato (*Ralstonia*), and others. *Ralstonia* race 3 biovar 2 strains are of particular concern because they are cold tolerant and potentially threaten potato cultivation in temperate climates. As a result, *Ralstonia* race 3 biovar 2 strains are strictly regulated quarantine pathogens in Europe and North America and is on the United States Select Agent list. The ability of *Roq1* to protect tomato from the race 3 biovar 2 strain UW551 (**Supplementary Figure S8**) suggests that *Roq1* can also protect potato from this high-concern pathogen. This work demonstrates the widespread potential of using naturally occurring plant immune receptors to safely, sustainably, and economically manage diverse and difficult to control pathogen species.

DATA AVAILABILITY STATEMENT

All datasets generated for this study are included in the article/**Supplementary Material**.

AUTHOR CONTRIBUTIONS

NT and AS wrote the manuscript and performed *Pseudomonas* and *Ralstonia* petiole infection assays. AS carried out

Xanthomonas infection and *Agrobacterium* transient expression experiments. UG and SH performed *Xanthomonas* field experiments. CH constructed the *Ralstonia* knockout and performed *Ralstonia* soil soak assays, supervised by CA. All authors analyzed the results and edited and approved the manuscript.

FUNDING

This work was supported in part by the National Institute of Food and Agriculture, US Department of Agriculture under award number 2016-67012-25106, and the UC Berkeley Innovative Genomics Institute. CH was supported by an NSF Predoctoral Fellowship.

ACKNOWLEDGMENTS

This manuscript has been released as a pre-print at bioRxiv (Thomas et al., 2019). We thank Shirley Sato and Tom Clemente of the University of Nebraska Plant Transformation Core Research Facility for the transformation of tomato. We thank Myeong-Je Cho and Julie Pham of the UC Berkeley Innovative Genomics Institute for transformation of *Nicotiana tabacum*.

SUPPLEMENTARY MATERIAL

The Supplementary Material for this article can be found online at: https://www.frontiersin.org/articles/10.3389/fpls.2020.00463/full#supplementary-material

REFERENCES

Boller, T., and He, S. Y. (2009). Innate immunity in plants: an arms race between pattern recognition receptors in plants and effectors in microbial pathogens. *Science* 324, 742–744. doi: 10.1126/science.1171647

Castañeda, A., Reddy, J. D., El-Yacoubi, B., and Gabriel, D. W. (2005). Mutagenesis of all eight avr genes in *Xanthomonas campestris* pv. *campestris* had no detected effect on pathogenicity, but one avr gene affected race specificity. *Mol. Plant. Microbe Interact.* 18, 1306–1317.

Coupat, B., Chaumeille-Dole, F., Fall, S., Prior, P., Simonet, P., Nesme, X., et al. (2008). Natural transformation in the *Ralstonia solanacearum* species complex: number and size of DNA that can be transferred. *FEMS Microbiol. Ecol.* 66, 14–24. doi: 10.1111/j.1574-6941.2008.00552.x

Coutu, C., Brandle, J., Brown, D., Brown, K., Miki, B., Simmonds, J., et al. (2007). pORE: a modular binary vector series suited for both monocot and dicot plant transformation. *Transgenic Res.* 16, 771–781. doi: 10.1007/s11248-007-9066-2

Dangl, J. L., Horvath, D. M., and Staskawicz, B. J. (2013). Pivoting the plant immune system from dissection to deployment. *Science* 341, 746–751. doi: 10.1126/science.1236011

Davis, R. M., Miyao, G., Subbarao, K. V., Stapleton, J. J., and Aegerter, A. B. J. (2013). *UC IPM: UC Management Guidelines - TOMATO:Diseases*. Available at: http://ipm.ucanr.edu/PMG/r783101611.html (Accessed June 17, 2019).

de Pontes, N. C., Nascimento, A. D. R., Golynski, A., Maffia, L. A., and Rogério de Oliveira, J. (2016). Intervals and number of applications of acibenzolar-S-methyl for the control of bacterial spot on processing tomato. *Plant Dis.* 100, 2126–2133. doi: 10.1094/pdis-11-15-1286-re

Denny, T. (2006). "Plant pathogenic *Ralstonia* species," in *Plant-Associated Bacteria*, ed. S. S. Gnanamanickam (Dordrecht: Springer), 573–644. doi: 10.1007/1-4020-4538-7_16

Deslandes, L., and Rivas, S. (2012). Catch me if you can: bacterial effectors and plant targets. *Trends Plant Sci.* 17, 644–655. doi: 10.1016/j.tplants.2012.06.011

Dillon, M. M., Almeida, R. N. D., Laflamme, B., Martel, A., Weir, B. S., Desveaux, D., et al. (2019). Molecular evolution of *Pseudomonas* syringae Type III secreted effector proteins. *Front. Plant Sci.* 10:418.

Ferrante, P., and Scortichini, M. (2009). Identification of *Pseudomonas syringae* pv. actinidiae as causal agent of bacterial canker of yellow kiwifruit (*Actinidia chinensis* Planchon) in Central Italy. *J. Phytopathol.* 157, 768–770. doi: 10.1111/j.1439-0434.2009.01550.x

Freeman, J. H., McAvoy, E. J., Boyd, N. S., Kanissery, R., Smith, H. A., Desaeger, J., et al. (2018). "Tomato production," in *Vegetable Production Handbook of Florida 2018–2019*, eds H. A. Smith, J. H. Freeman, P. J. Dittmar, M. L. Paret, and G. E. Vallad (Lincolnshire, IL: Vance Publishing Corporation), 349–393.

Gibson, D. G., Young, L., Chuang, R.-Y., Venter, J. C., Hutchison, C. A. III, and Smith, H. O. (2009). Enzymatic assembly of DNA molecules up to several hundred kilobases. *Nat. Methods* 6, 343–345. doi: 10.1038/nmeth.1318

Giska, F., Lichocka, M., Piechocki, M., Dadlez, M., Schmelzer, E., Hennig, J., et al. (2013). Phosphorylation of HopQ1, a type III effector from *Pseudomonas syringae*, creates a binding site for host 14-3-3 proteins. *Plant Physiol.* 161, 2049–2061. doi: 10.1104/pp.112.209023

Grant, S. R., Fisher, E. J., Chang, J. H., Mole, B. M., and Dangl, J. L. (2006). Subterfuge and manipulation: type III effector proteins of phytopathogenic bacteria. *Annu. Rev. Microbiol.* 60, 425–449. doi: 10.1146/annurev.micro.60.080805.142251

Griffin, K., Gambley, C., Brown, P., and Li, Y. (2017). Copper-tolerance in *Pseudomonas syringae* pv. *tomato* and *Xanthomonas* spp. and the control of diseases associated with these pathogens in tomato and pepper. A systematic literature review. *Crop Protoc.* 96, 144–150. doi: 10.1016/j.cropro.2017.02.008

Gudesblat, G. E., Torres, P. S., and Vojnov, A. A. (2009). *Xanthomonas campestris* overcomes *Arabidopsis* stomatal innate immunity through a DSF cell-to-cell signal-regulated virulence factor. *Plant Physiol.* 149, 1017–1027. doi: 10.1104/pp.108.126870

Guindon, S., Dufayard, J.-F., Lefort, V., Anisimova, M., Hordijk, W., and Gascuel, O. (2010). New algorithms and methods to estimate maximum-likelihood phylogenies: assessing the performance of PhyML 3.0. *Syst. Biol.* 59, 307–321. doi: 10.1093/sysbio/syq010

Hann, D. R., Domínguez-Ferreras, A., Motyka, V., Dobrev, P. I., Schornack, S., Jehle, A., et al. (2014). The *Pseudomonas* type III effector HopQ1 activates cytokinin signaling and interferes with plant innate immunity. *New Phytol.* 201, 585–598. doi: 10.1111/nph.12544

Hayes, M. M., MacIntyre, A. M., and Allen, C. (2017). Complete genome sequences of the plant pathogens *Ralstonia solanacearum* Type Strain K60 and *R. solanacearum* race 3 biovar 2 strain UW551. *Genome Announc.* 5:e01088-17. doi: 10.1128/genomeA.01088-17

Horsfall, J. G., and Barrat, R. W. (1945). An improved grading system for measuring plant diseases. *Phytopathology* 35:655.

Horvath, D. M., Stall, R. E., Jones, J. B., Pauly, M. H., Vallad, G. E., Dahlbeck, D., et al. (2012). Transgenic resistance confers effective field level control of bacterial spot disease in tomato. *PloS One* 7:e42036. doi: 10.1371/journal.pone.0042036

Jones, J. D. G., and Dangl, J. L. (2006). The plant immune system. *Nature* 444, 323–329.

Jones, J. D. G., Vance, R. E., and Dangl, J. L. (2016). Intracellular innate immune surveillance devices in plants and animals. *Science* 354, doi: 10.1126/science.aaf6395

Jones, J. D. G., Witek, K., Verweij, W., Jupe, F., Cooke, D., Dorling, S., et al. (2014). Elevating crop disease resistance with cloned genes. *Philos. Trans. R. Soc. Lond. B Biol. Sci.* 369:20130087. doi: 10.1098/rstb.2013.0087

Kapos, P., Devendrakumar, K. T., and Li, X. (2019). Plant NLRs: from discovery to application. *Plant Sci.* 279, 3–18. doi: 10.1016/j.plantsci.2018.03.010

Kay, S., and Bonas, U. (2009). How *Xanthomonas* type III effectors manipulate the host plant. *Curr. Opin. Microbiol.* 12, 37–43. doi: 10.1016/j.mib.2008.12.006

Kennelly, M. M., Cazorla, F. M., de Vicente, A., Ramos, C., and Sundin, G. W. (2007). *Pseudomonas syringae* diseases of fruit trees: progress toward understanding and control. *Plant Dis.* 91, 4–17. doi: 10.1094/pd-91-0004

Khokhani, D., Tran, T. M., Lowe-Power, T. M., and Allen, C. (2018). Plant assays for quantifying *Ralstonia solanacearum* virulence. *Bio Protocol* 8:3028.

Kunwar, S., Iriarte, F., Fan, Q., Evaristo da Silva, E., Ritchie, L., Nguyen, N. S., et al. (2018). Transgenic expression of *EFR* and *Bs2* genes for field management of bacterial wilt and bacterial spot of tomato. *Phytopathology* 108, 1402–1411. doi: 10.1094/phyto-12-17-0424-r

Li, W., Yadeta, K. A., Elmore, J. M., and Coaker, G. (2013). The *Pseudomonas syringae* effector HopQ1 promotes bacterial virulence and interacts with tomato 14-3-3 proteins in a phosphorylation-dependent manner. *Plant Physiol.* 161, 2062–2074. doi: 10.1104/pp.112.211748

Li, X., Kapos, P., and Zhang, Y. (2015). NLRs in plants. *Curr. Opin. Immunol.* 32, 114–121. doi: 10.1016/j.coi.2015.01.014

Li, Z., Wu, S., Bai, X., Liu, Y., Lu, J., Liu, Y., et al. (2011). Genome sequence of the tobacco bacterial wilt pathogen *Ralstonia solanacearum*. *J. Bacteriol.* 193, 6088–6089. doi: 10.1128/jb.06009-11

Liu, Y., Kanda, A., Kiba, A., Hikichi, Y., and Ohnishi, K. (2009). Distribution of avirulence genes avrA and popP1 in 22 Japanese phylotype I strains of *Ralstonia solanacearum*. *J. Gen. Plant Pathol.* 75, 362–368. doi: 10.1007/s10327-009-0189-6

Malik, K., Wu, K., Li, X. Q., Martin-Heller, T., Hu, M., Foster, E., et al. (2002). A constitutive gene expression system derived from the tCUP cryptic promoter elements. *Theor. Appl. Genet.* 105, 505–514. doi: 10.1007/s00122-002-0926-0

Milling, A., Babujee, L., and Allen, C. (2011). *Ralstonia solanacearum* extracellular polysaccharide is a specific elicitor of defense responses in wilt-resistant tomato plants. *PLoS One* 6:e15853. doi: 10.1371/journal.pone.0015853

Mukaihara, T., and Tamura, N. (2009). Identification of novel *Ralstonia solanacearum* type III effector proteins through translocation analysis of hrpB-regulated gene products. *Microbiology* 155, 2235–2244. doi: 10.1099/mic.0.027763-0

Nakano, M., and Mukaihara, T. (2019). The type III effector RipB from *Ralstonia solanacearum* RS1000 acts as a major avirulence factor in *Nicotiana benthamiana* and other *Nicotiana* species. *Mol. Plant Pathol.* 20, 1237–1251. doi: 10.1111/mpp.12824

Peeters, N., Carrère, S., Anisimova, M., Plener, L., Cazalé, A.-C., and Genin, S. (2013). Repertoire, unified nomenclature and evolution of the Type III effector gene set in the *Ralstonia solanacearum* species complex. *BMC Genomics* 14:859. doi: 10.1186/1471-2164-14-859

Potnis, N., Timilsina, S., Strayer, A., Shantharaj, D., Barak, J. D., Paret, M. L., et al. (2015). Bacterial spot of tomato and pepper: diverse *Xanthomonas* species with a wide variety of virulence factors posing a worldwide challenge. *Mol. Plant Pathol.* 16, 907–920. doi: 10.1111/mpp.12244

Poussier, S., Prior, P., Luisetti, J., Hayward, C., and Fegan, M. (2000). Partial sequencing of the hrpB and endoglucanase genes confirms and expands the known diversity within the *Ralstonia solanacearum* species complex. *Syst. Appl. Microbiol.* 23, 479–486. doi: 10.1016/s0723-2020(00)80021-1

Prior, P., and Fegan, M. (2004). "Recent developments in the phylogeny and classification of *Ralstonia solanacearum*," in *Proceedings of the I International Symposium on Tomato Diseases 695* (Leuven: International Society for Horticultural Science), 127–136. doi: 10.17660/actahortic.2005.695.14

Qi, T., Seong, K., Thomazella, D. P. T., Kim, J. R., Pham, J., Seo, E., et al. (2018). NRG1 functions downstream of EDS1 to regulate TIR-NLR-mediated plant immunity in *Nicotiana benthamiana*. *Proc. Natl. Acad. Sci. U.S.A.* 115, E10979–E10987.

Rivard, C. L., O'Connell, S., Peet, M. M., Welker, R. M., and Louws, F. J. (2012). Grafting tomato to manage bacterial wilt caused by *Ralstonia solanacearum* in the Southeastern united states. *Plant Dis.* 96, 973–978. doi: 10.1094/pdis-12-10-0877

Ryan, R. P., Vorhölter, F.-J., Potnis, N., Jones, J. B., Van Sluys, M.-A., Bogdanove, A. J., et al. (2011). Pathogenomics of *Xanthomonas*: understanding bacterium-plant interactions. *Nat. Rev. Microbiol.* 9, 344–355. doi: 10.1038/nrmicro2558

Sabbagh, C. R. R., Carrère, S., Lonjon, F., Vailleau, F., Macho, A. P., Genin, S., et al. (2019). Pangenomic type III effector database of the plant pathogenic *Ralstonia* spp. *PeerJ* 7:e7346. doi: 10.7287/peerj.preprints.27726v1

Safni, I., Cleenwerck, I., De Vos, P., Fegan, M., Sly, L., and Kappler, U. (2014). Polyphasic taxonomic revision of the *Ralstonia solanacearum* species complex: proposal to emend the descriptions of *Ralstonia solanacearum* and *Ralstonia syzygii* and reclassify current *R. syzygii* strains as *Ralstonia syzygii* subsp. syzygii subsp. nov., *R. solanacearum* phylotype IV strains as *Ralstonia syzygii* subsp. indonesiensis subsp. nov., banana blood disease bacterium strains as *Ralstonia syzygii* subsp. celebesensis subsp. nov. and *R. solanacearum* phylotype I and III strains as *Ralstonia pseudosolanacearum* sp. nov. *Int. J. Syst. Evol. Microbiol.* 64, 3087–3103. doi: 10.1099/ijs.0.066712-0

Schultink, A., Qi, T., Lee, A., Steinbrenner, A. D., and Staskawicz, B. (2017). Roq1 mediates recognition of the *Xanthomonas* and *Pseudomonas* effector proteins XopQ and HopQ1. *Plant J.* 92, 787–795. doi: 10.1111/tpj.13715

Schwartz, A. R., Potnis, N., Timilsina, S., Wilson, M., Patané, J., Martins, J., et al. (2015). Phylogenomics of *Xanthomonas* field strains infecting pepper and tomato reveals diversity in effector repertoires and identifies determinants of host specificity. *Front. Microbiol.* 6:535.

Sharma, S., and Bhattarai, K. (2019). Progress in developing bacterial spot resistance in tomato. *Agronomy* 9:26. doi: 10.3390/agronomy9010026

Sievers, F., Wilm, A., Dineen, D., Gibson, T. J., Karplus, K., Li, W., et al. (2011). Fast, scalable generation of high-quality protein multiple sequence alignments using Clustal Omega. *Mol. Syst. Biol.* 7:539. doi: 10.1038/msb.2011.75

Sohn, K. H., Segonzac, C., Rallapalli, G., Sarris, P. F., Woo, J. Y., Williams, S. J., et al. (2014). The nuclear immune receptor RPS4 is required for RRS1SLH1-dependent constitutive defense activation in *Arabidopsis thaliana*. *PLoS Genet.* 10:e1004655. doi: 10.1371/journal.pgen.1004655

Staskawicz, B. J., and Schultink, A. C. (2019). *Roq1 Provides Resistance to Both Xanthomonas and Pseudomonas in Plants*. World Patent WO2019040483. Geneva: WIPO.

Tai, T. H., Dahlbeck, D., Clark, E. T., Gajiwala, P., Pasion, R., Whalen, M. C., et al. (1999). Expression of the *Bs2* pepper gene confers resistance to bacterial spot disease in tomato. *Proc. Natl. Acad. Sci. U.S.A.* 96, 14153–14158. doi: 10.1073/pnas.96.24.14153

Teper, D., Salomon, D., Sunitha, S., Kim, J.-G., Mudgett, M. B., and Sessa, G. (2014). *Xanthomonas euvesicatoria* type III effector XopQ interacts with tomato and pepper 14-3-3 isoforms to suppress effector-triggered immunity. *Plant J.* 77, 297–309. doi: 10.1111/tpj.12391

Thomas, N. C., Hendrich, C. G., Gill, U. S., Allen, C., Hutton, S. F., and Schultink, A. (2019). Roq1 confers resistance to *Xanthomonas*, *Pseudomonas syringae* and *Ralstonia solanacearum* in tomato. *bioRxiv* [Preprint]. doi: 10.1101/813758

Vasse, J., Frey, P., and Trigalet, A. (1995). *Microscopic Studies of Intercellular Infection and Protoxylem Invasion of Tomato Roots by Pseudomonas Solanacearum*. Available at: https://pubag.nal.usda.gov/catalog/1443867 (Accessed July 1, 2019).

Vincelli, P. (2016). Genetic engineering and sustainable crop disease management: opportunities for case-by-case decision-making. *Sustain. Sci. Pract. Policy* 8:495. doi: 10.3390/su8050495

Wei, C. F., Kvitko, B. H., Shimizu, R., Crabill, E., Alfano, J. R., Lin, N. C., et al. (2007). A *Pseudomonas syringae* pv. *tomato* DC3000 mutant lacking the type III effector HopQ1-1 is able to cause disease in the model plant *Nicotiana benthamiana*. *Plant J.* 51, 32–46. doi: 10.1111/j.1365-313x.2007.03126.x

Xin, X.-F., Kvitko, B., and He, S. Y. (2018). *Pseudomonas syringae*: what it takes to be a pathogen. *Nat. Rev. Microbiol.* 16, 316–328. doi: 10.1038/nrmicro.2018.17

Yuliar, Nion, Y. A., and Toyota, K. (2015). Recent trends in control methods for bacterial wilt diseases caused by *Ralstonia solanacearum*. *Microbes Environ.* 30, 1–11. doi: 10.1264/jsme2.me14144

Zipfel, C. (2014). Plant pattern-recognition receptors. *Trends Immunol.* 35, 345–351.

Conflict of Interest: AS and NT are employees of and have a financial stake in Fortiphyte Inc., which has intellectual property rights related to the Roq1 resistance gene.

The remaining authors declare that the research was conducted in the absence of any commercial or financial relationships that could be construed as a potential conflict of interest.

frontiers in Microbiology

ORIGINAL RESEARCH
published: 19 May 2020
doi: 10.3389/fmicb.2020.00977

L-Amino Acid Oxidases From Mushrooms Show Antibacterial Activity Against the Phytopathogen *Ralstonia solanacearum*

Jerica Sabotič[1]†, Jože Brzin[1], Jana Erjavec[2], Tanja Dreo[2], Magda Tušek Žnidarič[2], Maja Ravnikar[2] and Janko Kos[1,3]*

[1] Department of Biotechnology, Jožef Stefan Institute, Ljubljana, Slovenia, [2] Department of Biotechnology and Systems Biology, National Institute of Biology, Ljubljana, Slovenia, [3] Faculty of Pharmacy, University of Ljubljana, Ljubljana, Slovenia

Ralstonia solanaceraum is the quarantine plant pathogenic bacterium that causes bacterial wilt in over 200 host plants, which include economically important crops such as potato, tomato, tobacco, banana, and ginger. Alternative biological methods of disease control that can be used in integrated pest management are extensively studied. In search of new proteins with antibacterial activity against *R. solanacearum*, we identified L-amino acid oxidases (LAOs) from fruiting bodies of *Amanita phalloides* (*Ap*LAO) and *Infundibulicybe geotropa* (*Cg*LAO). We describe an optimized isolation procedure for their biochemical characterization, and show that they are dimeric proteins with estimated monomer molecular masses of 72 and 66 kDa, respectively, with isoelectric point of pH 6.5. They have broad substrate specificities for hydrophobic and charged amino acids, with highest K_m for L-Leu, and broad pH optima at pH 5 and pH 6, respectively. An enzyme with similar properties is also characterized from the mycelia of *I. geotropa* (*Cg*mycLAO). Fractionated aqueous extracts of 15 species of mushrooms show that LAO activity against L-Leu correlates with antibacterial activity. We confirm that the LAO activities mediate the antibacterial actions of *Ap*LAO, *Cg*LAO, and *Cg*mycLAO. Their antibacterial activities are greater against Gram-negative *versus* Gram-positive bacteria, with inhibition of growth rate, prolongation of lag-phase, and decreased endpoint biomass. In Gram-positive bacteria, they mainly prolong the lag phase. These *in vitro* antibacterial activities of *Cg*LAO and *Cg*mycLAO are confirmed *in vivo* in tomato plants, while *Ap*LAO has no effect on disease progression *in planta*. Transmission electron microscopy shows morphological changes of *R. solanacearum* upon LAO treatments. Finally, broad specificity of the antibacterial activities of these purified LAOs were seen for *in vitro* screening against 14 phytopathogenic bacteria. Therefore, these fungal LAOs show great potential as new biological phytoprotective agents and show the fruiting bodies of higher fungi to be a valuable source of antimicrobials with unique features.

Keywords: bacterial wilt, antimicrobial, *Amanita phalloides*, *Clitocybe geotropa*, oxidative stress, L-amino acid oxidase, antibacterial, phytophatogen

Abbreviations: *Ap*LAO, *Amanita phalloides* L-amino acid oxidase; AUDPC, area under the disease progress curve; *Cg*LAO, *Infundibulicybe* (previously *Clitocybe) geotropa* L-amino acid oxidase; *Cg*mycLAO, mycelium-derived *Infundibulicybe* (previously *Clitocybe) geotropa* L-amino acid oxidase; CSM, complete supplement mixture; *Hc*LAO, *Hebeloma cylindrosporium* L-amino acid oxidase; LAO, L-amino acid oxidase; PBS, phosphate-buffered saline; PHA, polyhydroxyalkanoate; YPG, yeast peptone glucose.

OPEN ACCESS

Edited by:
Marc Valls, University of Barcelona, Spain

Reviewed by:
Anabela Portela Borges, University of Porto, Portugal
Yasufumi Hikichi, Kōchi University, Japan

***Correspondence:**
Jerica Sabotič
Jerica.Sabotic@ijs.si

†ORCID:
Jerica Sabotič
orcid.org/0000-0002-2404-0192

Specialty section:
This article was submitted to Plant Microbe Interactions, a section of the journal Frontiers in Microbiology

Received: *16 December 2019*
Accepted: *23 April 2020*
Published: *19 May 2020*

Citation:
Sabotič J, Brzin J, Erjavec J, Dreo T, Tušek Žnidarič M, Ravnikar M and Kos J (2020) L-Amino Acid Oxidases From Mushrooms Show Antibacterial Activity Against the Phytopathogen Ralstonia solanacearum. Front. Microbiol. 11:977. doi: 10.3389/fmicb.2020.00977

INTRODUCTION

The search for new antibacterial agents is especially important against plant pathogenic bacteria where there are no effective chemical or biological agents available for plant protection (Payne et al., 2007; Sahu et al., 2017). One such plant pathogen is the quarantine bacterium *Ralstonia solanacearum* (Smith, 1896) Yabuuchi et al., 1996, which is the active agent for bacterial wilt in the plant family *Solanaceae*. *R. solanacearum* is a species complex that can infect over 200 host plants, which include economically important crops such as potato, tomato, eggplant, tobacco, banana, pelargonium, and ginger (Allen et al., 2005). Overall, *R. solanacearum* results in approximately US$ 950 million annual losses worldwide. The most affected countries are China, Bangladesh, Uganda and Bolivia, which suffer between 30 and 90% annual crop losses, which can rise to 98% during crop storage (Allen et al., 2005; Yuliar et al., 2015).

L-amino acid oxidases (LAOs; E.C. 1.4.3.2) are enzymes that catalyze the oxidative deamination of L-amino acids to their corresponding α-keto acids, with the generation of ammonia and hydrogen peroxide. They are flavoenzymes, and they show high stereospecificity toward L-isomers of amino acids (Lukasheva et al., 2011; Hossain et al., 2014). LAOs are widely distributed in nature, and they fulfill a wide spectrum of biological roles in nitrogen metabolism and in the protection against antagonists, with antimicrobial activities representing one of their main functions. Moreover, LAOs represent a major component of snake venoms, where they serve as toxins, which have been studied in great detail to date. These are flavin adenine dinucleotide or flavin mononucleotide binding proteins, with molecular masses from 50 to 300 kDa, and isoelectric points between pH 4.0 and 9.4. They are usually glycosylated and form non-covalently associated homodimers. Most LAOs have a broad range of substrate specificities, with preference for hydrophobic amino-acid substrates, including L-Phe, L-Leu, L-Trp, L-Met, and L-Ile. On the other hand, some LAOs have very narrow substrate specificities, with high preference for basic L-amino acids, such as L-Lys oxidase from *Trichoderma viride*. The biological effects of LAOs are mediated through their enzymatic activity in two ways: (i) via elimination of amino acids from the extracellular environment, which can cause nutrient deficiency, and/or (ii) via binding to the surface of cells and generating high local concentrations of hydrogen peroxide, which can lead to cell death (Du and Clemetson, 2002; Lukasheva et al., 2011; Guo et al., 2012; Hossain et al., 2014). Several snake venom LAOs have strong antibacterial activities that show wide variations in their selectivities and specificities against Gram-positive and/or Gram-negative bacteria (Guo et al., 2012; Izidoro et al., 2014). Only a few LAOs have been isolated from fungi, however, a recent screening of LAO activities in fungal fruiting bodies revealed that they represent a new rich and readily accessible source of versatile and robust enzymes with LAO activities (Žun et al., 2017).

Although there have been extensive studies on biological control of *R. solanaceraum* (Anith et al., 2004; Ji et al., 2005; Messiha et al., 2007; Hong et al., 2011; Maji and Chakrabartty, 2014; Yuliar et al., 2015), to date there are no efficient chemical or biological agents available for its control. So far, only a few fungal proteins have been tested in the field of agricultural crop protection, including tamavidin (Takakura et al., 2012), mycocypins (Šmid et al., 2013, 2015) and different lectins (Pohleven et al., 2011; Sabotič et al., 2016). The only example of mushroom proteins that are active against bacterial plant pathogens was reported by Zheng et al. (2010), who isolated an antibacterial protein from dried fruiting bodies of the mushroom *Clitocybe sinopica*, however, they did not perform any *in vivo* tests (Zheng et al., 2010). A screening study for antibacterial activities against *R. solanacearum* that included 150 aqueous extracts of fungal fruiting bodies from 94 different species revealed complete growth inhibition of *R. solanacearum in vitro* for 11 of these extracts. Two extracts were selected for isolation and characterization of the antibacterial active substance. One was from the poisonous death cap *Amanita phalloides* (Fries) Link (1833), which showed broad antibacterial activity *in vitro* against Gram-negative bacteria but no *in vivo* activity. The other was from the edible trooping funnel mushroom *Infundibulicybe geotropa* (Buillard ex DeCandolle) Harmaja (2003), which showed antibacterial activity against different strains of *Ralstonia* spp., and also antibacterial activity *in vivo* for both tomato and potato (Erjavec et al., 2016).

Here, we describe the biochemical characterization of proteins with antibacterial activity against *R. solanacearum* that are isolated from fruiting bodies of *A. phalloides* and *I. geotropa*, and from *I. geotropa* cultured mycelia. *I. geotropa* has been reclassified taxonomically from *Clitocybe geotropa*, however, the abbreviation of the protein name (*Cg*LAO) as well as that from the mycelium (*Cg*mycLAO) is maintained here for continuity of the characterization of these proteins, as their apoptosis-inducing activities on cancer cell lines were published previously (Pišlar et al., 2016). We determined the antibacterial activities of these isolated proteins against *R. solanacearum* both *in vitro* and *in vivo*. We finally indicate a possible mechanism of action for the *I. geotropa* protein through electron microscopy analysis of *R. solanacearum* cells in the presence of the purified protein fraction from *I. geotropa*, and through determining the effects of these isolated antibacterial proteins on model Gram-positive and Gram-negative bacteria.

MATERIALS AND METHODS

Materials and Fungal Samples

The L-amino acids L-Thr, L-Gly, L-Ala, L-Met, L-Phe, and L-Tyr were from Serva (Heidelberg, Germany), L-Arg, L-Val, and L-Trp from Fluka (Buchs, Switzerland), L-Pro from Merck (Darmstadt, Germany) and L-His, L-Lys, L-Asp, L-Glu, L-Ser, L-Asn, L-Gln, L-Cys, L-Ile, and L-Leu from Sigma-Aldrich (St. Louis, MO, United States). Complete supplement mixture (CSM) was from Formedium (Norfolk, United Kingdom), and peptide N-glycosidase F was from Roche Diagnostics (Basel, Switzerland). Horseradish peroxidase, catalase and other reagents (all of analytical or sequencing grade) were from Sigma-Aldrich (St. Louis, MO, United States). Glutaraldehyde, osmium

tetroxide, and uranyl acetate were from SPI Supplies (West Chester, PA, United States), Paraformaldehyde, epoxy resins agar 100 and lead citrate were from Agar Scientific (Essex, United Kingdom). Yeast extract and casamino acids were from Difco (Detroit, MI, United States), proteose peptone, bacto-peptone and agar from Oxoid (Basingstoke, United Kingdom), glucose and sucrose from Kemika (Zagreb, Croatia), malt extract from BioMerieux (Marcy l'Etoile, France), and M17 from Merck (Darmstadt, Germany). Fruiting bodies of *Agaricus bisporus* (J. E. Lange) Imbach 1946, *Macrolepiota procera* (Scop.) Singer 1948, *Coprinopsis cinerea* (Schaeff.) Redhead, Vilgalys and Moncalvo 2001, *Amanita phalloides* (Vaill. ex Fr.) Link 1833, *Amanita rubescens* Pers. 1797, *Hygrophorus erubescens* (Fr.) Fr. (1838), *Hygrophorus russula* (Schaeff. ex Fr.) Kauffman (1918), *Infundibulicybe geotropa* (Bull.) Harmaja (2003), *Clitocybe nebularis* (Batsch) P. Kumm. (1871), *Lepista nuda* (Bull.) Cooke (1871), *Tricholoma saponaceum* (Fr.) P. Kumm. (1871), *Imleria badia* (Fr.) Vizzini (2014), *Suillus variegatus* (Sw.) Richon and Roze (1888), *Cantharellus cibarius* Fr. (1821), and *Tuber mesentericum* Vittad. (1831) (**Table 1**) were collected in their natural habitat in forest stands or grasslands in central and western Slovenia and frozen at −20°C. The taxonomic classification follows the Index Fungorum database[1].

Isolation of *I. geotropa* LAO From Fruiting Bodies and Vegetative Mycelia

After thawing, 240 mL of crude aqueous extract was pressed out of 500 g of the fruiting bodies. After addition of 2 M NaSCN and 3 M urea, the extract was concentrated by ultrafiltration using 3-kDa cut-off membranes. The precipitated material was removed by centrifugation at 8000 × *g* for 20 min at 4°C. The samples were then divided into three equal portions, with each applied to a preparative gel filtration chromatography column (4 × 110 cm; flow rate, 42 mL/h; fraction volume, 17 mL) using Sephacryl S200 (GE Healthcare Life Sciences, Uppsala, Sweden) equilibrated in 0.02 M Tris–HCl, pH 7.5, with 0.3 M NaCl and 3 M urea (buffer A). The fractions with antibacterial activity were pooled, concentrated by ultrafiltration, and dialyzed against 50 mM phosphate buffer, pH 6.8 (buffer B), which contained 0.85 M ammonium sulfate. They were then applied to a hydrophobic interaction chromatography column (3 × 35 cm; flow rate, 19.2 mL/h; fraction volume, 12 mL) using phenyl-Sepharose (GE Healthcare Life Sciences, Uppsala, Sweden) equilibrated in buffer B. The bound protein was eluted using a linear gradient of ammonium sulfate, from 0.85 to 0 M in buffer B (1200 mL), followed by a gradient of 0 to 20% ethanol in buffer B (400 mL). The fractions with the highest antibacterial activities were pooled and concentrated by ultrafiltration. This is an optimized protocol from the previously published *Cg*LAO purification (Pišlar et al., 2016) with highly improved yield.

Infundibulicybe geotropa mycelia were cultivated as described previously (Erjavec et al., 2016), collected by filtration through cheesecloth, and centrifuged (8000 × *g* for 10 min at 4°C) and stored at −20°C until use. The solid mycelia (15 g) were homogenized in liquid nitrogen, and the protein from this hyphal powder was extracted overnight in 100 mL buffer A. The insoluble material was removed by centrifugation (16000 × *g* for 5 min at 4°C), and the resulting crude *I. geotropa* mycelium extract was subjected to the same purification procedure as the crude fruiting body extracts.

[1]http://www.indexfungorum.org

TABLE 1 | Antibacterial activities against *R. solanacearum* and LAO activities (at pH 5.5) in the fungal fruiting body extracts and their gel filtration fractions.

Family	Species	Estimated Mw of active fraction (kDa)	*In vitro* antibacterial activity		LAO activity of gel filtration fractions		
			Extract	Active fraction	In-gel vs. amino acids in CSM	In-solution vs. amino acids in CSM	In-solution vs. L-Leu
Agaricaceae	*Agaricus bisporus*	25	−	−	+	+	−
	Macrolepiota procera	na	−	−	−	−	−
Psathyrellaceae	*Coprinopsis cinerea*	na	−	−	−	−	−
Amanitaceae	*Amanita phalloides*	120	+	+	+	+	+
	Amanita rubescens	na	nd	−	−	−	−
Hygrophoraceae	*Hygrophorus erubescens*	na	−	−	−	−	−
	Hygrophorus russula	na	−	−	−	−	−
Tricholomataceae	*Infundibulicybe geotropa*	80	+	+	+	+	+
	Clitocybe nebularis	30	+	±	+	+	−
	Lepista nuda	150	−	+	+	−	−
	Tricholoma saponaceum	na	+	−	−	−	−
Boletaceae	*Imleria badia*	30	nd	−	+	+	−
Suillaceae	*Suillus variegatus*	na	−	−	−	−	−
Hydnaceae	*Cantharellus cibarius*	na	nd	−	−	−	−
Tuberaceae	*Tuber mesentericum*	50	−	+	+	+	+

Details of the elution profiles for the LAO and antibacterial activities of the gel filtration fractions are illustrated in ***Supplementary Figure S4****. ±, Antibacterial activity detected in a different fraction than LAO activity. na, not applicable (no activity); nd, not determined. CSM, complete supplement mixture.*

Isolation of *A. phalloides* LAO From Fruiting Bodies

The isolation procedure for *A. phalloides* LAO (*Ap*LAO) was the same as that used for *I. geotropa* LAO (*Cg*LAO), except that 2 M NaSCN was omitted in the extract preparation. The two separation steps using gel filtration and hydrophobic interaction chromatography were as described above for *Cg*LAO.

SDS-PAGE, Two-Dimensional SDS-PAGE, Native PAGE, and Isoelectric Focusing

The proteins were routinely analyzed on 10% polyacrylamide gels under denaturing and reducing conditions, and visualized using Coomassie brilliant blue staining or silver staining. Non-denaturing and non-reducing conditions were used for analyses of protein complexes and LAO activities. Low molecular weight markers of 14.4 to 97 kDa (GE Healthcare, Chicago, IL, United States) were used for molecular mass estimations.

For the two-dimensional SDS-PAGE analysis, the protein was precipitated by trichloroacetic acid/acetone, vacuum dried, and reconstituted in 125 μL rehydration buffer (7 M urea, 2 M thiourea, 30 mM Tris, 0.25% amidosulphobetaine-14, 2.5% 3-[(3-cholamidopropyl)dimethylammonio]-1-propanesulfonate (CHAPS), 0.002% bromophenol blue, 1% ampholytes, 12 μL/mL destreak reagent). A Ettan IPGphor II isoelectric focusing (IEF) system (GE Healthcare, Chicago, IL, United States) was used, and 7 cm Immobiline DryStrip pH gradient (IPG) strips 3-11 NL (GE Healthcare, Chicago, IL, United States) were passively rehydrated overnight with the protein samples. The IEF was performed at 20°C using the following sequential steps: 300 V for 45 min; 300 V to 1000 V linear gradient for 30 min; 1000 V to 5000 V linear gradient for 72 min; and 5000 V to the final 6000 Vh. The current was restricted to 50 μA/strip. The focused IPG strips were exposed to 65 mM dithiothreitol followed by 135 mM iodoacetamide in 75 mM Tris–HCl buffer with 6 M urea, 4% sodium dodecyl sulfate, 30% glycerol and 0.002% bromophenol blue. Then, 10% polyacrylamide gels were used for the second dimension of the SDS-PAGE, which were stained by the highly sensitive imidazole-zinc negative staining, as described previously (Fernandez-Patron et al., 1992). The protein spots were excised and stored at −20°C before further processing.

The proteins were analyzed under non-denaturing conditions using blue native PAGE with a Novex NativePAGE Bis-Tris gel system with 4 to 16% gradient protein gels (Life Technologies, Carlsbad, CA, United States), according to the manufacturer instructions. NativeMark unstained protein standards (ThermoFisher Scientific, Waltham MA, United States) was used for the molecular mass estimations.

Isoelectric focusing was carried out with a Pharmacia PhastSystem, using commercial precast pH 3-9 gradient gels (GE Healthcare, Chicago, IL, United States) following the manufacturer instructions. Alternatively, precast Novex pH 3-7 IEF protein gels (Life Technologies, Carlsbad, CA, United States) were used. Marker proteins with pI values from 3.5 to 9.3 were used for calibration (GE Healthcare, Chicago, IL, United States).

Protein Glycosylation Analysis

The glycosylation of proteins was assessed using treatment with peptide N-glycosidase (Magnelli et al., 2011). Protein samples were denatured by heating to 100°C for 10 min in 1% sodium dodecyl sulfate, and were then mixed with 50 mM Na_2HPO_4, pH 7.5, with 1.5% CHAPS before peptide N-glycosidase F (3 U) was added to half of each sample; the other half of each sample served as the controls. Both of these samples were incubated at 37°C for 24 h, and then subjected to SDS-PAGE analysis under reducing conditions.

Mass Spectrometry and N-Terminal Sequence Analysis

The proteins were resolved in one- or two-dimensional SDS-PAGE, and the individual bands and spots were excised. After in-gel trypsin digestion, they were identified by peptide mass fingerprinting (Ganten et al., 2006) using an ion trap mass spectrometer (1200 series HPLC-Chip-LC/MSD Trap XCT Ultra; Agilent Technologies, Santa Clara, CA, United States). Database searches were performed using the Mascot in-house server for the MS/MS ion searches.

The N-terminal amino-acid sequences of the proteins were determined by automated amino-acid sequencing using Procise Protein Sequencing System 492 (Applied Biosystems, Foster City, CA, United States). The proteins were resolved by SDS-PAGE, electroblotted onto polyvinylidene difluoride membranes, and stained with Coomassie blue. The individual protein bands were then excised and analyzed (Reim and Speicher, 2001).

LAO Activity Assay

The LAO activities of the protein samples were determined spectrophotometrically, as described previously (Kishimoto and Takahashi, 2001). Briefly, each protein sample was mixed with the reaction mixture that contained the substrate (5 mM L-amino acid or amino acids in 0.1% CSM), 2 mM o-phenylenediamine and 0.81 U/mL horseradish peroxidase in 0.1 M bis-Tris, pH 5.5, in 96-well microplates. Absorbance at 420 nm was measured at constant time intervals over 30 min at 30°C in a microplate reader (Infinite M1000; Tecan, Grödig, Austria). For substrate specificity analysis, the individual L-amino acids (5 mM) were used in the reaction mixture. For inhibition of LAO activity, ascorbic acid was added to the reaction mixture to final concentrations of 0.1 to 5 mg/mL.

For the optimum pH analysis for the LAO activities, these were analyzed as described above with L-Leu as the substrate and in phosphate-citrate buffer from pH 2.6 to pH 7.8, K-phosphate buffer from pH 6 to pH 9, and carbonate-bicarbonate buffer from pH 9 to pH 11.

In-gel analysis of the LAO activities was performed as described previously (Žun et al., 2017). Briefly, non-denatured samples were subjected to SDS-PAGE in 10% polyacrylamide gels. After electrophoresis, the gels were washed in 0.1 M bis-Tris, pH 5.5, and then incubated in the reaction mixture containing substrate (5 mM L-amino acid or amino acids in 0.1% CSM), 1 mM o-phenylenediamine and 0.5 U/mL horseradish peroxidase, in the same buffer at room temperature in the dark

for 1 to 20 h. After stopping the reaction by adding 2 M H_2SO_4, the brown bands of the LAO activity were analyzed using an image scanner (Canon LiDE 110, Middlesex, United Kingdom).

Bacterial Cultures and Inoculum Preparation

The National Collection of Plant Pathogenic Bacteria strain 4156 *Ralstonia solanacearum* (Smith, 1896) Yabuuchi et al., 1996 (phylotype IIB, race 3, biovar 2) (Wullings et al., 1998) was isolated from potatoes in 2001 in Netherlands. This was used as the study reference isolate for the *in vitro* testing of antibacterial activity. *R. solanacearum* were grown at 28°C on yeast peptone glucose (YPG) agar plates (per liter: 5 g yeast extract, 5 g proteose peptone, 10 g glucose, 12 g agar; pH 7.2-7.4). Bacterial suspensions were prepared in 0.01 M phosphate-buffered saline (PBS) (per liter: 1.071 g Na_2HPO_4, 0.4 g $NaH_2PO_47H_2O$, 8.0 g NaCl; pH 7.2). The bacterial concentrations were determined according to absorbance at 595 nm (A_{595}), and they were dilution plated on YPG agar (CFU/mL). Alternatively, BG medium (per liter: 10 g bacto-peptone, 1 g yeast extract, 1 g casamino acids, 5 g glucose) was used for *R. solanacearum* cultivation.

In vitro Testing of Antibacterial Activity Against *R. solanacearum* and Other Plant Pathogenic Bacteria

The *in vitro* testing for antibacterial activities was performed in microtiter plates following a previously published protocol (Erjavec et al., 2016). Briefly, the 200 μL testing wells contained YPG (75 μL), the suspension of *R. solanacearum* (10^7 cells/mL, 75 μL), 0.01 M PBS (42.5 μL) and the mushroom extract or protein fraction (7.5 μL). The following controls were included for each plate: positive control (no extract added) indicating the normal growth of *R. solanacearum* in these conditions; negative control (no extract and *R. solanacearum* added); and controls of extract sterility (no *R. solanacearum* added). All of the controls were supplemented to 200 μL with 0.01 M PBS. Each sample (i.e., mushroom extract) and the controls were tested in at least two parallel wells. After 24 h, absorbance at 595 nm was measured and 30 μL of the mixture from each well was plated onto fresh YPG agar plates, to determine whether the effects were bactericidal (i.e., no bacterial growth observed when transferred onto fresh medium) or bacteristatic (i.e., bacterial growth observed when transferred onto fresh medium). The effects of the fungal extracts on selected plant pathogenic bacteria [*Dickeya* spp. (NIB B16 and NIB S1), *Dickeya fangzhongdai* (DSMS 101947), *Erwinia amylovora* (NCPPB 683), *Pseudomonas syringae* pv. *syringae* (NCPPB 281), *Clavibacter michiganensis* subsp *michiganensis* (NCPPB 2979), *Agrobacterium tumefaciens* (NCPPB 2437), *Enterobacter* sp. (NCCPB 4168), *Pectobacterium atrosepticum* (NIB Z 620), *Pectobacterium carotovorum* (NIB Z 623), *Dickeya chrysanthemi* (NCPPB 402), *Escherichia coli* (GSPB 48), *Ralstonia mannitolilytica* (CFBP 6737), and *Xanthomonas arboricola* pv. pruni (NCPPB 416)] were tested in media that support good bacterial growth, which included casamino acid-peptone-glucose (CPG) medium (per liter: 1 g casamino acids, 10 g peptone, 5 g glucose), King's medium B (KB; per liter: 20 g proteose peptone, 1.5 g K_2HPO_4, 1.5 g MgSO4 $7H_2O$, 10 mL glycerol), nutrient broth yeast extract (NBYE; per liter: 8 g nutrient broth, 5 g yeast extract, pH 7.5) and YPG (Schaad et al., 2001). *Ap*LAO, *Cg*LAO and the LAO extracted from mycelia of *I. geotropa* (*Cg*mycLAO) were tested for their effect on the growth of *R. solanacearum* using the highest concentration available for each sample at different concentrations, as indicated in **Table 3**.

The combined effects of the purified LAO enzymes and catalase (1000 U/mL) on *R. solanacearum* were tested in liquid YPG and BG media.

In vitro Testing of Antibacterial Activities Against *Escherichia coli* and *Lactococcus lactis*

The Gram-negative bacterium *Escherichia coli* DH5α and the Gram-positive bacterium *Lactococcus lactis* NZ9000 were used to define the antimicrobial mechanism of the LAO activities. Growth curves were followed in rich media, S.O.C. (2% tryptone, 0.5% yeast extract, 10 mM NaCl, 2.5 mM KCl, 10 mM $MgSO_4$, 0.4% glucose) for *E. coli*, and GM17 (M17 from Merck supplemented with 0.5% glucose) for *L. lactis*. Overnight cultures were diluted 100-fold in the corresponding fresh medium, to which the filter sterilized LAO samples were added at different concentrations (*Ap*LAO, 64-0.08 μg/mL; *Cg*LAO, 99-1.6 μg/mL; *Cg*mycLAO, 129-21 μg/mL). Alternatively, *E. coli* growth was followed in M9 minimal medium (0.24 M Na_2HPO_4, 0.24 M KH_2PO_4, 0.09 M NaCl, 0.19 M NH_4Cl, 1 mM $MgSO_4$, 0.1 mM $CaCl_2$, 2% glucose) without or with 5 mM L-Leu. The effects of catalase addition were determined in the rich medium using bovine catalase at 1000 U/mL. Growth curves (as triplicates) were followed at 30°C by measuring A_{595} in 96-well plates using a microplate reader (Sunrise; Tecan, Grödig, Austria) and the XFluor4 software, and analyzed using DMFit Microsoft Excel Add-In, version 3.5 (Baranyi and Roberts, 1994).

Tomato Pathogenicity Test

Tomato pathogenicity tests were used to determine the *in vivo* activities of the *A. phalloides* and *I. geotropa* extracts and the purified LAO enzymes. The same protocols were used as described by Erjavec et al. (2016). Briefly, tomato plants (*Solanum lycopersicon* cv. "Moneymaker") were used as the test plant. The plants were inoculated at the two-to-three true-leaf stage with mixtures of the *R. solanacearum* suspensions and mushroom extracts or protein samples (10:1 ratio). The bacterial concentration in the inoculation suspension was 10^5 CFU/mL, and the concentrations of the purified LAO enzymes were 2.14 mg/mL for *Ap*LAO, 3.3 mg/mL for *Cg*LAO, and 4.3 mg/mL for *Cg*mycLAO. The *R. solanacearum* suspension and 0.01 M PBS were used for the inoculation of the positive and negative control plants, respectively. Using a sterile needle (Icogamma plus, 0.6 mm × 25 mm; Novico, Italy), each suspension was inoculated between the cotyledons, with approximately 20 μL of each suspension used per plant.

In total, 42 plants were inoculated with each extract, 42 plants with the positive controls, and 20 plants with the negative controls. After the inoculations, the plants were grown at a 28°C day temperature, with a 16 h photoperiod at 90 μmol m^{-2} s^{-1} photon irradiance, and at a 20°C night temperature. The severities of the symptoms were evaluated regularly over 14 days, following the numerical grades of Winstead and Kelman (1952): 0 (no symptoms), 1 (one leaf wilted), 2 (2-3 leaves wilted), 3 (all leaves except the tip of the plant wilted), 4 (all leaves and the tip of the plant wilted), and 5 (plant dead).

Chi-squared tests were used for symptom severities and disease progression in plants inoculated with mixtures of *R. solanacearum* and protein samples, compared with the positive control plants. The area under the disease progress curve (AUDPC) was used as a measure of quantitative disease resistance, as calculated for the pathogenicity tests (Madden et al., 2007) using the R-statistical (R Development Core Team, 2008) Agricolae package (De mendiburu, 2020).

Transmission Electron Microscopy

The ultrastructure of the bacterial cells was examined using transmission electron microscopy. Overnight cultures were mixed with *Cg*LAO (50 μg/mL) for 2 h and compared with untreated cells. The cells were fixed in 3% glutaraldehyde and 1% paraformaldehyde in 0.1 M phosphate buffer, post-fixed in 2% osmium tetroxide, and embedded in epoxy resin. Ultrathin sections were cut and examined under transmission electron microscopy (CM 100; Philips, Amsterdam, Netherlands), operating at 80 kV. Micrographs were recorded with a CCD camera (Orius SC 200; Gatan Inc., United States).

RESULTS

Isolation of Antibacterial Substances From Crude Protein Extracts of *Amanita phalloides* and *Infundibulicybe geotropa*

Proteins that showed antibacterial activities against *R. solanacearum* were isolated from the fruiting bodies of *A. phalloides* and *I. geotropa* using a two-step procedure of gel filtration (**Figure 1**) and hydrophobic-interaction chromatography (**Figure 2**). These yielded purified proteins of 72 and 66 kDa from A. *phalloides* and *I. geotropa*, respectively, as shown by SDS-PAGE analysis (**Figure 3**). For the preparation of the crude protein extract from *A. phalloides*, little benefit was seen for the inclusion of NaSCN with the 3 M urea, and so this potential activation step of NaSCN was omitted from the protocol. On the other hand, for the preparation of the crude protein extract from *I. geotropa* fruiting bodies, the addition of 2 M NaSCN with the 3 M urea resulted in an approximately 10-fold increase in the total LAO activity of the extract, so this step was included in the purification scheme.

In a typical preparation, 3.8 and 9.0 mg of the antibacterial proteins were obtained from 500 g of *A. phalloides* and *I. geotropa* fruiting bodies, respectively.

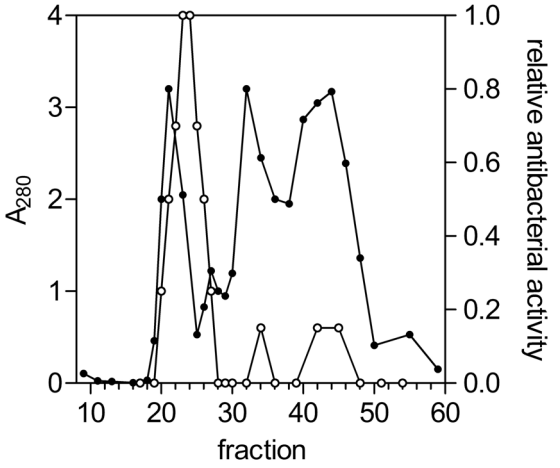

FIGURE 1 | Gel-filtration chromatography of the *Infundibulicybe geotropa* extract. Protein elution profile (A_{280}; closed circles) from gel filtration chromatography using Sephacryl S200, for relative antibacterial activity against *Ralstonia solanacearum* (open circles). Fractions 21 to 25 were collected and further purified.

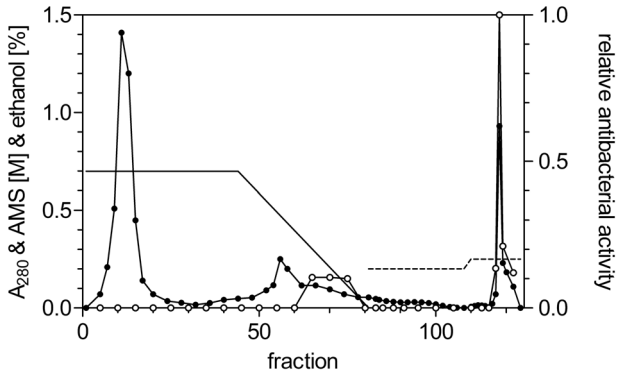

FIGURE 2 | Hydrophobic-interaction chromatography of the fractions with antibacterial activity against *R. solanacearum* from the gel filtration of the *I. geotropa* extract. Protein elution profile (A_{280}; closed circles) from hydrophobic interaction chromatography using Phenyl-Sepharose for relative antibacterial activity against *R. solanacearum* (open circles). Solid line, ammonium sulfate gradient; dotted line, ethanol concentration. Fractions 118–120 were collected and concentrated by ultrafiltration.

The Proteins With Antibacterial Activity Are L-Amino Acid Oxidases

Under native conditions, the molecular masses of the purified antibacterial proteins from *A. phalloides* and *I. geotropa* were estimated to be in the 120 to 130 kDa range from the elution volumes on a calibrated gel filtration column (data not shown), which suggested that both proteins form dimers. Furthermore, apparent molecular masses in the 180 to 300 kDa range were obtained using native PAGE analysis (**Figure 4B**). The antibacterial protein purified from *A. phalloides* fruiting bodies ran at 220 kDa as a diffuse band, whereas two bands of approximately 180 and 360 kDa were observed for the

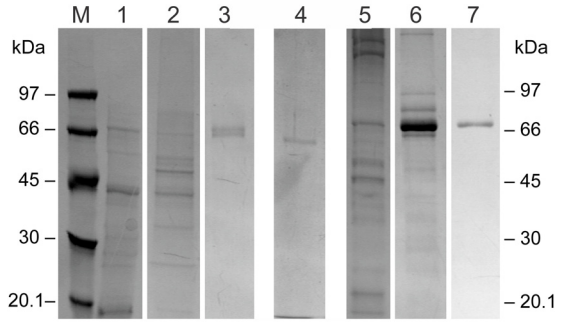

FIGURE 3 | Representative SDS-PAGE analysis of the fractions showing antibacterial activity after the two-step purification procedure of the *I. geotropa* and *A. phalloides* extracts. SDS-PAGE in a 10% polyacrylamide gel under denaturing conditions visualized by Coomassie blue staining. Lane M, molecular mass markers; lane 1, crude aqueous extract of *I. geotropa* fruiting bodies; lane 2, gel filtration fractions 21–25 of *Cg*LAO; lane 3, fraction 118 after hydrophobic-interaction chromatography of *Cg*LAO; lane 4, purified *Cg*mycLAO; lane 5, crude aqueous extract of *A. phalloides* fruiting bodies; lane 6, gel filtration fractions 23–32 of *Ap*LAO; lane 7, fractions 113–117 after hydrophobic-interaction chromatography of *Ap*LAO.

antibacterial protein purified from *I. geotropa* fruiting bodies. The bands were excised from native PAGE, with the proteins eluted overnight by diffusion from gel pieces and the antibacterial activities against *Ralstonia solanacearum* were confirmed *in vitro*. The molecular masses revealed by PAGE analysis under native and denaturing conditions (**Figure 4**), together with the gel filtration of the crude extracts and the purified proteins, indicated that the antibacterial proteins from both of these species form higher molecular aggregates or multimers in the fruiting body extracts. Furthermore, during the purification procedures these higher molecular protein complexes dissociated mostly into dimers in solution.

Analysis of the isoelectric points revealed that both of these proteins have similar isoelectric points, at approximately pH 6.5. The antibacterial protein from *A. phalloides* showed higher heterogeneity (**Figure 4C**). Several bands were observed for the *A. phalloides* protein with isoelectric focusing, which were probably the result of glycosylation variants, as N-glycosylation was confirmed for the antibacterial protein from *A. phalloides* (**Figure 4D**). On the other hand, N-glycosylation was not confirmed for the *I. geotropa* antibacterial protein (**Figure 4D**).

N-terminal sequencing of both of these proteins did not provide conclusive data to enable primer design for gene sequence retrieval. Therefore, the individual spots from the *I. geotropa* 2D-PAGE separation (**Supplementary Figure S1**) were cut out, eluted and subjected to mass spectrometry analysis. However, only similarity to a bacterial dihydrolipoyl dehydrogenase (EC 1.8.1.4) with limited coverage was detected, which was not considered a significant hit. On the other hand, using mass spectrometry analysis the protein from *A. phalloides* with antibacterial activity was identified as toxophallin, an LAO that was isolated from *A. phalloides* fruiting bodies (Stasyk et al., 2010). Poor outcome of the N-terminal amino acid sequencing and mass spectrometry peptide fingerprinting is probably the consequence of the fact that genomes of these two fungal species are not yet available and the similarity to characterized LAOs from other organisms is too low to be detected.

L-amino acid oxidase activities were confirmed in the fractions with antibacterial activity after the gel filtration and hydrophobic interaction chromatography for both species. The proteins with antibacterial activities are therefore termed *Ap*LAO and *Cg*LAO. The in-gel LAO activities (**Figure 4A**, lanes 5, 6) corresponded well to the bands of the non-denatured *Ap*LAO (**Figure 4A**, lane 4) and *Cg*LAO (**Figure 4A**, lane 2), as observed under conditions of SDS-PAGE analysis.

I. geotropa Produces LAO in Vegetative Mycelia

A protein with antibacterial activity and LAO activity was also isolated from *I. geotropa* mycelia following the same procedures as for that from the fruiting bodies. Both the mycelium extract and the gel filtration fractions showed LAO activities that completely inhibited *R. solanacearum* growth

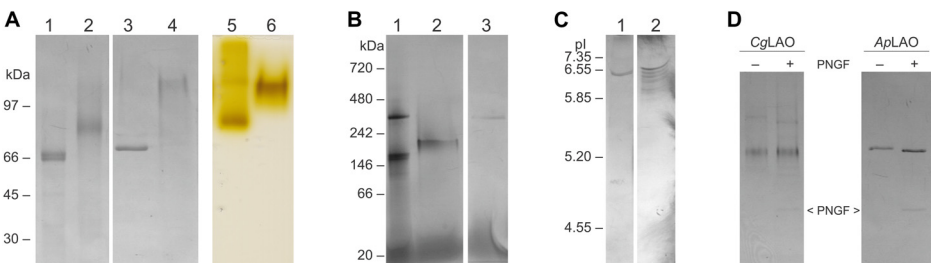

FIGURE 4 | Representative polyacrylamide electrophoretic analyses of purified proteins with antibacterial activity from *I. geotropa* and *A. phalloides*. **(A)** SDS-PAGE analysis in a 10% polyacrylamide gel under denaturing and non-denaturing conditions showing Coomassie blue staining (lanes 1–4) and H_2O_2 production (LAO activity; lanes 5, 6). Lanes 1, 2, 5, *Cg*LAO; lanes 3, 4, 6, *Ap*LAO; lanes 1, 3, samples heated to 100°C for 10 min; lanes 2, 4, samples incubated at room temperature. Lanes 5, 6, LAO activities for *Cg*LAO (lane 5) and *Ap*LAO (lane 6). For H_2O_2 production, following SDS-PAGE under non-denaturing conditions in a 10% polyacrylamide gel, the LAO activity was revealed by staining for H_2O_2 production for 1 h using the *o*-phenylenediamine–horseradish peroxidase system with 5 mM L-Leu as substrate in 0.1 M bis-Tris, pH 5.5. **(B)** Blue native PAGE analysis. Lane 1, purified *Cg*LAO; lane 2, purified *Ap*LAO; lane 3, purified *Cg*mycLAO. **(C)** Isoelectric focusing analysis. Lane 1, purified *Cg*LAO; lane 2, purified *Ap*LAO. **(D)** SDS-PAGE analysis for deglycosylation using peptide-N-glycosidase F (PNGF) in a 10% silver-stained polyacrylamide gel. Left, purified *Cg*LAO; right, purified *Ap*LAO.

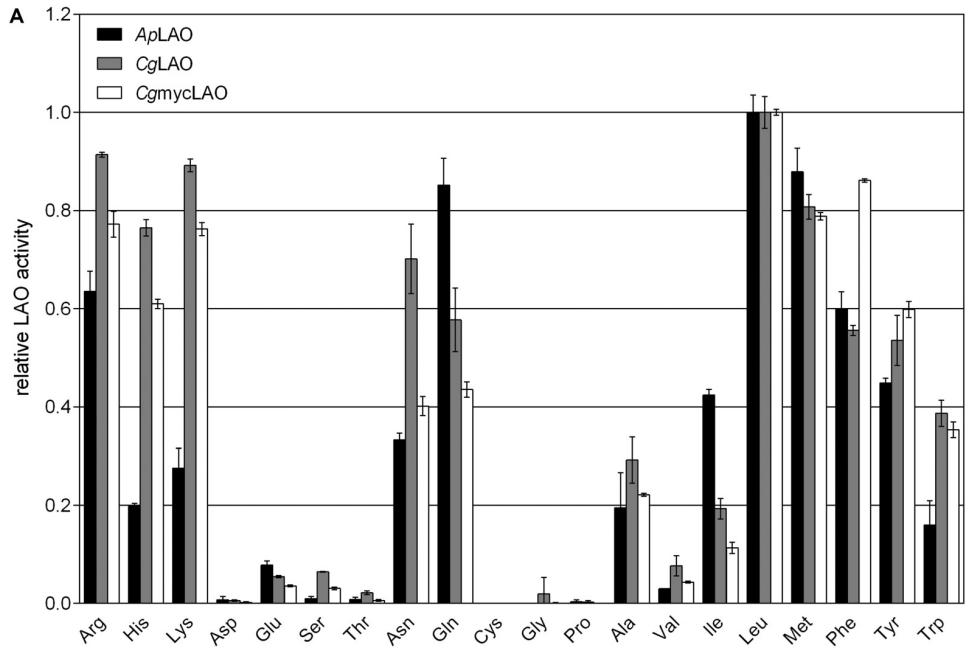

B

	L-Leu		L-Arg		L-Gln	
	K_m [mM]	V_{max} [μmol/s]	K_m [mM]	V_{max} [μmol/s]	K_m [mM]	V_{max} [μmol/s]
*Ap*LAO	0.096 ± 0.009	1.98 ± 0.05	2.71 ± 0.08	1.82 ±0.06	0.27 ± 0.04	2.31 ± 0.05
*Cg*LAO	0.55 ± 0.06	1.13 ± 0.03	0.59 ± 0.12	1.22 ± 0.09	12.1 ± 0.6	1.53 ± 0.04
*Cg*mycLAO	1.52 ± 0.06	0.34 ± 0.04	ND	ND	ND	ND

FIGURE 5 | Substrate specificities and kinetic properties of *Ap*LAO, *Cg*LAO and *Cg*mycLAO. **(A)** Quantitative analysis of different L-amino acid substrates (5 mM) at pH 7.5 and 37°C. Data are means ± standard deviation normalized to L-Leu, the optimal substrate for both enzymes. **(B)** K_m and V_{max} were determined experimentally and using Michaelis-Menten equation.

(**Supplementary Figure S2**). Furthermore, concentrated spent medium from mycelium growth had no effect on *R. solanacearum* growth indicating that the antibacterial LAO is not secreted. The LAO isolated from the cultured vegetative mycelia of *I. geotropa* was termed *Cg*mycLAO, and it showed very similar characteristics to that from *I. geotropa* fruiting bodies (*Cg*LAO). *Cg*mycLAO showed a single band of approximately 400 kDa on native PAGE (**Figure 4B**), and one prominent band of approximately 65 kDa on SDS-PAGE (**Figure 3**). Identification of *Cg*mycLAO by mass spectrometry analysis was also not successful, as no similarity to identified peptides was found in the available databases.

L-Amino Acid Oxidase Activity

The *Ap*LAO, *Cg*LAO, and *Cg*mycLAO showed similar broad substrate specificities for L-amino acids with hydrophobic and charged side chains (**Figure 5A**). They all showed their highest LAO activity against L-Leu, with K_m in the low millimolar range (**Figure 5B**). *Ap*LAO showed approximately 2-fold higher specific activity compared to *Cg*LAO. Addition of the antioxidant agent ascorbic acid (at 0.1 mg/mL or higher) inhibited *Ap*LAO, *Cg*LAO, and *Cg*mycLAO activities *in vitro* (**Supplementary Figure S3**) similarly, as previously shown for toxophallin (Stasyk et al., 2010).

All three enzymes had a broad pH optimum (**Figure 6**), which peaked at pH 6 for *Ap*LAO and at pH 5 for *Cg*LAO and *Cg*mycLAO. Furthermore, they had a wide pH range for their activities, with >50% enzymatic activity in the pH range from pH 3 to pH 10.

L-Leu LAO Activity Correlates With Antibacterial Activity in the Fractionated Extracts of Fungal Fruiting Bodies

This study is a follow-up to the screening study of antibacterial activities against *R. solanacearum* in mushrooms (Erjavec et al., 2016), therefore, analysis of LAO mediated antibacterial activity was broadened in order to assess, whether it is widely distributed among fungal species or limited to a few species. The fruiting body extracts of 15 species of mushrooms covering one ascomycete and seven basidiomycete families were fractionated using gel filtration chromatography (Sephacryl S300). Their antibacterial activities against *R. solanacearum* and their LAO activities against L-Leu and the defined mixture of amino acids in CSM were determined for the fractions (**Table 1** and

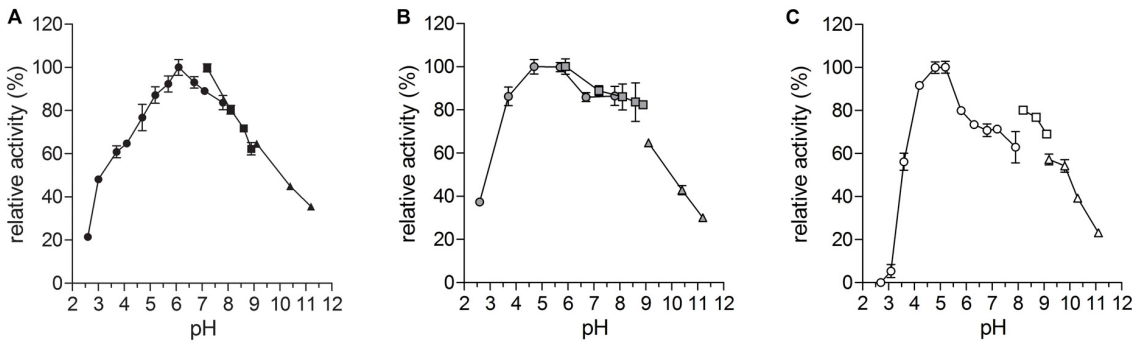

FIGURE 6 | pH optima of *Ap*LAO, *Cg*LAO and *Cg*mycLAO. pH range for activity of *Ap*LAO **(A)**, *Cg*LAO **(B)**, and *Cg*mycLAO **(C)** as analyzed using L-Leu as substrate: pH 2.6 to pH 7.8, phosphate-citrate buffer (circles); pH 6 to pH 9, K-phosphate buffer (squares); pH 9 to pH 11, carbonate-bicarbonate buffer (triangles). Data are means ± standard deviation.

Supplementary Figure S4). The LAO activities against the CSM amino acids of the fractions detected using the in-gel activity method were also determined spectrophotometrically, with the exception of the *Lepista nuda* fractions, which only showed in-gel LAO activities. The fractions of *A. phalloides*, *I. geotropa*, and *Tuber mesentericum* that showed LAO activity against the CSM amino acids were also active against L-Leu, and the same fractions also had antibacterial activities. On the other hand, the fractions of the *Agaricus bisporus* and *Xerocomus badius* extracts only showed LAO activities against the CSM amino acids, and they were not active against L-Leu and also did not have antibacterial activities. Similarly, the fractions of the *Clitocybe nebularis* extract that showed LAO activity only against the CSM amino acids were not active against L-Leu, and had no antibacterial activities. However, antibacterial activity was detected in one of the other fractions from the *C. nebularis* extract, which indicated the presence of a non-LAO antibacterial activity. Moreover, LAO activity was detected exclusively by the in-gel detection method using the CSM amino acids in one fraction of the *L. nuda* extract, which also showed antibacterial activity.

The LAO activities that were detected in-gel against the CSM amino acid substrate with apparent molecular masses of 50 kDa and above correlated with the antibacterial activities. On the other hand, the fractions that showed LAO activities with apparent molecular masses of 30 kDa or less did not have antibacterial activities.

A lack of antibacterial activity *in vitro* in the fruiting body extracts does not necessarily signify a lack of antibacterial compounds in these extracts. There were no antibacterial activities detected in the whole extracts from *L. nuda* and *T. mesentericum*, although there were antibacterial activities detected in their gel filtration fractions. Conversely, the *T. saponaceum* extract had antibacterial activity, but this was lost upon fractionation.

LAO Activity Mediates the Antibacterial Effects on *E. coli* and *L. lactis*

To determine the mode of action of these enzymes, the effects of *Ap*LAO, *Cg*LAO, and *Cg*mycLAO were examined on the growth of two model bacteria. Their antibacterial activities were greater against the Gram-negative *E. coli* than the Gram-positive *L. lactis* (**Figures 7**, **8**). *Ap*LAO, *Cg*LAO, and *Cg*mycLAO all slowed the growth rates of *E. coli*, and *Cg*LAO and *Cg*mycLAO also significantly prolonged the *E. coli* lag phase, which was up to 10-fold longer. Also, *Ap*LAO and *Cg*LAO, but not *Cg*mycLAO, promoted *E. coli* transition to the stationary phase at a lower optical density (A_{595}). On the other hand, the *L. lactis* growth rate and optical density at transition to the stationary phase was less affected by *Ap*LAO, *Cg*LAO and *Cg*mycLAO, and the main effect of all three of these LAOs was for prolongation of the lag phase. The effect was less substantial than for *E. coli*, as the lag phase was at most tripled (by the highest concentration of *Cg*LAO used).

Surprisingly, the catalase-negative *L. lactis* was more resistant to these LAO activities in terms of all of the growth parameters, as compared to *E. coli*, which expresses catalase. Nevertheless, the addition of catalase to the medium alleviated or abolished the effects of these LAO activities on both *E. coli* and *L. lactis* (**Supplementary Figure S5**). Furthermore, the addition of the preferred substrate of *Ap*LAO, *Cg*LAO, and *Cg*mycLAO to the minimal medium increased the antibacterial activity on *E. coli* of all three of these LAOs, and for all of the growth parameters (**Supplementary Figure S6**). These results confirm that the antibacterial effects of all three LAOs are indeed a consequence of the LAO activity by oxidative deamination of L-amino acids.

LAO Activity Mediates the Antibacterial Effects on *R. solanacearum*

The antibacterial activity of *Ap*LAO, *Cg*LAO, and *Cg*mycLAO is due to their enzymatic activity. *Ap*LAO and *Cg*LAO showed similar antibacterial activities against *R. solanacearum* in YPG and BG medium, with the minimum inhibitory concentration of 4.2 μg/mL in BG and 8.4 μg/mL in YPG for *Ap*LAO and 25.8 μg/mL for *Cg*LAO (**Figure 9**). The inhibitory activities of *Cg*mycLAO were minimal, and were only detected at 20-fold higher concentrations compared to *Cg*LAO. The addition of catalase reduced the inhibitory effects of the LAO activity in a concentration-dependent manner, which confirmed that this

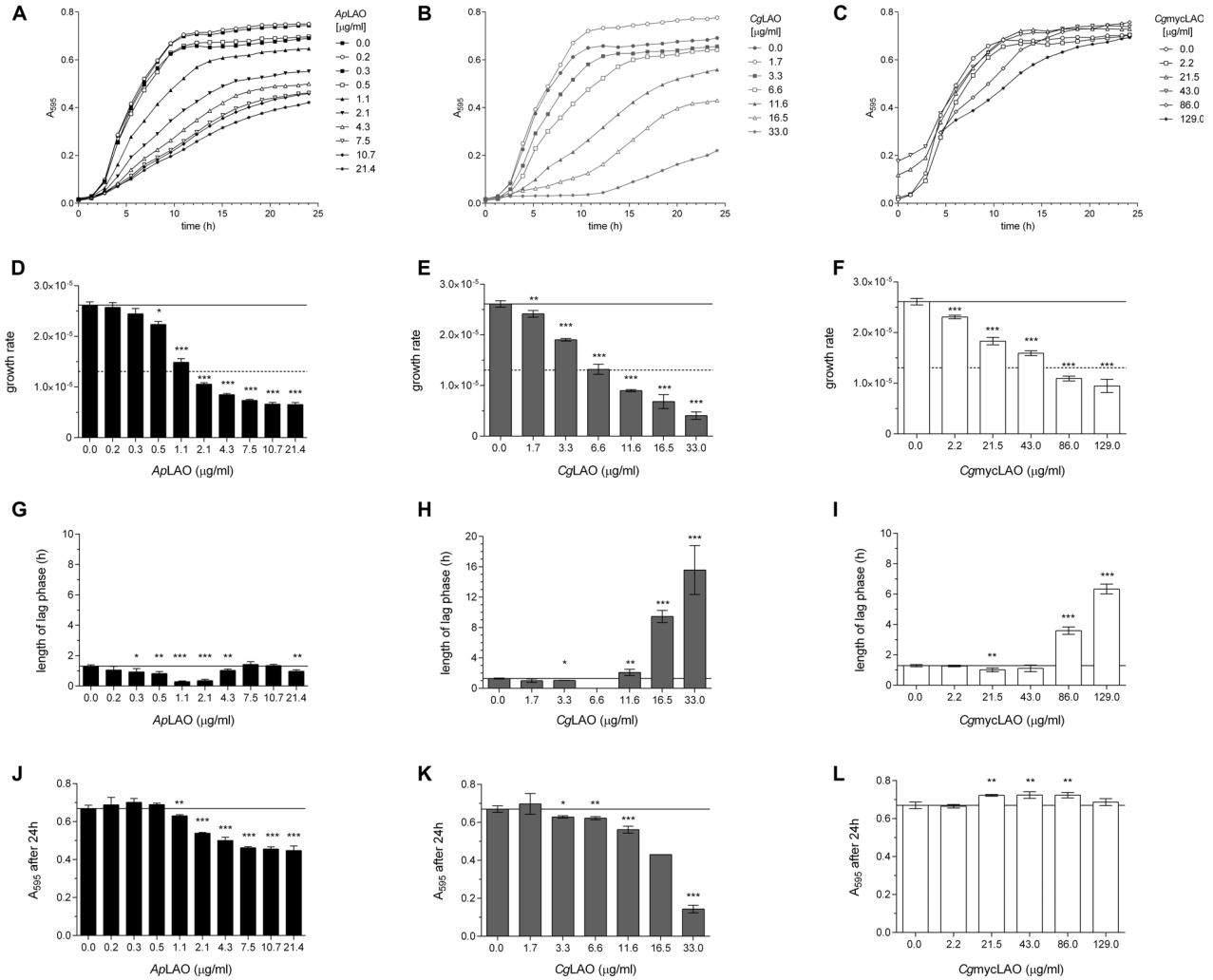

FIGURE 7 | Effects of *Ap*LAO, *Cg*LAO and *Cg*mycLAO on *E. coli* growth measures. Representative *E. coli* growth curves **(A–C)** and derived growth parameters as growth rate **(D–F)**, length of lag phase **(G–I)**, and absorbance after 24 h **(J–L)** in the absence and presence of increasing concentrations of *Ap*LAO **(A,D,G,J)**, *Cg*LAO **(B,E,H,K)** and *Cg*mycLAO **(C,F,I,L)**. Data are means ± standard deviation, with the analysis performed twice, each as three technical repeats. $^{*}p < 0.05$; $^{**}p < 0.01$; and $^{***}p < 0.001$ (Student's *t*-tests vs. no addition control). Guiding lines help visualize the control value.

inhibitory activity is the consequence of the LAO enzymatic activity (**Figure 9**).

Transmission Electron Microscopy of *R. solanacearum*

Micrographs of *R. solanacearum* were produced by transmission electron microscopy, and these revealed the influences of *Cg*LAO on the bacterial ultrastructure. The comparisons of the bacterial shapes before (**Figure 10A**) and after (**Figures 10B,C**) treatment with *Cg*LAO indicated presence of "bulges" on the cell surface (**Figures 10B,C**, black arrows) and increased filamentous structure around the PHA granules (**Figures 10B,C**, white arrows). Control cells had a wrinkled outer membrane with a visible periplasmic space (**Figure 10A**), which was sometimes enlarged due to invagination of the inner membrane. After the *Cg*LAO treatment, the volume of the periplasmic space appeared to increase mostly at the cell poles (**Figures 10B,C**, white arrowheads), although the plasma membrane was also seen to be detached from the cell wall in other places (**Figure 10B**, black arrowheads). The periplasmic space of the *Cg*LAO-treated cells also appeared to contain more granulated material compared to the control cells, and the outer membrane became less wrinkled and looked smooth, and in some cases, amorphous (**Figures 10B,C**).

In vivo Pathogenicity Tests

For *Cg*LAO and *Cg*mycLAO, the inhibitory activities against *R. solanacearum* disease progression *in vivo* in tomato plants were confirmed, while *Ap*LAO had no such activity *in vivo*. Tomato plants were used in the pathogenicity tests as these are an important *R. solanacearum* host plant, and they are also used as test plants in bacterial diagnostics. The *A. phalloides*

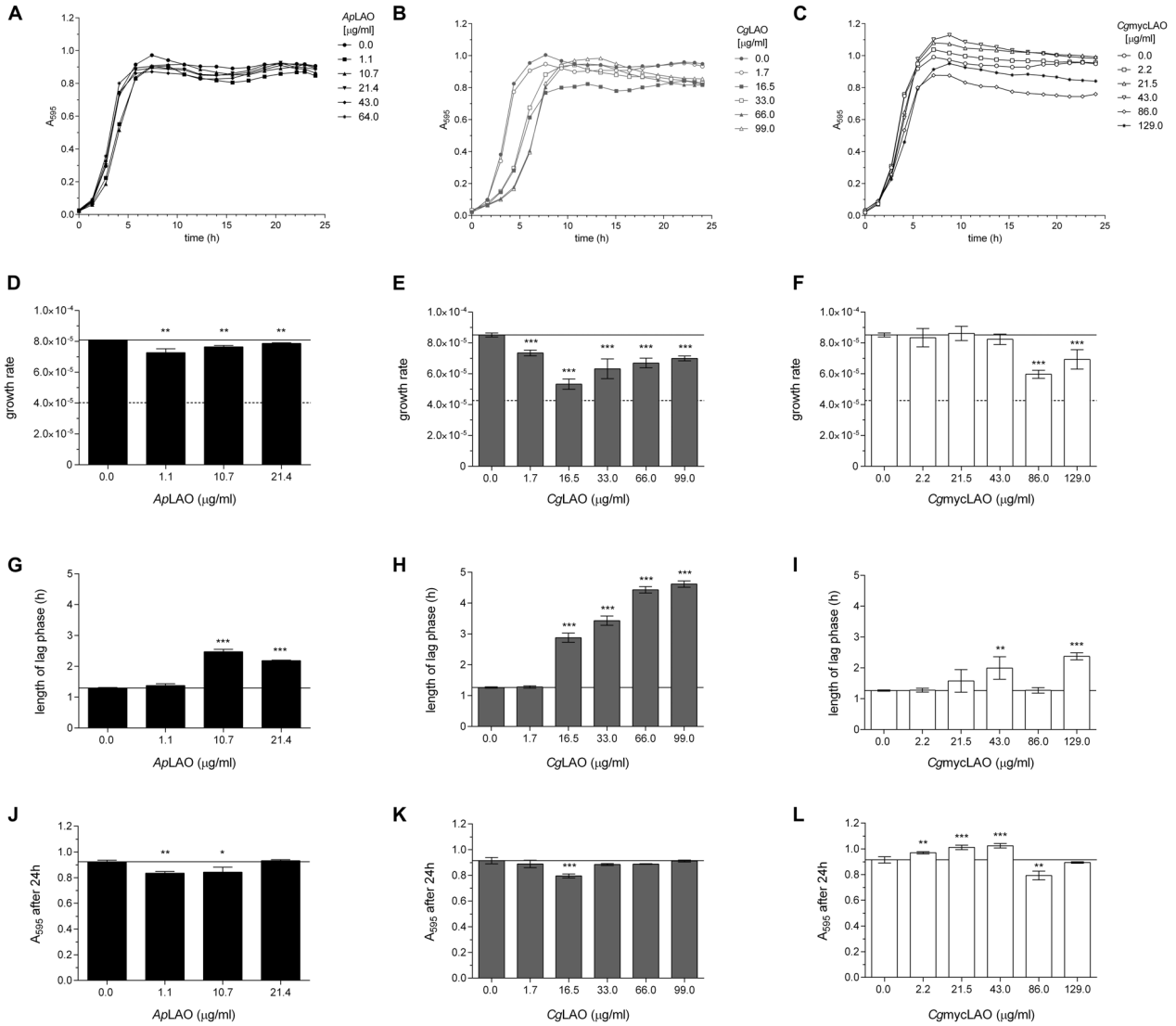

FIGURE 8 | Effects of *Ap*LAO, *Cg*LAO and *Cg*mycLAO on *L. lactis* growth measures. Representative *L. lactis* growth curves **(A–C)** and derived growth parameters as growth rate **(D–F)**, length of lag phase **(G–I)**, and absorbance after 24 h **(J–L)** in the absence and presence of increasing concentrations of *Ap*LAO **(A,D,G,J)**, *Cg*LAO **(B,E,H,K)** and *Cg*mycLAO **(C,F,I,L)**. Data are means ± standard deviation, with the analysis performed twice, each as three technical repeats. $^{*}p < 0.05$; $^{**}p < 0.01$; $^{***}p < 0.001$ (Student's *t*-tests vs. no addition control). Guiding lines help visualize the control value.

and *I. geotropa* extracts and their purified *Ap*LAO, *Cg*LAO, and *Cg*mycLAO fractions were tested for *in vivo* activities, through comparison of their AUDPC values (**Table 2**). *Ap*LAO had no effects on disease progression in the tomato plants, with AUDPC of 93, similar to previously observed effects (Erjavec et al., 2016). On the other hand, the *I. geotropa* extracts, *Cg*LAO, the mycelium extract and *Cg*mycLAO all significantly delayed disease progression in the tomato plants ($p < 0.05$ or < 0.01; **Figure 11**). This indicated that the protein in the extracts from the fruiting bodies and the mycelia of *I. geotropa* that had antibacterial activity was the purified *Cg*LAO and *Cg*mycLAO. The same observations were made previously for a *I. geotropa* extract, with AUDPC of 75% (Erjavec et al., 2016). The AUDPC for the *Cg*mycLAO extract (75%) was the same as that for the *Cg*LAO fruiting body extract. The AUDPCs for *Cg*LAO and *Cg*mycLAO were higher compared to the extracts, at 79 and 85%, respectively.

LAOs Have Antibacterial Activities Against Several Plant Pathogenic Bacteria

We assessed the scope of fungal LAOs antibacterial activities by analyzing their effect on the growth of different plant pathogenic bacteria. *Ap*LAO (33 μg/mL) and *Cg*LAO (103 μg/mL) showed inhibitory activities against several selected catalase-positive bacteria, with the exception of *Erwinia amylovora* (**Table 3**). Furthermore, *Ap*LAO (100 μg/mL) completely inhibited growth measured at 24h in YPG medium

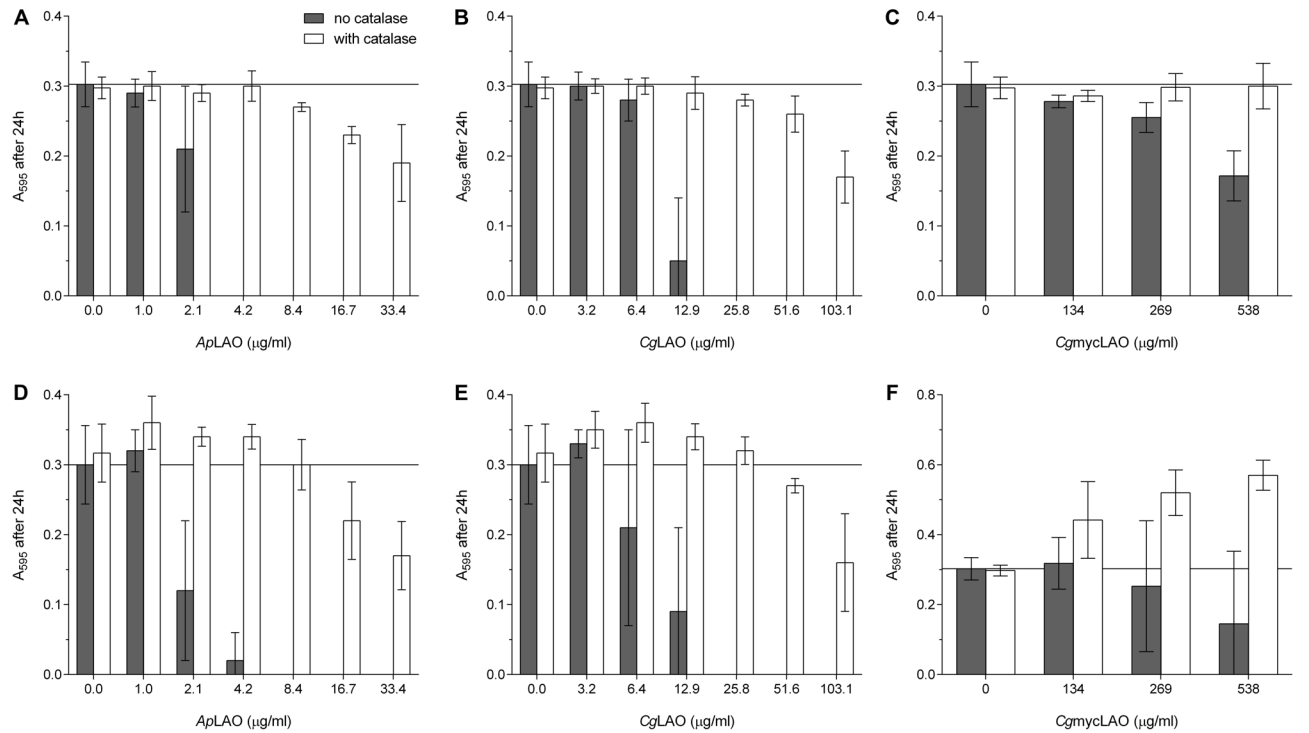

FIGURE 9 | Catalase removes the inhibition of *R. solanacearum* by *Ap*LAO, *Cg*LAO, and *Cg*mycLAO. Representative absorbance after 24 h in the absence and presence of increasing concentrations of *Ap*LAO **(A,D)**, *Cg*LAO **(B,E)** and *Cg*mycLAO **(C,F)** without (closed columns) and with (open columns) addition of catalase. The analyses were carried out in BG medium **(A–C)** and YPG medium **(D–F)**. Data are means ± standard deviation, with the analysis performed twice, each as three technical repeats. Guiding lines help visualize the control value.

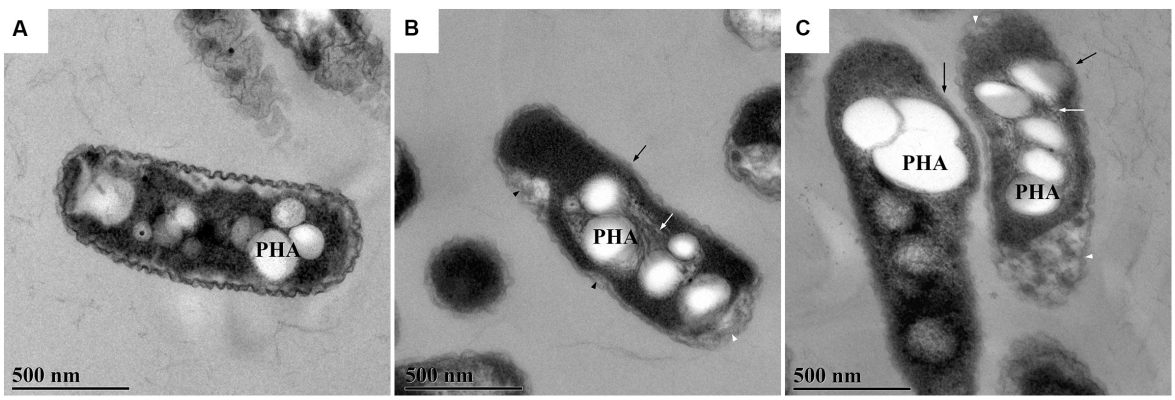

FIGURE 10 | Representative transmission electron microscopy after treatment of *R. solanacearum* with *Cg*LAO. *R. solanacearum* were left untreated **(A)** or were treated **(B,C)** with *Cg*LAO at 50 μg/mL for 2 h. PHA, polyhydroxyalkanoate granules. **(B,C)** White arrows, filaments around granules; black arrows, bulge in the bacterial surface; black arrowheads, detachment of plasma membrane; white arrowheads, large periplasmic spaces at the poles of the cell.

of the following bacteria: *A. tumefaciens* (NCPPB 2437), *Enterobacter* sp. (NCCPB 4168), *P. atrosepticum* (NIB Z 620), *P. carotovorum* (NIB Z 623), *D. chrysanthemi* (NCPPB 402), *E. coli* (GSPB 48), *R. mannitolilytica* (CFBP 6737), and *X. arboricola* pv. pruni (NCPPB 416). *Cg*mycLAO appeared to be less effective *in vitro* compared to *Ap*LAO and *Cg*LAO, as the similar activities were seen at higher *Cg*mycLAO concentrations.

DISCUSSION

Here, we have described the purification of antibacterial LAOs from two mushrooms: the poisonous death cap *A. phalloides* (*Ap*LAO) and the edible trooping funnel *I. geotropa* (*Cg*LAO). These were purified through two chromatographic steps following the initial activation and solubilization of the active LAO species using NaSCN and urea. More complex procedures

TABLE 2 | *In vitro* antibacterial activities against *R. solanacearum* and *in vivo* (tomato cv. "Moneymaker") disease activities of the protein extracts and purified proteins.

Extract/ purified protein fraction	***In vitro* antibacterial activity vs. *R. solanacearum***		**Pathogenicity (tomato cv. "Moneymaker")**		
	Level	**Type**	**AUDPC[a] (% positive control)**		**Significance vs. positive control[b] (Yes/No)**
			1	**2**	
A. phalloides fruiting body	+++	Bactericidal	114[c]	98[c]	No
*Ap*LAO	+++	Bactericidal	nt	93	No
I. geotropa fruiting body	+++	Bactericidal	76[c]	75[c]	Yes
*Cg*LAO	+++	Bactericidal	nt	79	Yes
I. geotropa mycelium	+++	Bactericidal	nt	75	Yes
*Cg*mycLAO	+++	Bactericidal	nt	85	Yes

[a]*AUDPC, area under the disease progress curve: quantitative summary of disease intensity over time, calculated for tomato plants infected with mixtures of R. solanacearum NIB Z 30 and protein samples. Symptom severity evaluated 14 days post-inoculation. AUDPC expressed relative to tomato positive control.* [b]*Within groups, the time points at which the distribution of symptoms differs from the corresponding distribution in the positive control group, are marked by asterisk above columns in* ***Figure 11*** *(chi-squared test; *p < 0.05; **p < 0.01).* [c]*Published previously (Erjavec et al., 2016). +++, complete inhibition of bacteria: no growth observed (≤15% positive control A_{595}). nt, not tested.*

TABLE 3 | Inhibitory activities of *Ap*LAO, *Cg*LAO and *Cg*mycLAO against the selected bacteria.

Bacteria	**Strain**	**Medium[a]**	**Growth after 24 h (% positive control)**		
			***Ap*LAO 33 μg/mL**	***Cg*LAO 103 μg/mL**	***Cg*mycLAO 2.1 mg/mL**
Ralstonia solanacearum	NCPPB 4156	CPG	0	0	0
Dickeya sp.	NIB B16	CPG	77.7	0	0
Dickeya sp.	NIB S1	CPG	50.0	0	0
Dickeya fangzhongdai	DSMS 101947	CPG	278	0	0
Erwinia amylovora	NCPPB 683	KB	100	69.7	90.9
Pseudomonas syringae pv. syringae	NCPPB 281	KB	97.4	0	0
Clavibacter michiganensis subsp. *michiganensis*	NCPPB 2979	NBYE	0	0	0

[a]*composition of media as described in Schaad et al. (2001).*

have been used previously for the isolation of LAOs from fungal fruiting bodies and mycelia. Four- to six-step procedures comprising several steps of different types of chromatographies and protein precipitation were used for toxophallin and Trp-oxidase purification (Furuya et al., 2000; Stasyk et al., 2008).

In our initial purification and identification of the antibacterial component in crude extracts of *A. phalloides*, *I. geotropa*, and *I. geotropa* mycelia, in all cases the antibacterial activities following gel filtration ran close to the void volume of the column. This indicated a relatively high molecular mass species of around 200 to 300 kDa. This would be attributable to relatively large protein assemblies, which can result from aggregation with other proteins or from multimerization of LAOs in the mushroom tissues and the crude extracts. Another observation was that there was significant precipitation of bioactive material during the concentrating of the crude extracts. When dissolved in 3 M urea, these precipitates contained a significant amount of bioactive material. With the aim to help with the purification, the chaotropic agents NaSCN and urea were included in all of the crude extracts and gel filtration buffers with *I. geotropa*, as this provided an immediate several-fold increase in the measurable LAO activities in the *I. geotropa* extracts, and eventually in greater final yield of the corresponding LAO enzymes. This tendency to precipitate also remained during the next purification step of hydrophobic chromatography. A relatively low concentration of ammonium sulfate (0.85 M) had to be used to achieve binding of the sample to the phenyl-Sepharose, the use of higher concentrations resulted in increased precipitation of protein that showed antibacterial and LAO activities.

The molecular masses of the purified *Ap*LAO and *Cg*LAO were estimated as 72 and 66 kDa, respectively, from the SDS-PAGE analysis, and between 120 and 130 kDa by gel filtration using native conditions, which suggested that these enzymes were dimeric in nature. This is consistent with the molecular masses of LAOs isolated from fruiting bodies and mycelia of other basidiomycetes. Monomers of L-Trp-oxidase from *Coprinus* sp. (Furuya et al., 2000) and an LAO from *Hebeloma cylindrosporium* (*Hc*LAO) (Nuutinen et al., 2012) had molecular masses of 68 and 67 kDa, respectively, and assembled into hexamers (420 kDa) and dimers (140 kDa), respectively. Monomers of toxophallin (Stasyk et al., 2010) and toxovirin (Antonyuk et al., 2010) were identified as 55 kDa proteins. The differences in the previously reported molecular mass of toxophallin compared to that in the present study can be attributed to the low accuracy of molecular mass estimations with SDS-PAGE. A range of molecular masses of LAO monomeric subunits have been reported from various

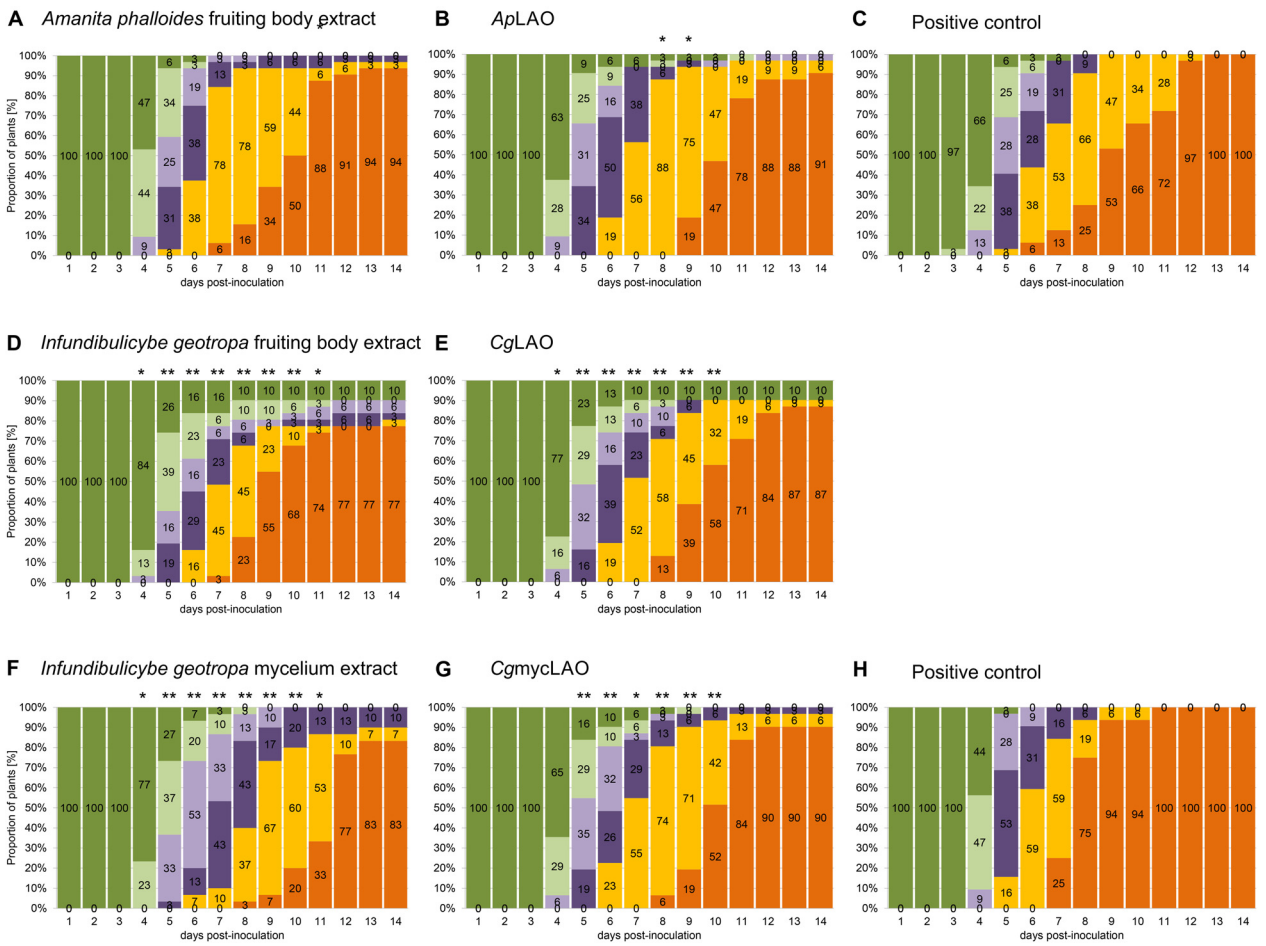

FIGURE 11 | Effects of extracts and purified LAOs on bacterial wilt disease progression in artificially inoculated potted tomato plants of cv. "Moneymaker." Plants were stem-inoculated with mixture of *R. solanacearum* (10^5 CFU/mL) and the extracts from the fruiting bodies of *A. phalloides* **(A)** and *I. geotropa* **(D)** and the mycelia of *I. geotropa* **(F)**, or the purified *Ap*LAO **(B)**, *Cg*LAO **(E)** or *Cg*mycLAO **(G)**, or with *R. solanacearum* alone (**C,H**; positive control). The experiments were performed in two growing chambers, one with plants for groups **(A–C)** and the other for groups **(D–H)**. For each time point from 1 to 14 days, the symptoms are expressed as proportion of plants with symptoms for each grade according to Winstead and Kelman (1952): dark green, grade 0 (no symptoms); light green, grade 1 (one leaf wilted); light purple, grade 2 (2–3 leaves wilted); dark purple, grade 3 (all leaves except the tip of the plant wilted); yellow, grade 4 (all leaves and the tip of the plant wilted); orange, grade 5 (plant dead). Within groups, the times at which the distribution of the symptoms differed significantly from the corresponding distribution in the positive control group, are indicated: $^*p < 0.05$ and $^{**}p < 0.01$ (chi-squared tests). The plants in the negative control groups did not show any symptoms.

microbial and animal sources, which have ranged from 43 kDa for LAO from *Streptococcus oligofermentas* (Tong et al., 2008) to 85 kDa for LAO from sea hare *Aplysia kurodai* (Kamiya et al., 1986). The molecular masses of the newly identified fungal LAOs are within the prevalent range of LAO molecular masses between 60 and 70 kDa. With the exception of the monomeric LAO escapin from sea hare *Aplysia californica* (Yang et al., 2005), these enzymes are mostly active as oligomers. They have included mainly dimers (Geueke and Hummel, 2002; Kitani et al., 2007; Yang et al., 2011; Guo et al., 2012), but also trimers (Kitani et al., 2010), and tetramers (Kamiya et al., 1986), with molecular masses ranging from 100 to 340 kDa. The initial isolation procedures that have generally been adapted to allow for such high molecular mass protein assemblies have indicated the presence of an array of possible aggregates or multimeric proteins in the fruiting bodies that show strong antibacterial activities. These have then generally been dissociated using chaotropic ions and urea during the purification procedures, which has resulted in predominantly LAO dimers present under the conditions described.

The isoelectric points of LAOs can be relatively variable. While most are acidic proteins with pI between pH 4 and pH 5, a few have higher pIs, above pH 8 (Geueke and Hummel, 2002; Guo et al., 2012; Vargas et al., 2013). In contrast to the isoelectric points of *Ap*LAO and *Cg*LAO here as approximately at pH 6.5, slightly lower isoelectric points have been reported for toxophallin (pH 5.7) (Stasyk et al., 2008) and *Hc*LAO (pH 5.4) (Nuutinen et al., 2012).

N-glycosylation was shown here for *Ap*LAO, while *Cg*LAO did not appear to be N-glycosylated. The glycosylation status of the LAOs from basidiomycetes has not been investigated, however, an indication of glycosylation of *Hc*LAO was shown by 2D-PAGE analysis, which yielded several spots (Nuutinen et al., 2012).

Animal and fungal LAOs with antibacterial activities have been shown to be glycoproteins (Yang et al., 2005, 2011; Kitani et al., 2007; Alves et al., 2008), although N-glycans appear not to be involved in the antibacterial activities, as deglycosylation did not reduce the antibacterial activity for a LAO from rockfish (Kitani et al., 2007), and a non-glycosylated bacterial LAO has shown antibacterial activity (Tong et al., 2008). Our results confirm that N-glycans are not essential for antibacterial activity of LAOs as both non N-glycosylated *Cg*LAO and N-glycosylated *Ap*LAO showed strong antibacterial activity.

The slightly acidic pH optimum between pH 5 and pH 6 seen here for *Ap*LAO and *Cg*LAO differs from more basic pH optima reported for L-Trp oxidase, at pH 7 (Furuya et al., 2000), and for LAOs from *Hebeloma* spp. and *Laccaria bicolor*, at pH 8 (Nuutinen and Timonen, 2008; Nuutinen et al., 2012). LAO activities that show a broad pH range are, however, common to basidiomycete LAOs, thus being similar to, although not as expanded as, *Ap*LAO and *Cg*LAO here. LAO activities with broad pH ranges have been reported, such as from pH 6 to pH 10 for *Hebeloma* LAOs, and from pH 5 to pH 11 for *Coprinus* L-Trp-oxidase (Furuya et al., 2000; Nuutinen and Timonen, 2008). Snake venom LAOs have their pH optimum between pH 7 and 8.5 (Tan and Fung, 2008), and microbial LAOs show a broader pH optimum usually between pH 6 and pH 9 (Geueke and Hummel, 2002; Kurosawa et al., 2009; Yang et al., 2011; Pollegioni et al., 2013). Here described fungal LAOs showed extraordinarily wide pH optimum, which strengthens their potential for a wide array of applications.

L-amino acid oxidases have shown either broad or very narrow substrate specificities. The broad substrate specificities reported here for *Ap*LAO and *Cg*LAO were similarly reported for *Hc*LAO and toxovirin (Antonyuk et al., 2010; Nuutinen et al., 2012), while L-Trp-oxidase from *Coprinus* has a narrow substrate specificity (Furuya et al., 2000). Converesely, snake venom LAOs generally have high specificities toward hydrophobic or aromatic amino acids, such as L-Phe, L-Leu, L-Met, and L-Ile (Lukasheva et al., 2011; Guo et al., 2012), and several marine animal LAOs have high specificities toward positively charged amino acids, such as L-Lys and L-Arg (Jimbo et al., 2003; Yang et al., 2005; Kitani et al., 2007, 2010). Broad substrate specificities for charged and aromatic amino acids have been shown for some bacterial (Geueke and Hummel, 2002; Tong et al., 2008) and fungal (Davis et al., 2005) LAOs, while others have shown very narrow specificities against one L-amino acid, and these have been named accordingly (Kusakabe et al., 1980; Arima et al., 2009; Pollegioni et al., 2013; Hossain et al., 2014).

Amanita phalloides and *Cg*LAO are particularly stable enzymes that are resistant to repeated freezing and thawing cycles (our observations). In this regard, fungal LAOs are more similar to microbial enzymes that tend to be more robust and stable compared to those from animals. With a few exceptions, snake venom LAOs are thermo-labile enzymes that are inactivated by freezing but remain stable at 4°C (Tan and Fung, 2008; Guo et al., 2012; Pollegioni et al., 2013).

Amanita phalloides, *Cg*LAO and *Cg*mycLAO all showed broad specificities for their antibacterial actions, as they showed activities against both Gram-negative and Gram-positive bacteria, albeit that these were less pronounced for the Gram-positive bacteria. Some degree of specificity was shown in the screening of their activities on the various plant pathogenic bacteria, where *Dickeya* spp. showed some resistance, and growth of *Erwinia amylovora* was not affected. This is consistent with other known LAOs, which in general have broad antibacterial activities that encompass both Gram-positive and Gram-negative bacteria, while their activities against fungi and yeast are generally lower (Yang et al., 2005; Guo et al., 2012).

The mechanism of the antibacterial activities here is attributed to the LAO enzymatic activity that leads to formation of the toxic H_2O_2. Therefore, their antimicrobial activities can be abolished by addition of catalase. The addition of catalase suppressed the antibacterial activities of *Ap*LAO, *Cg*LAO, and *Cg*mycLAO against *R. solanacearum*, *E. coli* and *L. lactis*, which confirmed that these antibacterial activities are the consequence of H_2O_2 formation. Furthermore, significant contributions to these LAO activities comes from depletion of substrate L-amino acids and accumulation of other intermediates and their final products. For example, production of ammonia leads to a less acidic medium, and α-keto acids can act as siderophores (Lukasheva et al., 2011; Hossain et al., 2014). In the present study, the addition of L-Leu to the minimal medium significantly enhanced the antibacterial activities of *Ap*LAO, *Cg*LAO, and *Cg*mycLAO by providing more substrate for the LAO enzymatic activity and boost the production of H_2O_2.

The effects of LAO activities against the different parameters of the bacterial growth curves were more pronounced in terms of the extended lag phase on Gram-positive *L. lactis*, while all three monitored growth parameters were affected in *E. coli*. These were most probably caused by the oxidative stress mediated by H_2O_2 as similar effects comprising a prolonged lag phase and lower growth rates upon exposure to different H_2O_2 levels have been shown for different *Aeromonas* and *Vibrio* spp. (Wang et al., 2004), as well as for *E. coli* (Sahu and Behuria, 2018).

Binding of LAOs to the bacterial surface has been shown, which presumably enhances their antibacterial activities by the consequent increased local concentrations of H_2O_2 (Ehara et al., 2002; Lee et al., 2011). Despite several attempts, we have not been able to conclusively confirm the binding of *Ap*LAO or *Cg*LAO to the surface of *R. solanacearum*.

Another aspect of these LAO activities is the morphological changes that were detected for *R. solanacearum* after the addition of *Cg*LAO here. These changes were mainly evident as the formation of bulges in the bacterial surface, and as a consequence, many bacteria became more curved than rod shaped. The *S. schlegeli* antibacterial protein and H_2O_2 have been shown to produce similar morphological changes to bacteria. However, these changes differ among the bacterial species, and can include bleb-like protrusions on the surface, cell elongation, and pore formation, which can be accompanied by the rough appearance of the cell surfaces (Kitani et al., 2008; Wang et al., 2011).

The morphological and ultrastructural changes in *R. solanacearum* were probably the consequences of the rearrangement of the PHA granules, which are believed to be involved in oxidative stress tolerance (Castro-Sowinski et al., 2010). This was also confirmed here by the increased

fibrillated structure around the PHA granules. It has been shown that PHA synthesis enhances the tolerance of plant pathogenic *Pseudomonas* to oxidative stress (Fones and Preston, 2012). Reactive oxygen species, such as H_2O_2, can even stimulate PHA synthesis, as a protective function against stress. This is in part mediated by the protection of proteins from oxidative damage, with a protective efficiency greater than that of trehalose (Obruca et al., 2016; Al Rowaihi et al., 2018). The present study also indicated changes in the cell wall structure of *R. solanacearum* after the treatment with *Cg*LAO. Instead of the cell wall being visibly divided into the inner and outer membranes, with the *Cg*LAO treatment the majority of the cells had a less pronounced and structured cell wall. Interestingly, morphological changes to mammalian cells in culture have been reported after treatments with *Ap*LAO, which showed a periplasmic localization (Pišlar et al., 2016).

The pathogenicity tests in the present study confirm that the *I. geotropa* LAO isolated from the fruiting bodies and mycelia can delay disease progression in tomato plants. To the best of our knowledge, this is the only study that has repeated *in vivo* testing and confirmed previously published results (Erjavec et al., 2016). Furthermore, in addition to the antibacterial activities defined for the extracts, these antibacterial activities were substantiated *in vivo* using the proteins purified from the extracts. The effect of the *Cg*LAO fruiting body extract was stronger compared to the purified proteins *Cg*LAO and *Cg*mycLAO. This indicated that these enzymes might interact with other proteins, peptides or compounds in the extracts that enhanced their antibacterial activities but were lost during the purification. Interestingly, the antibacterial activities of *Ap*LAO appeared to be greater *in vitro*, while the pathogenicity tests showed it as ineffective *in vivo*. Although *Ap*LAO and *Cg*LAO are both LAOs and they show similar biochemical characteristics, their LAO enzymatic activities do not appear to be sufficient to provide antibacterial protection to these plants *in vivo*. Potentially, the glycosylation state or interactions with other proteins confer this specificity and enhanced activity. The stronger activity of *Cg*LAO in terms of the prolongation of the lag phase might have provided the plant with more time to mount an antibacterial response. On the other hand, the different *in vivo* activities of *Ap*LAO and *Cg*LAO might be the consequence of their interactions with the plant defense system. Importantly, the protective activity of *Cg*LAO purified from the fruiting bodies was mirrored by *Cg*mycLAO purified from the mycelia, as well by the simple aqueous extracts of the cultured mycelia, thus indicating their potential for their use as plant protection agents.

CONCLUSION

We identified new fungal LAOs with antibacterial activity and described the process of their purification from higher fungi as well as their comprehensive biochemical characterization. We showed their antibacterial activity *in vitro* against a broad range of Gram-negative and Gram-positive bacteria encompassing several species of phytopathogens. Moreover, *in vivo* antibacterial activity was demonstrated for LAOs from *I. geotropa* fruiting bodies and mycelia in tomato plants, while the strong antibacterial effect of *Ap*LAO *in vitro* had no effect on disease progression *in planta*. This raises an important point to test the antibacterial effect of new candidate phytoprotective agents observed *in vitro*, also *in vivo* in the early steps of their development. We have also demonstrated that antibacterial and LAO activity is present and expressed in cultured mycelia of *I. geotropa*, which indicates that a constant source is available and strengthens their potential to be used as new biological phytoprotective agents. Similar antibacterial activity based on LAOs was observed in other fungal species showing fruiting bodies of higher fungi to be a valuable source of antimicrobials.

DATA AVAILABILITY STATEMENT

All datasets generated for this study are included in the article/**Supplementary Material**.

AUTHOR CONTRIBUTIONS

JB designed the study and purified proteins. JS designed and performed biochemical experiments and those using model microorganisms. JE and TD designed and performed experiments with *R. solanacearum*. MT performed and analyzed TEM. MR and JK provided the resources. JB and JS wrote the manuscript. JE, MT, MR, and JK reviewed and edited the manuscript.

FUNDING

This study was supported by the Slovenian Research Agency (Grants Nos. P4-0127 to JK and P4-0165 to MR). The funders had no role in study design, data collection and analysis, decision to publish, or preparation of the manuscript.

ACKNOWLEDGMENTS

The authors are grateful to Adrijana Leonardi for help with the 2D-PAGE and protein N-terminal sequence analysis, to Jure Pohleven for help with the mass spectrometry analysis, to Lidija Matičič for help with the *in vitro* testing of antibacterial activity, and to Chris Berrie for critical reading and language editing of the manuscript.

SUPPLEMENTARY MATERIAL

The Supplementary Material for this article can be found online at: https://www.frontiersin.org/articles/10.3389/fmicb.2020.00977/full#supplementary-material

REFERENCES

Al Rowaihi, I. S., Paillier, A., Rasul, S., Karan, R., Grotzinger, S. W., Takanabe, K., et al. (2018). Poly(3-hydroxybutyrate) production in an integrated electromicrobial setup: Investigation under stress-inducing conditions. *PLoS One* 13:e0196079. doi: 10.1371/journal.pone.0196079

Allen, C., Prior, P., and Hayward, A. C. (2005). *Bacterial wilt Disease and the Ralstonia Solanacearum Species Complex*. St. Paul, MN: American Phytopathological Society.

Alves, R. M., Antonucci, G. A., Paiva, H. H., Cintra, A. C., Franco, J. J., Mendonca-Franqueiro, E. P., et al. (2008). Evidence of caspase-mediated apoptosis induced by l-amino acid oxidase isolated from Bothrops atrox snake venom. *Comp. Biochem. Physiol. Pt. A Mol. Integr. Physiol.* 151, 542–550. doi: 10.1016/j.cbpa.2008.07.007

Anith, K. N., Momol, M. T., Kloepper, J. W., Marois, J. J., Olson, S. M., and Jones, J. B. (2004). Efficacy of plant growth-promoting rhizobacteria, acibenzolar-S-methyl, and soil amendment for integrated management of bacterial wilt on tomato. *Plant Dis.* 88, 669–673. doi: 10.1094/PDIS.2004.88.6.669

Antonyuk, V. O., Klyuchivska, O. Y., and Stoika, R. S. (2010). Cytotoxic proteins of *Amanita virosa* Secr. mushroom: purification, characteristics and action towards mammalian cells. *Toxicon* 55, 1297–1305. doi: 10.1016/j.toxicon.2010.01.023

Arima, J., Sasaki, C., Sakaguchi, C., Mizuno, H., Tamura, T., Kashima, A., et al. (2009). Structural characterization of L-glutamate oxidase from *Streptomyces* sp. X-119-6. *FEBS J.* 276, 3894–3903. doi: 10.1111/j.1742-4658.2009.07103.x

Baranyi, J., and Roberts, T. A. (1994). A dynamic approach to predicting bacterial growth in food. *Int. J. Food Microbiol.* 23, 277–294. doi: 10.1016/0168-1605(94)90157-0

Castro-Sowinski, S., Burdman, S., Matan, O., and Okon, Y. (2010). "Natural Functions of Bacterial Polyhydroxyalkanoates," in *Plastics from Bacteria: Natural Functions and Applications*, ed. G.-Q. Chen (Berlin: Springer-Verlag).

Davis, M. A., Askin, M. C., and Hynes, M. J. (2005). Amino acid catabolism by an *areA*-regulated gene encoding an L-amino acid oxidase with broad substrate specificity in *Aspergillus nidulans*. *Appl. Environ. Microbiol.* 71, 3551–3555. doi: 10.1128/AEM.71.7.3551-3555.2005

De mendiburu, F. (2020). *Statistical Procedures for Agricultural Research using R. Package Agricolae. (Online publication)*. Available online at: https://tarwi.lamolina.edu.pe/~fmendiburu (accessed January 19, 2020).

Du, X. Y., and Clemetson, K. J. (2002). Snake venom L-amino acid oxidases. *Toxicon* 40, 659–665.

Ehara, T., Kitajima, S., Kanzawa, N., Tamiya, T., and Tsuchiya, T. (2002). Antimicrobial action of achacin is mediated by L-amino acid oxidase activity. *FEBS Lett.* 531, 509–512. doi: 10.1016/s0014-5793(02)03608-6

Erjavec, J., Ravnikar, M., Brzin, J., Grebenc, T., Blejec, A., Želko Gosak, M., et al. (2016). Antibacterial activity of wild mushroom extracts on bacterial wilt pathogen, *Ralstonia solanacearum*. *Plant Dis.* 100, 453–464. doi: 10.1094/PDIS-08-14-0812-RE

Fernandez-Patron, C., Castellanos-Serra, L., and Rodriguez, P. (1992). Reverse staining of sodium dodecyl sulfate polyacrylamide gels by imidazole-zinc salts: sensitive detection of unmodified proteins. *Bio. Tech.* 12, 564–573.

Fones, H., and Preston, G. M. (2012). Reactive oxygen and oxidative stress tolerance in plant pathogenic *Pseudomonas*. *FEMS Microbiol. Lett.* 327, 1–8. doi: 10.1111/j.1574-6968.2011.02449.x

Furuya, Y., Sawada, H., Hirahara, T., Ito, K., Ohshiro, T., and Izumi, Y. (2000). A novel enzyme, L-tryptophan oxidase, from a basidiomycete, *Coprinus* sp. SF-1: purification and characterization. *Biosci. Biotechnol. Biochem.* 64, 1486–1493. doi: 10.1271/bbb.64.1486

Ganten, D., Ruckpaul, K., Birchmeier, W., Epplen, J. T., Genser, K., Gossen, M. (eds), et al. (2006). "Peptide mass fingerprinting," in *Encyclopedic Reference of Genomics and Proteomics in Molecular Medicine*, (Berlin: Springer Berlin Heidelberg), 1377–1377.

Geueke, B., and Hummel, W. (2002). A new bacterial L-amino acid oxidase with a broad substrate specificity: purification and characterization. *Enzyme Microb. Technol.* 31, 77–87.

Guo, C., Liu, S., Yao, Y., Zhang, Q., and Sun, M. Z. (2012). Past decade study of snake venom L-amino acid oxidase. *Toxicon* 60, 302–311. doi: 10.1016/j.toxicon.2012.05.001

Hong, J. C., Momol, M. T., Ji, P. S., Olson, S. M., Colee, J., and Jones, J. B. (2011). Management of bacterial wilt in tomatoes with thymol and acibenzolar-S-methyl. *Crop. Protect.* 30, 1340–1345.

Hossain, G. S., Li, J., Shin, H. D., Du, G., Liu, L., and Chen, J. (2014). L-Amino acid oxidases from microbial sources: types, properties, functions, and applications. *Appl. Microbiol. Biotechnol.* 98, 1507–1515. doi: 10.1007/s00253-013-5444-2

Izidoro, L. F., Sobrinho, J. C., Mendes, M. M., Costa, T. R., Grabner, A. N., Rodrigues, V. M., et al. (2014). Snake venom L-amino acid oxidases: trends in pharmacology and biochemistry. *BioMed Res. Int.* 2014, 196754. doi: 10.1155/2014/196754

Ji, P., Momol, M. T., Olson, S. M., Pradhanang, P. M., and Jones, J. B. (2005). Evaluation of thymol as biofumigant for control of bacterial wilt of tomato under field conditions. *Plant Dis.* 89, 497–500. doi: 10.1094/PD-89-0497

Jimbo, M., Nakanishi, F., Sakai, R., Muramoto, K., and Kamiya, H. (2003). Characterization of L-amino acid oxidase and antimicrobial activity of aplysianin A, a sea hare-derived antitumor-antimicrobial protein. *Fish. Sci.* 69, 1240–1246.

Kamiya, H., Muramoto, K., and Yamazaki, M. (1986). Aplysianin-A, an antibacterial and antineoplastic glycoprotein in the albumen gland of a sea hare. Aplysia kurodai. *Experientia* 42, 1065–1067. doi: 10.1007/bf01940736

Kishimoto, M., and Takahashi, T. (2001). A spectrophotometric microplate assay for L-amino acid oxidase. *Analy. Biochem.* 298, 136–139. doi: 10.1006/abio.2001.5381

Kitani, Y., Ishida, M., Ishizaki, S., and Nagashima, Y. (2010). Discovery of serum L-amino acid oxidase in the rockfish *Sebastes schlegeli*: isolation and biochemical characterization. *Comp. Biochem. Physiol. B Biochem. Mol. Biol.* 157, 351–356. doi: 10.1016/j.cbpb.2010.08.006

Kitani, Y., Kikuchi, N., Zhang, G., Ishizaki, S., Shimakura, K., Shiomi, K., et al. (2008). Antibacterial action of L-amino acid oxidase from the skin mucus of rockfish *Sebastes schlegelii*. *Comp. Biochem. Physiol. Pt. B Biochem. Mol. Biol.* 149, 394–400. doi: 10.1016/j.cbpb.2007.10.013

Kitani, Y., Tsukamoto, C., Zhang, G., Nagai, H., Ishida, M., Ishizaki, S., et al. (2007). Identification of an antibacterial protein as L-amino acid oxidase in the skin mucus of rockfish *Sebastes schlegeli*. *FEBS J.* 274, 125–136. doi: 10.1111/j.1742-4658.2006.05570.x

Kurosawa, N., Hirata, T., and Suzuki, H. (2009). Characterization of putative tryptophan monooxygenase from *Ralstonia solanacearum*. *J. Biochem.* 146, 23–32. doi: 10.1093/jb/mvp040

Kusakabe, H., Kodama, K., Kuninaka, A., Yoshino, H., Misono, H., and Soda, K. (1980). A new antitumor enzyme, L-lysine alpha-oxidase from *Trichoderma viride*. Purification and enzymological properties. *J. Biol. Chem.* 255, 976–981.

Lee, M. L., Tan, N. H., Fung, S. Y., and Sekaran, S. D. (2011). Antibacterial action of a heat-stable form of L-amino acid oxidase isolated from king cobra (*Ophiophagus hannah*) venom. *Compar. Biochem. Physiol. Toxicol. Pharmacol.* 153, 237–242. doi: 10.1016/j.cbpc.2010.11.001

Lukasheva, E. V., Efremova, A. A., Treshalina, E. M. Y., Medentzev, A. G., and Berezov, T. T. (2011). L-Amino oxidases: properties and molecular mechanisms of action. *Biochemistry (Moscow)* 5, 337–345. doi: 10.18097/pbmc20125804372

Madden, L. V., Hughes, G., and Van Den Bosch, F. (2007). *The Study of Plant Disease Epidemics*. St. Paul, MN: APS Press.

Magnelli, P., Bielik, A., and Guthrie, E. (2012). "Identification and characterization of protein glycosylation using specific endo- and exoglycosidases," in *Protein Expression in Mammalian Cells. Methods in Molecular Biology (Methods and Protocols)*, Vol. 801, ed. J. Hartley (New Jersey: Humana Press).

Maji, S., and Chakrabartty, P. K. (2014). Biocontrol of bacterial wilt of tomato caused by *Ralstonia solanacearum* by isolates of plant growth promoting rhizobacteria. *Austr. J. Crop Sci.* 8, 208–214. doi: 10.1007/s11274-011-0975-0

Messiha, N. A. S., Van Bruggen, A. H. C., Van Diepeningen, A. D., De Vos, O. J., Termorshuizen, A. J., Tjou-Tam-Sin, N. N. A., et al. (2007). Potato brown rot incidence and severity under different management and amendment regimes in different soil types. *Eur. J. Plant Pathol.* 119, 367–381.

Nuutinen, J. T., Marttinen, E., Soliymani, R., Hilden, K., and Timonen, S. (2012). L-Amino acid oxidase of the fungus *Hebeloma cylindrosporum* displays substrate preference towards glutamate. *Microbiology* 158, 272–283. doi: 10.1099/mic.0.054486-0

Nuutinen, J. T., and Timonen, S. (2008). Identification of nitrogen mineralization enzymes, L-amino acid oxidases, from the ectomycorrhizal fungi *Hebeloma* spp.

and *Laccaria bicolor*. *Mycol. Res.* 112, 1453–1464. doi: 10.1016/j.mycres.2008.06.023

Obruca, S., Sedlacek, P., Mravec, F., Samek, O., and Marova, I. (2016). Evaluation of 3-hydroxybutyrate as an enzyme-protective agent against heating and oxidative damage and its potential role in stress response of poly(3-hydroxybutyrate) accumulating cells. *Appl. Microbiol. Biotechnol.* 100, 1365–1376. doi: 10.1007/s00253-015-7162-4

Payne, D. J., Gwynn, M. N., Holmes, D. J., and Pompliano, D. L. (2007). Drugs for bad bugs: confronting the challenges of antibacterial discovery. *Nat. Rev. Drug Discover.* 6, 29–40. doi: 10.1038/nrd2201

Pišlar, A., Sabotič, J., Šlenc, J., Brzin, J., and Kos, J. (2016). Cytotoxic L-amino-acid oxidases from *Amanita phalloides* and *Clitocybe geotropa* induce caspase-dependent apoptosis. *Cell Death Discover.* 2:16021. doi: 10.1038/cddiscovery.2016.21

Pohleven, J., Brzin, J., Vrabec, L., Leonardi, A., Cokl, A., Strukelj, B., et al. (2011). Basidiomycete *Clitocybe nebularis* is rich in lectins with insecticidal activities. *Appl. Microbiol. Biotechnol.* 91, 1141–1148. doi: 10.1007/s00253-011-3236-0

Pollegioni, L., Motta, P., and Molla, G. (2013). L-amino acid oxidase as biocatalyst: a dream too far? *Appl. Microbiol. Biotechnol.* 97, 9323–9341. doi: 10.1007/s00253-013-5230-1

R Development Core Team (2008). *A Language and Environment for Statistical Computing. Online publication*. Vienna: R Development Core Team.

Reim, D. F., and Speicher, D. W. (2001). N-terminal sequence analysis of proteins and peptides. *Curr. Protoc. Protein Sci.* Chapter 11, Unit 11.10. doi: 10.1002/0471140864.ps1110s57

Sabotič, J., Ohm, R. A., and Kunzler, M. (2016). Entomotoxic and nematotoxic lectins and protease inhibitors from fungal fruiting bodies. *Appl. Microbiol. Biotechnol.* 100, 91–111. doi: 10.1007/s00253-015-7075-2

Sahu, P. K., Gupta, A., Kumari, K. P., Kedarnath, Lavanya, G., and Yadav, A. K. (2017). "Attempts for biological control of *Ralstonia solanacearum* by using beneficial microorganisms," in *Agriculturally Important Microbes for Sustainable Agriculture*, eds V. S. Meena, P. K. Mishra, J. K. Bisht, and A. Pattanayak (Singapore: Springer Nature Singapore Pte Ltd).

Sahu, S. K., and Behuria, H. G. (2018). Biochemical characterization of H_2O_2-induced oxidative stress in *E.coli*. *J. Appl. Microbiol. Biochem.* 2:10. doi: 10.1371/journal.pone.0106942

Schaad, N. W., Jones, J. B., and Chun, W. (2001). *Laboratory Guide for Identification of Plant Pathogenic Bacteria*. St. Paul, MN: American Phytopathological Society.

Šmid, I., Gruden, K., Buh Gašparič, M., Koruza, K., Petek, M., Pohleven, J., et al. (2013). Inhibition of the growth of Colorado potato beetle larvae by macrocypins, protease inhibitors from the parasol mushroom. *J. Agricult. Food Chem.* 61, 12499–12509. doi: 10.1021/jf403615f

Šmid, I., Rotter, A., Gruden, K., Brzin, J., Buh Gašparič, M., Kos, J., et al. (2015). Clitocypin, a fungal cysteine protease inhibitor, exerts its insecticidal effect on Colorado potato beetle larvae by inhibiting their digestive cysteine proteases. *Pesticide Biochem. Physiol.* 122, 59–66. doi: 10.1016/j.pestbp.2014.12.022

Stasyk, T., Lootsik, M., Hellman, U., Wernstedt, C., Souchelnytskyi, S., and Stoika, R. (2008). A new protein from death cap *Amanita phalloides*: isolation and study of cytotoxic activity. *Stud. Biol.* 2, 21–32.

Stasyk, T., Lutsik-Kordovsky, M., Wernstedt, C., Antonyuk, V., Klyuchivska, O., Souchelnytskyi, S., et al. (2010). A new highly toxic protein isolated from the death cap *Amanita phalloides* is an L-amino acid oxidase. *FEBS J.* 277, 1260–1269. doi: 10.1111/j.1742-4658.2010.07557.x

Takakura, Y., Oka, N., Suzuki, J., Tsukamoto, H., and Ishida, Y. (2012). Intercellular production of Tamavidin 1, a biotin-binding protein from tamogitake mushroom, confers resistance to the blast fungus *Magnaporthe oryzae* in transgenic rice. *Mol. Biotechnol.* 51, 9–17. doi: 10.1007/s12033-011-9435-1

Tan, N.-H., and Fung, S.-Y. (2008). Snake venom L-amino acid oxidases and their potential biomedical applications. *Malays. J. Biochem. Mol. Biol.* 16, 1–10.

Tong, H., Chen, W., Shi, W., Qi, F., and Dong, X. (2008). SO-LAAO, a novel L-amino acid oxidase that enables *Streptococcus oligofermentans* to outcompete *Streptococcus mutans* by generating H_2O_2 from peptone. *J. Bacteriol.* 190, 4716–4721. doi: 10.1128/JB.00363-08

Vargas, L. J., Quintana, J. C., Pereanez, J. A., Nunez, V., Sanz, L., and Calvete, J. (2013). Cloning and characterization of an antibacterial L-amino acid oxidase from *Crotalus durissus* cumanensis venom. *Toxicon* 64, 1–11. doi: 10.1016/j.toxicon.2012.11.027

Wang, F., Li, R., Xie, M., and Li, A. (2011). The serum of rabbitfish (*Siganus oramin*) has antimicrobial activity to some pathogenic organisms and a novel serum L-amino acid oxidase is isolated. *Fish Shellf. Immunol.* 30, 1095–1108. doi: 10.1016/j.fsi.2011.02.004

Wang, Y., Leung, P. C., Qian, P., and Gu, J. D. (2004). Effects of UV, H_2O_2 and Fe^{3+} on the growth of four environmental isolates of *Aeromonas* and *Vibrio* species from a mangrove environment. *Microb. Environ.* 19, 163–171.

Winstead, N. N., and Kelman, A. (1952). Inoculation techniques for evaluating resistance to *Pseudomonas solanacearum*. *Phytopathology* 42, 628–634. doi: 10.1186/s13007-019-0530-9

Wullings, B. A., Van Beuningen, A. R., Janse, J. D., and Akkermans, A. D. L. (1998). Detection of *Ralstonia solanacearum*, which causes brown rot of potato, by fluorescent in situ hybridization with 23S rRNA-targeted probes. *Appl. Environ. Microbiol.* 64, 4546–4554.

Yang, C. A., Cheng, C. H., Lo, C. T., Liu, S. Y., Lee, J. W., and Peng, K. C. (2011). A novel L-amino acid oxidase from *Trichoderma harzianum* ETS 323 associated with antagonism of *Rhizoctonia solani*. *J. Agricult. Food Chem.* 59, 4519–4526. doi: 10.1021/jf104603w

Yang, H. C., Johnson, P. M., Ko, K. C., Kamio, M., Germann, M. W., Derby, C. D., et al. (2005). Cloning, characterization and expression of escapin, a broadly antimicrobial FAD-containing L-amino acid oxidase from ink of the sea hare *Aplysia californica*. *J. Exp. Biol.* 208, 3609–3622. doi: 10.1242/jeb.01795

Yuliar, Nion, Y. A., and Toyota, K. (2015). Recent trends in control methods for bacterial wilt diseases caused by *Ralstonia solanacearum*. *Microbes Environ.* 30, 1–11. doi: 10.1264/jsme2.ME14144

Zheng, S., Liu, Q., Zhang, G., Wang, H., and Ng, T. B. (2010). Purification and characterization of an antibacterial protein from dried fruiting bodies of the wild mushroom *Clitocybe sinopica*. *Acta Biochim. Polon.* 57, 43–48.

Žun, G., Kos, J., and Sabotič, J. (2017). Higher fungi are a rich source of L-amino acid oxidases. *3 Biotech* 7:230. doi: 10.1007/s13205-017-0813-7

Conflict of Interest: The authors declare that the research was conducted in the absence of any commercial or financial relationships that could be construed as a potential conflict of interest.

frontiers in Microbiology

ORIGINAL RESEARCH
published: 30 July 2020
doi: 10.3389/fmicb.2020.01683

Super-Multiple Deletion Analysis of Type III Effectors in *Ralstonia solanacearum* OE1-1 for Full Virulence Toward Host Plants

Ni Lei[1†], Li Chen[2†], Akinori Kiba[3], Yasufumi Hikichi[3], Yong Zhang[4,5] and Kouhei Ohnishi[6]**

[1] The United Graduate School of Agricultural Sciences, Ehime University, Matsuyama, Japan, [2] College of Food Engineering and Nutritional Science, Shaanxi Normal University, Xi'an, China, [3] Faculty of Agriculture and Marine Science, Kochi University, Kochi, Japan, [4] College of Resources and Environment, Southwest University, Chongqing, China, [5] Interdisciplinary Research Center for Agriculture Green Development in Yangtze River Basin, Southwest University, Chongqing, China, [6] Research Institute of Molecular Genetics, Kochi University, Kochi, Japan

OPEN ACCESS

Edited by:
Paulo José Pereira Lima Teixeira, University of São Paulo, Brazil

Reviewed by:
Brian H. Kvitko, University of Georgia, United States
Marc Tad Nishimura, Colorado State University, United States

***Correspondence:**
Yong Zhang
bioyongzhang@swu.edu.cn
Kouhei Ohnishi
kouheio@kochi-u.ac.jp

† These authors have contributed equally to this work

Specialty section:
This article was submitted to Microbe and Virus Interactions with Plants, a section of the journal Frontiers in Microbiology

Received: *29 April 2020*
Accepted: *29 June 2020*
Published: *30 July 2020*

Citation:
Lei N, Chen L, Kiba A, Hikichi Y, Zhang Y and Ohnishi K (2020) Super-Multiple Deletion Analysis of Type III Effectors in Ralstonia solanacearum OE1-1 for Full Virulence Toward Host Plants. Front. Microbiol. 11:1683. doi: 10.3389/fmicb.2020.01683

Ralstonia solanacearum species complex (RSSC) posses extremely abundant type III effectors (T3Es) that are translocated into plant cells via a syringe-like apparatus assembled by a type III secretion system (T3SS) to subvert host defense initiated by innate immunity. More than 100 T3Es are predicted among different RSSC strains, with an average of about 70 T3Es in each strain. Among them, 32 T3Es are found to be conserved among the RSSC and hence called the core T3Es. Here, we genetically characterized contribution of abundant T3Es to virulence of a Japanese RSSC strain OE1-1 toward host plants. While all the T3Es members of AWR family contributed slightly to virulence, those of the GALA, HLK, and SKWP families did not influence full virulence of OE1-1. Mutant OE1-1D21E (with deletion of all 21 T3Es members of four families) exhibited slightly impaired virulence, while mutant OE1-1D36E (deleting all 21 T3Es of 4 families and 15 core T3Es) exhibited substantially reduced virulence. Mutant OE1-1D42E (deleting all 21 T3Es of 4 families, 15 core T3Es and 6 extended core T3Es) failed to cause any disease on tobacco plants with leaf infiltration but retained faint virulence on tobacco plants with petiole inoculation. The proliferation of mutant OE1-1D42E in tobacco stems was substantially impaired with about three orders of magnitude less than that of OE1-1, while no impact in tobacco leaves if directly infiltrated into leaves. On the contrary, the OE1-1D42E mutant retained faint virulence on eggplants with leaf infiltration but completely lost virulence on eggplants with root-cutting inoculation. The proliferation of OE1-1D42E mutant both in eggplant leaves and stems was substantially impaired. Intriguingly, mutant OE1-1D42E still caused necrotic lesions in tobacco and eggplant leaves, indicating that some other than the 42 removed effectors are involved in expansion of necrotic lesions in host leaves. All taken together, we here genetically demonstrated that all the core and extended core T3Es are nearly crucial for virulence of OE1-1 toward host plants and provided currently a kind of T3Es-free strain that enables primary functional studies of individual T3Es in host cells.

Keywords: *Ralstonia solanacearum*, type III effector, multiple deletion, pathogenesis, core effectors

INTRODUCTION

Ralstonia solanacearum is a soil-borne Gram-negative plant vascular bacterium that is widely distributed and can cause lethal bacterial wilt on more than 450 plant species belonging to 50 botanical families worldwide (Mansfield et al., 2012; Jiang et al., 2017). Like in many pathogenic bacteria of animals and plants, a syringe-like type III secretion system (T3SS) is one of the essential pathogenicity determinants in *R. solanacearum* that is a translocation apparatus and ensures direct translocation of virulence proteins (called type III effectors, T3Es) into plant cell cytosol to subvert host defense initiated by innate immunity (Poueymiro and Genin, 2009; Genin, 2010). *R. solanacearum* strains are currently referred to as a *Ralstonia solanacearum* species complex (RSSC) due to their extreme heterogeneity, while the T3SS is considerably conserved among the RSSC (Genin and Denny, 2012; Coll and Valls, 2013). Different from the T3SS, T3Es are hugely variable among different RSSC strains (Mukaihara et al., 2010; Peeters et al., 2013; Sabbagh et al., 2019). There are more than 100 T3Es predicated among different RSSC strains with an average of about 70 T3Es per strain that is significantly more abundant than those of any other plant pathogenic bacteria (less than 30 T3Es in each plant pathogenic bacterium, such as *Pseudomonas syringae* or the *Xanthomonads*) (Sébastien et al., 2011; Genin and Denny, 2012; Peeters et al., 2013). Abundant studies have now demonstrated that highly variable repertoires of T3Es might be responsible for the host range of different RSSC strains (Genin and Denny, 2012; Coll and Valls, 2013). Two RSSC strains of GMI1000 and RS1000 are virulent on tomato plants, and they are avirulent on tobacco plants that elicit a hypersensitive response (HR) in tobacco leaves. Two strains have almost identical repertoires of T3Es that comprise 72 and 74 T3Es, respectively (Mukaihara et al., 2010; Peeters et al., 2013). Deletion of T3Es of both RipAA and RipP1 enables GMI1000 to cause wilt symptoms on tobacco plants (Poueymiro et al., 2009), while removal of RipB enables RS1000 to cause wilt symptoms on tobacco plants, and RipAA and RipP1 contribute in part to avirulence of RS1000 on tobacco plants (Nakano and Mukaihara, 2019), indicating that different effector repertories are recognized by different plants, which ultimately leads to virulence or avirulence of the pathogen.

A feature of T3Es repertoires in the RSSC is the existence of functional redundancy with several multigenic families, including the AWR (RipA in a unified nomenclature, five members), GALA (RipG, seven members), HLK (RipH, three members), PopP (RipP, two members) and SKWP (RipS, six members) (Peeters et al., 2013; Sabbagh et al., 2019). Abundant studies have been to date carried out on these multigenic families that are collectively, but not individually, required for full virulence of RSSC strains toward host plants (Angot et al., 2006; Remigi et al., 2011; Solé et al., 2012). Comparing T3Es of 11 sequenced strains representative of four RSSC phylotypes demonstrates that 22 T3Es are conserved among all 11 RSSC strains and are assigned as the core T3Es. 10 T3Es are conserved among 10 out of 11 RSSC strains and are designated as the additional core T3Es (Peeters et al., 2013). We refer to the additional core as the extended core in this study. Note that four multigenic families of the AWR, GALA, HLK, and SKWP contain nine core and extended core T3Es. In addition to T3Es of above four multigenic families, more and more individual T3Es are currently demonstrated to be functional for *R. solanacearum* to invade host cells (Nakano and Mukaihara, 2018, 2019; Sun et al., 2019; Zhuo et al., 2020). We recently announced complete genome sequence of OE1-1 (chromosome: NZ_CP009764.1, megaplasmid: NZ_CP009763.1) that was initially isolated from eggplant in Japan. Both OE1-1 and GMI1000 belong to phylotype I, sharing more than 99% of genomic similarity (data not shown), while OE1-1 is virulent in both tomato and tobacco plants (Kanda et al., 2003). Blast search analysis indicates that OE1-1 possesses more than 70 T3Es, including 21 T3E members of above 4 multigenic families. Generally, OE1-1 contains 21 core T3Es and 9 extended core T3Es (**Figure 1**).

To date, several hundred papers have focused on a either few or single T3Es to decipher their functional roles in host cells that mainly focus on molecular interaction with host innate immunity, such as manipulating host proteasome, eliciting host cell death, triggering expression of plant genes, and/or displaying biochemical activities on plant protein targets (Deslandes and Genin, 2014). There are a limited number of studies focusing on coordinate contribution of abundant T3Es to the infection process of RSSC strains toward host plants. We currently characterized coordinated contribution of each T3Es family to full virulence of OE1-1 and demonstrated that one or more T3Es of the GALA family, SKWP family, or HLK family did not contribute to virulence of OE1-1 toward host plants. All the T3Es members of the GALA family or HLK family slightly contribute to full virulence of OE1-1 toward host tomato and tobacco plants, which is consistent with previous reports in other RSSC strains (Remigi et al., 2011; Solé et al., 2012; Chen et al., 2013, 2018). We here focused on dozens of T3Es (over 40 T3Es including the core and extended core T3Es) to clarify their joint contribution to full virulence of OE1-1 toward host plants.

MATERIALS AND METHODS

Bacterial Strains and Culture Conditions

R. solanacearum T3Es mutants used in this study (listed in **Supplementary Table S1** and **Figure 1**) are derivatives of OE1-1, which is virulent against tomato, tobacco, and eggplants (Kanda et al., 2003). *R. solanacearum* strains were grown at 28°C in nutrient-rich medium containing casamino acids, peptone, yeast extract, and glucose (Boucher et al., 1985). *Escherichia coli* strains of DH12S and S17-1 were grown in Luria-Bertani (LB) medium at 37°C for plasmid construction and conjugational transfer, respectively.

Mutants Generation With an In-Frame Deletion of Target Genes

In the present study, target genes were in-frame deleted with the pK18mobsacB-based homologous recombination as previously described (Zhang et al., 2018), and many genes could be removed one by one with this system. In brief, two DNA

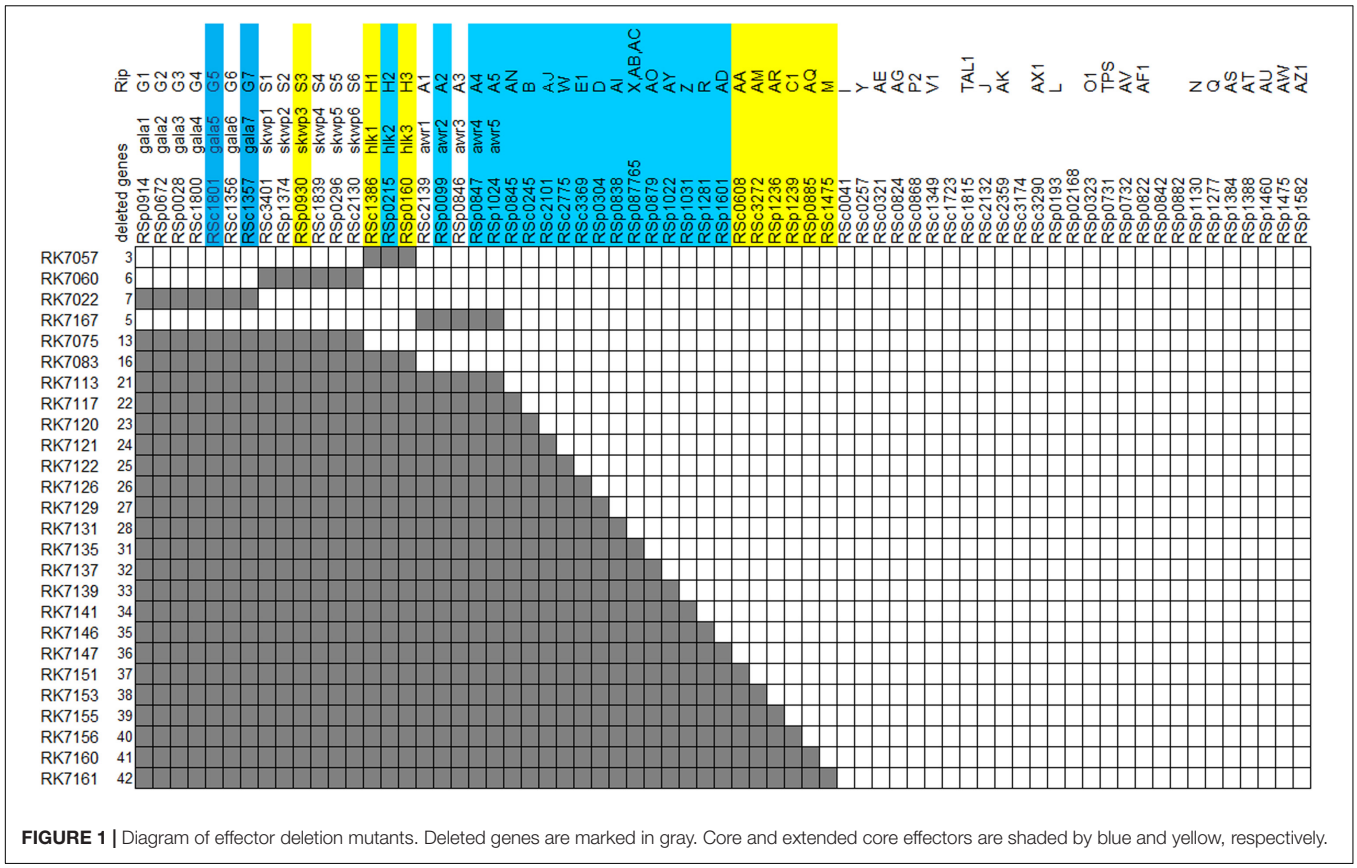

FIGURE 1 | Diagram of effector deletion mutants. Deleted genes are marked in gray. Core and extended core effectors are shaded by blue and yellow, respectively.

fragments flanking a target gene were conjugated with joint PCR and cloned into pK18mobsacB to generate the desired plasmid (**Supplementary Table S1**). After validated sequences, each plasmid was individually transferred into OE1-1 or its derivate T3Es mutants by conjugation with *E. coli* S17-1 to generate desired mutants that were confirmed by colony PCR with respective primer pairs (**Supplementary Table S1**).

Virulence Assay and Necrotic Lesion Test

Virulence assay was performed in two wilt-susceptible plants of tobacco (*Nicotiana benthamiana*) and eggplant (*Solanum melongena* cv. Senryo-nigou) as previously described (Zhang et al., 2018). *R. solanacearum* cells were inoculated to testing plants cultivated in a culture room at 25°C for 3–4 weeks with two methods of root-cutting and leaf-infiltration. The first method is a more natural way, and the second one allows cells to invade intercellular spaces of leaves directly. Each assay was performed with four biological replicates using 12 plants per trail. Wilt symptoms of plants were daily inspected as a 1–4 disease index. Statistical significance was assessed using a *t*-test or a Tukey-Kramer.

Necrotic lesions were observed in leaves of tobacco and eggplant with leaf infiltration. Briefly, bacterial cells at an OD_{600} of 0.1 (ca. 50 μl) were infiltrated into plant leaves, and the development of necrotic lesions was recorded periodically. Each test was performed with four biological replicates using four plants per trail.

The *in planta* Bacterial Proliferation Assay

In the present study, the *in planta* bacterial proliferation assay was performed both in leaves and stems of tobacco and eggplant as previously described (Zhang et al., 2019). For proliferation in leaves, bacterial cells at 10^6 cfu ml^{-1} (ca. 50 μl) were infiltrated into plant leaves, and leaf disks were punched periodically for quantification of cell densities. For proliferation in stems, 2 μl of a bacterial suspension at 10^7 cfu ml^{-1} was dropped onto the fresh-cut surface of petioles, and cells in stems were harvested periodically for quantification of cell densities. Cell densities were quantified by dilution plating and that in leaves and stems was expressed in cfu cm^{-2} and cfu g^{-1}, respectively. Each assay was performed with four biological replicates using six plants per trial. Statistical significance was assessed using a *t*-test.

RESULTS

All the T3Es Members of GALA, SKWP, HLK, and AWR Families Contribute Together but in Part to Full Virulence of OE1-1 Toward Tobacco Plants

We generated a series of mutants with deletion of single T3Es, while all of them showed quite similar virulence as OE1-1 on tobacco plants (data not shown). The *gala* mutant RK7022

(deletion of all 7 T3Es of GALA family, D*gala*) and *hlk* mutant RK7057 (deletion of all 3 T3Es of HLk family, D*hlk*) exhibited similar virulence as the wild type OE1-1 on tobacco plants with leaf infiltration (**Figures 2A,C**; Chen et al., 2013, 2018). The *skwp* mutant RK7060 (deletion of all 6 T3Es of the SKWP family, D*skwp*) also showed similar virulence as OE1-1 (**Figure 2B**), while the *awr* mutant RK7167 (deletion of all 5 T3Es of AWR family, D*awr*) is substantially less virulent than OE1-1 on tobacco plants with leaf infiltration (**Figure 2D**). As a control, the T3SS deficient mutant RK5438 (Δ*hrcV*) did not show any virulence on tobacco plants (data not shown; Vasse et al., 2000).

We, therefore, generated a series of mutants with combined deletion of T3Es from 4 families, RK7075 (D*gala* D*skwp*, deleting 13 T3Es, OE1-1D13E), RK7083 (D*gala* D*skwp* D*hlk*, OE1-1D16E) and RK7113 (D*gala* D*skwp* D*hlk* D*awr*, OE1-1D21E), to evaluate their combined contribution to full virulence of OE1-1 on tobacco plants. Intriguingly, RK7075, and RK7083 exhibited similar virulence as OE1-1 on tobacco plants with leaf infiltration (**Figures 3A,B**). In contrast, RK7113 showed significantly less virulence than OE1-1 on tobacco plants with leaf infiltration (**Figure 3C**). All together, all the T3Es members of 4 families contribute together, but partially, to full virulence of OE1-1 toward tobacco plants. These results indicated that some other T3Es besides these four families might be required for full virulence of OE1-1.

All the Core and Extended Core T3Es Are Jointly Crucial for Virulence of OE1-1 on Tobacco Plants With Leaf Infiltration

Although T3E members of four families of the AWR, GALA, SKWP, and HLK have been functionally validated to be able to alter pathogenic behavior of some RSSC strains on specific hosts (Deslandes and Genin, 2014), RK7113 (OE1-1D21E) was slightly less virulent than OE1-1 on tobacco plants. These four families contain six core T3Es (Peeters et al., 2013), and OE1-1 possesses another 15 core T3Es (**Figure 1**). We further deleted all these 15 core T3Es one by one from RK7113 (OE1-1D21E)

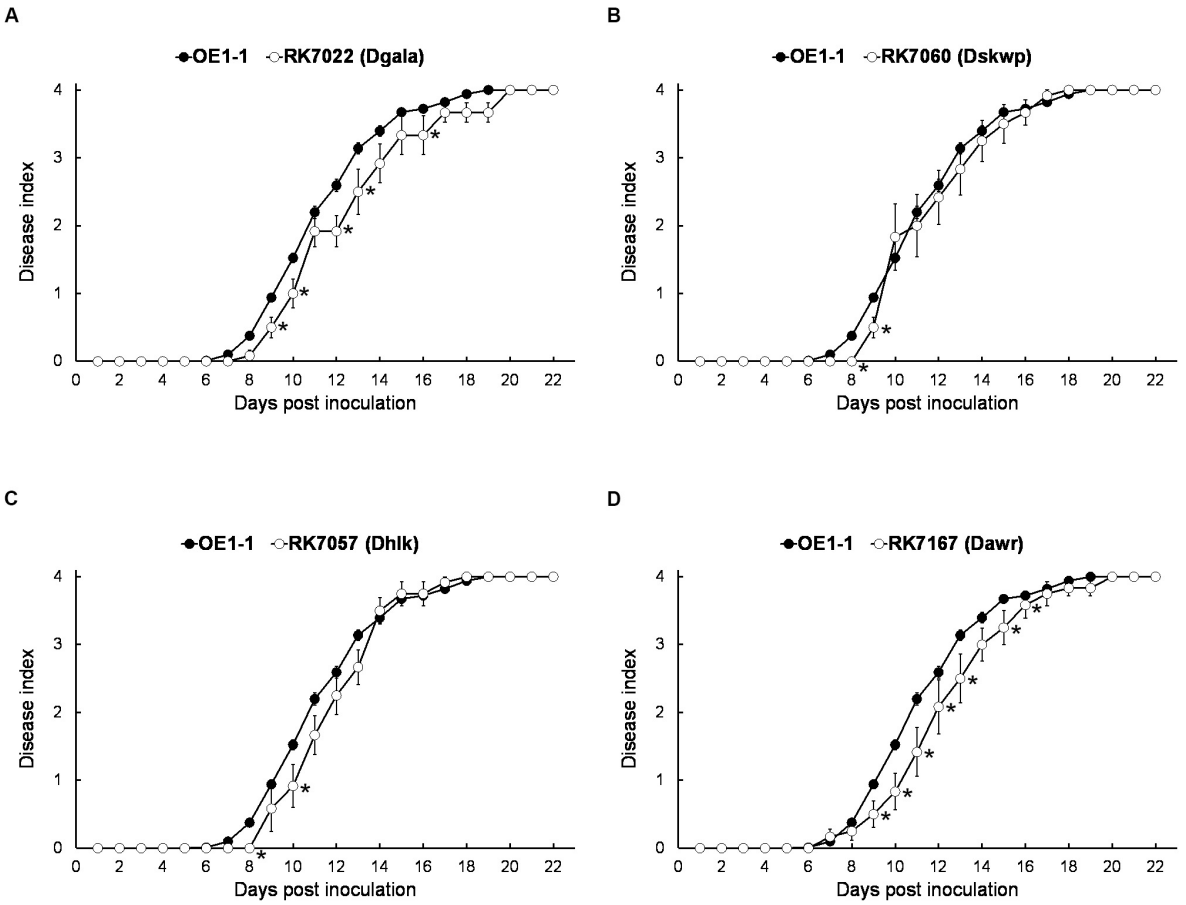

FIGURE 2 | Virulence assay of *R. solanacearum* mutants with T3Es deletion of single-family on tobacco plants with leaf infiltration. Virulence of OE1-1 (the wild type strain) was compared with that of **(A)** RK7022 (D*gala*), **(B)** RK7060 (D*skwp*), **(C)** RK7057 (D*hlk*), and **(D)** RK7167 (D*awr*). About 50 μl of a bacterial suspension at an OD_{600} of 0.1 was infiltrated into *N. benthamiana* leaves with a blunt-end syringe. Wilt symptoms were inspected daily and scored on a disease index scale from 0 to 4 (0, no wilting; 1, 1–25% wilting; 2, 26–50% wilting; 3, 51–75% wilting; and 4, 76–100% wilted or dead). Each assay was repeated with at least four biological replicates using 12 plants per trial. The mean values of all experiments were averaged with standard error (SE). A *t*-test was conducted each day, and asterisks indicated a significant difference ($p < 0.05$).

to clarify whether these core T3Es contribute together to full virulence of OE1-1. As expected, mutants deleting more T3Es exhibited less virulence than those with less T3Es deletion on tobacco plants. For instance, mutants of RK7135 (OE1-1D31E) and RK7137 (OE1-1D32E) were less virulent than mutants of RK7126 (OE1-1D26E), RK7129 (OE1-1D27E) and RK7131 (OE1-1D28E) on tobacco plants (**Supplementary Figure S1**). Mutants of RK7146 (OE1-1D35E) and RK7147 (OE1-1D36E) were much less virulent than mutants of RK7139 (OE1-1D33E) and RK7141 (OE1-1D34E) (**Supplementary Figure S1**). All the core T3Es were deleted in RK7147 (OE1-1D36E, deletion of 15 more core T3Es from RK7113), which indeed exhibited substantially impaired virulence on tobacco plants (**Figure 4A**), while it retained faint virulence to some extent since RK7147-inoculated tobacco plants started wilting at 15 days post-inoculation (dpi) and reached disease index one at about 22 dpi (**Figure 4A**).

OE1-1 possesses 6 extended core T3Es (**Figure 1**), and we further deleted these 6 T3Es one by one from RK7147 (OE1-1D36E) to clarify whether full virulence of OE1-1 was determined by all the core and extended core T3Es. Mutants of RK7155 (OE1-1D39E) and RK7156 (OE1-1D40E) were less virulent than mutants of RK7151 (OE1-1D37E) and RK7153 (OE1-1D38E) (**Supplementary Figure S2**). Mutants of RK7160 (OE1-1D41E) and RK7161 (OE1-1D42E, deletion of all 6 extended T3Es from RK7147) failed to cause any wilting symptoms on tobacco plants with leaf infiltration (**Figure 4B**), confirming that all the core and extended core T3Es are crucial for virulence of OE1-1 on tobacco plants. Different from that with inoculation method of leaf infiltration, RK7161 (OE1-1D42E) caused slight wilting symptoms on eggplants with the petiole inoculation, which enables direct invasion into xylem vessels (**Figure 4C**). RK7161-inoculated eggplants with petiole inoculation started wilting at 12 dpi and reached disease index one at 22 dpi (**Figure 4C**),

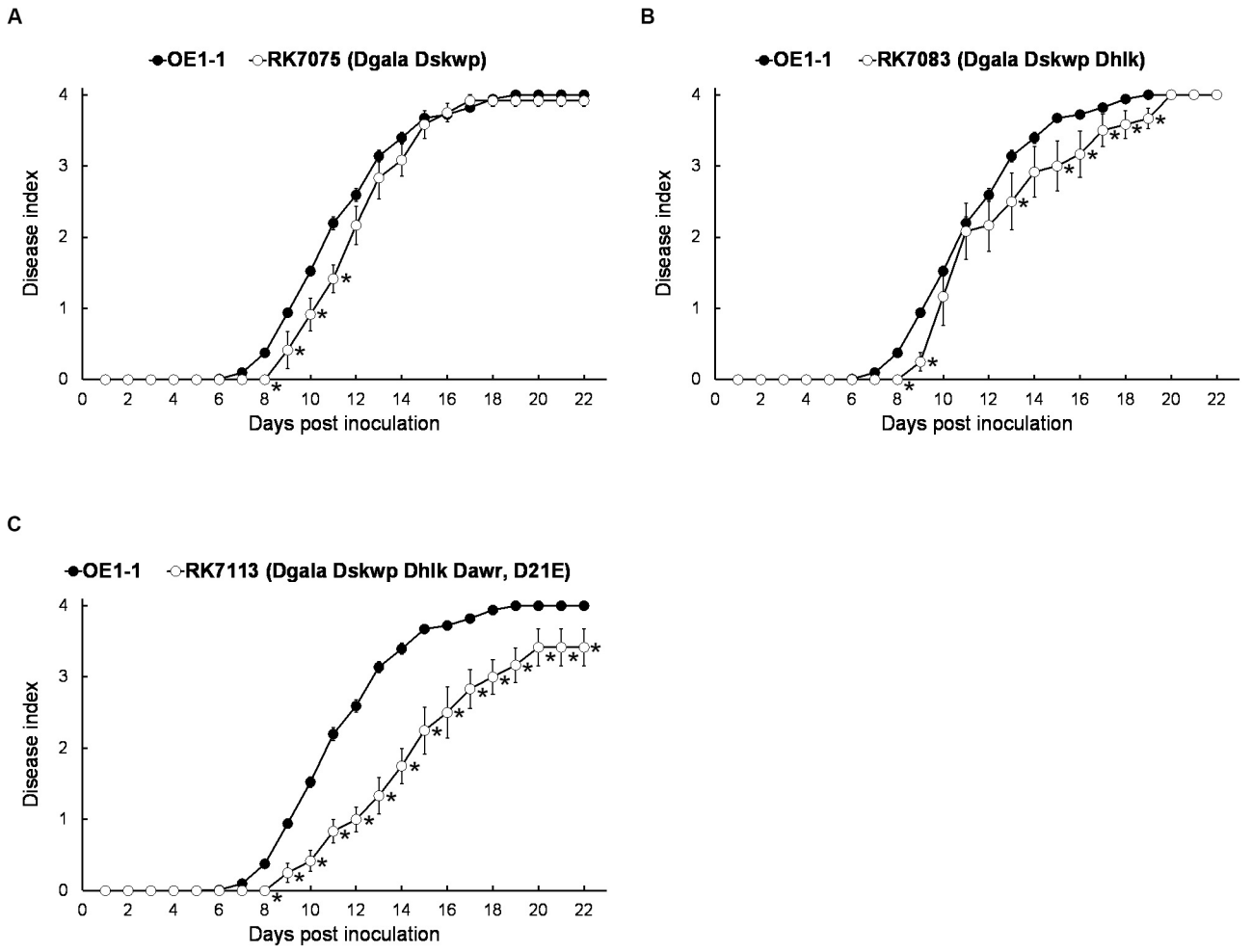

FIGURE 3 | Virulence assay of *R. solanacearum* T3Es mutants with combined deletion of four families in tobacco plants with leaf infiltration. Virulence of OE1-1 was compared with that of **(A)** RK7075 (D*gala* D*skwp*, OE1-1D13E), **(B)** RK7083 (D*gala* D*skwp* D*hlk*, OE1-1D16E), and **(C)** RK7113 (D*gala* D*skwp* D*hlk* D*awr*, OE1-1D21E). Wilt symptoms were inspected daily and scored on a disease index scale from 0 to 4. Each assay was repeated with at least four biological replicates using 12 plants per trial. The mean values of all experiments were averaged with SE. A *t*-test was conducted each day, and asterisks indicated a significant difference ($p < 0.05$).

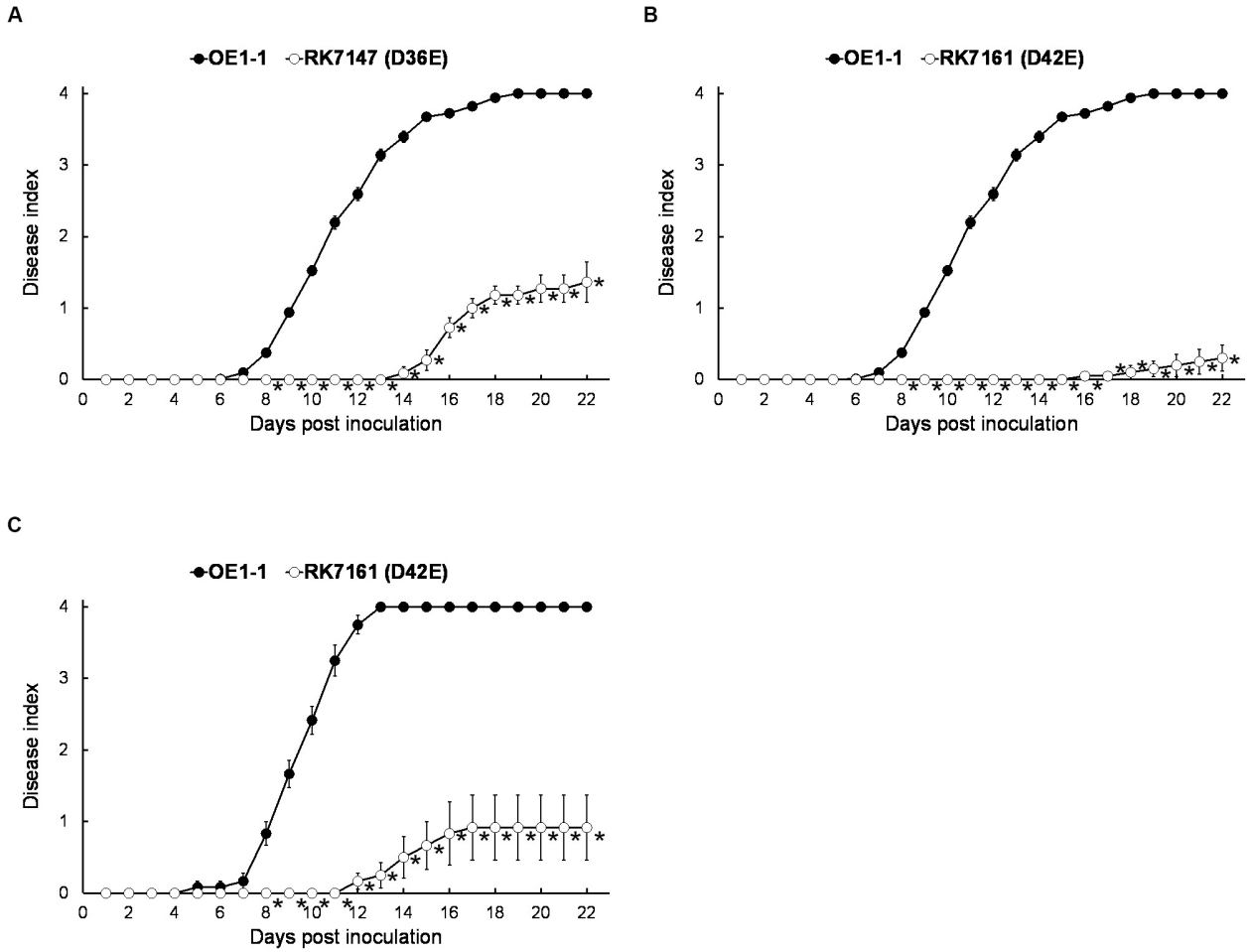

FIGURE 4 | Virulence assay of *R. solanacearum* T3Es mutants with deletion of more core and extended T3Es. OE1-1; RK7147 (D*gala* D*skwp* D*hlk* D*awr*, deletion of 15 more core T3Es, OE1-1D36E); RK7161 (D*gala* D*skwp* D*hlk* D*awr*, deletion of 15 core and six more extended T3Es deletion, OE1-1D42E) were used. Bacterial cells were infiltrated into **(A,B)** tobacco and **(C)** eggplants (*S. melongena* cv. Senryo-nigou). Wilt symptoms were inspected daily and scored on a disease index scale from 0 to 4. Each assay was repeated with at least four biological replicates using 12 plants per trial. The mean values of all experiments were averaged with SE. A *t*-test was conducted each day, and asterisks indicated a significant difference ($p < 0.05$).

indicating that some other T3Es of OE1-1 besides the core and extended core T3Es could function, especially in xylem vessels of tobacco plants.

Removal of 42 T3Es From OE1-1 Does Not Eliminate the Formation of Necrotic Lesions in Tobacco and Eggplant Leaves

The T3SS is essential for *R. solanacearum* to inject abundant T3Es into host cell cytosol that subverts host defense, and T3SS deficient mutants are well known to fail to cause any wilting symptoms in host plants. For instance, GMI1000 elicits HR in non-host tobacco leaves within 24 h post infiltration (hpi), while its *hrcV* mutant fails to elicit HR (Poueymiro et al., 2009). OE1-1 caused necrotic lesions in tobacco leaves at about 3 dpi and then started to wilt tobacco leaves at about 6 dpi. The *hrcV* mutant of OE1-1, RK5438, failed to cause any necrotic lesions in tobacco leaves (**Figure 5A**). Intriguingly, RK7161 (OE1-1D42E) caused necrotic lesions in tobacco leaves at about 4 dpi that was about 1-day delayed than OE1-1 (**Figure 5A**). This phenomenon was also observed in eggplant leaves at about 6 dpi (**Figure 5B**), indicating that all the core and extended core T3Es are not required for OE1-1 to cause necrotic lesions in host leaves. Some other T3Es besides the 42 removed effectors of OE1-1 might be required to expand necrotic lesions in host leaves.

All the Core and Extended Core T3Es Are Jointly Crucial for Virulence of OE1-1 in Eggplants

RK7161 (OE1-1D42E) caused necrotic lesions in tobacco and eggplant leaves, and we assessed whether RK7161 could cause wilting disease on eggplants. RK7147 (OE1-1D36E) and RK7161 exhibited significantly less virulence on eggplants with leaf infiltration (**Figure 6A**), which were similar to those on tobacco plants. When eggplants were challenged with a more natural inoculation method of the root-cutting, RK7147 exhibited significantly less virulence, while RK7161 failed

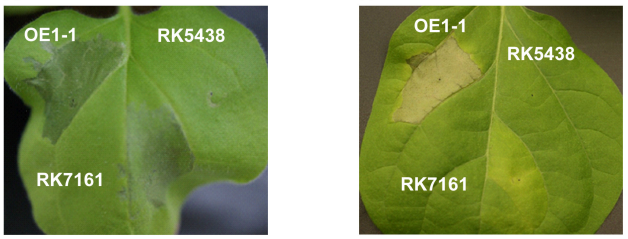

FIGURE 5 | Symptoms of bacterial infiltrated leaves. OE1-1, RK5438 (OE1-1 Δ*hrcV*), and RK7161 (OE1-1D42E) were infiltrated into leaves of **(A)** tobacco and **(B)** eggplant. Approximately 50 μl of a bacterial suspension at an OD_{600} of 0.1 was infiltrated into leaves, and the development of necrotic lesions was observed daily. The representative results are presented, and similar results were obtained in all experiments.

to cause any wilting symptoms on eggplants (**Figure 6B**). Eggplants inoculated with RK5438, the *hrcV* mutant were healthy throughout the experiments (data not shown).

The Core and Extended Core T3Es Are Essential for OE1-1 to Multiply Both in Leaved and Xylem Vessels of Eggplants, but Only in Xylem Vessels of Tobacco Plants

Extensive proliferation in host plants is another essential pathogenicity determinants of *R. solanacearum*. We thus assessed whether the core and extended core T3Es are required for *in planta* proliferation. Tobacco leaves were infiltrated with the bacterial suspension at a concentration of 10^6 cfu ml^{-1}, and cell growth in tobacco leaves was daily assessed until 3 dpi when tobacco leaves became withered and dried. The wild-type strain OE1-1 and RK7161 (OE1-1D42E) grew almost the same ways in tobacco leaves from 1 to 3 dpi (**Figure 7A**), indicating that these core and extended core T3Es are independent for the intercellular proliferation of OE1-1 at least in tobacco leaves.

We also assessed cell proliferation in xylem vessels of tobacco plants. Tobacco plants were inculcated by dropping a bacterial suspension onto the fresh-cut surface of petioles, and stem pieces were daily harvested for quantification of cell densities. OE1-1 reached to approximately 10^8 cfu g^{-1} at 3 dpi and got to a maximum of about 10^{10} cfu g^{-1} at 5–6 dpi (**Figure 7B**). RK7161 grew slowly to a maximum of 5×10^7 cfu g^{-1} at 5–6 dpi. The T3SS deficient *hrcV* mutant, RK5438, did not grow in xylem vessels (**Figure 7B**). These results confirmed that all the core and extended core T3Es are important for OE1-1 to multiply in tobacco xylem vessels.

Proliferation assay of RK7161 was also performed both in leaves and xylem vessels of eggplants. When directly infiltrated into eggplants leaves, RK7161 grew slowly to the maximum of about 10^5 cfu cm^{-2} at 3 dpi (**Figure 7C**), which is about three orders less than that of OE1-1. When directly invaded xylem vessels of eggplants, RK7161 grew slowly to the maximum of 10^7 cfu g^{-1} at 5 dpi, which was about four orders less than OE1-1 (**Figure 7D**), confirming that all the core and extended core T3Es are important for OE1-1 to multiply both in the intercellular spaces and xylems of eggplants.

DISCUSSION

In the present study, we provided genetic evidence to demonstrate that all the core and extended core T3Es are together crucial for virulence of OE1-1 on host tobacco plants. Dozens of T3Es have been confirmed to individually manipulate plant cellular functions and alter plant signal transduction, which results in extensive proliferation of RSSC strains in host plants

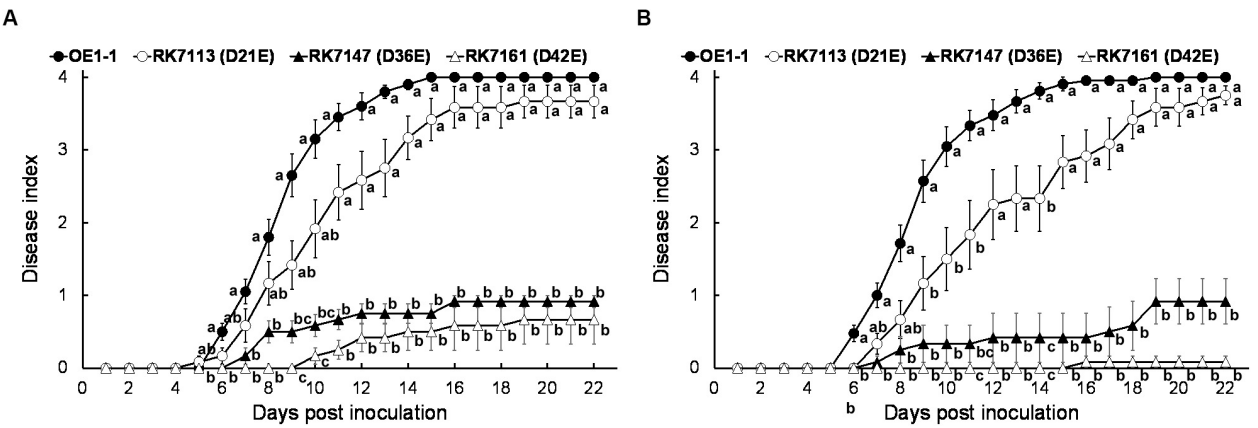

FIGURE 6 | Virulence assay of *R. solanacearum* T3Es mutants in eggplants. Bacterial cells were inoculated with methods of **(A)** leaf infiltration and **(B)** root-cutting inoculation. OE1-1; RK7113 (OE1-1D21E); RK7147 (OE1-1D36E); RK7161 (OE1-1D42E). For leaf infiltration, approximately 50 μl of a bacterial suspension at an OD_{600} of 0.1 was infiltrated into leaves. For root-cutting inoculation, a bacterial suspension was poured onto the root wounded plants at a final concentration of 10^6 cfu g^{-1} soil. Wilt symptoms were inspected daily and scored on a disease index scale from 0 to 4. Each assay was repeated with at least four biological replicates using 12 plants per trial. The mean values of all experiments were averaged with SE. A Tukey-Kramer test was conducted each day, and the alphabets indicated significant differences ($p < 0.05$).

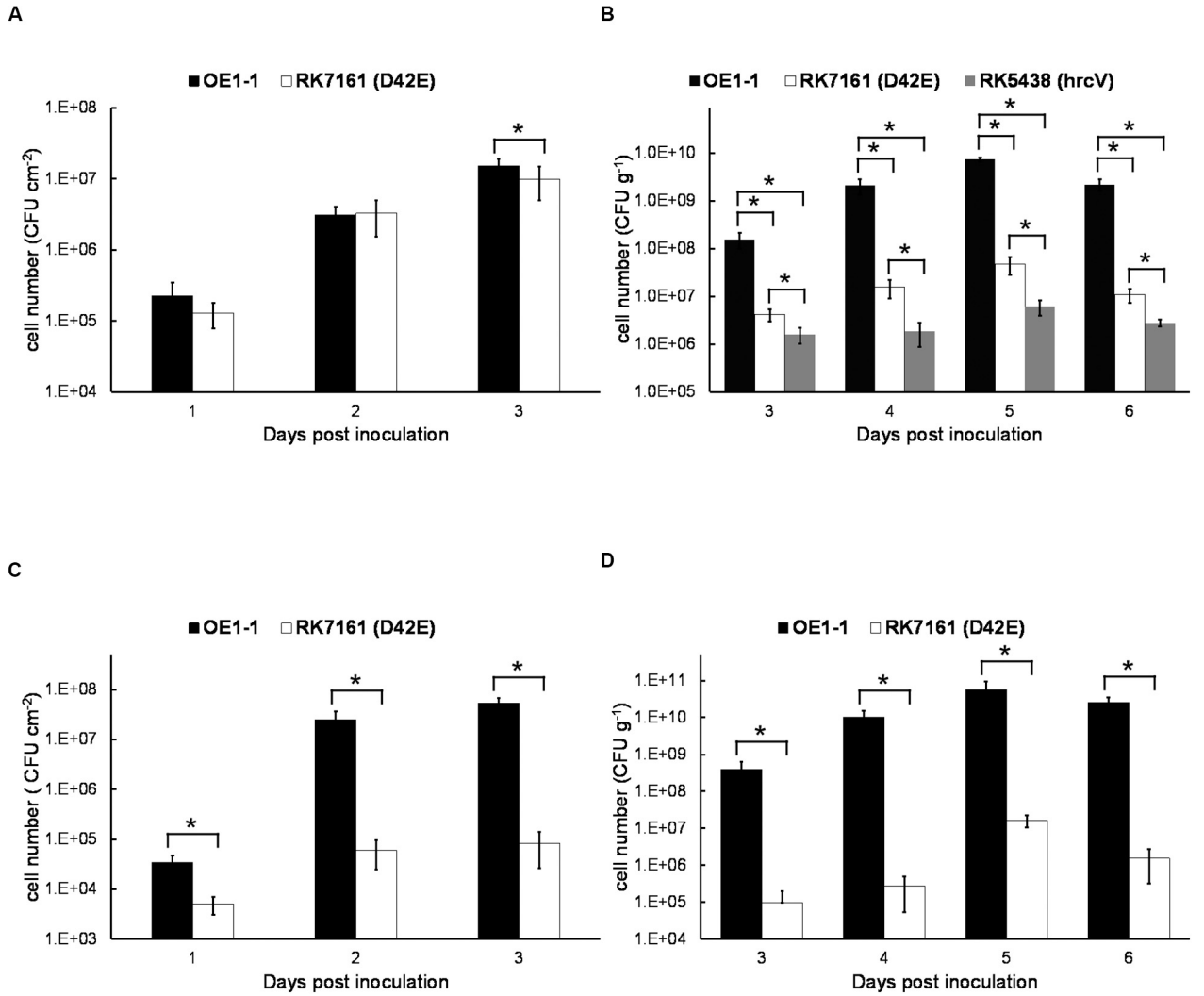

FIGURE 7 | The *in planta* proliferation of bacterial cells. For cell growth in leaves, a bacterial suspension at 10^6 cfu ml^{-1} was infiltrated into leaves of **(A)** tobacco and **(C)** eggplant with a blunt-end syringe, and leaf disks (0.38 cm^2) were daily punched for quantification of cell densities by dilution plating. For cell growth in stems, 2 μl of a bacterial suspension at a density of 10^7 cfu ml^{-1} was dropped onto a freshly cut petiole surface of **(B)** tobacco and **(D)** eggplant. The stem species (1 cm in length) were daily cut for quantification of cell densities by dilution plating. Black bars, white bars, and gray bars indicate cell growth of OE1-1, RK7161 (OE1-1D42E), and RK5438 (Δ*hrcV*), respectively. Each assay was carried out at least three times. The mean values of all experiments were averaged with SE. A *t*-test was conducted each day, and asterisks indicated a significant difference ($p < 0.05$).

and gives rise to disease development on host plants. At the same time, some T3Es can be detected by intracellular receptors in non-host plants that activate the immune response to effectively suppress the proliferation of RSSC strains in non-host plants and prevent disease development (Deslandes and Genin, 2014; Macho, 2016). Only limited numbers of studies are focused on the coordinate contribution of abundant T3Es to virulence of the RSSC. Our results demonstrated that mutants with increasing deletion numbers of T3Es exhibited gradually impaired virulence on host tobacco plants (**Supplementary Figures S1,S2**).

T3Es repertoires are greatly diversified among different RSSC strains, and 32 T3Es are proposed to compose the core and extended core T3Es, which are detected in most of the RSSC strains with genomic searching and probably present in an ancestral *R. solanacearum* strain (Peeters et al., 2013). Our results indeed confirmed that all these core and extended core T3Es play an essential role on virulence of OE1-1 since the mutant deleting all the core and extended core T3Es lost virulence toward host plants. The RSSC has a vast host range, with more than 450 plant species belonging to 50 botanical families. The core and extended core T3Es can probably explain the great adaption of the RSSC to a wide broad range of host species, although there are no apparent clues on T3Es with host specificity determinants (Coll and Valls, 2013; Peeters et al., 2013). Based on unique protein structures, especially carrying various internal repeats, a total of 23 T3Es are classified into five multigenic families of GALA, SKWP, HLK, AWR, and PopP. The construction of mutants lacking one or

more T3Es reveals functional overlap among the T3Es network, and highly variable repertoires of T3Es are believed to be able to hinder the biochemical function of some T3Es in different RSSC strains (Deslandes and Genin, 2014). Our results suggested that all the T3Es members of the AWR family, but not GALA, SKWP, or HLK families, jointly contributed slightly to full virulence of OE1-1 on tobacco plants. This result is consistent with previous reports that cumulative disruption of the seven RipG (GALA) or the five RipA (AWR) or the three RipH (HLK) resulted in attenuated virulence on some hosts but had modest or no impact on others (Angot et al., 2006; Solé et al., 2012; Chen et al., 2013). For instance, T3Es members of the AWR family can induce necrotic reactions on plants and are required for full virulence of some RSSC strain (Popa et al., 2016). T3Es members of the GALA family are previously demonstrated that different GALA members display different requirements for pathogenicity on *Arabidopsis thaliana*, tomato, and eggplant (Remigi et al., 2011). We also showed that all the T3Es members of the GALA family contributed jointly in part to virulence of OE1-1 on tobacco but not on tomato plants with root-cutting inoculation (Chen et al., 2018). Mutant with deletion of all the T3Es members of 4 families of GALA, SKWP, HLK, and AWR exhibited less virulent than OE1-1 on tobacco plants (**Figure 3C**), probably because the six core and three extended core T3Es were deleted in the mutant. All the core and extended T3Es seem to be critical for virulence on tobacco plants in the intercellular spaces and xylem (**Figures 4B,C**). Intriguingly, some other T3Es besides these core and extended core T3Es contribute slightly to full virulence of OE1-1 on tobacco plants, especially in xylem vessels, indicating that different T3Es function differently in different parts of same host plants.

The RSSC possesses extremely abundant T3Es, and some of them are validated to be functionally overlapped (Deslandes and Genin, 2014). Feature of functional overlap among T3Es will inevitably hinder the individual function of single T3Es in host RSSC strains with traditional genetic disruption. Studies of single T3E function are hence usually performed by over-expressed in engineered strains. The final goal of this study is to generate a T3Es-free strain for functional studies on individual T3Es in host cells. RK7161 (OE1-1D42E) is almost T3E free that completely lost virulence on tobacco plants with leaf infiltration, and on eggplants with root-cutting inoculation. It is reported that a polymutant with deletion of 28 well-expressed T3Es in *P. syringae* pv. *tomato* DC3000 is functionally effectorless for growth in *N. benthamiana* (Sébastien et al., 2011). With the Tn*7* based chromosomal integration system, target gene of each T3Es with its native promoter can be integrated into chromosome of the T3E-free RK7161 strain at 25-bp downstream of *glmS* gene (Choi et al., 2005; Zhang et al., 2020). This sole target T3E can be thus constitutively expressed in RSSC strain and injected into host cells via the T3SS. Once this single T3E is incorporated into host cells, we can observe several phenotypes of host plant cells, which will enable primary functional study of an individual T3E in host cells.

All taken together, our results demonstrated that virulence of OE1-1 was determined with all the core and extended core T3Es. We also provided a RSSC strain lacking 60% of its T3Es, which enables primary functional studies on individual T3Es in host cells.

DATA AVAILABILITY STATEMENT

The datasets presented in this study can be found in online repositories. The names of the repository/repositories and accession number(s) can be found at: https://www.ncbi.nlm.nih.gov/nuccore/; accession numbers CP009764.1 and CP009764.1 and at: https://www.ncbi.nlm.nih.gov/nuccore/; accession numbers CP009763.1 and CP009763.1.

AUTHOR CONTRIBUTIONS

YZ and KO conceived and designed the experiments. NL and LC performed the experiments. AK, YH, KO, and YZ analyzed and discussed the results. YZ and NL wrote and revised the manuscript. All authors contributed to the article and approved the submitted version.

FUNDING

This research was supported by JSPS KAKENHI Grant Numbers JP22580052 and JP20017020 and Cabinet Office grant in aid, the Advanced Next-Generation Greenhouse Horticulture by IoP (Internet of Plants), Japan.

SUPPLEMENTARY MATERIAL

The Supplementary Material for this article can be found online at: https://www.frontiersin.org/articles/10.3389/fmicb.2020.01683/full#supplementary-material

REFERENCES

Angot, A., Peeters, N., Lechner, E., Vailleau, F., Baud, C., Gentzbittel, L., et al. (2006). *Ralstonia solanacearum* requires F-box-like domain-containing type III effectors to promote disease on several host plants. *Proc. Natl. Acad. Sci. U.S.A.* 103, 14620–14625. doi: 10.1073/pnas.0509393103

Boucher, C., Barberis, P. A., Trigalet, A. P., and Demery, D. A. (1985). Transposon mutagenesis of *Pseudomonas solanacearum*: isolation of Tn*5*-induced avirulent mutants. *J. Gen. Microbiol.* 131, 2449–2457. doi: 10.1099/00221287-131-9-2449

Chen, L., Li, J., Shirota, M., Kiba, A., Hikichi, Y., and Ohnishi, K. (2018). Involvement of GALA effectors in *Ralstonia solanacearum* disease development towards two host plants. *Acta Microbiol. Sin.* 58, 131–141.

Chen, L., Shirota, M., Zhang, Y., Kiba, A., Hikichi, Y., and Ohnishi, K. (2013). Involvement of HLK effectors in *Ralstonia solanacearum* disease development in tomato. *J. Gen. Plant Pathol.* 80, 79–84. doi: 10.1007/s10327-013-0490-2

Choi, K. H., Gaynor, J. B., White, K. G., Lopez, C., Bosio, C. M., Karkhoff-Chweizer, R. R., et al. (2005). A Tn*7*-based broad range bacterial cloning and expression system. *Nat. Methods* 2, 443–448. doi: 10.1038/nmeth765

Coll, N. S., and Valls, M. (2013). Current knowledge on the *Ralstonia solanacearum* type III secretion system. *Microb. Biotechnol.* 6, 614–620.

Deslandes, L., and Genin, S. (2014). Opening the *Ralstonia solanacearum* type III effector tool box: insights into host cell subversion mechanisms. *Curr. Opin. Plant Biol.* 20, 110–117. doi: 10.1016/j.pbi.2014.05.002

Genin, S. (2010). Molecular traits controlling host range and adaptation to plants in *Ralstonia solanacearum*. *New Phytol.* 187, 920–928. doi: 10.1111/j.1469-8137.2010.03397.x

Genin, S., and Denny, T. P. (2012). Pathogenomics of the *Ralstonia solanacearum* species complex. *Annu. Rev. Phytopathol.* 50, 67–89.

Jiang, G., Wei, Z., Xu, J., Chen, H., Zhang, Y., She, X., et al. (2017). Bacterial wilt in china: history, current status, and future perspectives. *Front. Plant Sci.* 8:1549. doi: 10.3389/fpls.2017.01549

Kanda, A., Ohnishi, S., Tomiyama, H., Hasegawa, H., Yasukohchi, M., Kiba, A., et al. (2003). Type III secretion machinery-deficient mutants of *Ralstonia solanacearum* lose their ability to colonize resulting in loss of pathogenicity. *J. Gen. Plant Pathol.* 69, 250–257. doi: 10.1007/s10327-003-0041-3

Macho, A. P. (2016). Subversion of plant cellular functions by bacterial type-III effectors: beyond suppression of immunity. *New Phytol.* 210, 51–57. doi: 10.1111/nph.13605

Mansfield, J., Genin, S., Magori, S., Citovsky, V., Sriariyanum, M., Ronald, P., et al. (2012). Top 10 plant pathogenic bacteria in molecular plant pathology. *Mol. Plant Pathol.* 13, 614–629. doi: 10.1111/j.1364-3703.2012.00804.x

Mukaihara, T., Tamura, N., and Iwabuchi, M. (2010). Genome-wide identification of a large repertoire of *Ralstonia solanacearum* type III effector proteins by a new functional screen. *Mol. Plant Microb. Interact.* 23, 251–262. doi: 10.1094/mpmi-23-3-0251

Nakano, M., and Mukaihara, T. (2018). *Ralstonia solanacearum* type III effector RipAL targets chloroplasts and induces jasmonic acid production to suppress salicylic acid-mediated defense responses in plants. *Plant Cell Physiol.* 59, 2576–2589.

Nakano, M., and Mukaihara, T. (2019). The type III effector RipB from *Ralstonia solanacearum* RS1000 acts as a major avirulence factor in *Nicotiana benthamiana* and other *Nicotiana* species. *Mol. Plant Pathol.* 20, 1237–1251. doi: 10.1111/mpp.12824

Peeters, N., Carrère, S., Anisimova, M., Plener, L., Cazalé, A.-C., and Genin, S. (2013). Repertoire, unified nomenclature and evolution of the Type III effector gene set in the *Ralstonia solanacearum* species complex. *BMC Genomics* 14:859. doi: 10.1186/1471-2164-14-859

Popa, C., Li, L., Gil, S., Tatjer, L., Hashii, K., Tabuchi, M., et al. (2016). The effector AWR5 from the plant pathogen *Ralstonia solanacearum* is an inhibitor of the TOR signalling pathway. *Sci. Rep.* 6:27058.

Poueymiro, M., Cunnac, S., Barberis, P., Deslandes, L., Peeters, N., Cazale-Noel, A. C., et al. (2009). Two type III secretion system effectors from *Ralstonia solanacearum* GMI1000 determine host-range specificity on tobacco. *Mol. Plant Microb. Interact.* 22, 538–550. doi: 10.1094/mpmi-22-5-0538

Poueymiro, M., and Genin, S. (2009). Secreted proteins from *Ralstonia solanacearum*: a hundred tricks to kill a plant. *Curr. Opin. Microbiol.* 12, 44–52. doi: 10.1016/j.mib.2008.11.008

Remigi, P., Anisimova, M., Guidot, A., Genin, S., and Peeters, N. (2011). Functional diversification of the GALA type III effector family contributes to *Ralstonia solanacearum* adaptation on different plant hosts. *New Phytol.* 192, 976–987. doi: 10.1111/j.1469-8137.2011.03854.x

Sabbagh, C., Carrere, S., Lonjon, F., Vailleau, F., Macho, A. P., Genin, S., et al. (2019). Pangenomic type III effector database of the plant pathogenic *Ralstonia* spp. *Peer J.* 7:e7346. doi: 10.7717/peerj.7346

Sébastien, C., Suma, C., Brian, H. K., Alistair, B. R., Gregory, B. M., and Alan, C. (2011). Genetic disassembly and combinatorial reassembly identify a minimal functional repertoire of type III effectors in *Pseudomonas syringae*. *Proc. Natl. Acad. Sci. U.S.A.* 108, 2975–2980. doi: 10.1073/pnas.1013031108

Solé, M., Popa, C., Mith, O., Sohn, K. H., Jones, J. D. G., Deslandes, L., et al. (2012). The awr gene family encodes a novel class of *Ralstonia solanacearum* type III effectors displaying virulence and avirulence activities. *Mol. Plant Microb. Interact.* 25, 941–953. doi: 10.1094/mpmi-12-11-0321

Sun, Y., Li, P., Shen, D., Wei, Q., He, J., and Lu, Y. (2019). The *Ralstonia solanacearum* effector RipN suppresses plant PAMP-triggered immunity, localizes to the endoplasmic reticulum and nucleus, and alters the NADH/NAD+ratio in *Arabidopsis*. *Mol. Plant Pathol.* 20, 533–546. doi: 10.1111/mpp.12773

Vasse, J., Genin, S., Frey, P., Boucher, C., and Brito, B. (2000). The *hrpB* and *hrpG* regulatory genes of *Ralstonia solanacearum* are required for different stages of the tomato root infection process. *Mol. Plant Microb. Interact.* 13, 259–267. doi: 10.1094/mpmi.2000.13.3.259

Zhang, Y., Han, L., Zhang, L., Xu, C., Shi, X., Hikichi, Y., et al. (2020). Expression of *Ralstonia solanacearum* type III secretion system is dependent on a novel type 4 pili (T4P) assembly protein (TapV) but is T4P independent. *Mol. Plant Pathol.* 21, 777–793. doi: 10.1111/mpp.12930

Zhang, Y., Li, J., Zhang, W., Shi, H., Luo, F., Hikichi, Y., et al. (2018). A putative LysR-type transcriptional regulator PrhO positively regulates the type III secretion system and contributes to the virulence of *Ralstonia solanacearum*. *Mol. Plant Pathol.* 19, 1808–1819. doi: 10.1111/mpp.12660

Zhang, Y., Zhang, W., Han, L., Li, J., Shi, X., Hikichi, Y., et al. (2019). Involvement of a PadR regulator PrhP on virulence of *Ralstonia solanacearum* by controlling detoxification of phenolic acids and type III secretion system. *Mol. Plant Pathol.* 20, 1477–1490. doi: 10.1111/mpp.12854

Zhuo, T., Wang, X., Chen, Z., Cui, H., Zeng, Y., Chen, Y., et al. (2020). The *Ralstonia solanacearum* effector RipI induces a defence reaction by interacting with the bHLH93 transcription factor in *Nicotiana benthamiana*. *Mol. Plant Pathol.* 21, 999–1004. doi: 10.1111/mpp.12937

Conflict of Interest: The authors declare that the research was conducted in the absence of any commercial or financial relationships that could be construed as a potential conflict of interest.

frontiers in Plant Science

ORIGINAL RESEARCH
published: 31 July 2020
doi: 10.3389/fpls.2020.01156

KatE From the Bacterial Plant Pathogen *Ralstonia solanacearum* Is a Monofunctional Catalase Controlled by HrpG That Plays a Major Role in Bacterial Survival to Hydrogen Peroxide

María Laura Tondo[1,2†], *Roger de Pedro-Jové*[3,4†], *Agustina Vandecaveye*[5], *Laura Piskulic*[6], *Elena G. Orellano*[1,5*] *and Marc Valls*[3,4*]

[1] *Área Biología Molecular, Facultad de Ciencias Bioquímicas y Farmacéuticas, Universidad Nacional de Rosario, Rosario, Argentina,* [2] *Instituto de Ingeniería Ambiental, Química y Biotecnología Aplicada (INGEBIO), Facultad de Química e Ingeniería del Rosario, Pontificia Universidad Católica Argentina (UCA), Consejo Nacional de Investigaciones Científicas y Técnicas (CONICET), Rosario, Argentina,* [3] *Centre for Research in Agricultural Genomics (CSIC-IRTA-UAB-UB), Catalonia, Spain,* [4] *Department of Genetics, University of Barcelona, Barcelona, Spain,* [5] *Instituto de Biología Molecular y Celular de Rosario, Consejo Nacional de Investigaciones Científicas y Técnicas (CONICET), Rosario, Argentina,* [6] *Área Estadística y Procesamiento de Datos, Facultad de Ciencias Bioquímicas y Farmacéuticas, Universidad Nacional de Rosario, Rosario, Argentina*

Ralstonia solanacearum is the causative agent of bacterial wilt disease on a wide range of plant species. Besides the numerous bacterial activities required for host invasion, those involved in the adaptation to the plant environment are key for the success of infection. *R. solanacearum* ability to cope with the oxidative burst produced by the plant is likely one of the activities required to grow parasitically. Among the multiple reactive oxygen species (ROS)-scavenging enzymes predicted in the *R. solanacearum* GMI1000 genome, a single monofunctional catalase (KatE) and two KatG bifunctional catalases were identified. In this work, we show that these catalase activities are active in bacterial protein extracts and demonstrate by gene disruption and mutant complementation that the monofunctional catalase activity is encoded by *katE.* Different strategies were used to evaluate the role of KatE in bacterial physiology and during the infection process that causes bacterial wilt. We show that the activity of the enzyme is maximal during exponential growth *in vitro* and this growth-phase regulation occurs at the transcriptional level. Our studies also demonstrate that *katE* expression is transcriptionally activated by HrpG, a central regulator of *R. solanacearum* induced upon contact with the plant cells. In addition, we reveal that even though both KatE and KatG catalase activities are induced upon hydrogen peroxide treatment, KatE has a major effect on bacterial survival under oxidative stress conditions and especially in the adaptive response of *R. solanacearum* to this oxidant. The *katE* mutant strain also exhibited differences in the structural characteristics of the biofilms developed on an abiotic surface in comparison to wild-type cells, but not in the overall amount of biofilm production. The role of catalase KatE during the interaction with its host

OPEN ACCESS

Edited by:
Benjamin Gourion, UMR2594 Laboratoire Interactions Plantes-Microorganismes (LIPM), France

Reviewed by:
Anna Katherine Block, Center for Medical, Agricultural and Veterinary Entomology, United States
Claudia S. L. Vicente, Instituto Nacional Investigaciao Agraria e Veterinaria (INIAV), Portugal

***Correspondence:**
Elena G. Orellano
orellano@ibr-conicet.gov.ar
Marc Valls
marcvalls@ub.edu

[†]These authors have contributed equally to this work

Specialty section:
This article was submitted to Plant Pathogen Interactions, a section of the journal Frontiers in Plant Science

Received: *21 May 2020*
Accepted: *16 July 2020*
Published: *31 July 2020*

Citation:
Tondo ML, de Pedro-Jové R, Vandecaveye A, Piskulic L, Orellano EG and Valls M (2020) KatE From the Bacterial Plant Pathogen Ralstonia solanacearum Is a Monofunctional Catalase Controlled by HrpG That Plays a Major Role in Bacterial Survival to Hydrogen Peroxide. Front. Plant Sci. 11:1156. doi: 10.3389/fpls.2020.01156

plant tomato is also studied, revealing that disruption of this gene has no effect on *R. solanacearum* virulence or bacterial growth in leave tissues, which suggests a minor role for this catalase in bacterial fitness *in planta*. Our work provides the first characterization of the *R. solanacearum* catalases and identifies KatE as a *bona fide* monofunctional catalase with an important role in bacterial protection against oxidative stress.

Keywords: *Ralstonia solanacearum*, bacterial wilt, oxidative burst, KatE catalase, host adaptation

INTRODUCTION

Ralstonia solanacearum is a gram-negative, soil-borne β-proteobacterium that causes the bacterial wilt disease in more than 200 plant species, including economically important food crops such as potato, tomato, peanut, and eggplant (Allen et al., 2004). In addition to its extremely wide host range, *R. solanacearum* exhibits an increasingly broad geographic distribution and is able to survive for long periods in waterways, soil and in symptomless or latently infected plants (Denny, 2006; Genin and Denny, 2012).

Upon interaction with a susceptible host, the pathogen initiates the infection by entering the roots. After colonisation of the intercellular spaces of the root cortex, the bacterium enters the xylem vessels, spreading rapidly, and systemically through the vascular system. Intensive bacterial multiplication and production of large amounts of exopolysaccharides (EPSs) blocks water traffic in vascular bundles, ultimately resulting in complete wilting, plant death, and the release of the pathogen back to the soil (Genin and Denny, 2012). *R. solanacearum* requires multiple virulence factors that act additively to facilitate infection of the host plant. Bacterial motility mediated by flagella and type IV pili, plant cell wall-degrading enzymes, and type II-secreted proteins enable bacterial penetration into root tissues. Secretion of type III effectors inside plant cells evades plant immune responses and allows disease development (Peeters et al., 2013). In the plant environment, *R. solanacearum* must overcome different types of metabolic stresses in order to survive and proliferate. One of these challenges is the exposure to plant-generated reactive oxygen species (ROS) that accumulate in the apoplast as part of the primary defence response to pathogen invasion (Lamb and Dixon, 1997).

ROS are unavoidable by-products of plant metabolic pathways generated as a result of successive one-electron reductions of molecular oxygen (O_2). Under physiological steady state conditions, ROS accumulation is prevented by the action of protective antioxidant systems often confined to specific compartments. However, adverse environmental factors including pathogen infection disturb this fine balance between production and scavenging of ROS leading to a rapid increase in intracellular ROS levels or "oxidative burst" (Apel and Hirt, 2004). In plants challenged with pathogenic microorganisms, including fungi, bacteria, and viruses, the oxidative burst proved to be one of the earliest events after elicitation (Wojtaszek, 1997). In the interaction of *R. solanacearum* with tomato plants, a single-phase ROS increase was detected at 24 h post-inoculation (hpi) of a susceptible cultivar, while a bi-phasic ROS generation with peak levels at 12 and 36 hpi was observed after infection of a resistant tomato variety (Mandal et al., 2011). The second phase of ROS accumulation, usually more prolonged and higher in magnitude, has been correlated with disease resistance *via* the hypersensitive response during incompatible and non-host interactions (Lamb and Dixon, 1997).

The oxidative burst fulfils multiple functions to plant cells undergoing pathogen attack. ROS promote the oxidative cross-linking of plant cell walls to slow pathogen entry and spread, and act as key signal molecules that mediate the activation of plant defence responses and systemic resistance (Lamb and Dixon, 1997). In addition, the high reactivity of ROS with cellular macromolecules, including DNA and proteins, make ROS effective antimicrobial agents capable of either killing the pathogen or slowing down its growth (Peng and Kuc, 1992). To counter-attack ROS, oxidative stress response genes were shown to be expressed in plant-associated bacteria during the interaction with their hosts (Smith et al., 1996; Santos et al., 2001; Okinaka et al., 2002; Saenkham et al., 2007; Tamir-Ariel et al., 2007). Particularly, an *in vivo* expression technology (IVET) screen performed in *R. solanacearum* during pathogenesis of tomato plants revealed that at least 15 out of 153 *in planta*-expressed genes encoded proteins involved in the oxidative stress response, further supporting the notion that an oxidative challenge is associated with plant infection (Brown and Allen, 2004; Flores-Cruz and Allen, 2009).

Hydrogen peroxide (H_2O_2), the major ROS of the oxidative burst, is an electrically neutral and relatively stable species that can penetrate through cell membranes and diffuse to reach distant cellular components (Wojtaszec, 1997). H_2O_2 concentrations must be kept at low levels inside bacterial cells due to its ability to oxidize ferrous ions to generate highly reactive hydroxyl radicals (·OH; Fenton reaction), and to react with iron-sulphur clusters of key metabolic enzymes (Mishra and Imlay, 2012). Among the bacterial enzymes evolved to remove ROS and avoid toxicity, catalases (E.C. 1.11.1.6; H_2O_2:H_2O_2 oxidoreductase) constitute the primary scavengers of H_2O_2 by catalyzing its dismutation to water and oxygen. Based on phylogenetic analyses, three distinct catalase families can be distinguished: typical (monofunctional) heme catalases (KatEs), bifunctional heme catalase-peroxidases (KatGs), and (non-heme) manganese catalases (MnCats) (Zámocky et al., 2012). Most sequenced bacterial genomes encode multiple catalase isozymes that operate in different physiological or environmental conditions (Mishra and Imlay, 2012). Induction of specific catalases has been observed when bacteria detect environmental ROS and

upon entry into the stationary phase (Loewen, 1997; Mishra and Imlay, 2012). In addition, recent reports have demonstrated the role of particular catalases during pathogenesis, enhancing the bacterial ability to overcome host-induced oxidative burst (Jittawuttipoka et al., 2009; Tondo et al., 2010; Mishra and Imlay, 2012). The available *R. solanacearum* GMI1000 genome encodes numerous predicted ROS-scavenging enzymes, including three putative catalases. The *RSc0775* (KatGb) and *RSc0776* (KatGa) open reading frames (ORFs) encode predicted bifunctional catalase-peroxidases in the bacterial chromosome; whereas *RSp1581* (KatE) codes for a predicted typical monofunctional catalase and is located in the megaplasmid, which harbors most *R. solanacearum* pathogenicity functions (Salanoubat et al., 2002; Genin and Denny, 2012).

Our previous transcriptomic studies in *R. solanacearum* extracted from roots of early infected potato plants indicated that the transcription of *katE* and, to a lesser extent, *katGb* is induced during plant colonisation compared to growth in rich medium (Puigvert et al., 2017). We also identified *katE* among the genes specifically induced by HrpG, a key *R. solanacearum* pathogenicity regulator that responds to direct bacterial contact with plant cells (Valls et al., 2006). In addition, *R. solanacearum* catalases are up-regulated by the transcriptional regulator OxyR, whose deletion impaired bacterial virulence (Flores-Cruz and Allen, 2011). These observations collectively suggest a role for catalases during the infection process, but the contribution of these enzymes to bacterial wilt disease has not been investigated.

Here we present a thorough study of the *R. solanacearum* KatE. We prove that this gene encodes a *bona fide* catalase enzyme responsible for one of the two catalase activities detected in this pathogen, describe its expression pattern and study its role during bacterial life *in planta*.

MATERIALS AND METHODS

Bacterial Strains, Plasmids, and Growth Conditions

Relevant characteristics of the plasmids and bacterial strains used in this work are described in **Table 1**. The wild-type strain GMI1000 of *R. solanacearum* and its *hrpG*-derivative have been previously described (Boucher et al., 1985; Valls et al., 2006). The complemented (*ΔhrpG* + *hrpG*) strain was obtained by electroporation of the *ΔhrpG* mutant with pLT-HrpG, a vector

TABLE 1 | Bacterial strains, plasmids, and primers used in this study.

Strain/plasmid	Relevant genotype and description	Source/reference
Ralstonia solanacearum		
GMI1000	Wild-type strain	Boucher et al., 1985
ΔkatE	*katE* deletion mutant in the GMI1000 background, Gm^r	This study
ΔkatE + *katE*	*ΔkatE* strain complemented with *katE* from pRCT-katE, Gm^r, Tc^r	This study
ΔhrpG	*hrpG* deletion mutant in the GMI1000 background	Valls et al., 2006
ΔhrpG + *hrpG*	*ΔhrpG* strain complemented with the overexpressing plasmid pLT-HrpG, Tc^r	This study
Escherichia coli		
JM109	*HsdR17 endA1 recal thi gyrA96 relA1 recA1 supE44* $\lambda^-\Delta$*(lac-proAB)*, [F', traD36, $proA^+B^+$, $lacI^qZ\Delta M15$]	Promega Corp.
Plasmids		
pGEM-T Easy	PCR cloning and sequencing vector, Ap^r	Promega Corp.
pGEM-UkatE	PCR-amplified (945-bp) *katE* upstream fragment, cloned in pGEM-T easy, Ap^r	This study
pGEM-DkatE	PCR-amplified (892-bp) *katE* downstream fragment, cloned in pGEM-T easy, Ap^r	This study
pCM351	Allelic exchange vector, Ap^r, Tc^r, Gm^r	Marx and Lidstrom, 2002
pCM-UDkatE	Upstream (945-bp) and downstream (892-bp) fragments of *katE* cloned into *Eco*RI/*Not*I and *Hpa*I/*Sac*I sites of pCM351, Ap^r, Tc^r, Gm^r	This study
pRCT	pRC containing tetracycline resistance and cloning sites, Ap^r, Cl^r, Tc^r	Monteiro et al., 2012b
pRCT-katE	PCR-amplified (1960-bp) fragment containing *katE* ORF and promoter sequence, cloned into *Hpa*I/*Bgl*II sites of pRCT, Ap^r, Cl^r, Tc^r	This study
pLT-HrpG	pLAFR3 derivative including the *HrpG* coding sequence under the control of the *Ptac* promoter	Valls et al., 2006
pJBA128	Vector containing *gfpmut3* under a constitutive *PlacUV5* promoter, Tc^r	Lee et al., 2005

Primer name	Sequence[a]	Amplified fragment
katEU-F	5' tagaattcGGATACTGACCGTTGCCATC 3' (*Eco*RI)	This study
katEU-R	5' tagcggccgcGAGTCTCCTGTGGGGATGAG 3' (*Not*I)	This study
katED-F	5' tagttaacGCTGCAGGACTGATGATGTG 3' (*Hpa*I)	This study
katED-R	5' tagagctcGGTCACGGATATCGAACCAC 3' (*Sac*I)	This study
UkatEU-F	5' GAATGCTTTCCGCCTTGATATC 3'	This study
Gent-R	5' CCTGCTGCGTAACATCGTTGC 3'	This study
ckatE-F	5' tagttaacTGTTTGAAGACGGTGACGTT 3' (*Hpa*I)	This study
ckatE-R	5' taagatctTCAGTCCTGCAGCTTCG 3' (*Bgl*II)	This study
katE_qPCR-F	5' TGAACAAGAACCCGGAGAAC 3'	This study
katE_qPCR-R	5' TGTCGGCATACGAGAAGATG 3'	This study

Ap^r, Gm^r, Tc^r: resistance to ampicillin (Ap), gentamicin (Gm) and tetracycline (Tc), respectively; PCR, polymerase chain reaction.

[a]Capital letters correspond to nucleotides of the R. solanacearum GMI1000 genome sequence and small letters to nucleotides added to facilitate cloning (restriction sites underlined).

that overexpress HrpG from the isopropyl-b-D-thiogalactopyranoside (IPTG)-inducible *Ptac* promoter. The plasmid and transformation procedures are described in (Valls et al., 2006). *R. solanacearum* strains were routinely grown at 28°C in tetrazolium chloride (TZC) agar plates (Kelman, 1954), complete BG medium (10 g/L bactopeptone, 1 g/L yeast extract, 1 g/L casamino acids, 0.5% glucose), or MP minimal medium supplemented with 20 mM L-glutamate as a carbon source (Plener et al., 2010). To induce HrpG expression in the complemented *ΔhrpG* + *hrpG* strain IPTG was added to the cultures at a final concentration of 100 mM. Gentamicin and tetracycline were used for selection of *R. solanacearum* strains (5 and 10 μg/mL in liquid and solid cultures, respectively). Bacterial growth was monitored by measuring optical density at 600 nm. *Escherichia coli* strains were grown at 37°C in Luria-Bertani (LB) broth supplemented with appropriate antibiotics (Sambrook and Russell, 2001).

Molecular Biology and Microbiological Techniques

Molecular cloning procedures, including DNA restriction and analysis, DNA ligation, preparation of competent cells, and transformation of *E. coli* by electroporation, were performed according to standard protocols (Ausubel et al., 1994; Sambrook and Russell, 2001). Plasmid DNA was isolated using Wizard Plus SV Minipreps DNA Purification System (Promega Corp., Madison, WI). Restriction enzymes, DNA ligase, and other DNA enzymes were used according to the manufacturers' recommendations. Total genomic DNA from *R. solanacearum* was isolated from fresh bacterial cultures as described by Chen and Kuo (Chen and Kuo, 1993). For RNA extraction and quantitative real-time PCR analysis, total RNA was extracted using the SV Total RNA Isolation Kit (Promega) following manufacturer's instructions for Gram-negative bacteria. cDNA was synthesized using the High Capacity cDNA reverse transcriptase kit (Applied Biosystems) following manufacturer's instructions. The Sybr Green Master Mix (Sigma Aldrich) was used for quantitative real-time PCR with the LightCycler 480 Instrument (Roche Life Science) using the katE_qPCR-F and katE_qPCR-R oligonucleotides as primers. Per each biological condition, duplicates were run and the phosphoserine aminotransferase gene (*serC*) was used as a reference gene for normalisation of expression as described in (Monteiro et al., 2012a).

Construction of the *R. solanacearum ΔkatE* Mutant and Complemented Strain

The *R. solanacearum ΔkatE* mutant strain was generated by inserting a gentamicin resistance cassette in substitution of the open reading frame *RSp1581* in the GMI1000 strain. Primers were designed in order to amplify 945-bp (primer pair katEU-F/katEU-R) and 892-pb (primer pair katED-F/katED-R) fragments located upstream and downstream of the gene *RSp1581*, respectively (**Table 1**). Specific restriction sites were incorporated to each primer to be used in subsequent cloning steps. PCR amplifications were performed with the proofreading Phusion DNA polymerase (New England Biolabs, Inc., Ipswich, MA, U.S.A.) following the manufacturer's conditions. The resulting fragments were cloned into pGEM-T easy (Promega Corp.) creating pGEM-UkatE and pGEM-DkatE for the upstream and downstream regions of the *katE* gene, respectively; and the identity of the inserts were confirmed by sequencing with vector primers SP6 and T7. Inserts were then excised by double digestion with *Eco*RI/*Not*I (upstream region) and *Hpa*I/*Sac*I (downstream region), and inserted into the multiple cloning sites of pCM351 (Marx and Lidstrom, 2002) on both sides of the gentamicin resistance cassette, creating pCM-UDkatE. This construction was then linearized by *Eco*RI and introduced into the wild type *R. solanacearum* GMI1000 by natural transformation following the protocol described by Boucher and associates (Boucher et al., 1985). Double recombination events were selected by gentamicin resistance on TZC agar plates and the correct insertion in the genome was confirmed by PCR using primers UkatEU-F and Gent-R, which hybridize upstream of the upper region used for the homologous recombination and in the gentamicin resistance cassette, respectively (**Table 1**). This mutant strain, denoted as *ΔkatE*, was used for phenotypic characterization.

For *ΔkatE* complementation, a 1960-bp DNA fragment containing the *katE* coding region and extending 430 pb upstream of the 5' end of the ORF was PCR amplified with primers ckatE-F and ckatE-R (**Table 1**). The amplified sequence included the putative promoter region of the *katE* gene as predicted with SoftBerry (www.softberry.com). This amplicon was double digested with *Hpa*I/*Bgl*II and cloned into the integration element of the suicide vector pRCT (Monteiro et al., 2012b) to generate recombinant plasmid pRCT-katE. This plasmid was then linearized by *Nco*I and introduced into the mutant strain *ΔkatE* by natural transformation as described above. Complemented strains were selected by tetracycline resistance on TZC agar plates. The complemented mutant strain selected for further studies was designated *ΔkatE* + *katE*.

Enzyme Activity Assay and Staining

R. solanacearum soluble cell extracts were prepared from 10 mL cultures harvested by centrifugation at 4,000 *g* for 10 min at 4°C. Bacteria were washed and resuspended in 500 μL of ice-cold 50 mM potassium phosphate buffer (pH 7.0) containing 1 mM PMSF, and then disrupted by intermittent sonication. Suspensions were clarified by centrifugation at 12,000 *g* for 20 min at 4°C. Protein concentrations in soluble cell extracts were determined by the Sedmak and Grossberg method (Sedmak and Grossberg, 1977) with bovine serum albumin as standard. Catalase activity in cell extracts was monitored through the decomposition of hydrogen peroxide by following the decrease in absorbance at 240 nm (Beers and Sizer, 1952). The assays were performed at 25°C in 50 mM potassium phosphate buffer (pH 7.0) containing 10 mM H_2O_2. To calculate the catalase specific activity an extinction coefficient of 43.6 M^{-1} cm^{-1} at 240 nm was used. One unit of catalase activity was defined as the amount of activity required to decompose 1 μmol of H_2O_2 per minute under the assay conditions.

For evaluation of catalase activity in gels, soluble protein extracts (15–25 μg) were separated by continuous electrophoresis in 8% (w/v) non-denaturing polyacrylamide gels in glycine buffer (pH 9.5). To eliminate the likelihood of multiple, potentially artifactual catalase bands, non-denaturing gels were electrophoresed

at a constant current of 10 mA. Staining for catalase activity was performed as previously described (Scandalios, 1968).

Peroxidase activity staining was performed according to Kang and associates (Kang et al., 1999) with some modifications. Briefly, aliquots of cell extracts containing 100 μg of soluble protein were electrophoresed on 8% (w/v) native polyacrylamide gels as previously described. Gels were then incubated in 0.1 M Tris-HCl (pH 7.5) containing 0.1 mg/mL 3,3'-diaminobenzidine, 9 mM H_2O_2, and 0.4 mg/mL $NiCl_2$ for approximately 30 min in the dark, until appearance of the bands.

Coomassie-stained gels were run in parallel to those used for catalase and peroxidase activity measurements to ascertain comparable protein loadings between samples.

Bacterial Survival in the Presence of Hydrogen Peroxide

To test bacterial resistance to hydrogen peroxide *R. solanacearum* overnight cultures were inoculated into fresh BG medium and grown to early exponential phase (6.5 h at 28°C and 200 rpm). Aliquots of the cultures were diluted and plated on BG-agar in order to quantify the bacterial population and then hydrogen peroxide was added to the cultures at final concentrations of 1 and 2.5 mM. After 15 min of exposure to the oxidant, samples were removed, washed once with fresh medium, serially diluted and plated on BG-agar plates.

For the induction experiments, *R. solanacearum* cultures were grown to early exponential phase (6.5 h) and incubated with sub-lethal concentrations of hydrogen peroxide (25, 50, and 100 μM) for an additional hour before being used in the killing experiments. After the induction treatment, aliquots of the cultures were washed, diluted and plated on BG-agar plates. Cultures were then treated with a lethal concentration of H_2O_2 (5 mM) for 15 min, after which samples were taken, washed once with fresh medium, serially diluted and plated on BG-agar plates.

In all cases, growth of liquid cultures was monitored spectrophotometrically by optical density at 600 nm (OD_{600}). Colonies were counted after 72 h incubation at 28°C. The percentage of survival was defined as the number of colony forming units (CFU) after treatment divided by the number of CFU prior to treatment ×100.

Biofilm Observation and Quantification

For analyses of biofilm formation *R. solanacearum* strains were modified to express the green fluorescent protein (GFP) by electroporation with plasmid pJBA128 (Lee et al., 2005). Saturated cultures of the GFP-labeled bacteria in BG medium were adjusted to an optical density at 600 nm of 0.1 and diluted 1:20 in fresh CPG medium (1 g/L casamino acids, 5 g/L glucose and 10 g/L bacteriological peptone). Then, 300 μL of the bacterial suspensions were placed onto chamber-covered glass slides (nu155411, Lab-Tek, NUNC, Naperville. IL, U.S.A.) that were statically incubated in a humidified PVC box at 28°C. All microscopic observations were performed on a Zeiss LSM880 confocal laser scanning microscope (Carl Zeiss, Jena, Germany) equipped with an argon laser and detector and filter sets for monitoring of GFP expression (excitation, 488 nm; emission, 517 nm). The images obtained were analyzed with ImageJ software (https://imagej.nih.gov).

Biofilm quantification analyses were carried out following crystal violet assay. In short, CPG overnight cultures were adjusted in CPG to an OD_{600} of 0.1. Next, 95 μL of fresh CPG and 5 μL of the adjusted culture to OD_{600} of 0.1 were added in each of the 96-well polystyrene microplates (Greiner, Kremsmünster, Austria) and incubated without shaking at 30°C during 24 h. After incubation, biomass growth was measured at OD_{600}. Next, 100 μL of 0.1% crystal violet stain was added to each well and incubated at room temperature for 30 min. Wells were washed three times with MQ-water and the stained biofilm was solubilised with 100 μL of 95% ethanol and measured at OD_{580}. Measurements were performed using SpectraMax multi-plate reader and the results normalised to biomass (OD_{580}/OD_{600}).

Pathogenicity and Bacterial Multiplication Assays in Tomato

The susceptible tomato (*Solanum lycopersicum*) cv. Marmande cultivar was grown under long-day light conditions at 25°C and 60% relative humidity. Prior to infection, three- to four-week-old plants were acclimated for 3 days at 27°C with constant light conditions (12 h light/12 h darkness). For the pathogenicity assays, plants not watered for two days were drench inoculated without root wounding with 40 mL of the bacterial suspension adjusted to 10^7 CFU/mL from an overnight culture. 20–25 plants were inoculated per strain and wilting symptoms were recorded per plant using an established semi-quantitative wilting scale ranging from 0 (no wilting) to 4 (death) (Monteiro et al., 2012b).

For bacterial growth assays *in planta*, tomato leaves were vacuum-infiltrated submerging the aerial plant into water or 10^5 CFU/mL bacterial suspensions for 20 s. In both cases, the adjuvant Silwet L-77 was added (80 μL/L suspension) to facilitate infiltration. At day 0 and 3 post infiltration, bacterial concentrations in the plant tissues were measured. To this end, three 5-mm diameter disks per biological replicate were taken from infiltrated leaves, homogenised and 10 μL of serial ten-fold dilutions were plated in selective plates. The plates were incubated at 28°C until colonies could be counted. Three biological replicas were used per bacterial strain.

Statistical Analyses

Quantitative analyses were performed with at least three independent biological samples. Data were subjected to a multifactorial mixed model ANOVA and Tukey's multiple comparison tests along with residual analysis and validation using Infostat software (Infostat 2006H, http://www.infostat.com.ar).

RESULTS

R. solanacearum RSp1581 Encodes an Active Monofunctional Catalase Induced During Exponential Growth

In order to investigate the role of *katE* in the *R. solanacearum* physiology and plant interaction, we generated a *katE* deletion mutant by genetic replacement of the *RSp1581* open reading

frame by a gentamicin resistance cassette in the GMI1000 strain background. The resulting mutant, named *ΔkatE*, exhibited typical colony morphology on tetrazolium chloride (TZC)-containing agar plates and similar growth curves to its wild-type parental strain, demonstrating that disruption of *katE* does not affect bacterial growth *in vitro* (**Supplementary Figure 1**).

To analyze the effect of *katE* deletion on *R. solanacearum* catalase activity, soluble protein extracts from cultures grown in BG medium to early exponential and stationary phase were separated on non-denaturing polyacrylamide gels and stained for catalase activity. As shown in **Figure 1A**, we detected two distinct catalase bands at both growth stages in the wild-type strain GMI1000. On the contrary, the upper, slow-migrating band was completely absent in the *ΔkatE* mutant, suggesting that this band corresponds to the KatE isozyme. As a final proof that the *RSp1581* open reading frame is functional and encodes this enzyme, complementation of *ΔkatE* with a single copy of the open reading frame under its own promoter restored the catalase activity pattern. Soluble protein extracts of the wild type, *ΔkatE* and complemented (*ΔkatE* + *katE*) strains were also run in parallel on a non-denaturing polyacrylamide gel stained for peroxidase activity (**Figure 1B**). This assay revealed that the fast-migrating catalase band detected in all three strains exhibits peroxidase activity as well, suggesting that it corresponds to one of the KatG isozymes identified in the *R. solanacearum* genome (Salanoubat et al., 2002). In adittion, the upper KatE band did not appear in the peroxidase assay further corroborating its monofunctional enzymatic nature.

The activity levels of KatE observed in native gels (**Figure 1A**) seemed to indicate that expression of this gene in *R. solanacearum* is regulated by growth phase, as previously reported for other bacterial species (Loewen, 1997; Vattanaviboon and Mongkolsuk, 2000; Tondo et al., 2010). To test this hypothesis, we measured the *katE* mRNA levels in early exponential and stationary phase cultures by quantitative real-time RT-PCR. As illustrated in **Figure 1C**, mRNA levels of *katE* significantly decreased in stationary wild type cells, being approximately 5-fold lower in the stationary phase with respect to early exponential growth phase. This expression pattern was similar in the complemented *ΔkatE* strain whereas expression was undetectable in the *katE* mutant.

KatE Expression Is Transcriptionally Activated by the HrpG Regulator

Using genome-wide expression analyses in *R. solanacearum*, we previously identified *katE* among a group of virulence and environmental adaptation genes specifically regulated by the HrpG transcriptional regulator (Valls et al., 2006). To better investigate the role of HrpG in the regulation of *katE*, we measured *katE* transcript levels in the wild-type GMI1000 strain, a *hrpG* deletion mutant (*ΔhrpG*) and the complemented mutant strain overexpressing this regulator (*ΔhrpG* + *hrpG*). *katE* mRNA levels were significantly lower in the *ΔhrpG* strain with respect to the wild-type or the complemented overexpressing strain (**Figure 2A**). This effect was more pronounced (significant differences in 95% Tukey HSD test) in minimal medium -known to specifically induce HrpG activity- than in cells grown in rich BG medium (**Figure 2A**). To evaluate the influence of this regulation at the protein level, we then measured the effect of *hrpG* on the catalase activity. Measurements of catalase activity in native polyacrylamide gels revealed the same expression pattern obtained for *katE* transcripts, with markedly lower levels in the *ΔhrpG* background that could be complemented by overexpression of this regulator (**Figure 2B**). These results show a clear correlation between *hrpG* and *katE* transcript levels and with the catalase activity as well.

R. solanacearum KatE Activity Is Enhanced Upon H_2O_2 Treatment and Protects Against Oxidative Stress

To assess the involvement of catalases in the *R. solanacearum* oxidative stress response, we exposed early exponential phase

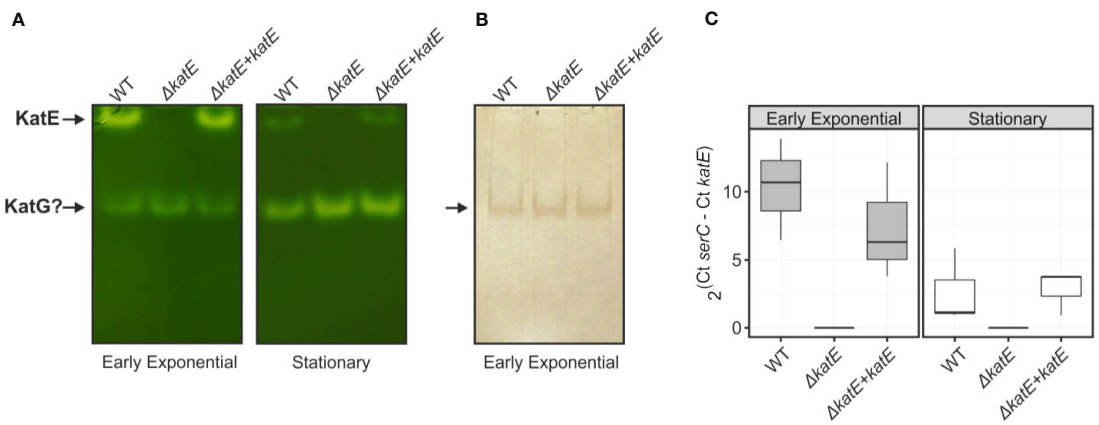

FIGURE 1 | Catalase/peroxidase activity patterns and *katE* expression in *R. solanacearum*. Equal amounts of total soluble protein extracts (25 μg) from wild-type GMI1000 strain (WT), the *katE* deletion mutant (*ΔkatE*), and the complemented (*ΔkatE* + *katE*) strain grown in BG medium to early exponential or stationary growth phases were separated on non-denaturing polyacrylamide gels stained for catalase **(A)** and peroxidase **(B)** activities. **(C)** *katE* mRNA levels measured by quantitative real-time PCR from cultures grown in the same conditions described in A. In the Y-axis is represented the $2^{\Delta Ct}$ normalised expression from three biological replicas with two technical replicas each. Experiments in A and B were repeated at least three times with similar results.

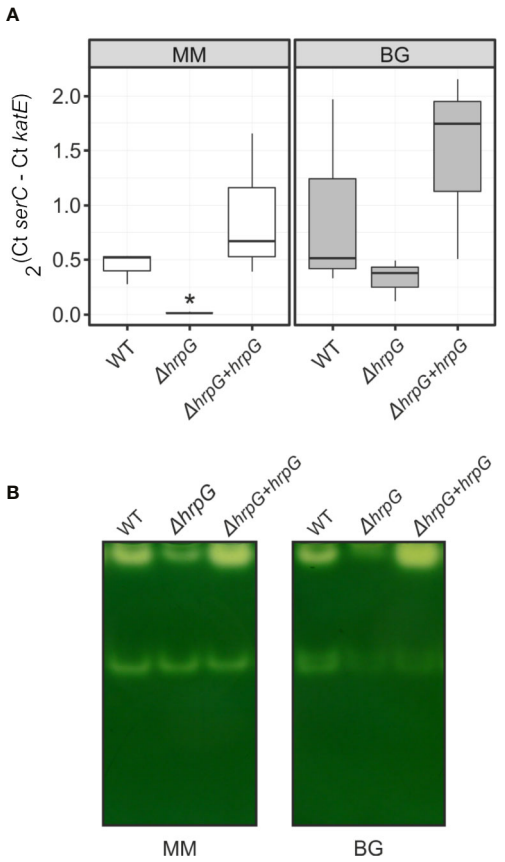

FIGURE 2 | Expression of *katE* in the wild-type (WT), *ΔhrpG* mutant, and complemented overexpressing (*ΔhrpG* + *hrpG*) strains. **(A)** mRNA levels of *katE* were measured by quantitative real-time PCR in RNAs extracted from *R. solanacearum* cells grown in rich BG or minimal medium supplemented with glutamate. In the Y-axis is represented the $2^{\Delta Ct}$ normalised expression from three biological replicas with two technical replicas each. The asterisk indicates the strain showing statistically significant differences to the other two strains tested in the same condition (95% Tukey HSD test). **(B)** Catalase activity patterns in native gels. Equal amounts of soluble proteins (25 μg) were separated by 8% non-denaturing PAGE and stained for catalase activity. A simultaneously run Coomassie-stained gel (not shown) indicated equal protein loadings between samples. This experiment was repeated three times with similar results.

cultures to a range of sub-lethal doses (25, 50, and 100 μM) of H_2O_2 for 1 h and the catalase activity patterns were compared to untreated control cultures on native polyacrylamide gels. As shown in **Figure 3A**, the activity of the two detected catalase bands increased upon H_2O_2 treatment, suggesting a clear induction of both isoforms under oxidative stress. To further evaluate the contribution of KatE to this response, we quantified the catalase activity levels in the wild type, the *ΔkatE* mutant and the complemented (*ΔkatE* + *katE*) strains grown in the conditions previously stated (**Figure 3B**). H_2O_2 treatment caused a ~5-fold increase of catalase activity in the wild-type strain, being this increment almost equivalent at all H_2O_2 concentrations tested. On the contrary, no catalase induction was observed in the *katE* mutant after peroxide exposure, suggesting an impaired ability to face the oxidative challenge.

Resistance of bacterial cells to lethal doses of H_2O_2 was then evaluated. As illustrated in **Figure 3C**, the *ΔkatE* mutant exhibited increased sensitivity to the oxidant compared to the parental wild-type strain, a phenotype that was more pronounced at higher H_2O_2 doses and maximal at the highest concentration tested (2.5 mM). Moreover, pre-adaptation of the cultures with a sub-lethal concentration of H_2O_2 (100 μM) led to a significant increase in the resistance of wild-type cells to an elevated dose (5 mM) of the agent (**Figure 3D**). This effect, commonly known as *adaptive response*, was not observed in the *ΔkatE* strain, which did not evidence higher tolerance to the oxidant after the adaptation treatment, reinforcing the notion that *katE* encodes the only catalase activity that contributes to bacterial adaptation to an oxidative environment.

Biofilm Formation Is Affected by the Deletion of *katE*

Bacterial antioxidant activities have been shown to influence biofilm formation (Kim et al., 2006; Simmons and Dybvig, 2015; Tondo et al., 2016). To analyze the structural characteristics of the *R. solanacearum* biofilm, we generated Green Fluorescent Protein (GFP)-labeled strain derivatives (**Table 1**) and observed their growth development on chambered cover glass slides by confocal laser scanning microscopy over a 5-day period. At two days post inoculation (dpi), formation of cell aggregates was apparent for the wild-type strain (**Figure 4A**), and a well-established biofilm with more complex structures was clearly observed at 5 dpi. In contrast, the *katE* mutant failed to form a structured biofilm after 5 days, exhibiting minor aggregation and reduced interstitial spaces. Besides observing the biofilm structure, we also quantified the amount of biofilm produced by measuring the intensity of crystal violet staining after growth on 96-well plates. As shown in **Figure 4B**, these experiments resulted in comparable quantities of biofilm in the wild type, the *katE* mutant and its genetically complemented derivative, demonstrating that KatE influences the development of biofilm structures but does not alter the overall amount of biofilm produced.

Pathogenicity Tests

As mentioned previously, *katE* transcription is activated by the master regulator of pathogenicity HrpG (**Figure 2**). In addition, our preliminary data show that *katE* from *R. solanacearum* strain UY031 is highly expressed when the bacterium grows in the plant apoplast and in the xylem (unpublished data). This information, together with our finding that catalase activity was key to survive oxidative stress led us to test whether it is required for *R. solanacearum* GMI1000 pathogenicity on tomato, its natural host. Plants of the susceptible tomato cultivar Marmande were inoculated with suspensions of the wild type, mutant, and complemented strains by soil drenching and symptom appearance was recorded over time (**Figure 5A**). No statistical differences in wilting symptoms in plants inoculated with the wild type, the *katE* disruption mutant or the complemented strain were observed in three biological replicas,

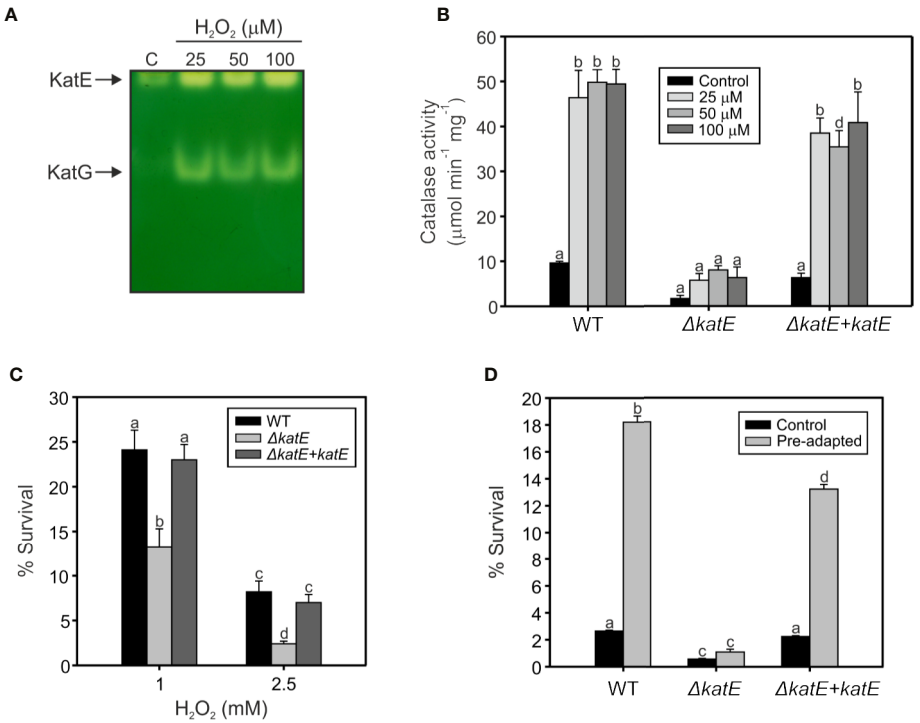

FIGURE 3 | Hydrogen peroxide response in wild type, the *ΔkatE* mutant, and its complemented counterpart. **(A)** Catalase activities detected after exposure to sub-lethal levels of hydrogen peroxide. Equal amounts (15 μg) of soluble protein extracts from early exponential phase cultures exposed to 25, 50, and 100 μM of H_2O_2 for 60 min, and from an untreated control (C), were separated on a native polyacrylamide gel stained for catalase activity. **(B)** Catalase activities quantified through H_2O_2 decomposition in soluble cell extracts obtained from cells treated as in A. **(C)** Sensitivity of *R. solanacearum* strains to 1 and 2.5 mM H_2O_2. Cells in early exponential phase of growth were exposed to the indicated concentrations of H_2O_2 for 15 min. The number of Colony Forming Units (CFU) was determined for each culture before and after the peroxide treatment by plating of appropriate dilutions. The percentage of survival is defined as the number of CFU after treatment divided by the number of CFU prior to H_2O_2 exposure ×100. **(D)** Sensitivity of pre-adapted cultures of WT, *ΔkatE*, and the complemented *ΔkatE* + *katE* strains to 5 mM H_2O_2. Exponential phase cultures were first adapted with 100 μM H_2O_2 for 60 min and then exposed to 5 mM H_2O_2 for 15 min. The number of CFU was determined for each culture before and after the 5 mM H_2O_2 treatment by plating of appropriate dilutions and percentage of survival calculated as the number of CFU after treatment divided by the number of CFU prior to treatment ×100. Data represent the mean and standard deviation of three independent experiments. Different letters indicate significant differences among strains and/or treatment according to the Tukey's multiple comparison test ($p<0.0001$).

suggesting no major role of the gene in the virulence of *R. solanacearum* GMI1000. The importance of apoplastic ROS led us to quantify whether bacterial fitness was affected during growth in this plant compartment. To this end, we infiltrated susceptible tomato leaves with solutions of the wild type, the *ΔkatE*, and the complemented strain and quantified bacterial concentrations in recovered leaf disk samples immediately after inoculation and at three days post inoculation (dpi). Results from a representative experiment are presented in **Figure 5B** and show that no differences in bacterial multiplication in the apoplast were observed for any of the three tested strains.

DISCUSSION

It has been shown that hydrogen peroxide is a central component of the oxidative burst during plant-pathogen interaction, as it accumulates in plants attacked by pathogenic microorganisms including fungi, bacteria and viruses (Baker and Orlandi, 1995; Wojtaszek, 1997). In this context, the antioxidant system adequacy by the invading microorganism must be fundamental to minimize the oxidative stress generated by the host plant, thus achieving the establishment of the infection. In this work, we demonstrated that monofunctional KatE and bifunctional KatG catalase activities can be detected in *R. solanacearum* soluble protein extracts using non-denaturing polyacrylamide gels (**Figure 1A**). Furthermore, a single mutant in the *katE* gene was generated and genetically complemented corroborating that the upper band revealed in the native gel corresponds to the KatE catalase.

We evaluated catalase activities during the different growth phases, detecting that the monofunctional catalase was induced during exponential growth (**Figures 1A, C**). These results collectively suggest that *katE* expression is growth phase regulated at the transcriptional level. Similar results were previously reported for other bacteria such as *E. coli, Xanthomonas campestris* pv. *campestris* and *Xanthomonas citri* subsp. *citri*, although the expression pattern of particular catalase isozymes may vary between species (Loewen, 1997; Vattanaviboon and Mongkolsuk,

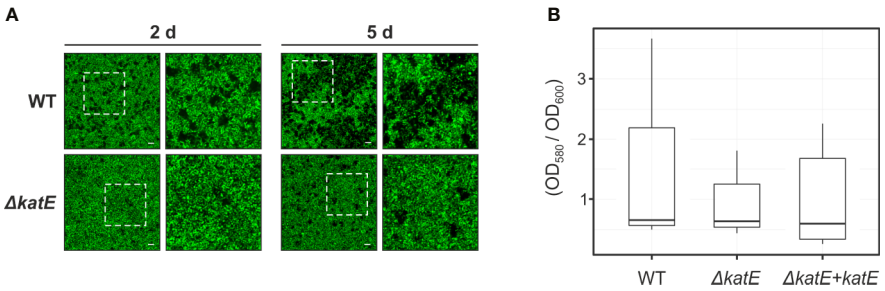

FIGURE 4 | Effect of *katE* disruption on *R. solanacearum* biofilm formation ability. **(A)** GFP-labeled wild-type and *ΔkatE* strains were grown on chambered cover slides and visualized under confocal laser scanning microscopy after 2 and 5 days of bacterial growth. Left panels show the biofilms developed at the bottom of the chambered cover slides with a magnification of 400X and right panels show a 2X zoom of the regions marked in the previous panels. Scale bars, 50 μm. **(B)** Biofilm quantification. Bacterial suspensions were grown for 24 h in 96 well plates at 30°C, stained with crystal violet and the biofilm was quantified as the OD_{580} normalized by the bacterial growth measured at OD_{600}. Boxplots of the values obtained per each tested strain from 5-6 biological replicas (N=5-6) are presented.

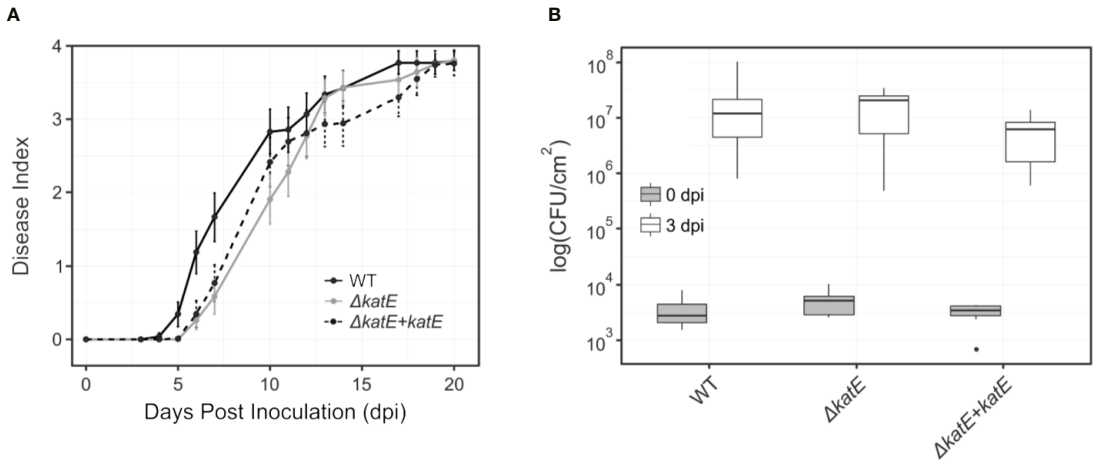

FIGURE 5 | Effect of *katE* in *R. solanacearum* virulence and fitness in the apoplast. **(A)** Bacterial pathogenicity assay on tomato. Wilting symptoms were recorded after soil-drench inoculation with the wild type *R. solanacearum* GMI1000 strain (black line), the *katE* disruption mutant derivative (grey line) and its complemented strain (dotted black line). Disease symptoms are plotted over time in a scale ranging from 0 (no symptoms) to 4 (wilted plant). Each data point represents the average of 20-25 plants and their standard errors. Three independent biological replicates were performed with similar results. **(B)** Bacterial growth in leave tissues. Tomato plants were vacuum infiltrated with 10^5 CFU/mL suspensions of GMI1000, the *katE* mutant, and the complemented strain. Leaf disks were sampled at day 0 and 3 post inoculation, and bacterial counts in the tissue were determined as CFU from plated dilutions normalized to the disk area sampled (N=3). All experiments were repeated three times with similar results.

2000; Tondo et al., 2010). In *X. citri* subsp. *citri*, *katE* gene was also regulated by growth phase but contrary to the pattern observed in *R. solanacearum*, it exhibited an strong induction in stationary phase cells (Tondo et al., 2010).

Our results show that *katE* is transcriptionally activated by HrpG but also responds to other inducing cues besides the growth phase, as shown by the higher transcriptional output observed upon growth in BG rich medium than in minimal medium, a condition known to induce HrpG activity (**Figure 2A**). This specific induction in rich medium independently of HrpG is corroborated by the high *katE* mRNA levels in the *ΔhrpG* mutant strain grown in this medium. Finally, *katE* expression seems to be controlled mostly at the transcriptional level, as the levels of the KatE enzyme mostly correlate with its mRNA abundance, although protein stability may be increased post-translationally in minimal medium, as indicated by the fact that it can be detected in the *ΔhrpG* mutant strain grown in this condition, where it shows minimal transcription levels (**Figures 2A, B**).

On the other hand, we studied the participation of the two *Ralstonia* catalases in the resistance against the oxidizing compound hydrogen peroxide. *R. solanacearum* exponential cultures were exposed to sub-lethal doses of peroxide, detecting

a clear induction of both catalase isoforms under oxidative stress (**Figure 3A**). These results are in agreement with those obtained by Florez-Cruz and Allen, who observed an OxyR-dependent induction of *katE* and *katG* mRNA levels after exposure to H_2O_2 (Flores-Cruz and Allen, 2009). Here, the contribution of KatE to this response was analyzed (**Figure 3B**). Quantification of *R. solanacearum* catalase activity in the *ΔkatE* mutant showed that it is almost residual and that its induction is undetectable (**Figure 3B**). The catalase activity was recovered in the complemented strain, where *katE* was reintroduced into the mutant background, and showing that KatE plays a significant role in the *R. solanacearum* protection to oxidative stress. To prove this, bacterial cultures were confronted to lethal doses of H_2O_2 detecting that the *ΔkatE* mutant was more susceptible to the oxidative compound than the wild type strain (**Figure 3C**). This is in agreement with the reported observations that disruption of the monofunctional catalase *katE* in *X. citri* subsp. *citri* and *katB* in *Pseudomonas syringae* pv. tomato DC3000 rendered these bacteria more susceptible to oxidative stress (Tondo et al., 2010; Guo et al., 2012). The other monofunctional catalase in *P. syringae* pv. tomato (KatE), which is clearly less induced by exposure to exogenous H_2O_2, also showed a minor role in resistance to the oxidative compound (Guo et al., 2012).

The adaptive response to oxidative agents has been previously proposed to play a fundamental role in plant-pathogen interactions, allowing bacteria to withstand increased oxidative stress conditions (Ausubel, 2005). Exposure to sub-lethal concentrations of oxidative stress agents usually have a priming effect on bacteria, which then tolerate higher doses of the same oxidant (adaptive response), and even others (cross-protection). These responses are due to the induction of numerous genes involved in oxidant removal and damage repair, including catalases (Demple, 1991; Tartaglia et al., 1991). Evaluation of this response in *R. solanacearum* showed that *katE* mutant does not significantly induce catalase activity upon treatment with low doses of H_2O_2 and its remained activity is not enough to protect bacteria against higher doses of the oxidant (**Figures 3B, D**). Consequently, even though KatG activity was found induced in peroxide-treated cultures according to in-gel catalase staining, our results suggest a minor role for the additional KatG catalases in the response to H_2O_2, being KatE the only catalase activity contributing to the bacterial adaptive response to an oxidative environment.

Our finding that KatE catalase activity was essential for survival in oxidative environments and the fact that ROS is a major player in plant defence responses (Wojtaszec, 1997; Flores-Cruz and Allen, 2009) led us to investigate its role in bacterial virulence. Surprisingly, we found no effect of the *katE* mutation on pathogenicity assays on tomato (**Figure 5A**). This could be due to the limited sensitivity of soil drench inoculation and disease scoring to detect minor differences in bacterial pathogenicity. An alternative explanation is that ROS accumulate mainly in the apoplast (Lamb and Dixon, 1997) and *R. solanacearum* grows mostly inside the xylem vessels of host plants. Thus, we measured the capacity of the bacterium to multiply in the tomato apoplast as a more quantitative measurement of its virulence and fitness. Again, disruption of *katE* did not cause any effect (**Figure 5B**). Although bacterial multiplication in the host is not always correlated with its aggressiveness (Angot et al., 2006), this result was somehow unexpected due to the important role played by the KatE catalase in *in vitro* protection to oxidative stress, a condition that is commonly encountered by bacteria inside the plant host (Lamb and Dixon, 1997).

In addition, the *katE* mutant strain did not show reduced ability to produce biofilms, another important trait for the wilting disease development (**Figure 4**). Biofilm-growing cells usually experience endogenous oxidative stress and many antioxidant systems were shown to be induced under this growth condition (Resch et al., 2005; Ram et al., 2005; Mikkelsen et al., 2007; Shanks et al., 2007; Chung et al., 2016). In fact, the role of catalase and superoxide dismutase in the development of mature biofilms was previously demonstrated in *X. citri* subsp. *citri* and *E. coli*, respectively (Kim et al., 2006; Tondo et al., 2016). According to our results, disruption of *katE* in *R. solanacearum* only alters the structure of the biofilm produced on an abiotic surface, but not the overall quantity of biofilm production. This is in agreement with previous reports indicating that perturbations of the physiological steady-state levels of ROS or the addition of catalase to the medium affects the quality and structural characteristics of the biofilms developed by *Azotobacter vinelandii* (Villa et al., 2012) and *Mycoplasma pneumoniae* (Simmons and Dybvig, 2015), with diverse effects on the amounts of biofilm produced.

However, the minor role that KatE seems to play *in planta* is in agreement with a previous screening for *R. solanacearum* genes essential for growth *in planta*, in which *katE* was not identified (Brown and Allen, 2004). The two possible explanations for the undetectable effect of *R. solanacearum katE* disruption on plant infection are, that ROS are not key players in the defence against this pathogen in tomato cv Marmande or that functional redundancy with other genes with catalase activity exists. The three catalases in *P. syringae* pv. tomato DC3000 are all plant induced and play non-redundant roles in virulence (Guo et al., 2012). Our results corroborate the hypothesis proposed by Guo *et al.* that catalases play different roles in each plant pathogen where they independently adapted to overcome the plant defensive production of H_2O_2. Our ongoing characterisation of the KatG catalases-peroxidases will be essential to shed light into this question.

DATA AVAILABILITY STATEMENT

All datasets presented in this study are included in the article/ **Supplementary Material**.

AUTHOR CONTRIBUTIONS

MLT, MV, and EO conceived and designed the work. MLT, RP-J, and AV performed the experiments. LP and RP-J contributed to

statistical analyses. EO and MV provided reagents and materials. All authors contributed to analysis and interpretation of results. MLT, RP-J, MV, and EO wrote the manuscript. All authors contributed to the article and approved the submitted version.

FUNDING

This work was supported by the Agencia Nacional de Promoción Científica y Tecnológica (ANPCyT PICT 2014-2487 to EO and PICT 2014-2485 to MLT) and the Spanish Ministry of Economy and Competitiveness (AGL2016-78002-R and PID2019-108595RB-I00 to MV). We also acknowledge financial support from the "Severo Ochoa Program for Centers of Excellence in R&D" (SEV/2015/0533), and the CERCA Program from the Catalan Government (Generalitat de Catalunya). The funders had no role in study design, data collection and analysis, decision to publish, or preparation of the manuscript. EO and MLT are staff members and AV is Fellow of the Consejo Nacional de Investigaciones Científicas y Técnicas (CONICET, Argentina).

ACKNOWLEDGMENTS

We are grateful to Núria S. Coll and the Bacterial Pathogens and Plant Cell Death Team (Center for Research in Agricultural Genomics, CRAG) for critical comments and Jordi Corral (Autonomous University of Barcelona) for useful suggestions. We also thank Rodrigo Vena (IBR-CONICET) for confocal microscopy analyses.

SUPPLEMENTARY MATERIAL

The Supplementary Material for this article can be found online at: https://www.frontiersin.org/articles/10.3389/fpls.2020.01156/full#supplementary-material

SUPPLEMENTARY FIGURE 1 | Growth curves of *R. solanacearum* GMI1000 wild-type (WT), *katE* mutant (*ΔkatE*) and complemented (*ΔkatE* + *katE*) strains in BG medium. *R. solanacearum* cultures were grown aerobically at 28°C with shaking at 200 rpm. Aliquots were taken at the indicated times and measured for colony-forming capacity by serial dilution and plating on BG-agar. Colonies were counted after 48 h incubation at 28°C.

REFERENCES

Allen, C., Prior, P., and Hayward, A. C. (2004). *Bacterial Wilt Disease and the Ralstonia solanacearum Species Complex* (St. Paul (Minnesota): American Phytopathological Society Press).

Angot, A., Peeters, N., Lechner, E., Vailleau, F., Baud, C., Gentzbittel, L., et al. (2006). *Ralstonia solanacearum* requires F-box-like domain-containing type III effectors to promote disease on several host plants. *Proc. Natl. Acad. Sci. U.S.A.* 103 (39), 14620–14625. doi: 10.1073/pnas.0509393103

Apel, K., and Hirt, H. (2004). Reactive oxygen species: metabolism, oxidative stress, and signal transduction. *Annu. Rev. Plant Biol.* 55, 373–399. doi: 10.1146/annurev.arplant.55.031903.141701

Ausubel, F. M., Brent, R., Kingston, R. E., Moore, D. D., Seidman, J. G., Smith, J. A., et al. (1994). *Current Protocols in Molecular Biology* (New York: John Wiley and Sons).

Ausubel, F. M. (2005). Are innate immune signaling pathways in plants and animals conserved? *Nat. Immunol.* 6, 973–979. doi: 10.1038/ni1253

Baker, C. J., and Orlandi, E. W. (1995). Active oxygen in plant pathogenesis. *Annu. Rev. Phytopathol.* 33, 299–321. doi: 10.1146/annurev.py.33.090195.001503

Beers, R. F. Jr, and Sizer, I. W. (1952). A spectrophotometric method for measuring the breakdown of hydrogen peroxide by catalase. *J. Biol. Chem.* 195, 133–140.

Boucher, C. A., Barberis, P. A., Trigalet, A. P., and Demery, D. A. (1985). Transposon mutagenesis of *Pseudomonas solanacearum*: Isolation of Tn5-induced avirulent mutants. *J. Gen. Microbiol.* 131, 2449–2457. doi: 10.1099/00221287-131-9-2449

Brown, D. G., and Allen, C. (2004). *Ralstonia solanacearum* genes induced during growth in tomato: an inside view of bacterial wilt. *Mol. Microbiol.* 53 (6), 1641–1660. doi: 10.1111/j.1365-2958.2004.04237.x

Chen, W. P., and Kuo, T. T. (1993). A simple and rapid method for the preparation of gram-negative genomic DNA. *Nucleic Acids Res.* 21, 2260. doi: 10.1093/nar/21.9.2260

Chung, C.-H., Fen, S., Yu, S.-C., and Wong, H. (2016). Influence of *oxyR* on growth, biofilm formation, and mobility of *Vibrio parahaemolyticus*. *Appl. Environ. Microbiol.* 82, 788–796. doi: 10.1128/AEM.02818-15

Demple, B. (1991). Regulation of bacterial oxidative stress genes. *Annu. Rev. Genet.* 25, 315–337. doi: 10.1146/annurev.ge.25.120191.001531

Denny, T. P. (2006). "Plant pathogenic Ralstonia species," in *Plant-Associated Bacteria*. Ed. S. S. Gnanamanickam (Dordrecht, The Netherlands: Springer), 573–644.

Flores-Cruz, Z., and Allen, C. (2009). *Ralstonia solanacearum* encounters an oxidative environment during tomato infection. *Mol. Plant-Microbe Interact.* 22, 773–782. doi: 10.1094/MPMI-22-7-0773

Flores-Cruz, Z., and Allen, C. (2011). Necessity of OxyR for the hydrogen peroxide stress response and full virulence in *Ralstonia solanacearum*. *Appl. Environ. Microbiol.* 77, 6426–6432. doi: 10.1128/AEM.05813-11

Genin, S., and Denny, T. P. (2012). Pathogenomics of the *Ralstonia solanacearum* species complex. *Annu. Rev. Phytopathol.* 50, 67–89. doi: 10.1146/annurev-phyto-081211-173000

Guo, M., Block, A., Bryan, C. D., Becker, D. F., and Alfano, J. R. (2012). *Pseudomonas syringae* catalases are collectively required for plant pathogenesis. *J. Bacteriol.* 194, 5054–5064. doi: 10.1128/JB.00999-12

Jittawuttipoka, T., Buranajitpakorn, S., Vattanaviboon, P., and Mongkolsuk, S. (2009). The catalase-peroxidase KatG is required for virulence of *Xanthomonas campestris* pv. campestris in a host plant by providing protection against low levels of H_2O_2. *J. Bacteriol.* 191, 7372–7377. doi: 10.1128/JB.00788-09

Kang, K.-S., Lim, C.-J., Han, T.-J., Kim, J.-C., and Jin, C.-D. (1999). Changes in the isozyme composition of antioxidant enzymes in response to aminotriazole in leaves of *Arabidopsis thaliana*. *J. Plant Biol.* 42, 187–193. doi: 10.1007/BF03030477

Kelman, A. (1954). The relationship of pathogenicity of *Pseudomonas solanacearum* to colony appearance in tetrazolium medium. *Phytopathology* 44, 693–695.

Kim, Y. H., Lee, Y., Kim, S., Yeom, J., Yeom, S., Seok, K. B., et al. (2006). The role of periplasmic antioxidant enzymes (superoxide dismutase and thiol peroxidase) of the Shiga toxin-producing *Escherichia coli* O157:H7 in the formation of biofilms. *Proteomics* 6, 6181–6193. doi: 10.1002/pmic.200600320

Lamb, C., and Dixon, R. A. (1997). The oxidative burst in plant disease resistance. *Annu. Rev. Plant Physiol. Plant Mol. Biol.* 48, 251–275. doi: 10.1146/annurev.arplant.48.1.251

Lee, B., Haagensen, J. A., Ciofu, O., Andersen, J. B., Hoiby, N., and Molin, S. (2005). Heterogeneity of biofilms formed by nonmucoid *Pseudomonas aeruginosa* isolates from patients with cystic fibrosis. *J. Clin. Microbiol.* 43, 5247–5255. doi: 10.1128/JCM.43.10.5247-5255.2005

Loewen, P. C. (1997). "Bacterial catalases," in *Oxidative Stress and the Molecular Biology of Antioxidant Defenses*. Ed. J. G. Scandalios (New York: Cold Spring Harbor Laboratory Press), 273–308.

Mandal, S., Das, R. K., and Mishra, S. (2011). Differential occurrence of oxidative burst and antioxidative mechanism in compatible and incompatible interactions of *Solanum lycopersicum* and *Ralstonia solanacearum*. *Plant Physiol. Biochem.* 49 (2), 117–123. doi: 10.1016/j.plaphy.2010.10.006

Marx, C. J., and Lidstrom, M. E. (2002). Broad-host-range *cre-lox* system for antibiotic marker recycling in Gram-negative bacteria. *Biotechniques* 33 (5), 1062–1067. doi: 10.2144/02335rr01

Mikkelsen, H., Duck, Z., Lilley, K. S., and Welch, M. (2007). Interrelationships between colonies, biofilms, and planktonic cells of *Pseudomonas aeruginosa*. *J. Bacteriol.* 189, 2411–2416. doi: 10.1128/JB.01687-06

Mishra, S., and Imlay, J. (2012). Why do bacteria use so many enzymes to scavenge hydrogen peroxide? *Arch. Biochem. Biophys.* 525 (2), 145–160. doi: 10.1016/j.abb.2012.04.014

Monteiro, F., Genin, S., van Dijk, I., and Valls, M. (2012a). A luminescent reporter evidences active expression of *Ralstonia solanacearum* type III secretion system genes throughout plant infection. *Microbiology* 158, 2107–2116. doi: 10.1099/mic.0.058610-0

Monteiro, F., Solé, M., van Dijk, I., and Valls, M. (2012b). A chromosomal insertion toolbox for promoter probing, mutant complementation, and pathogenicity studies in *Ralstonia solanacearum*. *Mol. Plant-Microbe Interact.* 25, 557–568. doi: 10.1094/MPMI-07-11-0201

Okinaka, Y., Yang, C.-H., Perna, N. T., and Keen, N. T. (2002). Microarray profiling of *Erwinia chrysanthemi* 3937 genes that are regulated during plant infection. *Mol. Plant-Microbe Interact.* 15, 619–629. doi: 10.1094/MPMI.2002.15.7.619

Peeters, N., Guidot, A., Vailleau, F., and Valls, M. (2013). *Ralstonia solanacearum*, a widespread bacterial plant pathogen in the post-genomic era. *Mol. Plant Pathol.* 14 (7), 651–662. doi: 10.1111/mpp.12038

Peng, M., and Kuc, J. (1992). Peroxidase-generated hydrogen peroxide as a source of antifungal activity *in vitro* and on tobacco leaf disks. *Phytopathology* 82, 696–699. doi: 10.1094/Phyto-82-696

Plener, L., Manfredi, P., Valls, M., and Genin, S. (2010). PrhG, a transcriptional regulator responding to growth conditions, is involved in the control of the type III secretion system regulon in *Ralstonia solanacearum*. *J. Bacteriol.* 192, 1011–1019. doi: 10.1128/JB.01189-09

Puigvert, M., Guarischi-Sousa, R., Zuluaga, P., Coll, N. S., Macho, A. P., Setubal, J. C., et al. (2017). Transcriptomes of *Ralstonia solanacearum* during root colonization of *Solanum commersonii*. *Front. Plant Sci.* 8, 370. doi: 10.3389/fpls.2017.00370

Ram, R. J., Verberkmoes, N. C., Thelen, M. P., Tyson, G. W., Baker, B. J., Blake, R. C., et al. (2005). Community proteomics of a natural microbial biofilm. *Science* 308, 1915–1920. doi: 10.1126/science.1109070

Resch, A., Rosenstein, R., Nerz, C., and Gotz, F. (2005). Differential gene expression profiling of *Staphylococcus aureus* cultivated under biofilm and planktonic conditions. *Appl. Environ. Microbiol.* 71, 2663–2676. doi: 10.1128/AEM.71.5.2663-2676.2005

Saenkham, P., Eiamphungporn, W., Farrand, S., Vattanaviboon, P., and Mongkolsuk, S. (2007). Multiple superoxide dismutases in *Agrobacterium tumefaciens*: functional analysis, gene regulation, and influence on tumorigenesis. *J. Bacteriol.* 189, 8807–8817. doi: 10.1128/JB.00960-07

Salanoubat, M., Genin, S., Artiguenave, F., Gouzy, J., Mangenot, S., Arlat, M., et al. (2002). Genome sequence of the plant pathogen *Ralstonia solanacearum*. *Nature* 415, 497–502. doi: 10.1038/415497a

Sambrook, J., and Russell, D. W. (2001). *Molecular Cloning: A Laboratory Manual* (New York: Cold Spring Harbor Laboratory Press).

Santos, R., Franza, T., Laporte, M. L., Sauvage, C., Touati, D., and Expert, D. (2001). Essential role of superoxide dismutase on the pathogenicity of *Erwinia chrysanthemi* strain 3937. *Mol. Plant-Microbe Interact.* 14, 758–767. doi: 10.1094/MPMI.2001.14.6.758

Scandalios, J. G. (1968). Genetic control of multiple molecular forms of catalase in maize. *Ann. N. Y. Acad. Sci.* 151, 274–293. doi: 10.1111/j.1749-6632.1968.tb11896.x

Sedmak, J. J., and Grossberg, S. E. (1977). A rapid, sensitive, and versatile assay for protein using Coomassie brilliant blue G250. *Anal. Biochem.* 79, 544–552. doi: 10.1016/0003-2697(77)90428-6

Shanks, R. M., Stella, N. A., Kalivoda, E. J., Doe, M. R., O'Dee, D. M., Lathrop, K. L., et al. (2007). A *Serratia marcescens* OxyR homolog mediates surface attachment and biofilm formation. *J. Bacteriol.* 189, 7262–7272. doi: 10.1128/JB.00859-07

Simmons, W. L., and Dybvig, K. (2015). Catalase enhances growth and biofilm production of *Mycoplasma pneumoniae*. *Curr. Microbiol.* 71 (2), 190–194. doi: 10.1007/s00284-015-0822-x

Smith, S. G., Wilson, T. J., Dow, J. M., and Daniels, M. J. (1996). A gene for superoxide dismutase from *Xanthomonas campestris* pv. campestris and its expression during bacterial-plant interactions. *Mol. Plant-Microbe Interact.* 9, 584–593. doi: 10.1094/mpmi-9-0584

Tamir-Ariel, D., Navon, N., and Burdman, S. (2007). Identification of genes in *Xanthomonas campestris* pv. vesicatoria induced during its interaction with tomato. *J. Bacteriol.* 189, 6359–6371. doi: 10.1128/JB.00320-07

Tartaglia, L. A., Storz, G., Farr, S. B., and Ames, B. N. (1991). "The bacterial adaptation to hydrogen peroxide stress," in *Oxidative stress, oxidants and antioxidant*. Ed. H. Sies (New York: Academic Press), 155–169.

Tondo, M. L., Petrocelli, S., Ottado, J., and Orellano, E. G. (2010). The monofunctional catalase KatE of *Xanthomonas axonopodis* pv. citri is required for full virulence in citrus plants. *PloS One* 5 (5), e10803. doi: 10.1371/journal.pone.0010803

Tondo, M. L., Delprato, M. L., Kraiselburd, I., Fernández Zenoff, M. V., Farías, M. E., and Orellano, E. G. (2016). KatG, the bifunctional catalase of *Xanthomonas citri* subsp. citri, responds to hydrogen peroxide and contributes to epiphytic survival on citrus leaves. *PloS One* 11 (3), e0151657. doi: 10.1371/journal.pone.0151657

Valls, M., Genin, S., and Boucher, C. (2006). Integrated regulation of the type III secretion system and other virulence determinants in *Ralstonia solanacearum*. *PloS Pathog.* 2 (8), e82. doi: 10.1371/journal.ppat.0020082

Vattanaviboon, P., and Mongkolsuk, S. (2000). Expression analysis and characterization of the mutant of a growth-phase- and starvation-regulated monofunctional catalase gene from *Xanthomonas campestris* pv. phaseoli. *Gene* 241, 259–265. doi: 10.1016/s0378-1119(99)00483-7

Villa, F., Remelli, W., Forlani, F., Gambino, M., Landini, P., and Cappitelli, F. (2012). Effects of chronic sub-lethal oxidative stress on biofilm formation by *Azotobacter vinelandii*. *Biofouling* 28 (8), 823–833. doi: 10.1080/08927014.2012.715285

Wojtaszek, P. (1997). Oxidative burst: an early plant response to pathogen infection. *Biochem. J.* 322 (3), 681–692. doi: 10.1042/bj3220681

Zámocky, M., Gasselhuber, B., Furtmüller, P. G., and Obinger, C. (2012). Molecular evolution of hydrogen peroxide degrading enzymes. *Arch. Biochem. Biophys.* 525 (2), 131–144. doi: 10.1016/j.abb.2012.01.017

Conflict of Interest: The authors declare that the research was conducted in the absence of any commercial or financial relationships that could be construed as a potential conflict of interest.

frontiers in Microbiology

ORIGINAL RESEARCH
published: 21 August 2020
doi: 10.3389/fmicb.2020.01978

Sound Vibration-Triggered Epigenetic Modulation Induces Plant Root Immunity Against *Ralstonia solanacearum*

Jihye Jung[1,2†], Seon-Kyu Kim[3†], Sung-Hee Jung[1,4], Mi-Jeong Jeong[5] and Choong-Min Ryu[1,4*]*

[1] Molecular Phytobacteriology Laboratory, Korea Research Institute of Bioscience and Biotechnology (KRIBB), Daejeon, South Korea, [2] Department of Biological Sciences, Korea Advanced Institute of Science and Technology (KAIST), Daejeon, South Korea, [3] Personalized Genomic Medicine Research Center, Korea Research Institute of Bioscience and Biotechnology (KRIBB), Daejeon, South Korea, [4] Biosystems and Bioengineering Program, University of Science and Technology, Daejeon, South Korea, [5] National Institute of Agricultural Science, Rural Development Administration, Wanju, South Korea

OPEN ACCESS

Edited by:
Marc Valls,
University of Barcelona, Spain

Reviewed by:
Gabriele Berg,
Graz University of Technology, Austria
Jia-He Wu,
Institute of Microbiology (CAS), China
Cris Argueso,
Colorado State University, United States

***Correspondence:**
Mi-Jeong Jeong
center1097@korea.kr
Choong-Min Ryu
cmryu@kribb.re.kr

[†] These authors have contributed equally to this work

Specialty section:
This article was submitted to Microbe and Virus Interactions with Plants, a section of the journal Frontiers in Microbiology

Received: 24 December 2019
Accepted: 27 July 2020
Published: 21 August 2020

Citation:
Jung J, Kim S-K, Jung S-H, Jeong M-J and Ryu C-M (2020) Sound Vibration-Triggered Epigenetic Modulation Induces Plant Root Immunity Against Ralstonia solanacearum. Front. Microbiol. 11:1978. doi: 10.3389/fmicb.2020.01978

Sound vibration (SV) is one of the several environmental stimuli that induce physiological changes in plants including changes in plant immunity. Immune activation is a complicated process involving epigenetic modifications, however, SV-induced epigenetic modifications remain unexplored. Here, we performed an integrative analysis comprising chromatin immunoprecipitation (ChIP) and microRNA sequencing (miRNA-seq) to understand the role of SV-mediated epigenetic modifications in immune activation in *Arabidopsis thaliana* against the root pathogen *Ralstonia solanacearum*. Plants exposed to SV (10 kHz) showed abundant H3K27me3 modification in the promoter regions of aliphatic glucosinolate biosynthesis and cytokinin signaling genes, leading to transcriptional changes that promote immunity. Additionally, 10 kHz SV down-regulated *miR397b* expression, thus activating three target *LACCASE* transcripts that mediate cell wall reinforcement via lignin accumulation. Taken together, SV triggers epigenetic modification of genes involved in secondary metabolite biosynthesis, defense hormone signaling, and pre-formed defense in *A. thaliana*, leading to the activation of plant immunity against *R. solanacearum*.

Keywords: epigenetics, ChIP-seq, miRNA-seq, RNA-seq, sound vibration, plant immunity, *Ralstonia solanacearum*

INTRODUCTION

Being sessile, plants have to withstand various harsh environmental conditions such as wind, rain, and pathogen invasion (Basu and Haswell, 2017). Sound vibration (SV) is one of the natural stimuli that induce physiological changes in plants (Jung et al., 2018). Recent studies show that SV increases disease resistance in plants. In *Arabidopsis thaliana,* it has been shown that the chewing sound of an insect causes increased production of plant immunity-related chemicals such as glucosinolates (GSs) and anthocyanins (Appel and Cocroft, 2014). In addition, exposure of *Arabidopsis* plants to 500 Hz of SV has been shown to increase the production of plant defense-related hormones such as

salicylic acid and jasmonic acid (Ghosh et al., 2016). In tomato (*Solanum lycopersicum*), 0.08–2 kHz SV treatment decreases the population of multiple pests and pathogens, including spider mites, aphids, viruses, and gray mold, in the greenhouse (Tianzhen et al., 2009; Hassanien et al., 2014).

Besides physiological changes, SV also causes transcriptional changes in genes involved in plant immunity. Recently, microarray analysis suggested that *Arabidopsis* plants pre-exposed to 1 kHz SV showed induced resistance against *Botrytis cinerea* and transcriptional changes in defense-related genes (Choi et al., 2017). However, studies investigating the effect of SV on plant immunity are generally limited to insects and fungi, and lack research on the transcriptome. Enhancement of the plant immune system via transcriptional changes involves a complex epigenetic regulatory network comprising modification of chromatin (histone proteins and DNA) and modulation of small RNAs [short interfering RNAs (siRNAs) and microRNAs (miRNAs)] (Vaucheret, 2006; Kouzarides, 2007; Kaikkonen et al., 2011; Gan et al., 2013; Catalanotto et al., 2016). Many studies have investigated epigenetic changes in defense-related genes due to histone modifications (Mengel et al., 2017; Ramirez-Prado et al., 2018b). For instance, hyperacetylation of histone H3 lysine (K) residue at amino acid position 9 or 14 (H3K9/14) activates stress-responsive genes in *Arabidopsis* (Mengel et al., 2017). Similarly, H3K9 acetylation (H3K9ac) induces the expression of defense-related genes such as *PR1*, *WRKY46*, and *WRKY53* (Ramirez-Prado et al., 2018a). Therefore, chromatin immunoprecipitation (ChIP) assay using specific histone modification markers could help to understand the epigenetic mechanisms underlying defense-related gene regulation (Park, 2009).

Gene transcription is also regulated by miRNAs (Vaucheret, 2006). For example, *miR393* and *miR160* promote immunity against *Pseudomonas syringae* pv. tomato DC3000 in *Arabidopsis* by suppressing the expression of genes encoding F-box auxin receptors and auxin response factors (ARFs), respectively. Nucleotide-binding site leucine-rich repeat (NBS-LRR) receptor proteins, another component of the plant innate immune system, recognize species-specific pathogen effectors, resulting in effector-triggered immunity (ETI) (Jones and Dangl, 2006; Zhang et al., 2019). Notably, miRNA-modulated *NBS-LRR* genes have been reported in various plant species such as *Arabidopsis*, alfalfa (*Medicago truncatula*), peanut (*Arachis hypogea*), tobacco (*Nicotiana tabacum*), and tomato (Zhai et al., 2011; Boccara et al., 2014; Zhang et al., 2019).

The soil-borne root pathogen, *Ralstonia solanacearum*, infects more than 200 plant species worldwide, causing enormous losses in crop yield (Lowe-Power et al., 2016; Lopes and Rossato, 2018). *R. solanacearum* enters the plant through root hairs and colonizes the stem tissue. Exopolysaccharides secreted by *R. solanacearum* directly cause wilting by physically blocking water flow in the densely colonized xylem vessels of the infected host. To date, no effective control strategies have been developed to control the spread of *R. solanacearum*. In the current study, we attempted to assess the epigenetic changes during SV-mediated immunity in plant roots. Although epigenetic changes in plant immunity are important, the effect of SV on these changes has not yet been reported. Here, we identified a specific frequency of SV that increases plant immunity against *R. solanacearum*. To understand the regulatory mechanisms of epigenetic changes required for the activation of plant immunity, we employed ChIP-seq, RNA-seq, and miRNA-seq. Our results provide strong evidence showing that SV is an effective physical trigger to induce resistance against *R. solanacearum* via epigenetic regulation of secondary metabolites and defense hormones, leading to SV-activated defenses. This is the first report of SV-mediated epigenetic modification of plant immunity-related genes.

MATERIALS AND METHODS

Plant Material and SV Treatment

Arabidopsis thaliana ecotype Columbia (Col-0) and *dcl2/4*, *rdr2-1/6-15*, *cyp79, cyp83, sur1, ahk2, ahk2/3*, and *cre1* mutants were used in this study. Plants were grown in pots containing soil at 23°C under a 15 h light/9 h dark photoperiod. After 12–14 days, plants were transferred to a plant culture incubator (23°C, 15 h light/9 h dark) for SV treatment. Plants were exposed to SV (0.2, 1, 5, 10, 15, and 20 kHz) at 90 dB every 3 h for 10 days using the Pro Tools M-Powered software (Avid Technology, Burlington, MA, United States) (**Figure 1A**). Background noise was ∼40 dB in the silencing box. After inoculation with *Ralstonia solanacearum*, plants were transferred to a plant culture incubator maintained at 30°C and a 12 h light/12 h dark photoperiod for monitoring disease progression.

Pathogen Inoculation and Disease Severity Assay

R. solanacearum GMI1000 was cultured on CPG (1 g/L casein, 10 g/L peptone, and 5 g/L glucose) agar medium for 1 day. A colony was picked and cultured in CPG broth for 8–10 h. A 2% volume of seed culture was inoculated in CPG broth and cultured for 20 h. The culture was then centrifuged at 8,000 rpm for 10 min. The pellet was resuspended in 10 mM $MgCl_2$ prepared in sterilized distilled water (SDW). Each plant was drenched with 10 mL (5×10^7 cells/mL) of the pathogen suspension. Disease severity was measured daily on a scale from 0 to 5 (0, no symptoms; 1, < 50% of rosette leaves wilted; 2, < 100% of rosette leaves wilted; 3, 100% of rosette leaves wilted; 4, 100% of rosette leaves wilted and stems partially wilted; 5, complete plant collapse). A drench application of 10 mL 0.3 mM benzothiadiazole (BTH) 3 days before pathogen inoculation was used as a positive control.

Chromatin Immunoprecipitation (ChIP) and Quantitative PCR (qPCR)

ChIP experiments were conducted, as described previously, with minor modifications (Yamaguchi et al., 2014). Roots of five plants were pooling for one replication and three replication were used ($n = (3)$. Each sample was immediately immersed in 1X phosphate buffered-saline (PBS). Roots were vacuum infiltrated with 1% formaldehyde in PBS for 15 min. Crosslinking reactions were quenched with 0.125 M glycine, and samples were washed with cold PBS. Samples were then ground in liquid nitrogen and solubilized in nuclei lysis buffer ([50 mM HEPES

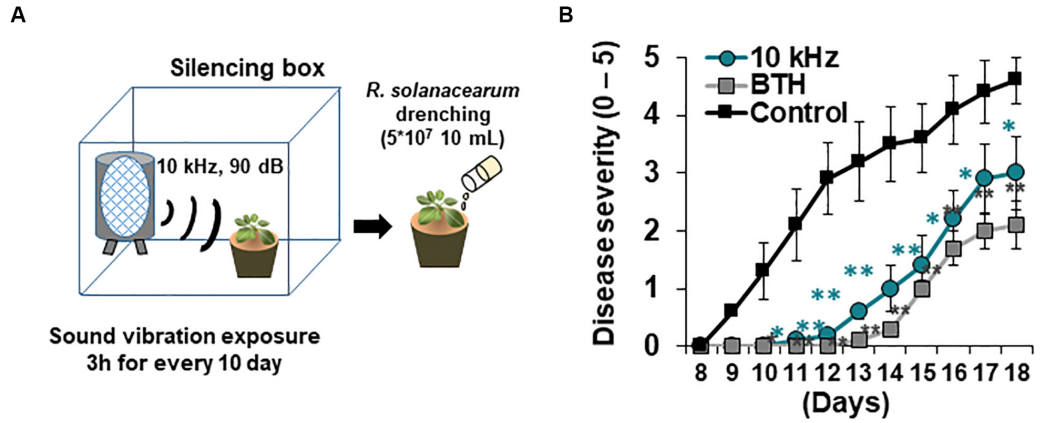

FIGURE 1 | Elicitation of induced resistance by 10 kHz sound vibration (SV) application in *Arabidopsis thaliana* plants against a soil-borne bacterial pathogen, *Ralstonia solanacearum*. **(A)** Schematic representation of SV treatment and *R. solanacearum* GMI1000 inoculation. **(B)** Disease severity in SV (10 kHz)-treated, benzothiadiazole (BTH)-treated, and control plants during disease progression. Disease severity was scored on a scale of 0 (no symptoms) to 5 (complete plant collapse). Data represent mean ± standard error (SE; $n = 10$; $^{*}p < 0.05$; $^{**}p < 0.01$).

[(pH 7.5]), 150 mM NaCl, 1% Triton X-100, 0.1% sodium deoxycholate, 0.1% SDS, and protease inhibitor).]. Chromatin was sheared to 0.1–1 kb fragments using a sonicator (Covaris M220) at 10% amplitude and 4°C temperature. The sheared chromatin was harvested after centrifugation at 14,000 rpm for 10 min. The supernatant was pre-cleared with 40 μL Dynabeads Protein A/G (1001D, 1003D; Invitrogen) at 4°C for 2 h with rotation. The pre-cleared samples were incubated overnight with 2 μL anti-H3k27me3 or anti-H3k36ac antibody (07-449, 07-540; Milipore). The supernatant was mixed with 40 μL Dynabeads Protein A/G for 4 h with rotation. The beads were washed with nuclei lysis buffer, followed by low-salt buffer ([20 mM Tris-Cl [(pH 8.0]), 150 mM NaCl, 2 mM EDTA, 1% Triton X-100, and 0.1% SDS),], high-salt buffer ([20 mM Tris-Cl [(pH 8.0]), 500 mM NaCl, 2 mM EDTA, 1% Triton X-100, and 0.1% SDS),], LNDET buffer ([0.25 M LiCl, 1% Nonidet Non-idet P-40, 1% deoxycholic acid, 1 mM EDTA, and 10 mM Tris-Cl [(pH 8.0])))], and TE buffer (pH 8.0). Samples were eluted twice using 100 (μL elution buffer (0.1 M NaHCO3 and 1% SDS) for 30 min at 65°C. The eluates were incubated overnight with 12 (μL 5 M NaCl and 1 (μL protease K at 65°C for reverse crosslinking. Finally, the samples were purified using MinElute Reaction Cleanup Kit (28204; Qiagen) for ChIP-seq analysis. To determine gene expression, 0.3 μg purified DNA and 2 μg input DNA (control) were subjected to qPCR using sequence-specific primers (**Supplementary Table S6**).

ChIP-Seq and Data Analysis

Genomic DNA libraries (insert size: 250–400 bp) were generated from the input and immunoprecipitated DNA and sequenced using Illumina HiSeq2500 to generate 100 bp paired-end reads. The sequenced reads were aligned to the *Arabidopsis* reference genome sequence (TAIR10) using Bowtie2 (v.2.2.2). The identification, estimation, and annotation of ChIP-seq peaks were carried out using the Homer (v.4.10) platform (Zhang et al., 2008).

Total RNA Isolation and qPCR

The roots of five plants were pooled together for each replicate ($n = 3$–4). The harvested roots were immediately washed with water to remove soil and other debris, and frozen in liquid nitrogen. Total RNA extraction and qPCR were conducted, as described previously, with a minor modification (Tata et al., 2016). The primers used in qPCR analysis are listed in **Supplementary Table S6**.

RNA-Seq and Data Analysis

Total RNA was isolated from *Arabidopsis* roots using the RNeasy Mini Kit (Qiagen), according to the manufacturer's instructions. The quality and integrity of total RNA were confirmed by agarose gel electrophoresis and ethidium bromide staining, followed by a visual examination of RNA under ultraviolet light. RNA-seq library was prepared using the TruSeq RNA Sample Prep Kit v2 (Illumina, San Diego, CA, United States) and sequenced on the Illumina Hiseq2500 platform to generate 100 bp paired-end reads. Reads were quantified and mapped to the *Arabidopsis* reference genome (TAIR10) using the STAR software (Dobin et al., 2013). Differentially expressed genes (DEGs) were selected from the RNA-seq count data using the edgeR package (Robinson et al., 2010). Counts per million (CPM) mapped reads in each sample were used to estimate the expression level of each gene. Enrichment analysis was performed using DAVID, and data were visualized using ReviGO ($p < 0.05$).

Small RNA-Seq and Data Analysis

Small RNA-seq libraries were constructed as described previously (Lu et al., 2007), with minor modifications. Total RNA was isolated using the mirVana miRNA Isolation Kit (Ambion). Small RNAs (20–30 nt) were separated on a 15% Novex TBE-Urea gel (Invitrogen) and purified. The purified small RNAs were ligated first with the 5′ RNA adapter and then with the 3′ RNA adapter provided in the TruSeq Small RNA Library Prep Kit (Illumina). At each step, the ligated product

was subjected to polyacrylamide gel electrophoresis (PAGE) and gel purified. After first-strand synthesis and 11 cycles of PCR amplification, the product was separated by PAGE, gel purified, and submitted for sequencing on the Illumina NextSeq500 platform. Adapter sequences were removed from the raw sequences using Trimommatic (v.0.33), and then the cleaned sequences were mapped onto the *Arabidopsis* reference genome (TAIR10) using bowtie2 (v.2.2.2). The quantification and statistical analysis of mapped reads were carried out using HTSeq (Kim et al., 2013; Anders et al., 2015) and edgeR (Robinson et al., 2010) packages, respectively.

Prediction of miRNA Targets and Generation of Heatmaps

Targets of the identified miRNAs were predicted based on the *Arabidopsis* reference genome (TAIR10 from the JGI genomic project, Phytozome 11) using target prediction software.[1] Targets with < 3 expectation were selected according to the following parameters: (1) less than two mismatches in the seed region (2–13 nt) between miRNA and the target; (2) a penalty of 0.5 for G–U mismatches and of 1 for other mismatches; (3) a penalty of 1.5 for extra weight in the seed region; and (4) a penalty of 2 and 0.5 for opening gap and extending gap, respectively. Heatmaps for miRNAs and target genes were constructed using the R software (version 3.5.2).

Lignin Quantification

Lignin was quantified as described previously (Schenk and Schikora, 2015), with a minor modification. Approximately 25–50 *Arabidopsis* roots (3–9 mg) per treatment were harvested and freeze-dried for 1 day. One milliliter of 80% methanol was added to the samples, followed by incubation at 25°C for 1 h. Next, the samples were centrifuged at 1,300 × *g* for 10 min, and supernatants were discarded. The pellets were washed with 1 mL 80% methanol, followed by SDW and acetone. To conduct alkaline hydrolysis, the pellets were incubated in 1 mL 1 M NaOH at 80°C for 1 h and subsequently overnight at room temperature. On the next day, 100 (μL of 86% phosphoric acid and 500 L of ethyl acetate were added to the samples and incubated on a rotary shaker at 25°C for 30 min. The samples were centrifuged at 1,300 × *g* for 5 min, and supernatants were discarded. To extract lignin, 500 μL of 80% methanol was added to the pellets, and the samples were centrifuged at 1,300 × *g* for 10 min. The pellets were first washed with 1 mL 80% methanol, followed by SDW and acetone, and then dried in a SpeedVac for 10 min. Next, 1.5 mL 2 M HCl and 0.3 mL thioglycolic acid were added to the dried pellets, and the samples were incubated on a shaker at 95°C for 4 h. Samples were cooled briefly on ice and then centrifuged at 13,000 × *g* for 5 min. The pellets were washed with SDW twice and centrifuged at 13,000 × *g* for 10 min. The residues were incubated with 1 mL 0.5 M NaOH overnight on a shaker. On the next day, samples were centrifuged at 13,000 × *g* for 5 min, and supernatants were collected. Then, 0.5 mL NaOH was added to the pellets, and samples were centrifuged at 13,000 × *g* for 5 min. Supernatants were combined and acidified with 300 μL 32% HCl. Samples were incubated on a shaker at 4°C for 4 h and then centrifuged at 13,000 × *g* for 5 min. The lignin pellet was dissolved in 100–200 μL 0.5 M NaOH. A standard curve (alkali, 2-hydroxy-proyl ether, Aldrich 370967) was generated for sample quantification, and lignin content was determined by measuring the absorbance at 340 nm and expressed as μg alkali lignin mg^{-1} dry root.

Statistical Analysis

To estimate the statistical significance of differences in gene expression data obtained by RNA-seq or small RNA-seq, DEGs were identified based on count data using an EdgeR package that uses a negative binomial model. The gene count dispersion was estimated using the adjusted profile likelihood method of Cox and Reid. After model fitting and dispersion estimation, DEGs were selected using a generalized linear model (GLM) likelihood ratio test that specifies probability distributions according to the mean-variance relationship. The GLM likelihood ratio test is based on the principle of fitting negative binomial GLMs with Cox-Reid dispersion estimates. Expression level differences in genes were considered statistically significant if the *P-value* was < 0.05 and the fold difference in expression between two sample groups was ≥ 1.5. To detect differentially bound peaks between two sample groups in ChIP-seq data, we used the Homer software platform, which adopts a cumulative Poisson distribution. In this test, differences in ChIP-seq peaks were considered statistically significant if the Poisson enrichment *P-value* over the background tag count was 0.0001 and fold enrichment over the background tag count was 4. To identify significant gene sets associated with biological processes, functional enrichment analysis was conducted using the DAVID software, in which the significance of over-represented gene sets was estimated by Fisher's Exact test ($P < 0.05$). The experimental data sets were subjected to the analysis of variance (ANOVA) using the JMP software (version 5.0; SAS Institute, Inc., Cary, NC, United States). Significant effects of treatments were determined based on the magnitude of the *F*-value ($P = 0.05$). When a significant F-test was obtained, separation of means was accomplished by Fisher's protected least significant difference (LSD) test ($P = 0.05$).

RESULTS

SV Treatment Triggers Induced Resistance Against *R. solanacearum* in Arabidopsis

Aboveground plant parts of *Arabidopsis* seedlings were treated with six different SVs (0.2, 1, 5, 10, 15, and 20 kHz) each at 90 dB. Among these SV treatments, the 10 kHz treatment triggered the greatest resistance against *R. solanacearum* in roots, similar to that triggered by the chemical trigger benzothiadiazole (BTH; positive control) (**Figures 1A,B** and **Supplementary Figure S1**). We performed RNA-sequencing (RNA-seq) of 10 kHz and BTH treated *Arabidopsis* roots to investigate 10 kHz SV-specific transcriptional changes. The results of Kyoto Encyclopedia of

[1] http://plantgrn.noble.org/psRNATarget

Genes and Genomes (KEGG) pathway enrichment analysis of DEGs (10 kHz vs. BTH treatments) conferred plant immunity group including "plant-hormone signal transduction," "plant-pathogen interaction," and "phenylpropanoid biosynthesis" (**Figure 2A** and **Supplementary Tables S1, S2**). In comparison with DEGs between 10 kHz SV and BTH treatment, 10 kHz SV specific DEGs were detected (**Figure 2A** and **Supplementary Table S1**). The results of Kyoto Encyclopedia of Genes and Genomes (KEGG) pathway enrichment analysis revealed that 10 kHz SV potentiated plant immunity (defense priming) in *Arabidopsis* after inoculation with *R. solanacearum* (**Figure 2A** and **Supplementary Table S1**).

Next, we investigated how 10 kHz SV triggers induced resistance in plants. To determine the effect of 10 kHz SV on plants, we selected DEGs showing 1.5-fold change in expression (p (0.05) between 10 kHz-treated plants and control plants (**Supplementary Figures S2A–C** and **Supplementary Table S3**). Arabidopsis plants were exposed to 10 kHZ for 10 days and then inoculated with *R. solanacearum*. DEGs identified at 0, 1, and 2 days post-inoculation (dpi) were involved in "response to stimulus," "phenylpropanoid catabolism," and "cell wall organization or biogenesis," respectively (**Supplementary Figures S2D–F**). These RNA-seq data were verified by qPCR (**Figure 2B**). The expression of phenylpropanoid biosynthetic genes, *LAC11* (AT5G03260), *PRR1* (AT1G32100), and *CTL2* (AT3G16920), increased in 10 kHz treated plants at 2 dpi compared with the control. Additionally, the qPCR results showed that the expression of secondary cell wall biosynthesis genes, *IRX6* (AT5G15630) and *NAC007* (AT1G12260), in SV-treated plants increased at 1 dpi, corroborating the RNA-seq data. These results indicate that activation of external reaction (0 dpi) by SV might lead to defense activation-like secondary metabolites (1 dpi) and physical barrier (2 dpi).

SV-Triggered Induced Resistance Mediates H3K27me3 Modification

In many case studies, induced resistance is coupled with defense priming involving epigenetic gene regulation (Park, 2009; Espinas et al., 2016). Therefore, we investigated two histone modifications as potential SV effectors, H3K36ac (transcription activation mark) and H3K27me3 (transcription repression mark), using ChIP-seq (**Figure 3A**). Significant differences were detected in the abundance of H3K27me3 modification, but not in that of H3K36ac modification, between 10 kHz-treated and control plants (**Figures 3B–E**). Next, to understand the functions of genes carrying the H3K27me3 mark in their promoter regions (total 174 genes), we performed gene ontology (GO) analysis (**Figures 3F–G** and **Supplementary Table S4**). The results revealed differential enrichment of histone modifications in the promoter regions of defense-related genes categorized as "glucosinolate biosynthetic process" and "cytokinin dehydrogenase activity" (Boivin et al., 2016; Liu et al., 2016; **Figure 3G**). Histone modification-mediated chromatin remodeling is one of the key epigenetic gene regulation strategies used to induce defense gene priming (Espinas et al., 2016). Therefore, H3K27me3 modification in the promoter regions of defense-related genes may lead to defense gene priming and adequate elicitation of induced resistance (an innate immune response).

SV-Induced H3K27me3 Modification Affects GS Biosynthesis and Cytokinin (CK) Signaling Genes

To conduct an integrative comparison of ChIP-seq and RNA-seq data, we examined the expression of 174 H3K27me3-modified genes (**Supplementary Tables S3, S4**). A total of 39 genes showed H3K27me3-mediated transcriptional changes, of which 12 genes (30.7%) encoded membrane-localized proteins (**Table 1**). Given that external stimuli are recognized by sensors in the cell membrane (Kumar, 2018), it is possible that these membrane-localized proteins are affected by SV.

Among the H3K27me3-modified genes, aliphatic GS biosynthesis-related genes, *MAM1*, *IPMI2*, and *GSTF11*, showed corresponding transcriptional changes (**Figures 4A–D** and **Table 1**). GSs are secondary metabolites in the Brassicaceae family with antimicrobial and antiherbivore properties (Appel and Cocroft, 2014; Sotelo et al., 2015; Liu et al., 2016). Therefore, we closely examined the expression of all GS biosynthesis genes (**Figures 4C,D**). Among the 14 GS biosynthesis genes, 12 were down-regulated at 0 dpi but up-regulated at 1 dpi (**Figures 4C,E**). Redundant H3K27me3 modification was detected in *GSTF11*, *IPMI2*, and *MAM1* promoters, *BACT4* intron, and *SUR1* intergenic region in SV-treated plants (**Figures 4A–C**). Thus, the expression of GS biosynthesis genes in SV-treated plants was tightly suppressed by the H3K27me3 modification at 0 dpi and subsequently released, suggesting SV-mediated epigenetic regulation of GS biosynthesis, thus triggering induced resistance. Similar to our results, Arabidopsis leaves pre-treated with caterpillar feeding-derived SV showed higher levels of aliphatic GS-mediated defenses than untreated plants when subsequently fed upon by *Pieris rapae* caterpillars (Appel and Cocroft, 2014). To investigate the effects of SV on the GS biosynthesis pathway, *cyp79*, *cyp83* and *sur1* mutants were treated with 10 kHz (**Figure 4F** and **Supplementary Figure S4A**). The disruption of upstream genes in the GS biosynthesis pathway mitigated the level of induced resistance. Thus, our results suggest that SV triggers the priming of GS-related genes in *Arabidopsis* for activating resistance against *R. solanacearum*.

We also identified H3K27me3 modification in CK signaling genes (**Table 1**). CK is a phytohormone that negatively regulates defense against root pathogens (Boivin et al., 2016). In our study, *CK oxidase/dehydrogenase* (*CKX*) genes (*CKX1*, *CKX3*, *CKX4*, and *CKX5*) and *type-A Arabidopsis response regulator* (*ARR*) genes (*ARR4*, *ARR6*, and *ARR7*; negative regulators of CK signaling) were up-regulated in 10 kHz-treated plants (**Figures 5A,C**), whereas *adenosine phosphate isopentenyltransferase* genes (*IPT5* and *IPT7*; CK biosynthesis genes) and a CK-responsive gene (*AT2G26695*) were down-regulated, thus inactivating CK signaling (**Figures 5B,D**; Bartrina et al., 2011). Among these genes, *CKX1* and *AT2G26695* were modulated by H3K27me3 modification (**Table 1** and

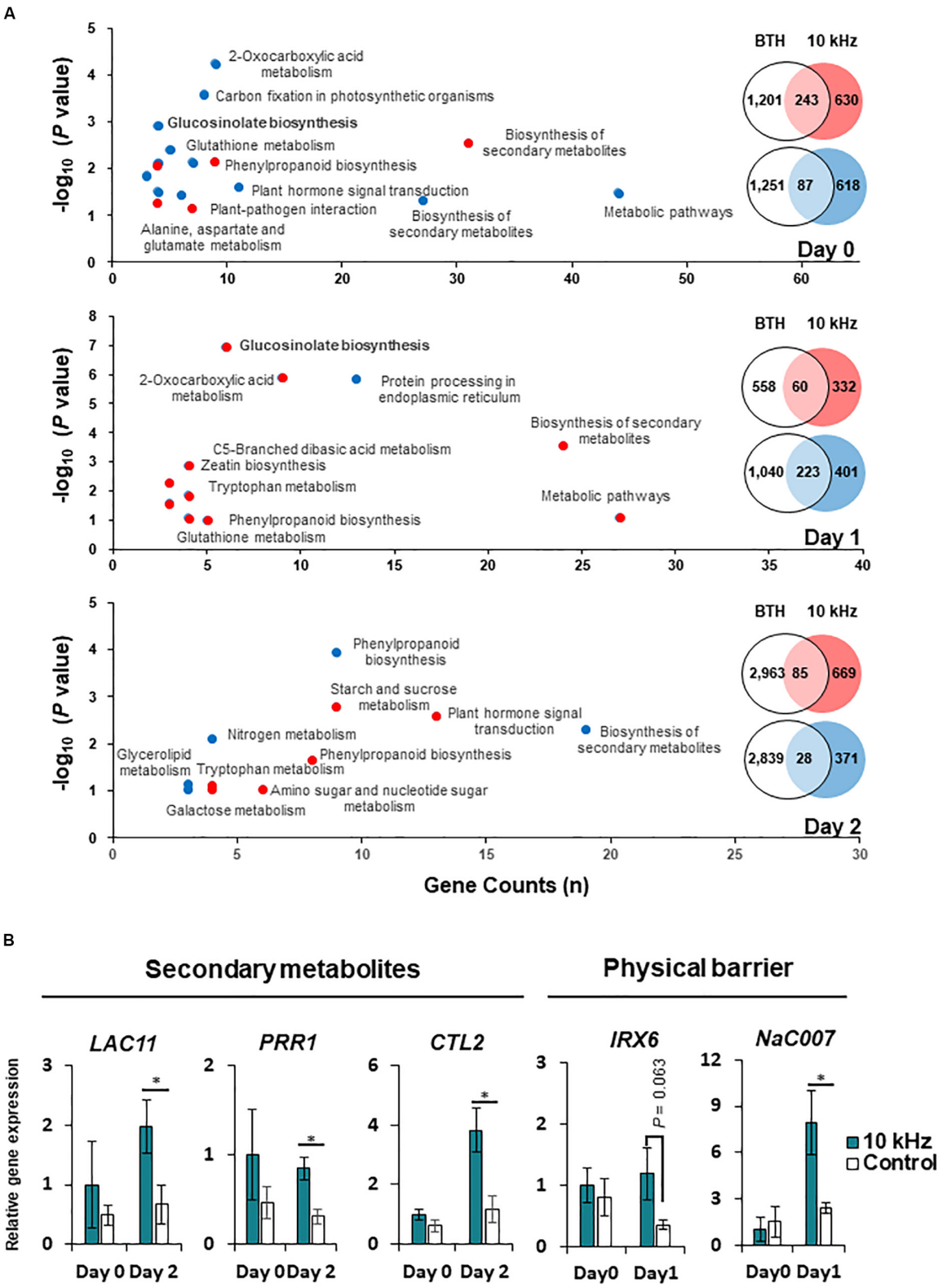

FIGURE 2 | Modification of gene expression in SV (10 kHz)-treated *Arabidopsis* plants compared with BTH-treated plants. **(A)** Venn diagram and major functions of differentially expressed genes (DEGs) in 10 kHz-treated plants compared with BTH-treated plants at 0, 1, and 2 days post-inoculation (dpi) with *R. solanacearum*. Up-regulated genes are indicated in red, and down-regulated genes are indicated in blue. **(B)** Quantitative PCR (qPCR)-based validation of RNA-seq data. The expression of genes related to biosynthesis of secondary metabolites and physical barrier were examined by qPCR. (n = 3–4; $^*p < 0.05$).

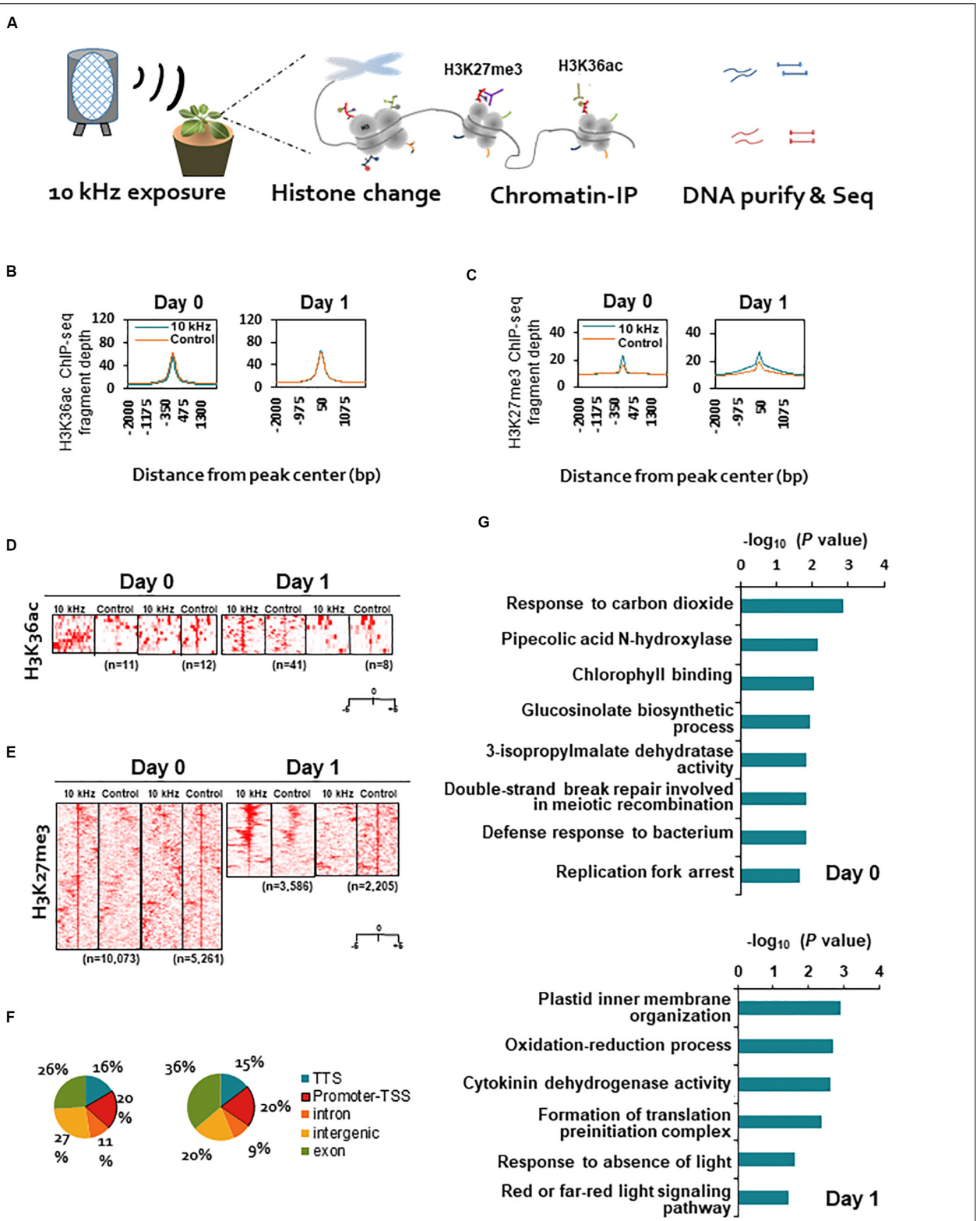

FIGURE 3 | Genome-wide profiling of H3K36ac and H3K27me3 modifications in SV-treated plants during *R. solanacearum* infection. **(A)** Schematic representation of the experimental design used for chromatin immunoprecipitation (ChIP)-seq analyses of H3K36ac and H3K27me3 modifications in 10 kHz-treated and control plants at 0 and 1 dpi. **(B,C)** Fragment depth from peak center of H3K36ac **(B)** or H3K27me3 **(C)**. **(D,E)** Heatmaps of ChIP-seq signals at ± 5 kb around the peak midpoints of H3K36ac **(D)** or H3K27me3 **(E)**. **(F)** Distribution of H3K27me3 sites within genic regions. A 1 kb region upstream of the transcription start site (TSS) was defined as the promoter. **(G)** Gene ontology (GO) analysis of genes carrying the H3K27me3 mark in promoter regions.

TABLE 1 | Correlation between H3K27me3 modification and RNA-seq data in *Arabidopsis* plants treated with sound vibration (SV) of 10 kHz.

Gene[§]	H3K27me3[‡]	$Log_2FC^{\dagger}$	*P-value	Description	Localization
CA1	+	−5.15	1.89E-06	Beta carbonic anhydrase 1	Plasma membrane, Chloroplast stroma
AT2G36220	+	−1.43	1.42E-08	Anaerobic respiration	–
GSTF11	+	−1.37	8.66E-05	Glutathione S-transferase F11, detoxification against herbicides	Cytosol
IPMI2	+	−1.35	2.44E-08	3-isopropylmalate dehydratase small subunit 1, glucosinolate biosynthetic process	Chloroplast stroma
AT3G03280	+	−1.22	1.39E-05	Uncharacterized	Transmembrane
AT2G26695	+	−0.98	2.19E-03	Metal ion binding, cytokinin responsive	–
AT1G43910	+	−0.92	2.99E-06	AAA-ATPase	Membrane
ERF011	+	−0.91	6.31E-08	Ethylene-responsive transcription factor ERF011	Nucleus
AT1G20990	+	−0.84	1.07E-02	Tubulin beta chain	Cytoskeleton
AT5G11620	+	−0.77	2.31E-03	Translation machinery-associated protein 22	Cytoplasm
AT4G30450	+	−0.72	7.40E-05	Glycine-rich protein	–
AT2G21185	+	−0.72	1.68E-04	Uncharacterized	Transmembrane
MYB32	+	−0.71	2.16E-04	Transcription factor MYB32	Nucleus
MAM1	+	−0.70	2.59E-03	Methylthioalkylmalate synthase 1, chloroplastic	Chloroplast
AT3G11591	+	−0.70	2.69E-02	Bric-a-brac protein	–
SYP125	+	−0.70	1.16E-02	SNAP receptor activity	Transmembrane
FAD4L2	+	−0.63	1.82E-03	Fatty acid desaturase 4-like 2, chloroplastic	Transmembrane (chloroplast)
ALMT10	+	−0.62	6.50E-04	Aluminum-activated malate transporter 10	Transmembrane
AT2G32190	+	−0.60	1.50E-02	Cysteine-rich/transmembrane domain A-like protein	Plasma membrane
AT5G57100	+	−0.59	2.02E-03	Nucleotide-sugar uncharacterized transporter 1	Transmembrane
AT1G44414	+	−1.45	4.07E-03	Uncharacterized	–
GRXS10	+	−1.01	2.06E-02	Monothiol glutaredoxin-S10	Nucleus
AT4G31470	+	−0.73	3.04E-02	CAP (Cysteine-rich secretory proteins, Antigen 5, and Pathogenesis-related 1 protein) superfamily protein	Extracellular space
SCY1	+	−0.59	6.60E-03	Preprotein translocase subunit SCY1, chloroplastic	Transmembrane (chloroplast)
AT2G27660	-	1.13	4.32E-04	Pectinesterase inhibitor activity	–
ARFD1A	-	1.12	5.39E-03	ADP-ribosylation factor D1A, transporter	Cytoplasm
AT4G16960	-	1.03	2.07E-03	Mitochondrial pyruvate carrier, Disease resistance protein (TIR-NBS-LRR class)	Transmembrane (Mitochondrion)
AT5G42010	-	0.98	8.64E-03	Transduction/WD40 repeat-like superfamily protein, uncharacterized	–
AT1G13480	-	0.95	2.16E-02	Proteasome subunit beta	Nucleus, cytoplasm
PLP3	-	0.89	6.25E-03	Patatin-like protein 3	Cytoplasm
AT3G50350	-	0.8	1.73E-03	Membrane insertase, putative (DUF1685)	–
WRKY43	-	0.80	1.91E-02	WRKY transcription factor 43, DNA binding	Nucleus
AT4G15810	-	0.76	2.31E-02	P-loop containing nucleoside triphosphate hydrolases superfamily protein	–
WRKY54	-	0.75	2.62E-03	Probable WRKY transcription factor 54	Nucleus
AT4G23540	-	0.73	2.23E-03	snRNA processing	Transmembrane, Nucleus
SNL6	-	0.64	2.63E-03	Paired amphipathic helix protein Sin3-like 6	Nucleus
PRP39-2	-	0.59	1.29E-02	Tetratricopeptide repeat (TPR)-like superfamily protein	Nucleus
CKX1	-	0.90	9.86E-03	Cytokinin dehydrogenase 1	Vacuole
HTR2	-	0.82	9.17E-03	Histone H3.2, nucleosomal DNA binding	Nucleus, Chromosome

[§]*Bold font indicates glucosinolate (GS) biosynthesis or cytokinin (CK) signaling genes.* [‡]*The + and - symbols indicate increased or decreased H3K27me3 modification determined from chromatin immunoprecipitation (ChIP) signals (2-fold difference; Poisson $P < 0.01$), respectively, in 10 kHz-treated plants compared with control plants. Genes with ± H3K27me3 modifications in promoter regions were identified from differentially expressed genes (DEGs) in RNA-seq data (1.5-fold change; $p < 0.05$).* [†]*Relative gene expression in 10 kHz-treated plants compared with control is presented as Log2 fold change (Log2FC). *P-value was obtained from a generalized linear model (GLM) likelihood ratio test.*

Figure 5). To confirm the relevance between CK signaling and SV-induced resistance, three CK receptor mutants, *ahk2*, *ahk2/3*, and *cre1*, were exposed to 10 kHz SV (**Figure 5E** and **Supplementary Figure S4B**). The *ahk2*, *ahk2/3*, and *cre1* mutants showed attenuated disease resistance. Given the overall tendency of the decline in CK signaling in 10 kHz-treated plants, our

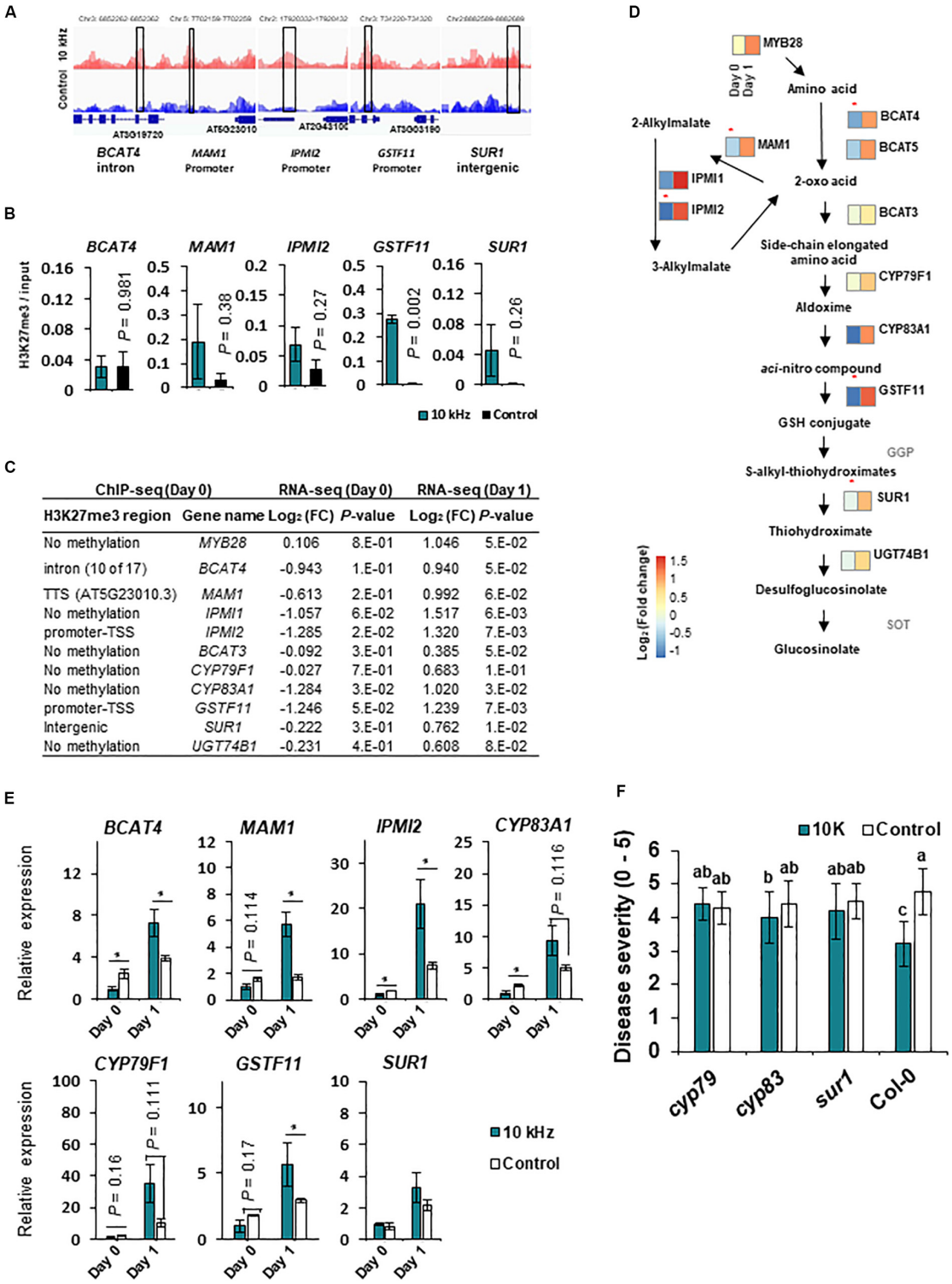

ChIP-seq (Day 0)		RNA-seq (Day 0)		RNA-seq (Day 1)	
H3K27me3 region	Gene name	Log_2 (FC)	*P*-value	Log_2 (FC)	*P*-value
No methylation	*MYB28*	0.106	8.E-01	1.046	5.E-02
intron (10 of 17)	*BCAT4*	-0.943	1.E-01	0.940	5.E-02
TTS (AT5G23010.3)	*MAM1*	-0.613	2.E-01	0.992	6.E-02
No methylation	*IPMI1*	-1.057	6.E-02	1.517	6.E-03
promoter-TSS	*IPMI2*	-1.285	2.E-02	1.320	7.E-03
No methylation	*BCAT3*	-0.092	3.E-01	0.385	5.E-02
No methylation	*CYP79F1*	-0.027	7.E-01	0.683	1.E-01
No methylation	*CYP83A1*	-1.284	3.E-02	1.020	3.E-02
promoter-TSS	*GSTF11*	-1.246	5.E-02	1.239	7.E-03
Intergenic	*SUR1*	-0.222	3.E-01	0.762	1.E-02
No methylation	*UGT74B1*	-0.231	4.E-01	0.608	8.E-02

FIGURE 4 | SV (10 kHz) modulates the expression of glucosinolate (GS) biosynthesis genes through chromatin remodeling**. (A)** Integrated Genome Browser (IGB) view of H3K27me3 modifications, as determined by ChIP-seq. Data represent the average of three biological replicates. Y-axis scale is identical for the different tracks. Blue diagrams indicate gene structure; boxes represent the regions tested in ChIP-qPCR experiments. **(B)** ChIP-qPCR validation ($n = 3$). **(C,D)** Expression of aliphatic GS biosynthesis genes. Heatmaps show expression levels of genes differentially expressed between 10 kHz-treated and control plants ($n = 3$–4). Asterisk indicates the enrichment of H3K27me3 modification in 10 kHz-treated plants vs. control plants. **(E)** Validation of GS biosynthesis gene expression by qPCR ($n = 3$–4; $^*p < 0.05$). **(F)** Disease severity in 10 kHz-treated and control GS biosynthesis mutant plants at 14 dpi with *R. solanacearum*. Data represent mean ± SE. Different letters indicate significant differences [$n = 10$; $p < 0.05$; Fisher's least significant difference (LSD) test].

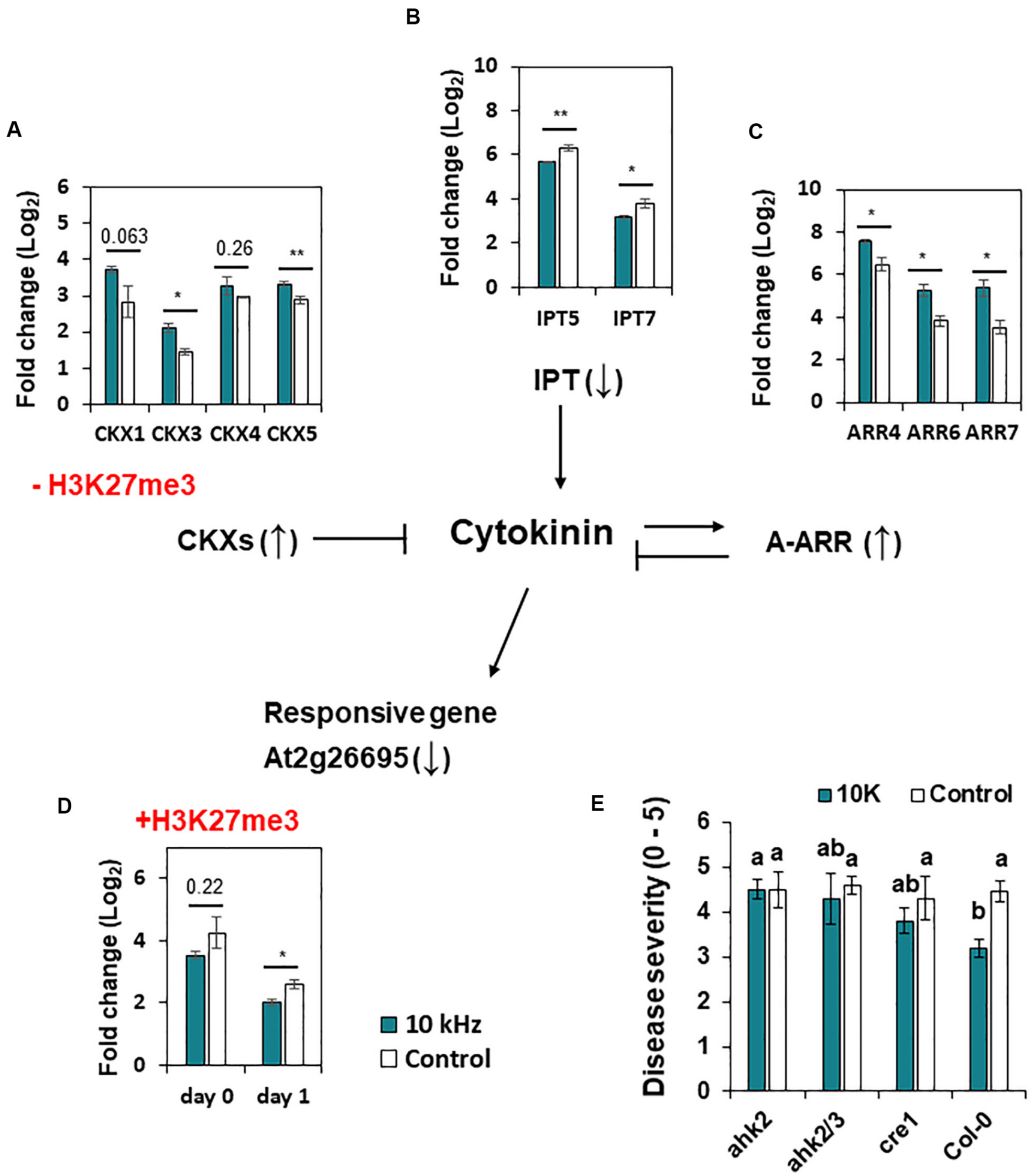

FIGURE 5 | Expression of cytokinin (CK) signaling genes and H3K27me3 modification in *A. thaliana*. **(A–D)** Expression of *CK dehydrogenase/oxidase* (*CKX*) genes at day 1 **(A)**, *adenosine phosphate isopentenyl-transferase* (*IPT*) genes at day 0 **(B)**, *type-A Arabidopsis thaliana response regulator* (*ARR*) genes at day 0 **(C)**, and CK-responsive genes (*At2g26695*) **(D)** in 10 kHz-treated and control plants. *CXK1* and *At2g26695* showed reduced and enhanced H3K27me3 modification in 10 kHz-treated and control plants, respectively. Data represent mean ± SE (n = 3–4). Asterisks indicate significant differences (*$p < 0.05$; **$p < 0.01$; Student's t-test). **(E)** Disease severity in 10 kHz-treated and control CK receptor mutant plants at 14 dpi with *R. solanacearum*. Data represent mean ± SE. Different letters indicate significant differences (n = 10; $p < 0.05$; Fisher's LSD test).

results imply that the inactivation of CK signaling by 10 kHz SV increases plant immunity against *R. solanacearum*.

Activities of Defense Response-Associated Genes

Based on the significant relationship between defense priming and SV, we further sought to identify an association between defense response-associated genes and SV. While exploring significantly enriched bio-functions associated with SV (**Figure 2A**), we observed that many genes with defense response-associated functions were significantly plentiful (**Supplementary Figure S3A**). Many genes were up- or down-regulated at 0 dpi, and the number of defense response-associated genes decreased after SV treatment (**Supplementary Figure S3B**). Among the 174 genes carrying the H3K27me3 mark in their promoter regions at 0 dpi (**Supplementary Table S4**), *CA1* and *CEJ1* (**Supplementary Figure S3C**), involved in defense against *R. solanacearum*, were significantly inhibited by SV, indicating that epigenetic activity of H3K27me3 regulates defense response at the early stage of SV treatment.

SV-Triggered Induced Resistance Is Accompanied by Changes in miRNA Expression

Similar to other epigenetic effectors, miRNAs modulate gene expression by post-transcriptional and transcriptional gene silencing (Vaucheret, 2006; Kaikkonen et al., 2011; Catalanotto et al., 2016). We performed miRNA-seq to identify miRNAs that regulate gene expression in 10 kHz-treated plants post-*R. solanacearum* inoculation. Differentially expressed (DE) miRNAs were compared with RNA-seq data to determine whether these miRNAs regulate gene expression (1.5-fold change; $p < 0.05$) (**Figure 6A** and **Supplementary Table S5**). A total of 15 DE miRNAs showed a negative correlation with the target mRNAs (**Figure 6B** and **Table 2**). Among these target mRNAs, lignin biosynthesis genes, *LAC2*, *LAC17*, and *IRX12 (LAC4)*, were up-regulated, while *miR397b* was down-regulated in 10 kHz-treated plants (**Figures 6B,C** and **Table 2**). Lignin concentration in the roots was increased in plants exposed to 10 kHz SV (**Figure 6D**). Since lignin is a component of plant secondary cell walls, biotrophic pathogen-induced lignification is a conserved pre-formed defense mechanism in *Arabidopsis* (Chezem et al., 2017). Because *LAC4* and *LAC17* are involved in lignin polymerization, disruption of these genes leads to narrower roots with lower lignification (Zhao et al., 2013). The *R. solanacearum*-resistant tomato cultivar LS-89 contains a higher number of redundant lignin biosynthesis genes than the susceptible cultivar Ponderosa (Ishihara et al., 2012). Additionally, using the MiEAA software,[2] we further investigated the functional annotations of 150 DE miRNAs (**Supplementary Table S5**). Among these 150 DE miRNAs, only two miRNAs (*ath-miR163* and *ath-miR398b-3p*) were enriched under the GO term "defense response to bacterium" (GO0042742), which was non-significant ($P > 0.05$; Fisher's Exact test) (data not shown). Therefore, the 10 kHz-induced *LAC2*, *LAC17*, and *LAC4* activation observed in our study may have contributed to plant cell wall reinforcement, thus strengthening the barrier against *R. solanacearum* in *Arabidopsis* roots.

Although 15 out of 120 DE miRNAs targeted host mRNAs, the functions of the remaining DE miRNAs were unknown. The majority of DE miRNAs identified at 0–2 dpi were 21 nt in length (**Figure 6E** and **Supplementary Table S5**). To obtain genetic evidence on the involvement of miRNAs in 10 kHz SV-mediated plant immunity, 21–22 nt miRNA processing mutants (*dcl2/4*) and 24-nt miRNA processing mutants (*rdr2-1/6-15*) were exposed to 10 kHz SV (Brosnan et al., 2007; Polydore and Axtell, 2018). Among these miRNA biogenesis mutants, induced resistance was abolished only in the *dcl2/4* mutant (**Figures 6F,G**), suggesting that 21–22-nt miRNAs affect 10 kHz-elicited induced resistance in *Arabidopsis* in a DCL2/4-dependent manner.

DISCUSSION

Previous research in plant immunity focused on chemical or biological materials for inducing disease resistance. In this study, we newly suggest that 10 kHz SV can be used as a physical trigger to induce plant resistance against *R. solanacearum*. Mostly, induced resistance is coupled with defense priming (Park, 2009; Espinas et al., 2016). The defense priming phenomenon enables plants to respond quickly and/or more strongly to each subsequent pathogen infection (Espinas et al., 2016). Therefore, we addressed two questions regarding the SV-mediated immune enhancement in *Arabidopsis*: (1) are SV-mediated transcriptional changes during pathogen infections accompanied by histone modifications?; and (2) are these changes regulated by miRNAs?

By exploring the H3K27me3 modification, we found changes in GS and CK pathway genes. Previously, GSs extracted from *Brassica* species showed direct antimicrobial activity against *Xanthomonas campestris* pv. *campestris* and *Pseudomonas syringae* pv. *maculicola* (Sotelo et al., 2015). In addition, the *walls are thin 1* (*wat1*) *Arabidopsis* mutant, which expresses GS biosynthesis genes to low levels in roots, shows enhanced susceptibility to *R. solanacearum* (Denance et al., 2013). Therefore, GSs seem to play an important role in the defense against *R. solanacearum* in *Arabidopsis*. In our results, GS biosynthesis genes showed a rapid increase in expression upon pathogen inoculation accompanied by H3K27me3 modification (Liu et al., 2016) (**Figure 4**). This indicates that the expression of GS biosynthesis genes is regulated epigenetically in SV-treated plants.

The plant hormone CK affects various processes during plant growth and development including cell division, shoot initiation, leaf senescence, and biotic and abiotic stress response (Kieber and Schaller, 2014). Moreover, CK plays a positive role in plant–microbe interactions, specifically symbiotic rhizobium nodulation (Gamas et al., 2017). However, CK accumulation in plants causes susceptibility to root pathogens such as *Agrobacterium tumefaciens*, *Plasmodiophora brassicae*, and *R. solanacearum* (Siemens et al., 2006; Hwang et al., 2010; Boivin et al., 2016). Overexpression of *CKX* genes in *Arabidopsis* increases resistance against *P. brassicae*, indicating the importance of CK in the progression of clubroot disease (Siemens et al., 2006). Similarly, the *M. truncatula* CK receptor mutant, *MTcre1*, showed enhanced resistance to *R. solanacearum*, supporting the negative role of CK in plants against *R. solanacearum* (Moreau et al., 2014). Therefore, epigenetic down-regulation of CK biosynthesis genes in SV-treated plants represents a key strategy for counteracting *R. solanacearum*.

Interestingly, we found that 12 out of 39 H3K27me3 modified genes at 0 dpi are localized in transmembrane (**Table 1**). Since the plants are sessile organisms, they have to cope with and adapt to various environments. In many cases, the environmental stress is detected by sensors located in the cell membrane (Kumar, 2018). In metalliferous soils, genes encoding transmembrane proteins play an important role in the environmental adaptation of plants (Sailer et al., 2018). Therefore, it seems that the genes related to the cell membrane have changed a lot in response to SV, which is the external stimulus in this study. Some cell membrane-related genes play a role in disease resistance (Vincent et al., 2017). For example, *glutamate receptor* (*GLR*) genes, which were differently expressed between treatments in our RNA-seq analysis, are known to activate defense-related genes by regulating Ca^{2+} signaling (Vincent et al., 2017;

[2]https://ccb-compute2.cs.uni-saarland.de/mieaa2/

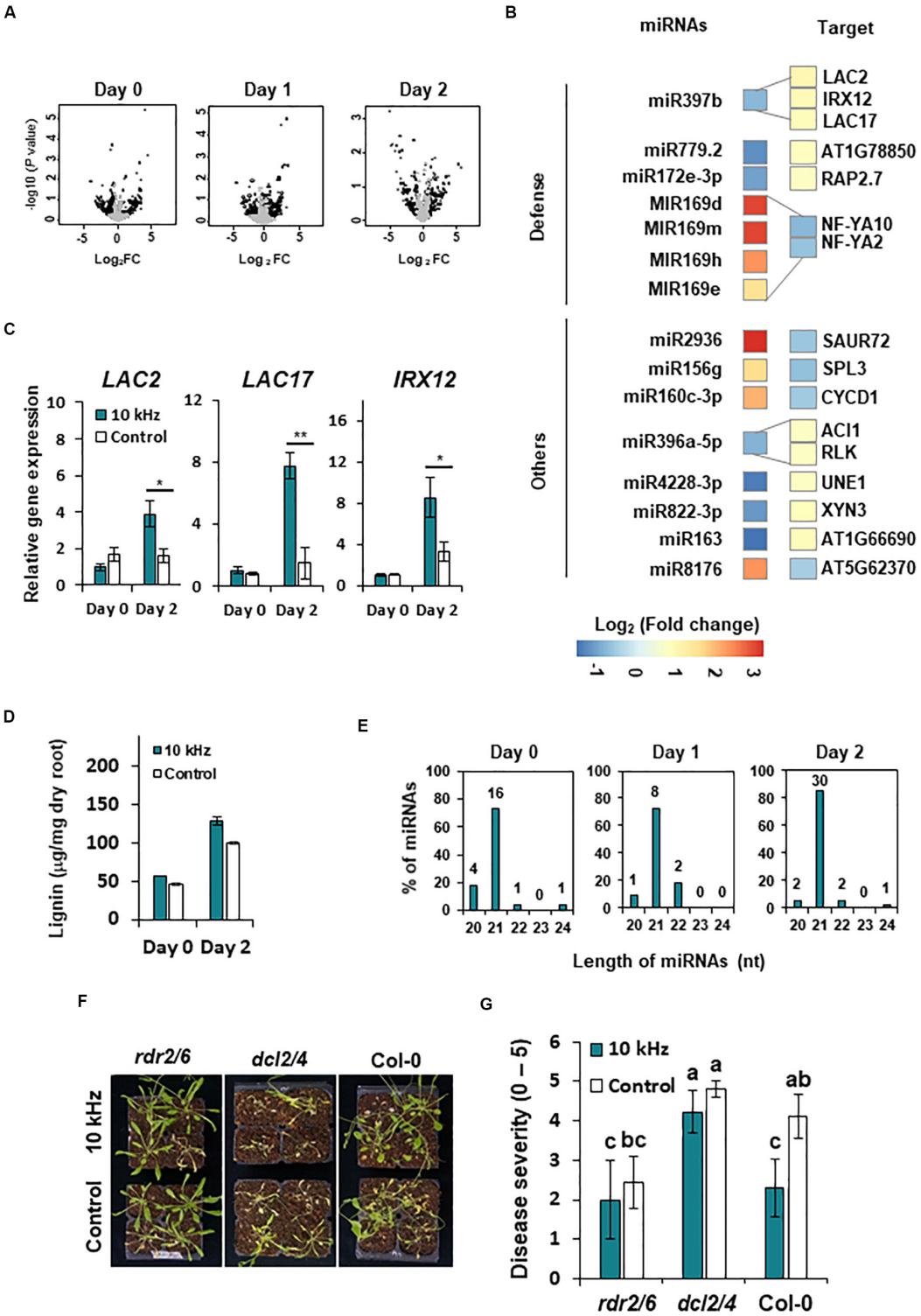

FIGURE 6 | SV (10 kHz) elicits miRNA modulation in *Arabidopsis* plants inoculated with *R. solanacearum*. **(A)** Volcano plots of miRNAs differentially expressed (DE) between 10 kHz-treated and control plants. Black dots indicate significantly DE miRNAs (1.5-fold change; $p < 0.05$). **(B)** Heatmaps showing relative gene expression levels in 10 kHz-treated vs. control plants (1.5-fold change; $p < 0.05$). Relative expression levels (log_2-transformed values) of miRNAs (left) and corresponding mRNAs (right) are indicated on a color scale. **(C)** Validation of *LAC2*, *LAC17*, and *IRX12* expression by qPCR. Data represent mean ± SE (*$p < 0.05$; **$p < 0.01$). **(D)** Quantification of lignin content. Data represent mean ± SE (**$p < 0.01$). **(E)** Length distribution of DE miRNAs. **(F,G)** Representative disease symptoms and disease severity in 10 kHz-treated and control plants at 14 dpi with *R. solanacearum*. Data represent mean ± SE. Different letters indicate significant differences ($n = 10$; $p < 0.05$; Fisher's LSD test).

TABLE 2 | Correlation between miRNA expression and RNA-seq data in 10 kHz-treated *Arabidopsis* plants.

miRNA[§]	Target genes	Log_2FC[†]	*P*-value	Description
Day 1				
miR156g	AT2G33810 (SPL3)	−0.86	3.55E-04	Metal binding
miR4228-3p	AT1G29300 (UNE1)	0.64	1.71E-01	Intracellular protein transporter, putative (DUF641)
Day 2				
miR2936	AT3G12830 (SAUR72)	−0.74	3.79E-02	Auxin–responsive protein
MIR169d				
MIR169h	AT5G06510 (NF-YA10)	−0.95	3.80E-03	Nuclear transcription factor Y subunit A-10
MIR169m	AT3G05690 (NF-YA2)	−0.81	6.25E-03	Nuclear transcription factor Y subunit A-2, DNA binding
MIR169e				
miR8176	AT5G62370	−0.64	3.62E-02	Pentatricopeptide repeat-containing protein
miR160c-3p	AT1G70210 (CYCD1)	−0.69	2.79E-03	Cell cycle activation, embryonic root protrusion
miR396a-5p	AT5G01370 (ACI1),	0.64	1.37E-02	ACL-interacting protein fruit dehiscence
	AT2G34530 (RLK)	0.63	8.20E-03	Protein kinase
MIR397b	AT2G29130 (LAC2)	0.93	1.09E-02	Cell wall lignification
	AT2G38080 (IRX12)	0.82	7.06E-03	
	AT5G60020 (LAC17)	0.75	5.14E-02	
MIR163	AT1G66690,	0.76	9.56E-02	Paraxanthine methyltransferase 2/
	AT2G12480 (SCPL43)	0.76	9.56E-02	Serine carboxypeptidase-like 43
miR822-3p	AT4G08160 (XYN3)	0.74	2.81E-02	Endo-1,4-beta-xylanase 3
miR172e-3p	AT2G28550 (RAP2.7)	0.64	6.16E-02	Ethylene-responsive transcription factor RAP2-7
miR779.2	AT1G78850	0.69	2.82E-02	EP1-like glycoprotein 3

[§]*Differentially expressed (DE) miRNAs showing at least 1.5-fold change ($p < 0.05$) in expression were selected. Among the DE miRNA target genes, those that met the selection criteria (1.5-fold change; $p < 0.05$) are presented.* [†]*Relative gene expression of 10 kHz-treated plants compared with control plants is presented as Log 2 fold change (Log2FC).*

Nguyen et al., 2018) (**Supplementary Table S3**). Our results also showed that *AT4G16960*, which is annotated as an *NLR* gene, is up-regulated by the reduction in H3K27me3 modification in SV-treated plants (**Table 1**). The NLR proteins are well-known plant membrane receptors that recognize pathogen-derived molecules and trigger immune responses (Qi and Innes, 2013). These results suggest the possibility that SV-mediated changes in transmembrane protein-encoding genes at 0 dpi lead to further intracellular responses against pathogen infection.

Plant cell wall is the first barrier against external stresses (Liu et al., 2018). Since lignin is a component of secondary cell wall in plants, increased accumulation of lignin strengthens the physical barrier, which minimizes the spread of pathogens, thus enhancing plant immunity (Liu et al., 2018). Studies show that the expression of lignin biosynthesis genes is up-regulated in plants infected with various pathogens such as necrotrophic bacteria, biotrophic bacteria, and fungi (Bonello et al., 2003; Ponce de Leon et al., 2007; Chezem et al., 2017). In potato (*Solanum tuberosum*) and tomato, *R. solanacearum*-resistant cultivars contain higher lignin content than susceptible cultivars (Ishihara et al., 2012; Ferreira et al., 2017). Therefore, SV-induced *LAC2, LAC17,* and *IRX12* activation in our study possibly contributed to plant cell wall reinforcement, thus strengthening the barrier against *R. solanacearum* in *Arabidopsis* root.

Among the DE miRNAs, the miR169 family members and their target genes, *NF-YA*, are known to regulate biotic and abiotic stress response and plant growth. The negative defense role of miR169 is reported in *Arabidopsis* and *Oryza sativa* against responsive *R. solanacearum and Magnaporthe oryzae* (Hanemian et al., 2016; Li et al., 2017). Abiotic stresses such as low phosphate, low nitrogen, and high sucrose induce *NF-YA2* and *NF-YA10* expression, indicating *NF-YA* is important to acclimate to abiotic stresses (Leyva-González et al., 2012). In addition, transgenic plants of miR169abc or miR169defg with increased *NF-YA* expression showed smaller rosettes and shorter primary roots (Sorin et al., 2014). Although our results showed increased accumulation of miR169 family members, and reduced *NF-YA2* and *NF-YA10* expression in SV-treated plants (**Figure 6B**), we speculate that the reduced *NF-YA2* and *NF-YA10* may be associated with adaptations, such as changing root architecture, for improving abiotic stress tolerance in an SV-dependent manner, rather than a response to pathogenesis.

In some plant species, miRNAs also regulate the mRNA of associated pathogens (Zhang et al., 2016; Liu et al., 2017; Wang et al., 2018). For instance, in cotton (*Gossypium arboretum*), miR398 and miR2950 directly target multiple open reading frames of the cotton leaf curl disease (CLCuD) virus, leading to translation inhibition and reduced disease severity (Akmal et al., 2017). Additionally, miR159 and miR166 target the mRNA of virulence genes encoding C-15 hydroxylase (HiC-15) and Ca^{2+}-dependent cysteine protease (Clp-1), respectively, conferring resistance to *Verticillium dahliae* (Zhang et al., 2016). In the current study, we showed enhanced miR398b, miR398b-5p, and miR398b-3p expression in SV-treated plants on day 2 (**Supplementary Table S5**). However, further research is needed to investigate whether the SV-induced plant miRNAs target *R. solanacearum* genes.

Overall, we confirmed that 10 kHz SV acts as a physical trigger and elicits induced resistance against *R. solancearum* in

Arabidopsis roots as well as transcriptional changes different from those caused by the chemical trigger BTH. Direct comparison of RNA-seq, ChIP-seq, and miRNA-seq data revealed the epigenetic response of GS biosynthesis, CK signaling, and lignin biosynthesis genes to 10 kHz SV. These data, therefore, support the role of a physical trigger in the epigenetic regulation of plant innate immunity. Taken together, our findings suggest that SV modulates the epigenetic regulation of genes involved in secondary metabolite biosynthesis, hormone signaling, and cell wall biosynthesis, thus enhancing induced resistance against *R. solanacearum*.

DATA AVAILABILITY STATEMENT

Sequencing data described in this manuscript have been deposited in the NCBI Gene Expression Omnibus (GEO) under the accession number GSE133325.

AUTHOR CONTRIBUTIONS

JJ designed the study, performed most of the experiments, interpreted the results, and wrote the manuscript. S-KK analyzed and interpreted the RNA-seq, miRNA-seq, and ChIP-seq data. S-HJ performed the mutant and qRT-PCR validation experiments. M-JJ designed the study. C-MR designed the study, interpreted the results, and wrote the manuscript. All authors contributed to the article and approved the submitted version.

FUNDING

This research was supported by the grants from the Agenda Project (Agenda Project Nos. PJ012814 and PJ01247201) of the Rural Development Administration (RDA), the Rural Development Administration, Strategic Initiative for Microbiomes in Agriculture and Food, Ministry of Agriculture, Food and Rural Affairs, Republic of Korea (as part of the multiministerial Genome Technology to Business Translation Program) (918017-4), and the KRIBB Initiative Program, South Korea.

SUPPLEMENTARY MATERIAL

The Supplementary Material for this article can be found online at: https://www.frontiersin.org/articles/10.3389/fmicb.2020.01978/full#supplementary-material

FIGURE S1 | Optimization of SV-triggered induced resistance in *Arabidopsis thaliana* plants against *Ralstonia solanacearum*. **(A,B)** Phenotype and disease severity in SV- (0.2, 1, 5, 10, 15, or 20 kHz) or BTH-treated plants and control plants at day 14. Disease severity was scored as 0 (no symptoms), 1 (< 50% of rosette leaves wilted), 2 (< 100% of rosette leaves wilted), 3 (100% of rosette leaves wilted), 4 (100% of rosette leaves wilted and stems partially wilted), and 5 (complete plant collapse). The 10 kHz (dark green) SV- and BTH-treated plants showed statistically reduced disease severity compared with control plants (gray) ($^{**}p < 0.01$).

FIGURE S2 | Transcriptomic profiling of 10 kHz-treated *A. thaliana* roots challenged with *R. solanacearum*. **(A–C)** Heatmaps of genes differentially expressed between 10 kHz-treated and control plants at 0 **(A)**, 1 **(B)**, and 2 **(C)** days post-inoculation (dpi; 1.5-fold change; $p < 0.05$). **(D–F)** Gene Ontology (GO) enrichment analyses of DEGs identified at 0 **(D)**, 1 **(E)**, and 2 **(F)** dpi.

FIGURE S3 | Gene set enrichment analysis and expression pattern of genes involved in defense response elicited by SV. **(A)** Gene set enrichment analysis of genes involved in defense response significantly associated with SV. **(B)** Heatmaps displaying expression patterns of defense response genes whose expression levels were highly correlated with SV. **(C)** Comparison of *CA1* and *CEJ1* expression levels between control and 10 KHz SV treatments. CPM, count per million mapped reads.

FIGURE S4 | Representative disease symptoms of 10 kHz-treated and control plants at 14 dpi with *R. solanacearum*. **(A,B)** Disease symptoms of 10 kHz-treated and control glucosinolate (GS) biosynthesis mutant plants **(A)** and cytokinin receptor mutant plants **(B)**.

TABLE S1 | Differentially expressed genes (DEGs) identified between sound vibration (SV; 10 kHz)- or benzothiadiazole (BTH)-treated plants vs. control plants.

TABLE S2 | Functional analysis of genes up- or down-regulated in 10 kHz-treated plants compared with control plants.

TABLE S3 | Normalized gene expression levels in 10 kHz-treated and control plants determined by RNA-seq.

TABLE S4 | Differential H3K27me3 enrichment in 10 kHz-treated vs. control plants.

TABLE S5 | Differentially expressed (DE) miRNAs identified between 10 kHz-treated and control plants.

TABLE S6 | List of primers used in this study.

REFERENCES

Akmal, M., Baig, M. S., and Khan, J. A. (2017). Suppression of cotton leaf curl disease symptoms in *Gossypium hirsutum* through over expression of host-encoded miRNAs. *J. Biotechnol.* 263, 21–29. doi: 10.1016/j.jbiotec.2017.10.003

Anders, S., Pyl, P. T., and Huber, W. (2015). HTSeq–a Python framework to work with high-throughput sequencing data. *Bioinformatics* 31, 166–169. doi: 10.1093/bioinformatics/btu638

Appel, H. M., and Cocroft, R. B. (2014). Plants respond to leaf vibrations caused by insect herbivore chewing. *Oecologia* 175, 1257–1266. doi: 10.1007/s00442-014-2995-6

Bartrina, I., Otto, E., Strnad, M., Werner, T., and Schmulling, T. (2011). Cytokinin regulates the activity of reproductive meristems, flower organ size, ovule formation, and thus seed yield in *Arabidopsis thaliana*. *Plant Cell* 23, 69–80. doi: 10.1105/tpc.110.079079

Basu, D., and Haswell, E. S. (2017). Plant mechanosensitive ion channels: an ocean of possibilities. *Curr. Opin. Plant Biol.* 40, 43–48. doi: 10.1016/j.pbi.2017.07.002

Boccara, M., Sarazin, A., Thiebeauld, O., Jay, F., Voinnet, O., Navarro, L., et al. (2014). The *Arabidopsis* miR472-RDR6 silencing pathway modulates PAMP- and effector-triggered immunity through the post-transcriptional control of disease resistance genes. *PLoS Pathog.* 10:e1003883. doi: 10.1371/journal.ppat.1003883

Boivin, S., Fonouni-Farde, C., and Frugier, F. (2016). How auxin and cytokinin phytohormones modulate root microbe interactions. *Front. Plant Sci.* 7:1240. doi: 10.3389/fpls.2016.01240

Bonello, P., Storer, A. J., Gordon, T. R., Wood, D. L., and Heller, W. (2003). Systemic effects of *Heterobasidion annosum* on ferulic acid glucoside and lignin of *presymptomatic ponderosa* pine phloem, and potential effects on bark-beetle-associated fungi. *J. Chem. Ecol.* 29, 1167–1182.

Brosnan, C. A., Mitter, N., Christie, M., Smith, N. A., Waterhouse, P. M., and Carroll, B. J. (2007). Nuclear gene silencing directs reception of long-distance mRNA silencing in *Arabidopsis*. *Proc. Natl. Acad. Sci. U.S.A.* 104, 14741–14746. doi: 10.1073/pnas.0706701104

Catalanotto, C., Cogoni, C., and Zardo, G. (2016). MicroRNA in control of gene expression: an overview of nuclear functions. *Int. J. Mol. Sci.* 17:1712. doi: 10.3390/ijms17101712

Chezem, W. R., Memon, A., Li, F.-S., Weng, J.-K., and Clay, N. K. (2017). SG2-type R2R3-MYB transcription factor MYB15 controls defense-induced lignification and basal immunity in *Arabidopsis*. *Plant Cell* 29, 1907–1926. doi: 10.1105/tpc.16.00954

Choi, B., Ghosh, R., Gururani, M. A., Shanmugam, G., Jeon, J., Kim, J., et al. (2017). Positive regulatory role of sound vibration treatment in *Arabidopsis thaliana* against *Botrytis cinerea* infection. *Sci. Rep.* 7:2527. doi: 10.1038/s41598-017-02556-9

Denance, N., Ranocha, P., Oria, N., Barlet, X., Riviere, M. P., Yadeta, K. A., et al. (2013). *Arabidopsis* wat1 (walls are thin1)-mediated resistance to the bacterial vascular pathogen, *Ralstonia solanacearum*, is accompanied by cross-regulation of salicylic acid and tryptophan metabolism. *Plant J.* 73, 225–239. doi: 10.1111/tpj.12027

Dobin, A., Davis, C. A., Schlesinger, F., Drenkow, J., Zaleski, C., Jha, S., et al. (2013). STAR: ultrafast universal RNA-seq aligner. *Bioinformatics* 29, 15–21. doi: 10.1093/bioinformatics/bts635

Espinas, N. A., Saze, H., and Saijo, Y. (2016). Epigenetic control of defense signaling and priming in plants. *Front. Plant Sci.* 7:1201. doi: 10.3389/fpls.2016.01201

Ferreira, V., Pianzzola, M. J., Vilaró, F. L., Galván, G. A., Tondo, M. L., Rodriguez, M. V., et al. (2017). Interspecific potato breeding lines display differential colonization patterns and induced defense responses after *Ralstonia solanacearum* Infection. *Front. Plant Sci.* 8:1424. doi: 10.3389/fpls.2017.01424

Gamas, P., Brault, M., Jardinaud, M. F., and Frugier, F. (2017). Cytokinins in symbiotic nodulation: when, where, what for? *Trends Plant Sci.* 22, 792–802. doi: 10.1016/j.tplants.2017.06.012

Gan, E.-S., Huang, J., and Ito, T. (2013). "Chapter three – functional roles of histone modification, chromatin remodeling and micrornas in *arabidopsis* flower development," in *International Review of Cell and Molecular Biology*, ed. K. W. Jeon (Cambridge, MA: Academic Press), 115–161. doi: 10.1016/b978-0-12-407695-2.00003-2

Ghosh, R., Mishra, R. C., Choi, B., Kwon, Y. S., Bae, D. W., Park, S.-C., et al. (2016). Exposure to sound vibrations lead to transcriptomic, proteomic and hormonal changes in *Arabidopsis*. *Sci. Rep.* 6:33370. doi: 10.1038/srep33370

Hanemian, M., Barlet, X., Sorin, C., Yadeta, K. A., Keller, H., Favery, B., et al. (2016). *Arabidopsis* CLAVATA1 and CLAVATA2 receptors contribute to *Ralstonia solanacearum* pathogenicity through a miR169-dependent pathway. *New Phytol.* 211, 502–515. doi: 10.1111/nph.13913

Hassanien, R. H. E., Hou, T.-Z., Li, Y.-F., and Li, B.-M. (2014). Advances in effects of sound waves on plants. *J. Integr. Agric.* 13, 335–348. doi: 10.1016/S2095-3119(13)60492-X

Hwang, H. H., Wang, M. H., Lee, Y. L., Tsai, Y. L., Li, Y. H., Yang, F. J., et al. (2010). *Agrobacterium*-produced and exogenous cytokinin-modulated *Agrobacterium*-mediated plant transformation. *Mol. Plant Pathol.* 11, 677–690. doi: 10.1111/j.1364-3703.2010.00637.x

Ishihara, T., Mitsuhara, I., Takahashi, H., and Nakaho, K. (2012). Transcriptome analysis of quantitative resistance-specific response upon *Ralstonia solanacearum* infection in tomato. *PLoS One* 7:e46763. doi: 10.1371/journal.pone.0046763

Jones, J. D., and Dangl, J. L. (2006). The plant immune system. *Nature* 444, 323–329. doi: 10.1038/nature05286

Jung, J., Kim, S. K., Kim, J. Y., Jeong, M. J., and Ryu, C. M. (2018). Beyond chemical triggers: evidence for sound-evoked physiological reactions in plants. *Front. Plant Sci.* 9:25. doi: 10.3389/fpls.2018.00025

Kaikkonen, M. U., Lam, M. T. Y., and Glass, C. K. (2011). Non-coding RNAs as regulators of gene expression and epigenetics. *Cardiovasc. Res.* 90, 430–440. doi: 10.1093/cvr/cvr097

Kieber, J. J., and Schaller, G. E. (2014). Cytokinins. *Arabidopsis Book* 12:e0168. doi: 10.1199/tab.0168

Kim, D., Pertea, G., Trapnell, C., Pimentel, H., Kelley, R., and Salzberg, S. L. (2013). TopHat2: accurate alignment of transcriptomes in the presence of insertions, deletions and gene fusions. *Genome Biol.* 14:R36. doi: 10.1186/gb-2013-14-4-r36

Kouzarides, T. (2007). Chromatin modifications and their function. *Cell* 128, 693–705. doi: 10.1016/j.cell.2007.02.005

Kumar, S. (2018). Epigenomics of plant responses to environmental stress. *Epigenomes* 2:6. doi: 10.3390/epigenomes2010006

Leyva-González, M. A., Ibarra-Laclette, E., Cruz-Ramírez, A., and Herrera-Estrella, L. (2012). Functional and transcriptome analysis reveals an acclimatization strategy for abiotic stress tolerance mediated by *Arabidopsis* NF-YA family members. *PLoS One* 7:e48138. doi: 10.1371/journal.pone.0048138

Li, Y., Zhao, S.-L., Li, J.-L., Hu, X.-H., Wang, H., Cao, X.-L., et al. (2017). Osa-miR169 negatively regulates rice immunity against the blast fungus *Magnaporthe oryzae*. *Front. Plant Sci.* 8:2. doi: 10.3389/fpls.2017.00002

Liu, Q., Luo, L., and Zheng, L. (2018). Lignins: biosynthesis and biological functions in plants. *Int. J. Mol. Sci.* 19:335. doi: 10.3390/ijms19020335

Liu, S. R., Zhou, J. J., Hu, C. G., Wei, C. L., and Zhang, J. Z. (2017). MicroRNA-mediated gene silencing in plant defense and viral counter-defense. *Front. Microbiol.* 8:1801. doi: 10.3389/fmicb.2017.01801

Liu, T., Zhang, X., Yang, H., Agerbirk, N., Qiu, Y., Wang, H., et al. (2016). Aromatic glucosinolate biosynthesis pathway in *Barbarea vulgaris* and its response to *Plutella xylostella* infestation. *Front. Plant Sci.* 7:83. doi: 10.3389/fpls.2016.00083

Lopes, C. A., and Rossato, M. (2018). History and status of selected hosts of the *Ralstonia solanacearum* species complex causing bacterial wilt in Brazil. *Front. Microbiol.* 9:1228. doi: 10.3389/fmicb.2018.01228

Lowe-Power, T. M., Jacobs, J. M., Ailloud, F., Fochs, B., Prior, P., and Allen, C. (2016). Degradation of the plant defense signal salicylic acid protects *Ralstonia solanacearum* from toxicity and enhances virulence on tobacco. *mBio* 7:e00656-16. doi: 10.1128/mBio.00656-16

Lu, C., Meyers, B. C., and Green, P. J. (2007). Construction of small RNA cDNA libraries for deep sequencing. *Methods* 43, 110–117. doi: 10.1016/j.ymeth.2007.05.002

Mengel, A., Ageeva, A., Georgii, E., Bernhardt, J., Wu, K., Durner, J., et al. (2017). Nitric oxide modulates histone acetylation at stress genes by inhibition of histone deacetylases. *Plant Physiol.* 173, 1434–1452. doi: 10.1104/pp.16.01734

Moreau, S., Fromentin, J., Vailleau, F., Vernie, T., Huguet, S., Balzergue, S., et al. (2014). The symbiotic transcription factor MtEFD and cytokinins are positively acting in the *Medicago truncatula* and *Ralstonia solanacearum* pathogenic interaction. *New Phytol.* 201, 1343–1357. doi: 10.1111/nph.12636

Nguyen, C. T., Kurenda, A., Stolz, S., Chetelat, A., and Farmer, E. E. (2018). Identification of cell populations necessary for leaf-to-leaf electrical signaling in a wounded plant. *Proc. Natl. Acad. Sci. U.S.A.* 115, 10178–10183. doi: 10.1073/pnas.1807049115

Park, P. J. (2009). ChIP–seq: advantages and challenges of a maturing technology. *Nat. Rev. Genet.* 10:669. doi: 10.1038/nrg2641

Polydore, S., and Axtell, M. J. (2018). Analysis of RDR1/RDR2/RDR6-independent small RNAs in *Arabidopsis thaliana* improves MIRNA annotations and reveals unexplained types of short interfering RNA loci. *Plant J.* 94, 1051–1063. doi: 10.1111/tpj.13919

Ponce de Leon, I., Oliver, J. P., Castro, A., Gaggero, C., Bentancor, M., and Vidal, S. (2007). Erwinia carotovora elicitors and *Botrytis cinerea* activate defense responses in *Physcomitrella patens*. *BMC Plant Biol.* 7:52. doi: 10.1186/1471-2229-7-52

Qi, D., and Innes, R. W. (2013). Recent advances in plant NLR structure, function, localization, and signaling. *Front. Immunol.* 4:348. doi: 10.3389/fimmu.2013.00348

Ramirez-Prado, J. S., Abulfaraj, A. A., Rayapuram, N., Benhamed, M., and Hirt, H. (2018a). Plant immunity: from signaling to epigenetic control of defense. *Trends Plant Sci.* 23, 833–844. doi: 10.1016/j.tplants.2018.06.004

Ramirez-Prado, J. S., Piquerez, S. J. M., Bendahmane, A., Hirt, H., Raynaud, C., and Benhamed, M. (2018b). Modify the histone to win the battle: chromatin dynamics in plant-pathogen interactions. *Front. Plant Sci.* 9:355. doi: 10.3389/fpls.2018.00355

Robinson, M. D., McCarthy, D. J., and Smyth, G. K. (2010). edgeR: a bioconductor package for differential expression analysis of digital gene expression data. *Bioinformatics* 26, 139–140. doi: 10.1093/bioinformatics/btp616

Sailer, C., Babst-Kostecka, A., Fischer, M. C., Zoller, S., Widmer, A., Vollenweider, P., et al. (2018). Transmembrane transport and stress response genes play an important role in adaptation of *Arabidopsis halleri* to metalliferous soils. *Sci. Rep.* 8:16085. doi: 10.1038/s41598-018-33938-2

Schenk, S. T., and Schikora, A. (2015). Lignin extraction and quantification, a tool to monitor defense reaction at the plant cell wall level. *Bio Protoc.* 5:e1430. doi: 10.21769/BioProtoc.1430

Siemens, J., Keller, I., Sarx, J., Kunz, S., Schuller, A., Nagel, W., et al. (2006). Transcriptome analysis of *Arabidopsis* clubroots indicate a key role for cytokinins in disease development. *Mol. Plant Microbe. Interact.* 19, 480–494. doi: 10.1094/mpmi-19-0480

Sorin, C., Declerck, M., Christ, A., Blein, T., Ma, L., Lelandais-Brière, C., et al. (2014). A miR169 isoform regulates specific NF-YA targets and root architecture in *Arabidopsis*. *New Phytol.* 202, 1197–1211. doi: 10.1111/nph.12735

Sotelo, T., Lema, M., Soengas, P., Cartea, M. E., and Velasco, P. (2015). In vitro activity of glucosinolates and their degradation products against brassica-pathogenic bacteria and fungi. *Appl. Environ. Microbiol.* 81, 432–440. doi: 10.1128/aem.03142-14

Tata, S. K., Jung, J., Kim, Y. H., Choi, J. Y., Jung, J. Y., Lee, I. J., et al. (2016). Heterologous expression of chloroplast-localized geranylgeranyl pyrophosphate synthase confers fast plant growth, early flowering and increased seed yield. *Plant Biotechnol. J.* 14, 29–39. doi: 10.1111/pbi.12333

Tianzhen, H., Baoming, L., Guanghui, T., Qing, Z., Yingping, X., and Lirong, Q. (2009). Application of acoustic frequency technology to protected vegetable production. *Trans. Chin. Soc. Agric. Eng.* 25, 156–159. doi: 10.3969/j.issn.1002-6819.2009.2.030

Vaucheret, H. (2006). Post-transcriptional small RNA pathways in plants: mechanisms and regulations. *Genes. Dev.* 20, 759–771. doi: 10.1101/gad.1410506

Vincent, T. R., Avramova, M., Canham, J., Higgins, P., Bilkey, N., Mugford, S. T., et al. (2017). Interplay of plasma membrane and vacuolar ion channels, together with BAK1, elicits rapid cytosolic calcium elevations in *Arabidopsis* during aphid feeding. *Plant Cell* 29, 1460–1479. doi: 10.1105/tpc.17.00136

Wang, W., Liu, D., Zhang, X., Chen, D., Cheng, Y., and Shen, F. (2018). Plant MicroRNAs in cross-kingdom regulation of gene expression. *Int. J. Mol. Sci.* 19:2007. doi: 10.3390/ijms19072007

Yamaguchi, N., Winter, C. M., Wu, M. F., Kwon, C. S., William, D. A., and Wagner, D. (2014). PROTOCOLS: chromatin immunoprecipitation from *Arabidopsis* Tissues. *Arabidopsis Book* 12:e0170. doi: 10.1199/tab.0170

Zhai, J., Jeong, D.-H., De Paoli, E., Park, S., Rosen, B. D., Li, Y., et al. (2011). MicroRNAs as master regulators of the plant NB-LRR defense gene family via the production of phased, trans-acting siRNAs. *Genes Dev.* 25, 2540–2553. doi: 10.1101/gad.177527.111

Zhang, R., Zheng, F., Wei, S., Zhang, S., Li, G., Cao, P., et al. (2019). Evolution of disease defense genes and their regulators in plants. *Int. J. Mol.* 20:335. doi: 10.3390/ijms20020335

Zhang, T., Zhao, Y. L., Zhao, J. H., Wang, S., Jin, Y., Chen, Z. Q., et al. (2016). Cotton plants export microRNAs to inhibit virulence gene expression in a fungal pathogen. *Nat. Plants* 2:16153. doi: 10.1038/nplants.2016.153

Zhang, Y., Liu, T., Meyer, C. A., Eeckhoute, J., Johnson, D. S., Bernstein, B. E., et al. (2008). Model-based analysis of ChIP-Seq (MACS). *Genome Biol.* 9:R137. doi: 10.1186/gb-2008-9-9-r137

Zhao, Q., Nakashima, J., Chen, F., Yin, Y., Fu, C., Yun, J., et al. (2013). Laccase is necessary and nonredundant with peroxidase for lignin polymerization during vascular development in *Arabidopsis*. *Plant Cell* 25, 3976–3987. doi: 10.1105/tpc.113.117770

Conflict of Interest: The authors declare that the research was conducted in the absence of any commercial or financial relationships that could be construed as a potential conflict of interest.

frontiers in Plant Science

ORIGINAL RESEARCH
published: 15 September 2021
doi: 10.3389/fpls.2021.726266

Streptomyces sp. JCK-6131 Protects Plants Against Bacterial and Fungal Diseases via Two Mechanisms

*Khanh Duy Le[1], Jeun Kim[2], Hoa Thi Nguyen[1], Nan Hee Yu[1], Ae Ran Park[1], Chul Won Lee[2] and Jin-Cheol Kim[1]**

[1] Department of Agricultural Chemistry, Institute of Environmentally Friendly Agriculture, College of Agriculture and Life Sciences, Chonnam National University, Gwangju, South Korea, [2] Department of Chemistry, Chonnam National University, Gwangju, South Korea

Plant bacterial and fungal diseases cause significant agricultural losses and need to be controlled. Beneficial bacteria are promising candidates for controlling these diseases. In this study, *Streptomyces* sp. JCK-6131 exhibited broad-spectrum antagonistic activity against various phytopathogenic bacteria and fungi. *In vitro* assays showed that the fermentation filtrate of JCK-6131 inhibited the growth of bacteria and fungi with minimum concentration inhibitory (MIC) values of 0.31–10% and 0.31–1.25%, respectively. In the *in vivo* experiments, treatment with JCK-6131 effectively suppressed the development of apple fire blight, tomato bacterial wilt, and cucumber *Fusarium* wilt in a dose-dependent manner. RP-HPLC and ESI-MS/MS analyses indicated that JCK-6131 can produce several antimicrobial compounds, three of which were identified as streptothricin E acid, streptothricin D, and 12-carbamoyl streptothricin D. In addition, the disease control efficacy of the foliar application of JCK-6131 against tomato bacterial wilt was similar to that of the soil drench application, indicating that JCK-6131 could enhance defense resistance in plants. Molecular studies on tomato plants showed that JCK-6131 treatment induced the expression of the *pathogenesis-related* (*PR*) genes *PR1*, *PR3*, *PR5*, and *PR12*, suggesting the simultaneous activation of the salicylate (SA) and jasmonate (JA) signaling pathways. The transcription levels of *PR* genes increased earlier and were higher in treated plants than in untreated plants following *Ralstonia solanacearum* infection. These results indicate that *Streptomyces* sp. JCK-6131 can effectively control various plant bacterial and fungal diseases via two distinct mechanisms of antibiosis and induced resistance.

Keywords: *Streptomyces*, priming defense, streptothricin, ISR, SAR

OPEN ACCESS

Edited by:
Yasufumi Hikichi, Kôchi University, Japan

Reviewed by:
Xingang Zhou, Northeast Agricultural University, China
Jiangang Li, Institute of Soil Science (CAS), China

****Correspondence:***
Jin-Cheol Kim
kjinc@jnu.ac.kr

Specialty section:
This article was submitted to Plant Pathogen Interactions, a section of the journal Frontiers in Plant Science

Received: *16 June 2021*
Accepted: *30 July 2021*
Published: *15 September 2021*

Citation:
Le KD, Kim J, Nguyen HT, Yu NH, Park AR, Lee CW and Kim J-C (2021) Streptomyces sp. JCK-6131 Protects Plants Against Bacterial and Fungal Diseases via Two Mechanisms. Front. Plant Sci. 12:726266. doi: 10.3389/fpls.2021.726266

HIGHLIGHTS

We found two mechanisms of *Streptomyces* JCK-6131 effective protect the plant against bacterial and fungal diseases, including production of streptothricin-like antibiotics and priming in host defense.

INTRODUCTION

Under field conditions, crops are often threatened by a variety of biotic pathogens including fungi, bacteria, nematodes, and viruses. Plant diseases caused by bacteria and fungi account for major losses in agricultural productivity (Lazarovits et al., 2014). Chemical bactericides and fungicides have been widely used to control various plant diseases. However, the misuse and indiscriminate use of chemical control agents have caused adverse effects on humans and the environment. Therefore, their application should be limited. Moreover, climate change and the rise of pesticide resistance also reduce the effectiveness of synthetic chemicals. This has led many scientists to search for potent alternative strategies against plant diseases (Ul Haq et al., 2020). The application of biological control methods is considered an effective alternative strategy (Lazarovits et al., 2014).

Plants have evolved a variety of defense mechanisms to protect themselves from pathogens, including physical and chemical defenses, which stop pathogen infection and the development of diseases (Nishad et al., 2020). Plants can alter their defense strategies depending on the pathogen. Plants distinguish and regulate their defense system based on the mechanism induced by the attacker and show suitable responses, such as the activation of the salicylic acid (SA) and jasmonic acid (JA)/ethylene (ET) pathways (De Vos et al., 2005). Plants interact with various microorganisms in the environment, and these interactions can be either positive or negative, either enhancing or compromising their defense system. Therefore, increasing research is being conducted on improving plant resistance against various pathogens (Bruce and Pickett, 2007).

Control of plant diseases using beneficial bacteria has great potential. Beneficial bacteria can enhance plant growth. Plant growth-promoting bacteria (PGPB) are classified according to their habitat; they can colonize between living tissues (endosphere), around the root (rhizosphere), on the surface of the root (rhizoplane), or on the aerial parts (phyllosphere) of plants (Mwajita et al., 2013; Dong et al., 2019). PGPB use various mechanisms to repress the growth of plant pathogens. They can directly repress pathogens by producing antibiotics, or through competition or parasitism. They can also indirectly repress pathogens by stimulating the plant's defense system (Niu et al., 2011; Chaparro et al., 2014). For example, they can produce bioactive substances that can kill or inhibit the growth of pathogens. Till date, many studies have reported the production of natural chemicals, such as antibiotics, iron-chelating siderophores, antimicrobial volatiles, and lytic and detoxification enzymes, by beneficial bacteria (Compant et al., 2005). Additionally, some PGPB can stimulate defense resistance in plants against a variety of pathogens. Induction of defense resistance includes induced systemic resistance (ISR) and systemic acquired resistance (SAR), which can suppress plant diseases by up to 85% (Walters et al., 2013). It has been elucidated that the SA-dependent signaling pathway controls SAR through the induction of the expression of SA-responsive *pathogenesis-related* (*PR*) genes (e.g., *PR1*, *PR4*, and *PR5*), which are associated with broad-spectrum plant defense responses. In contrast, the JA/ET-dependent signaling pathway regulates ISR and is associated with the expression of JA/ET-responsive genes (e.g., *PR3*, *PR4*, and defensin [*PR12*]) (Van Loon and Van Strien, 1999). Treating plants with PGPB or their products (elicitors) enhances defense resistance against pathogens in the future; this process is known as priming (Conrath et al., 2015).

Streptomyces species are aerobic and filamentous bacteria able to produce a large number of antibiotics and bioactive compounds, some of which have been applied in controlling plant diseases (Dhanasekaran et al., 2012). Numerous studies have reported that *Streptomyces* spp. serve as PGPB and biocontrol agents in plant protection against bacterial and fungal diseases (Cheng et al., 2010; Suárez-Moreno et al., 2019; Vergnes et al., 2020). Moreover, *Streptomyces* spp. are capable of stimulating plant defense resistance (Dias et al., 2017; Abbasi et al., 2019; Vergnes et al., 2020). However, only a few *Streptomyces* strains have been studied thus far; this limits their potential use.

During screening for *Streptomyces* strains that show antagonistic activity against phytopathogenic bacteria and fungi, we discovered JCK-6131, a strain that exhibited a broad-spectrum antimicrobial activity, leading us to conduct this study. The main objectives of this research were to: (1) identify *Streptomyces* sp. JCK-6131, (2) examine the antimicrobial activity of its fermentation filtrate against phytopathogenic bacteria and fungi, (3) evaluate the bio-control efficacy of its fermentation broth against plant bacterial and fungal diseases, and (4) assess the induction of the expression of *PR* genes in tomato plants treated with the fermentation broth of *Streptomyces* sp. JCK-6131.

MATERIALS AND METHODS

Culture and Fermentation of *Streptomyces*

Streptomyces sp. JCK-6131 was isolated from suppressive soil in Korea and maintained on international *Streptomyces* project 2 (ISP2; Becton, Dickinson, and Company, Franklin Lakes, NJ, United States) agar medium (yeast extract 4 g, malt extract 10 g, dextrose 4 g, agar 20 g, and distilled water for 1 L). The strain was stored in 30% glycerol at -80°C during the study period. For the purification of secondary metabolites, a single colony was transferred into ISP2 broth medium to make seed culture. After 48 h of incubation, 1% of the seed culture was inoculated into a 500-mL Erlenmeyer flask containing 100 mL of GSS medium (10 g soluble starch, 250 mg K_2HPO_4, 25 g soybean meal, 1 g beef extract, 4 g yeast extract, 2 g NaCl, 20 g glucose, 2 g $CaCO_3$, and distilled water for 1 L of medium, pH adjusted to 7.2) and fermented at 30°C and 180 rpm for 3 days. The obtained fermentation broth was centrifuged to divide the pellet and supernatant for further experiment.

Plant Pathogenic Microorganisms

Sixteen phytopathogenic bacteria were used in this study, including *Acidovorax avenae* subsp. *cattleyae* (Aac), *Acidovorax konjaci* (Ak), *Agrobacterium tumefaciens* (At), *Burkholderia glumae* (Bg), *Clavibacter michiganensis* subsp. *michiganensis*

(Cmm), *Erwinia pyrifoliae* (Ep), *Erwinia amylovora* (Ea), *Pectobacterium carotovorum* subsp. *carotovorum* (Pcc), *Pectobacterium chrysanthemi* (Pc), *Pseudomonas syringae* pv. *lachrymans* (Psl), *Pseudomonas syringae* pv. *actinidiae* (Psa), *Ralstonia solanacearum* (Rs), *Xanthomonas euvesicatoria* (Xe), *Xanthomonas axonopodis* pv. *citri* (Xac), *Xanthomonas arboricola* pv. *pruni* (Xap), and *Xanthomonas oryzae* pv. *oryzae* (Xoo). The bacteria were kindly supplied by Dr. S. D Lee of Rural Development Administration, Prof. S.-W. Lee of Dong-A University, and Prof. Y-G Ko of Suncheon National University, South Korea and stored in 30% glycerol at -80°C in Chonnam National University. The bacteria were cultured on tryptic soy agar (TSA; Becton, Dickinson, and Company) and tryptic soy broth (TSB; Becton, Dickinson, and Company) media at 30 ± 2°C. Four phytopathogenic fungi—*Botrytis cinerea* (Bc), *Colletotrichum coccodes* (Cc), *Fusarium oxysporum* f. sp. *cucumerinum* (Foc), and *Rhizoctonia solani* (Rhs)—were obtained from the Korea Research Institute of Chemical Technology, Daejeon, South Korea. *Raffaelea quercus-mongolicae* (Rq) and *Sclerotinia homoeocarpa* (Sh) were kindly supplied by the Korea Forest Research Institute, Seoul, South Korea. *Fusarium graminearum* (Fg) and *Pythium ultimum* (Pyu) were obtained from Seoul National University, Seoul, and Korea Agricultural Culture Collection, Jeonju, South Korea, respectively. All fungi were incubated on potato dextrose agar (PDA; Becton, Dickinson, and Company) and potato dextrose broth (PDB; Becton, Dickinson, and Company) media at 25°C.

Plant Materials

Tomato (cultivar "Seokwang"; Farmhannong Co., Ltd, Seoul, South Korea) was sown in vinyl pots (6.0 cm diameter) containing nursery soil and kept in an incubation room with 12 h daylight per day for 5 weeks. Cucumber (cultivar "Chungboksamchok"; Syngenta, South Korea) was soaked in warm water for 2 h then germinated in a petri dish containing wet paper at 30°C for 2 days. The germinated seeds were sown into nursery soil and grown at 25°C under the same light conditions for 7 days. *Arabidopsis thaliana* (*PR1:GUS* transgenic) seeds were surface-sterilized in a solution of 25% bleach plus 0.01% tween 20 for 5 min, followed by 70% ethanol for 5 min. Then, seeds were rinsed five times and soaked in sterilized water at 4°C for 2 days. These seeds were germinated on Murashige-Skoog (MS) agar medium (0.43 g MS salt, 1 g sucrose, and 0.7 g phyto-agar per 100 mL, pH 5.7) plus 50 μg/mL of kanamycin for 2 weeks at 25°C with a cycle of 16 h daylight per day in a growth-chamber.

Sequence and Whole-Genome Comparative Analysis

For identification of JCK-6131 strain, total DNA of JCK-6131 was extracted using an I-genomic BYF DNA Extraction mini kit (iNtRON Biotechnology, Inc., Seongnam-si, Gyeonggi-do, South Korea). The 16S rRNA was amplified by PCR using the primer pair 27f 5′- AGAGTTTGATCCTGGCTCAG – 3′ and 1492r 3′ – TTCAGCATTGTTCCATTGG – 5′. The PCR thermal profile was 95°C for 5 min; 30 cycles of 95°C for 30 s, annealing at 55°C for 30 s, and 72°C for 1 min 30 s; and a final extension at 72°C for 10 min. The sequence (1385 bp) was compared for similarity with the reference species of *Streptomyces* in the GenBank database using the BLAST search tool. Phylogenetic analysis was performed using the neighbor-joining DNA distance algorithm with MEGA (version X). Additionally, the whole gene sequences were uploaded and pairwise genome calculations of OrthoANI were performed using the Orthologous Average Nucleotide Identity tool (Lee et al., 2016).

Biochemical and Physiological Identification

The strain JCK-6131 was cultured on ISP media (ISP1, 2, 3, 4, 5, and 7) to observe the color of the colony and pigment production. The ability to enzymatic production, utilization of multiple carbon and nitrogen sources were also evaluated. The physiological tests were performed to estimate the growth of JCK-6131 on different concentrations of NaCl, temperatures as well as pH (Lima et al., 2017).

In vitro Antimicrobial Assay

The antimicrobial activity of the fermentation filtrate of *Streptomyces* sp. JCK-6131 was examined against all test microorganisms using a broth dilution method according to previous reports for bacteria (Le et al., 2020) and fungi (Kim et al., 2020). A serial two-fold dilution of the fermentation filtrate (10, 5, 2.5, 1.25, 0.63, 0.31, 0.16, and 0.08%) was prepared for these assays. Streptomycin sulfate was used as a positive control for phytopathogenic bacteria. The test microorganisms were incubated at 30°C for 1–2 days for bacteria and 25°C for 3–7 days for fungi. The minimum inhibitory concentration (MIC) value was the lowest concentration that can inhibit the growth of microorganisms. Each run of the experiment contained three replicates, and the entire experiment was repeated twice.

Isolation and Identification of Antimicrobial Metabolites

The fermentation broth was centrifuged to remove the cell mass and then the pH of the supernatant (1 L) was adjusted to 3.6 using 5 M HCl. Amberlite XAD-16N resin (50 g) was added to the culture supernatant and then the suspension was kept overnight, followed by filtering through a filter paper. The filtrate was precipitated in ice acetone (1:4, v/v), and the precipitate was obtained by centrifugation. The precipitate was dissolved in PBS (50 mM, pH 7.0) then loaded on a Sephadex LH20 open column that equilibrated and eluted the sample using water. Fractions that showed antibacterial activity against indicator bacteria were combined to get partially purified extract (PPE), and PPE were further purified by reverse-phase high-performance liquid chromatography (RP-HPLC; Shimadzu, Japan). The purified substances were collected and lyophilized based on their antibacterial activity, and their molecular masses were analyzed by liquid chromatography-mass spectrometry (LC-MS) (Shimadzu 6AD HPLC; API2000) in positive mode (100–1800 *m/z*) with a ZORBAX C18 column (4.6 × 250 mm). The mobile phases were distilled water and ACN containing 0.05% TFA. A linear gradient of 0–8% over 16 min was used

with a flow rate of 1 mL/min. The highly purified samples were used for electrospray ionization tandem mass spectrometry (ESI-MS/MS). The mass parameters were as follows: curtain gas, 30; spray voltage, 5500; ion source gas, 50 psi; and flow rate, 10 μ L/mL.

Historical GUS Staining Assay

Arabidopsis seedlings were transplanted to a liquid medium containing either fermentation broth or fermentation filtrate of *Streptomyces* sp. JCK-6131 at a final concentration of 1%. The plants were placed in a growth chamber with 12 h daylight per day at 25°C for 2 days. Salicylic acid (SA) was used as a positive control and GSS medium as a negative control. Historical GUS staining was conducted as previously reported (Kondo et al., 2014). Briefly, the seedlings were fixed in 90% ice acetone at -20°C for 1 h and washed twice in sodium phosphate buffer (pH 7.0). Washed plants were immersed in GUS staining solution that consisted of 0.1% Triton-X, 100 mM sodium phosphate buffer, 2.5 mM potassium ferrocyanide, 2.5 mM potassium ferricyanide, and 2 mM X-GlucA (Duchefa, X1405) overnight at 30°C. Reactions were stopped by 70% ethanol for 30 min and the stained samples were washed in 90% ethanol several times to remove chlorophyll. The GUS activity was qualitatively assayed by determining the blue color and observed under an optical microscope.

RNA Isolation and RT-qPCR

Tomato plants were sprayed with the 100-fold-diluted fermentation broth of *Streptomyces* sp. JCK-6131 at 3 days before Rs inoculation. Three plants from each group were taken at 1, 2, and 3 days after inoculation. The leaves were collected and ground in liquid nitrogen using a porcelain mortar. Total RNA was extracted using an Iqeasy^{TM} Plant RNA Extraction mini kit (iNtRON, Korea) and quantified using a NanoDrop spectrometer (NP80, IMPLEN, Germany). cDNA was synthesized from 1 μg of each RNA sample after treating with RNase-free DNase I using a SuperScript^{TM} IV First-Strand Synthesis System kit (Invitrogen). RT-qPCR was performed using a total reaction volume of 10 μL, containing 1 μL of cDNA template, 4 μL of 0.625 pM of forward and reverse primers, and 5 μL of 2 × iQ^{TM} SYBR Green supermix (BioRad) on a BioRad CFX96^{TM} Real-Time System. The PCR cycling parameters were denaturation at 95°C for 3 min; followed by 40 cycles at 95°C for 9 s, 55°C for 1 min, and 55°C for 3 s; and a final extension at 95°C for 30 s. Data was expressed as the normalized ratio of target genes to the internal reference *Ubiquitin* (*UBI*) gene. Primer sequences are provided in **Supplementary Table 1**. Experiments were conducted in triplicate.

In vivo Antimicrobial Assays

Preparation of Samples

The biocontrol efficacy of the fermentation broth of *Streptomyces* sp. JCK-6131 was evaluated against tomato bacterial wilt, fire blight of apple, and *Fusarium* wilt of cucumber. The fermentation broth was diluted in distilled water at 5-, 10-, 20-, and 100-fold, and then, Tween 20 was incorporated into each diluent at a concentration of 250 μg/mL. Additionally, PPE was also prepared in Tween 20 solution at 1,000, 100 and 10 μg/mL. Buramycin (streptomycin sulfate 20% WP; Farm Hannong Co., Seoul, Korea) and janroken (hymexazol 30% + penthiopyrad 5% WP; Hankook Samgong Co., Seoul, Korea) were used as positive controls for bacterial and fungal diseases, respectively. Tween 20 solution was used as a negative control.

Bacterial Wilt Disease of Tomato

During the fourth-leaf stage of tomato plants with bacterial wilt, soil was drenched with the fermentation broth of *Streptomyces* sp. JCK-6131 and PPE. The plants were treated with 20 mL of each sample per pot at 24 h before inoculation, and then 20 mL of Rs cell suspension (10^8 CFU/mL, 10 mM $MgCl_2$) was inoculated by soil drenching. A separate experiment was designed to evaluate the potential of ISR in tomato by *Streptomyces* sp. JCK-6131 against Rs infection. The tomato plant leaves were treated with the 100-fold-diluted fermentation broth and the fermentation filtrate three days before inoculation by foliar spraying. The inoculated plants were kept in the dark for 24 h and then transferred to an incubation room at 30°C and 75% RH with 12 h daylight per day for 10 days. The disease index was graded on the following scale: 0 = no leaf symptom, 1 = one leaf wilted, 2 = two or three leaves wilted, 3 = more than four leaves wilted, and 4 = plant dead (Le et al., 2020).

Fire Blight Disease of Apple

The biological efficacy of *Streptomyces* sp. JCK-6131 was evaluated against fire blight disease of apple using a detached leaf assay. The youngest true leaves were excised from the tips of growing shoots of 3-year-old apple trees (Hongro cultivar, moderately sensitive to fire blight disease) and sterilized in 1% bleach solution for 1 min, followed by rinsing three times in sterile water. The leaves were air-dried in a clean-beach, and then the detached leaf assay of fire blight disease was performed according to the method of Cabrefiga and Montesinos (2017). Briefly, each leaf was wounded with a sterile knife (or forceps) in the lamina in four positions, followed by treating with 10 μL of each sample onto each wound. After 1 h of air-drying, 10 μL of Ea suspension (10^7 CFU/ml) was inoculated at each pretreated position. The disease severity was recorded on the following scale: 0, no symptom; 1, necrosis located around the wound; 2, necrosis progressing far from the wound; and 3, necrosis of the whole leaf.

Fusarium Wilt Disease of Cucumber

The assay was conducted on seven-day-old seedlings of cucumber according to the method of Lee et al. (2014). The seedlings were pretreated with 20 mL of each sample per pot by soil drenching, and then the treated plants were inoculated with 20 mL solution of conidial suspension of Foc (10^6 conidia/ml) 24 h after treatment by soil drenching. The inoculated plants were kept in darkness for 24 h and incubated at 25°C and 75% RH with 12 h daylight per day for 4 weeks in an incubation room. The severity was calculated using the following scale: 0, no symptoms; 1, < 25% of leaves showing yellowing and or necrosis; 2, 26–50% of leaves showing yellowing and/or necrosis; 3, 51–75% of leaves showing yellowing and/or necrosis; and

4, 76–100% of leaves showing wilt, yellowing, and/or necrosis (Abro et al., 2019).

Calculation of Control Value

The *in vivo* experiments were repeated two times with three replicates per treatment and disease severity (DS) was transferred to a control percentage (±standard deviation) compared to the untreated control using the following equation:

$$\text{Control value}(\%) = \frac{(\text{DS of untreated control} - \text{DS of treatment})}{\text{DS of untreated control}} \times 100\%. \quad (1)$$

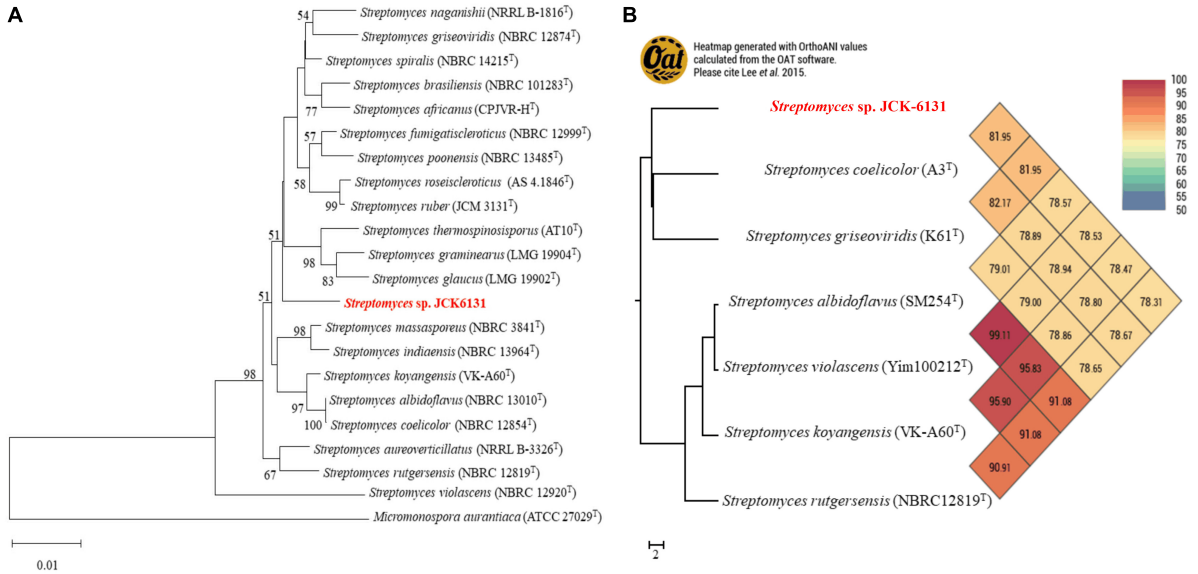

FIGURE 1 | Taxonomic classification of genome comparative of *Streptomyces* sp. JCK6131 compared to the genome of other related *Streptomyces*. **(A)** Phylogenetic relationships between JCK-6131 and related *Streptomyces* strains represented as a neighbor-joining (NJ) tree based on 16S rRNA gene sequences. The evolution history was determined using the NJ method with a Jukes-Cantor model. The numbers at the branching points represent the bootstrap values from 1,000 replications. *Micromonospora aurantiaca* ATCC 27029^T was used as the outgroup. Bar = 0.010 substitutions per nucleotide position. **(B)** Heatmap generated using the OrthoANI values for JCK-6131 and other type strains of *Streptomyces* species calculated using the OAT software.

TABLE 1 | Minimum inhibitory concentration (MIC) of the fermentation filtrate of *Streptomyces* sp. JCK-6131 against several plant pathogenic bacteria.

Plant pathogenic bacteria	MIC	
	Fermentation filtrate (%)	Streptomycin sulfate (μ g/mL)
Acidovorax avenae subsp. *cattleyae*	0.31 ± 0.00^{e}	500 ± 0.00^{b}
Acidovorax konjaci	0.42 ± 0.18^{e}	7.81 ± 0.00^{e}
Agrobacterium tumefaciens	10.00 ± 0.00^{a}	166.67 ± 72.17^{c}
Burkholderia glumae	10.00 ± 0.00^{a}	20.84 ± 9.02^{e}
Clavibacter michiganensis subsp. *michiganensis*	10.00 ± 0.00^{a}	20.84 ± 9.02^{e}
Erwinia amylovora TS3128	2.50 ± 0.00^{bcd}	5.21 ± 2.25^{e}
Erwinia pyrifoliae	3.33 ± 1.44^{bc}	5.21 ± 2.25^{e}
Pectobacterium carotovorum subsp. *carotovorum*	3.33 ± 1.44^{bc}	15.63 ± 0.00^{a}
Pectobacterium chrysanthemi	4.17 ± 1.44^{b}	500 ± 0.00^{b}
Pseudomonas syringae pv. *actinidiae*	3.33 ± 1.44^{bc}	15.63 ± 0.00^{e}
Pseudomonas syringae pv. *lachrymans*	3.33 ± 1.44^{bc}	15.63 ± 0.00^{e}
Ralstonia solanacearum	1.25 ± 0.00^{de}	10.42 ± 4.52^{e}
Xanthomonas euvesicatoria	2.50 ± 0.00^{bcd}	20.83 ± 9.02^{e}
Xanthomonas arboricola pv. *pruni*	2.50 ± 0.00^{bcd}	62.5 ± 0.00^{d}
Xanthomonas campestris pv. *citri*	3.33 ± 1.44^{bc}	31.25 ± 0.00^{e}
Xanthomonas oryzae pv. *oryzae*	1.25 ± 0.00^{de}	10.42 ± 4.52^{e}

Means within the same column followed by a different letter are significantly different ($p < 0.05$), according to Duncan's multiple range test. The names of bacteria are presented in alphabetical order.

Statistical Analysis

Results of the pot experiments were analyzed by one-way analysis of variance (ANOVA), and significant differences among treatments were evaluated with Fisher's least significant difference test. The comparison of two treatment methods was conducted by Student *t*-tests. *In vitro* data were analyzed by ANOVA with Duncan's multiple range test. A p-value of < 0.05 was considered significant. The statistical analysis was performed in SPSS 23.0 software (SPSS Inc. Chicago, IL, United States).

RESULTS

Taxonomical Identification of *Streptomyces* sp. JCK-6131

The partial 16S rRNA (1385-bp) gene sequence of JCK-6131 was deposited in GenBank under accession number MW911616. Comparison of 16S rRNA sequences indicated that JCK-6131 was closely related to *Streptomyces spiralis* NBRC 14215 and *Streptomyces thermospinosisporus* AT10, with similarity values of 98.34 and 98.13%, respectively. However, the phylogenetic tree analysis based on neighbor-joining algorithms indicated that JCK-6131 could not be identified as a known *Streptomyces* species (**Figure 1A**). Also, the ANI calculation was determined using complete genomes of six *Streptomyces* strains available in NCBI which included *Streptomyces coelicolor* A3^T, *Streptomyces griseoviridis* K61^T, *Streptomyces albidoflavus* SM254^T, *Streptomyces violascens* Yim1000212^T, *Streptomyces koyangensis* VK-A60^T, and *Streptomyces rutgersensis* NBRC12819^T (**Figure 1B**). Low relative identity values were obtained when comparing the genomic similarity between JCK-6131 and other type strains of the genus *Streptomyces*. OrthoANI values ranged from 78.31 to 81.95% (<95%), representing a different genome-species with other closely related *Streptomyces* strains within classified groups. The results clearly proved that *Streptomyces* sp. JCK-6131 represents a novel species in the genus *Streptomyces*. Additionally, the biochemical and physiological tests showed that the JCK-6131 have the ability to utilize multiple carbon and nitrogen sources, and growth on a wide range of temperature (15–45^{o}C, opt 30^{o}C), pH (5–10, opt 7), and concentration of NaCl up to 6%. Together with that, the JCK-6131 strain could produce some hydrolysis enzyme such as protease, lipase, amylase, and cellulase. Further studies for species identification showed that color of colony and pigment production of JCK-6131 on ISP media that also were different from *Streptomyces spiralis* (**Supplementary Table 2**).

Antagonistic Activity of JCK-6131 Against Plant Pathogenic Bacteria and Fungi

Streptomyces sp. JCK-6131 exhibited broad-spectrum antibacterial activity against all test pathogenic bacteria. Among the 16 test bacteria, Aac and Ak were the most sensitive to the fermentation filtrate with an MIC value of 0.31%. Cell growth of Ea, Ep, Xoo, and Rs were highly inhibited, with an MIC value of 1.25%, followed by Pcc, Psa, Xe, Xap, and Xac, which had an MIC value of 2.5%. Moderate sensitivity was recorded against Psl and Pc, with an MIC range of 3.33–4.17%. Three bacterial strains—At, Bg, and Cmm—were relatively insensitive to the fermentation filtrate (**Table 1**).

In addition, the fermentation filtrate of *Streptomyces* sp. JCK-6131 also inhibited the mycelial growth of eight phytopathogenic fungi. Bc was the most sensitive, followed by Fg and Rs. The mycelial growth of Rq, Foc, and Sh was moderately inhibited by the fermentation filtrate. Cc was the most insensitive to the fermentation filtrate (**Table 2**).

Identification of Antimicrobial Metabolites

The antimicrobial compounds remained in the aqueous layer after being partitioned with organic solvents, and they positively reacted with ninhydrin, suggesting that JCK-6131 produced amino acid-containing antimicrobial compounds. According to the mass analysis, we found that the partially purified fraction contained at least three compounds, including $[M + H]^+$ ion peaks at 649.6 (**Figure 2A**) and 759.8 *m/z* (**Figures 2B,C**). Each compound was predicted to correspond to streptothricin E acid, streptothricin D, and 12-carbamoylstreptothricin D, respectively, based on the collision-induced dissociation (CID) spectra of each compound by ESI-MS/MS analysis (**Figure 2**; Ji et al., 2008, 2009). Streptothricin E acid presented multiple product ions at 189.2 [S′], 382.4 [GLL-2H_2O-NH_2CO], 443.3 [GLL-H_2O], 461.3 [GLL], 613.5 [M-2NH_3], and 631.6 *m/z* [M-NH_3] (**Supplementary Figure 1**). Streptothricin D and 12-carbamoylstreptothricin D presented the same fragment ions at 171.3 [S], 296.8 [GS-2H_2O-NH_2CO], 444.4 [GLL-H_2O], and 570 *m/z* [GLLL-H_2O] (**Supplementary Figures 2**, **3**). The structures of streptothricin consist of a streptolidine (S/S'), a carbamoylated D-gulosamine (G), and a β-lysine chain (L) Ji et al. (2008).

Efficacy of *Streptomyces* sp. JCK-6131 in Controlling Plant Bacterial and Fungal Diseases

Results of the detached leaf assay showed that the fermentation broth suppressed the development of apple fire blight caused

TABLE 2 | Minimum inhibitory concentration (MIC) of the fermentation filtrate of *Streptomyces* sp. JCK-6131 against eight plant pathogenic fungi.

Plant pathogenic fungi	Fermentation filtrate (%)
Botrytis cinerea	0.42 ± 0.18^{d}
Colletotrichum coccodes	1.67 ± 0.72^{a}
Fusarium graminearum	0.63 ± 0.00^{cd}
Fusarium oxysporum f. sp. *cucumerinum*	1.25 ± 0.00^{ab}
Pythium ultimum	1.04 ± 0.36^{bc}
Raffaelea quercus-mongolicae	1.04 ± 0.63^{bc}
Rhizoctonia solani	0.63 ± 0.00^{cd}
Sclerotinia homoeocarpa	1.25 ± 0.00^{ab}

Means within the same column followed by a different letter are significantly different ($p < 0.05$), according to Duncan's multiple range test. The names of the fungi are presented in alphabetical order.

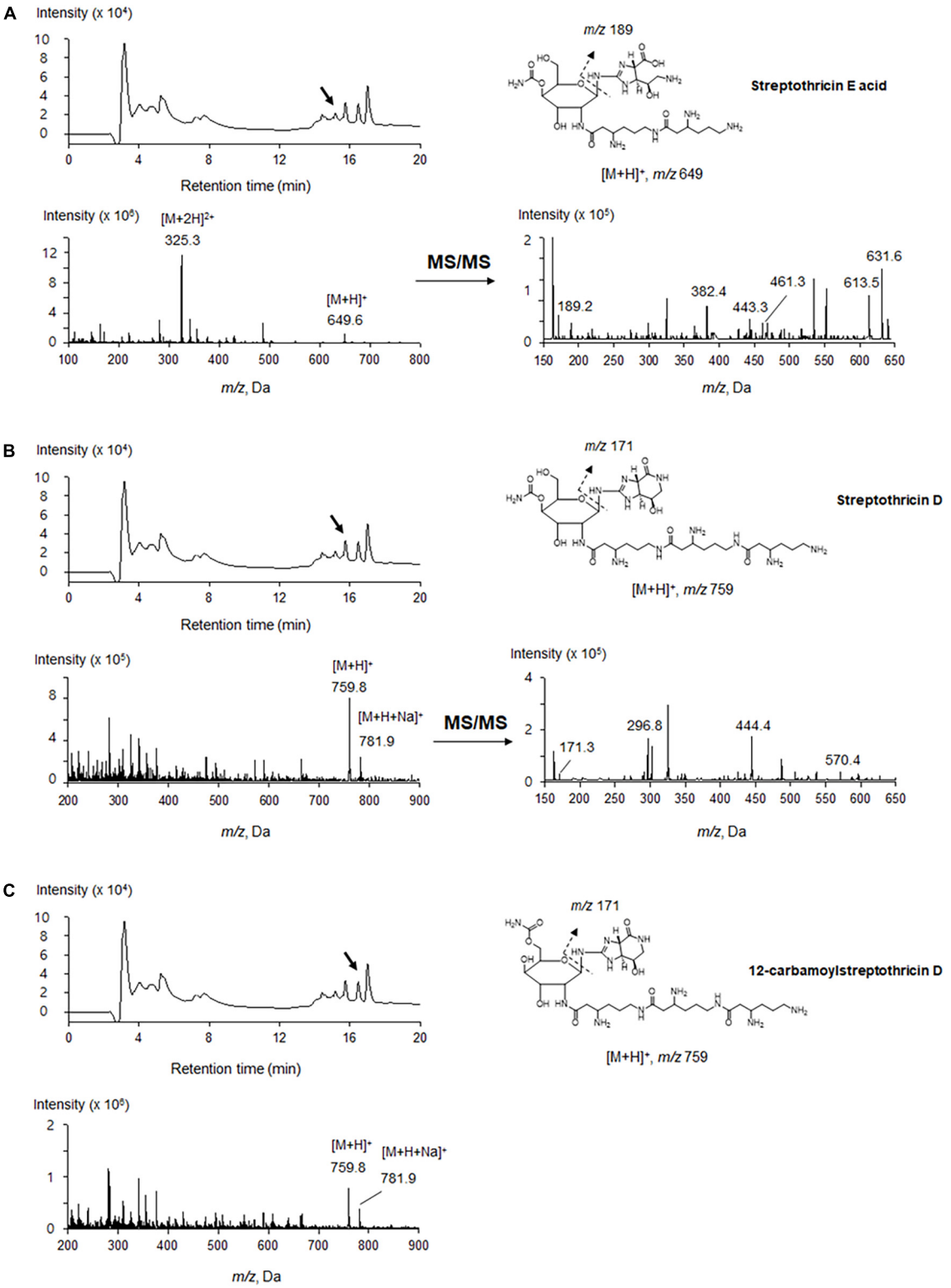

FIGURE 2 | LC-ESI-MS analysis of the compounds produced by *Streptomyces* sp. JCK-6131. Streptothricin E acid **(A)**, streptothricin D **(B)**, and 12-carbamoylstreptothricin D **(C)**. The LC chromatograms, mass spectra, and chemical structures with fragmentation patterns are shown.

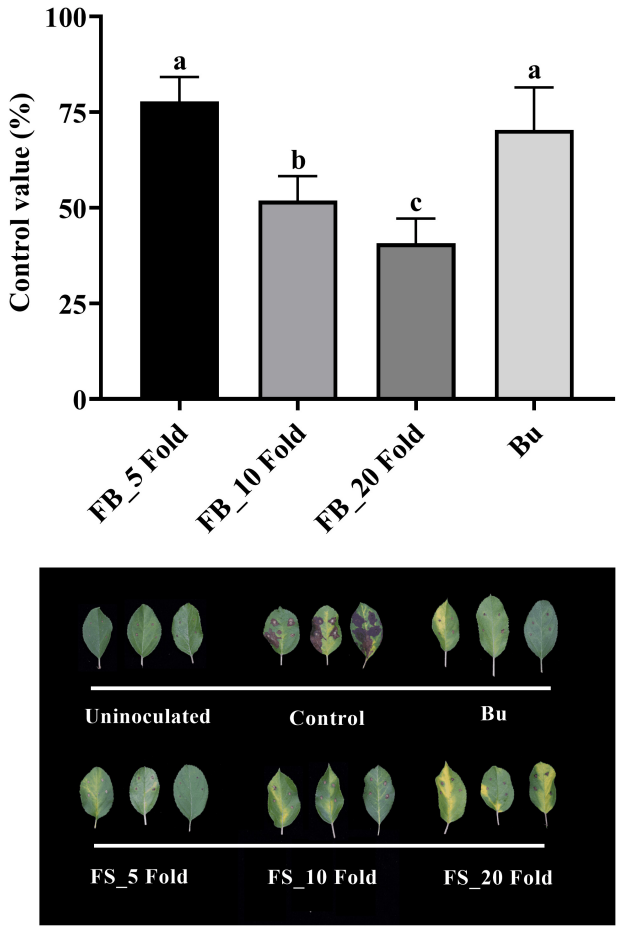

FIGURE 3 | Control efficacy of the fermentation broth of *Streptomyces* sp. JCK-6131 against apple fire blight in a detached leaf assay. FB = fermentation broth of *Streptomyces* sp. JCK-6131 and Bu = buramycin (×1000). Values are presented as the mean ± standard error of three runs, with three replicates each. The bars with the same letters represent non-significant differences between the treatments ($p < 0.05$, Fisher's least significant difference test).

by Ea in a dose-dependent manner (**Figure 3**). The highest protective activity was obtained by the treatment with the 5-fold-diluted fermentation broth of *Streptomyces* sp. JCK-6131 with a control value of 77.78% ($F_{3,8} = 13.94$, $p < 0.01$), which was not significantly different from the positive control buramycin treatment ($p = 0.549$). Likewise, the treatment with the 5-fold-diluted fermentation broth significantly reduced the severity of tomato bacterial wilt caused by Rs, with a control value of 86.11% ($F_{4,10} = 13.32$, $p < 0.001$), which was significantly higher than that of buramycin ($p = 0.014$) (**Figure 4A**). Interestingly, there was no significant difference in disease control between the treatment with the 20-fold-diluted fermentation broth and that with the 100-fold-diluted fermentation broth ($p = 0.260$), indicating the possibility of disease control efficacy via the ISR-activating effects of the fermentation broth of *Streptomyces* sp. JCK-6131. Hence, we further conducted the *in vivo* bioassay against tomato bacterial wilt, where the 100-fold-diluted fermentation broth was applied to the test plants by either soil drenching or foliar spraying. Both treatments suppressed the development of disease symptoms to similar extents, with a disease control efficacy of 55.55% for soil drenching and 52.78% for foliar spraying, which were not significantly different ($p = 0.678$) (**Figure 4B**).

On the other hand, PPE also reduced the development of tomato bacterial wilt disease in a dose-dependent manner with the highest control value of 88.89% by the treatment at 1,000 μg/mL ($F_{3,8} = 5.11$, $p < 0.05$, **Supplementary Figure 4**). Even at a low concentration of 10 μg/mL, it could control the plant disease with a control value of 58.33%.

The fermentation broth of *Streptomyces* sp. JCK-6131 also effectively suppressed the development of cucumber *Fusarium* wilt disease. The control efficacy was positively correlated with the concentration of fermentation broth at all dilutions between 5- and 20-fold, but not at 100-fold dilution (**Figure 5**). The development of *Fusarium* wilt on cucumber was significantly repressed by the treatment with the 5-fold-diluted fermentation broth, with a control value of 83.33% ($F_{4,10} = 23.67$, $p < 0.001$), which was quite similar to that of the positive control janroken treatment ($p = 0.125$). The treatment with the 100-fold-diluted fermentation broth also displayed a control value similar to that of the treatment with the 10-fold-diluted fermentation broth ($p = 0.588$).

Qualitative Induction of PR1 Gene Expression

Based on GUS activity analysis, either fermentation broth or filtrate treatment resulted in induction of *PR1:GUS* gene expression, which was slightly weaker than that of the SA control. In contrast, no expression of the *PR1:GUS* gene was observed on the medium-treated plants (negative control) (**Figure 6**).

Effect of JCK-6131 on Defense Responses in Tomato Against *Ralstonia solanacearum*

According to the above results, the fermentation broth of JCK-6131 induced the expression of the *PR1* gene. To clearly elucidate whether JCK-6131 plays a role in enhancing plant defense against pathogens, we analyzed the expression pattern of *PR* genes related to response to JCK-6131 treatment using RT-qPCR. The *PR* genes analyzed were *PR1*, *PR3*, *PR5*, and *PR12*, which are signature genes of the SA and JA signaling pathways. Tomato plants were foliar-sprayed with the 100-fold-diluted fermentation broth of JCK-6131, and the leaves were collected to measure the transcript levels of *PR* genes at 1, 2, and 3 days post-treatment (dpt) and post-inoculation (dpi). Compared with the negative control, the fermentation broth of JCK-6131 slightly induced the expression of *PR1*, *PR3*, *PR5*, and *PR12* genes in tomato plants at 1 dpt; however, the expression levels of these genes gradually decreased at 2 and 3 dpt. The expression levels of *PR1* and *PR5* were induced at higher levels than those of *PR3* and *PR12*. The expression levels of *PR1* and *PR5* in JCK-6131-treated plants were 2.99 and 2.80 times higher than those in the untreated plants, respectively (**Figures 7A,C**). The transcription levels of the *PR3* and *PR12* genes were 1.88 and 1.35 times higher in the treated

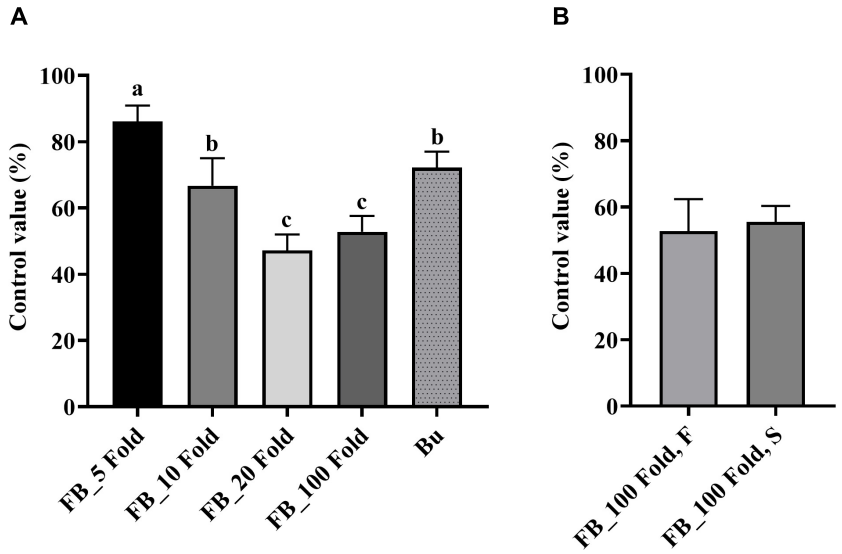

FIGURE 4 | Control efficacy of the fermentation broth of *Streptomyces* sp. JCK-6131 against tomato bacterial wilt in a pot experiment. **(A)** Treatment by soil drenching 1 day before inoculation. FB = fermentation broth of *Streptomyces* sp. JCK-6131, Bu = buramycin (×1000); analyzed by Fisher's least significant difference test. **(B)** Treatment by foliar spraying (F) and soil drenching (S) 3 days before inoculation; analyzed by student *t*-test. Values are presented as the mean ± standard error of three runs, with three replicates each. The bars with the same letters represent non-significant differences between the treatments ($p < 0.05$).

plants, respectively, compared to those in the untreated plants (**Figures 7B,D**).

To elucidate whether pre-treatment with the fermentation broth of JCK-6131 played a role in supporting plant defenses against pathogen infection, we further analyzed the transcription levels of four marker genes following the inoculation with Rs. Increased expression of target genes was observed in both the pretreated and untreated plants as a result of pathogen attack. The upregulation of *PR* genes in JCK-6131-treated plants was faster and stronger than in the untreated plants. In JCK-6131-treated plants, the expression levels of the *PR3* and *PR12* genes reached a maximum at 1 dpi and were then downregulated at 2 and 3 dpi (**Figures 7B,D**); their transcription levels were higher than those in the untreated plants by 1.9 and 5.3 times, respectively. In contrast, the expression levels of *PR1* and *PR5* in the JCK-6131-treated plants reached a maximum at 2 dpi, at which time it was 5.05 and 5.32 times higher, respectively, compared to those in the untreated plants (**Figures 7A,C**).

DISCUSSION

Given their abundance, biodiversity, and wide distribution in the natural environment, beneficial bacteria are promising candidates for plant protection (Compant et al., 2005). *Streptomyces* spp. have a great potential in the control of plant bacterial and fungal diseases by producing numerous antibiotics that can kill or inhibit the growth of plant pathogens (Kim et al., 1999; Dhanasekaran et al., 2012; Æimoviæ et al., 2015). *Streptomyces*-derived antibiotics were also reported to act as weapons in mediating *Streptomyces-Fusarium* interactions in soil (Essarioui et al., 2020).

We discovered a *Streptomyces* strain exhibiting a broad-spectrum antagonistic activity against various phytopathogenic bacteria and fungi. The fermentation broth of JCK-6131 effectively suppressed the development of fire blight of apple, bacterial wilt of tomato, and *Fusarium* wilt of cucumber. Together with that, the PPE also displayed effective disease control efficacy of tomato bacterial wilt. Additionally, the JCK-6131 strain can promote plant growth by producing IAA (data not shown), indicating that it belonged to the PGPB group. Identification of antimicrobial compounds showed that the strain produces streptothricin antibiotics, which have broad-spectrum antimicrobial activity against bacteria and fungi. Three compounds were identified: streptothricin E acid, streptothricin D, and 12-carbamoylstreptothricin D. Till date, many members of the streptothricin group have been identified. Their chemical structures consist of β-lysine, streptolidine, and ?-glucosamine; the number of β-lysine chains is known to play an important role in antibacterial activity (Ji et al., 2009). Moreover, streptothricins were tested as a fungicide in agriculture for controlling plant diseases and registered as an agrochemical in China in the 1990s (Ji et al., 2008).

Apart from their ability to produce antibiotics, *Streptomyces* spp. have also been recognized to induce the expression of defense mechanism-associated genes in plants (Vurukonda et al., 2018). They can directly trigger or produce elicitors that can induce systemic resistance in the plant against pathogens (Dias et al., 2017; Abbasi et al., 2019; Vergnes et al., 2020). Nasr-Eldin et al. (2019) reported that the foliar spraying of the fermentation filtrates of *Streptomyces* spp. showed effective protection against potato-virus Y in all potato cultivars. The disease incidence caused by Rs in tomato plants was reduced after pre-treatment with the cell suspensions of *Streptomyces flavotricini* vh8 and

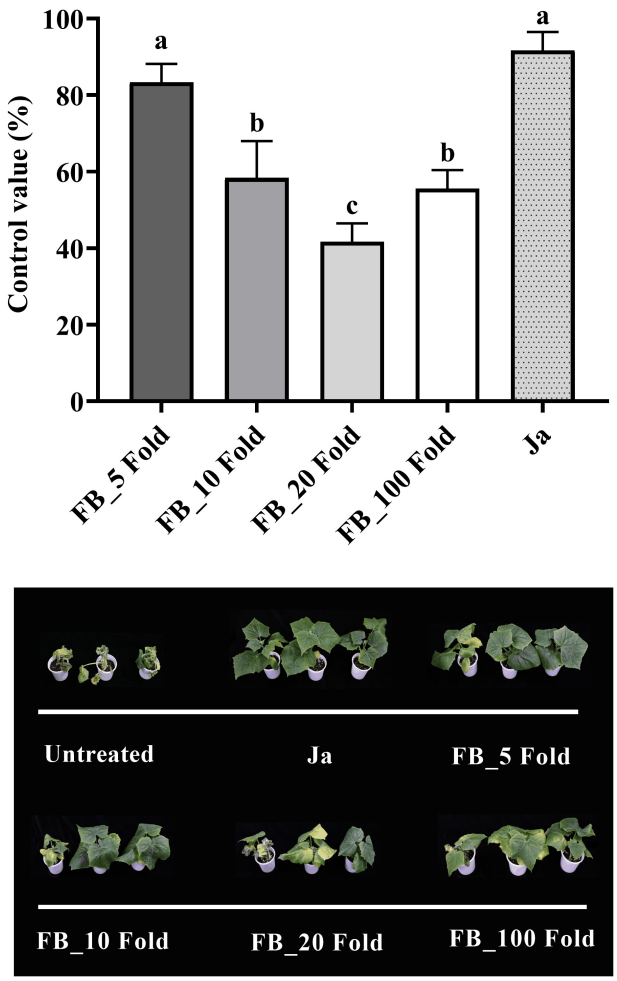

FIGURE 5 | Control efficacy of the fermentation broth of *Streptomyces* sp. JCK-6131 against cucumber *Fusarium* wilt in a pot experiment. FB = fermentation broth of *Streptomyces* sp. JCK-6131, Ja = janroken (×1000). Values are presented as the mean ± standard error of three runs, with three replicates each. The bars with the same letters represent non-significant differences between the treatments ($p < 0.05$, Fisher's least significant difference test).

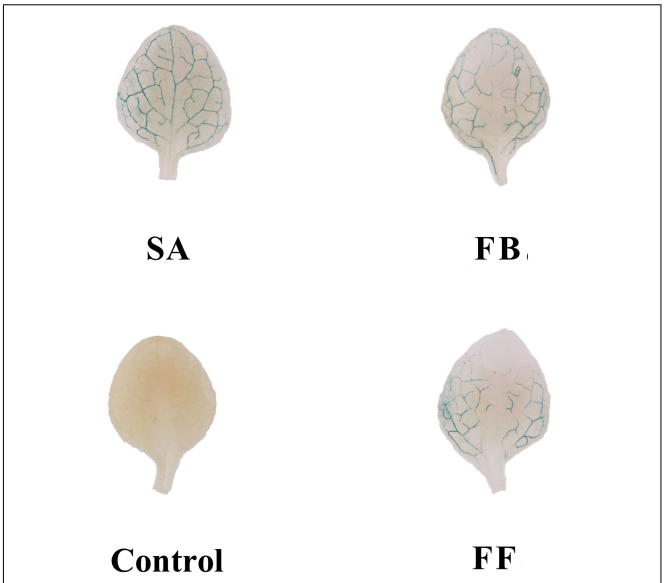

FIGURE 6 | GUS staining assay of *Arabidopsis* transgenic (PR1:GUS) seedlings treated with the fermentation broth (FB) and fermentation filtrate (FF) of *Streptomyces* sp. JCK-6131. SA = salicylic acid (0.1 mM), 1% GSS medium was used as a negative control.

Streptomyces toxytricini vh8 (Patil et al., 2011). Similarly, in the present study, the treatment with the 100-fold-diluted JCK-6131 fermentation broth suppressed the development of tomato bacterial wilt and cucumber *Fusarium* wilt by approximately 50%. Additionally, the disease control efficacy of the 100-fold-diluted JCK-6131 fermentation broth against tomato bacterial wilt was similar, regardless of the method of its application (foliar spraying or soil drenching). These results suggest that strain JCK-6131 could enhance defense resistance in plants.

Interactions between plants and pathogens results in the activation of defense signaling pathways such as the SA and JA signaling pathways, which leads to the accumulation of PR proteins that inhibit the growth of pathogens or repress the spread of disease to other organs (González-Bosch, 2018). The expression of *PR* genes is markedly induced by both biotic and abiotic stresses, making them important molecular markers for defense signaling pathways in plants (Van Loon and Van Strien, 1999). Among *PR* genes, the expression of the *PR1* gene has commonly been used as a marker of the activation of SAR, which enhances plant resistance to various pathogens (Park and Kloepper, 2000; Molinari et al., 2014; Li et al., 2015; Ali et al., 2018). In the present study, we found that the fermentation broth of the JCK-6131 strain induced the expression of the *PR1:GUS* gene in the transgenic plants, indicating that the SA signaling pathway was activated. A similar phenomenon was also reported by Vergnes et al. (2020), *PR1:GUS* gene expression in *Arabidopsis thaliana* plants was induced by 1% fermentation broth of *Streptomyces* sp. AgN23. Thus, these results suggest that JCK-6131 is capable of producing SAR elicitors.

The signaling crosstalk between the SA- and JA-signaling pathways are both synergistic and antagonistic. This crosstalk provides the potential for efficient regulation in plant defense responses according to the type of pathogen, and it depends on the relative concentration of these phytohormones (Li et al., 2019). Mur et al. (2006) reported that treatment with a relatively low concentration of both SA and JA resulted in the synergistic expression of the *PR1* and *defensin* genes in tobacco plants, whereas a high concentration of these two phytohormones led to an antagonistic effect. We observed the activation of both the SA and JA signaling pathways, as evident by the expression of their signature genes *PR1*, *PR3*, *PR5*, and *PR12*. The expression of marker genes for both pathways in this study showed a synergistic effect at a relatively moderate level in the tomato plant. In contrast, the overexpression of marker genes for the SA pathway led to a significant reduction in the expression of JA-marker genes at 2 dpi. Conversely, the fermentation

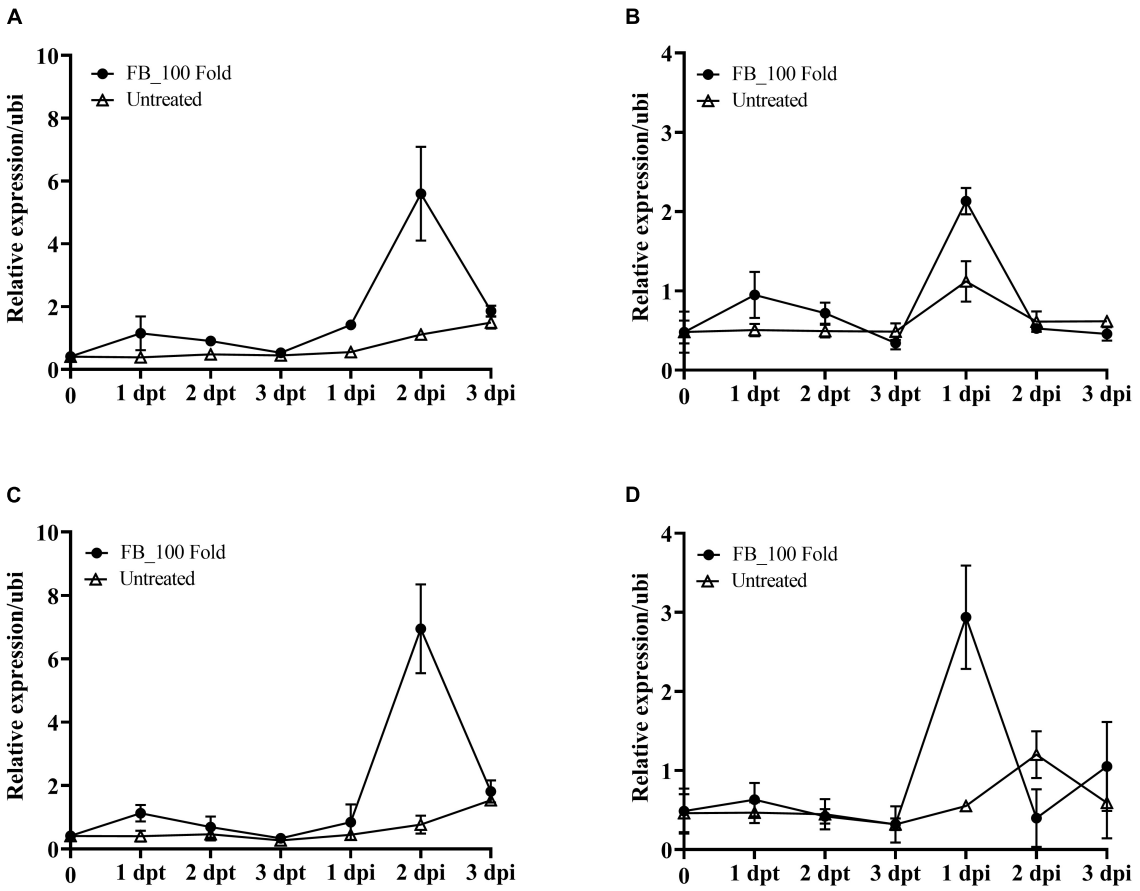

FIGURE 7 | Effect of the fermentation broth of *Streptomyces* sp. JCK-6131 on the gene expression levels of tomato plants before and after inoculation by *Ralstonia solanacearum*. The expression of the *PR1* **(A)**, *PR3* **(B)**, *PR5* **(C)**, and *PR12* **(D)** genes was analyzed from plants sprayed with 1% GSS (untreated) and treatment with 100-fold-diluted (FB_100 Fold) fermentation broth at different times, including 1, 2, and 3 days post treatment (dpt), and 1, 2, and 3 days post inoculation (dpi). The results display the average values ± SD (n = 3) of three runs with three replicates.

broth of JCK-6131 induced the early and weak expression of the *PR1*, *PR3*, *PR5*, and *PR12* genes in tomato plants 1 day after treatment. This suggests that both the SA- and JA-signaling pathways may be activated during priming with JCK-6131.

Van Wees et al. (2008) reported that the activation of both the SA and JA/ET pathways resulted in enhanced protection capability compared with the independent activation of each of these pathways. However, depending on the type of pathogen, the plant defense system will activate the suitable signaling pathway for infection characteristics. Ahn et al. (2011) and Liu et al. (2017) reported that Rs infection resulted in the early simultaneous expression of genes associated with the SA and JA signaling pathways in tomato and tobacco plants, respectively. In the present study, we found that the simultaneous expression of SA and JA marker genes was observed at 1 dpi, while they displayed an antagonistic effect at 2 dpi when the target genes of the SA-signaling pathway were strongly expressed. The expression of *PR* genes in JCK-6131-primed plants was faster and stronger than that of those in the unprimed plants after Rs inoculation. Because defense priming is considered a state of getting ready for battle, it contributes to enhancing plant resistance against a broad spectrum of pathogens. Therefore, primed plants display a more rapid and robust defense than unprimed plants when they are attacked by pathogens (Conrath et al., 2015). In this study, it was confirmed that both the SA and JA signaling pathways are involved in priming with JCK-6131.

CONCLUSION

In this study, we show that *Streptomyces* sp. JCK-6131 can effectively protect plants from bacterial and fungal pathogens via two major mechanisms. The first mechanism was the production of streptothricin antibiotics, which possessed a strong and broad-spectrum activity against various phytopathogenic bacteria and fungi. The second mechanism was the induction of plant systemic resistance against bacterial and fungal pathogens. Further studies regarding the identification of active metabolites responsible for plant resistance, optimization of fermentation culture conditions,

development of optimum formulation, and evaluation of disease control efficacy of such metabolites against various plant diseases in fields are necessary.

DATA AVAILABILITY STATEMENT

The original contributions presented in the study are included in the article/**Supplementary Material**, further inquiries can be directed to the corresponding author/s.

AUTHOR CONTRIBUTIONS

KDL and J-CK designed the study and wrote and revised the manuscript. KDL designed and performed experiments and analyzed the data. NHY, HTN, and KDL performed the RNA isolation and identified *Streptomyces* species. CWL and JK did the LC-MS/MS analysis. All authors read and approved the final version of this manuscript.

FUNDING

This research was supported by the Cooperative Research Program for Agricultural Science and Technology Development (Project PJ015296042021), Rural Development Administration, South Korea.

SUPPLEMENTARY MATERIAL

The Supplementary Material for this article can be found online at: https://www.frontiersin.org/articles/10.3389/fpls.2021.726266/full#supplementary-material

Supplementary Figure 1 | ESI-MS/MS fragmentation pattern of streptothricin E acid.

Supplementary Figure 2 | ESI-MS/MS fragmentation pattern of streptothricin D.

Supplementary Figure 3 | ESI-MS/MS fragmentation pattern of 12-carbamoylstreptothricin D.

Supplementary Table 1 | Primer sequences used in RT-qPCR analysis.

REFERENCES

Abbasi, S., Safaie, N., Sadeghi, A., and Shamsbakhsh, M. (2019). Streptomyces strains induce resistance to *Fusarium oxysporum f. sp. lycopersici* Race 3 in tomato through different molecular mechanisms. *Front. Microbiol.* 10:1505. doi: 10.3389/fmicb.2019.01505

Abro, M. A., Sun, X., Li, X., Jatoi, G. H., and Guo, L.-D. (2019). Biocontrol potential of fungal endophytes against *Fusarium oxysporum* f. sp. cucumerinum causing wilt in cucumber. *Plant Pathol. J.* 35, 598–608. doi: 10.5423/PPJ.OA.05.2019.0129

Aæimoviæ, S. G., Zeng, Q., McGhee, G. C., Sundin, G. W., and Wise, J. C. (2015). Control of fire blight (*Erwinia amylovora*) on apple trees with trunk-injected plant resistance inducers and antibiotics and assessment of induction of pathogenesis-related protein genes. *Front. Plant Sci* 6:16. doi: 10.3389/fpls.2015.00016

Ahn, I. P., Lee, S. W., Kim, M. G., Park, S. R., Hwang, D. J., and Bae, S. C. (2011). Priming by rhizobacterium protects tomato plants from biotrophic and necrotrophic pathogen infections through multiple defense mechanisms. *Mol. Cells* 32, 7–14. doi: 10.1007/s10059-011-2209-6

Ali, S., Ganai, B. A., Kamili, A. N., Bhat, A. A., Mir, Z. A., Bhat, J. A., et al. (2018). Pathogenesis-related proteins and peptides as promising tools for engineering plants with multiple stress tolerance. *Microbiol. Res.* 212-213, 29–37. doi: 10.1016/j.micres.2018.04.008

Bruce, T. J. A., and Pickett, J. A. (2007). Plant defence signalling induced by biotic attacks. *Curr. Opin. Plant Biol.* 10, 387–392. doi: 10.1016/j.pbi.2007.05.002

Cabrefiga, J., and Montesinos, E. (2017). Lysozyme enhances the bactericidal effect of BP100 peptide against *Erwinia amylovora*, the causal agent of fire blight of rosaceous plants. *BMC Microbiol.* 17:39. doi: 10.1186/s12866-017-0957-y

Chaparro, J. M., Badri, D. V., and Vivanco, J. M. (2014). Rhizosphere microbiome assemblage is affected by plant development. *ISME J.* 8, 790–803. doi: 10.1038/ismej.2013.196

Cheng, J., Yang, S. H., Palaniyandi, S. A., Han, J. S., Yoon, T.-M., Kim, T.-J., et al. (2010). Azalomycin F complex is an antifungal substance produced by Streptomyces malaysiensis MJM1968 isolated from agricultural soil. *J. Kor. Soc. Appl. Biol.Chem.* 53, 545–552. doi: 10.3839/jksabc.2010.084

Compant, S., Duffy, B., Nowak, J., Clément, C., and Barka, E. A. (2005). Use of plant growth-promoting bacteria for biocontrol of plant diseases: Principles, mechanisms of action, and future prospects. *Appl. Environ. Microbiol.* 71:4951. doi: 10.1128/AEM.71.9.4951-4959.2005

Conrath, U., Beckers, G. J. M., Langenbach, C. J. G., and Jaskiewicz, M. R. (2015). Priming for enhanced defense. *Annu. Rev. Phytopathol.* 53, 97–119. doi: 10.1146/annurev-phyto-080614-120132

De Vos, M., Van Oosten, V. R., Van Poecke, R. M., Van Pelt, J. A., Pozo, M. J., Mueller, M. J., et al. (2005). Signal signature and transcriptome changes of *Arabidopsis* during pathogen and insect attack. *Mol. Plant Microb. Interact.* 18, 923–937. doi: 10.1094/mpmi-18-0923

Dhanasekaran, D., Thajuddin, N., and Panneerselvam, A. (2012). "Applications of actinobacterial fungicides in agriculture and medicine, in fungicides for plant and animal diseases," in *Fungicides for Plant and Animal Diseases*, ed. D. Dharumadurai Dr (London: InTech Open), doi: 10.5772/25549

Dias, M. P., Bastos, M. S., Xavier, V. B., Cassel, E., Astarita, L. V., and Santarém, E. R. (2017). Plant growth and resistance promoted by *Streptomyces* spp. in tomato. *Plant Physiol. Biochem.* 118, 479–493. doi: 10.1016/j.plaphy.2017.07.017

Dong, C.-J., Wang, L.-L., Li, Q., and Shang, Q.-M. (2019). Bacterial communities in the rhizosphere, phyllosphere and endosphere of tomato plants. *PLoS One* 14:e0223847. doi: 10.1371/journal.pone.0223847

Essarioui, A., LeBlanc, N., Otto-Hanson, L., Schlatter, D. C., Kistler, H. C., and Kinkel, L. L. (2020). Inhibitory and nutrient use phenotypes among coexisting *Fusarium* and *Streptomyces* populations suggest local coevolutionary interactions in soil. *Environ. Microbiol.* 22, 976–985. doi: 10.1111/1462-2920.14782

González-Bosch, C. (2018). Priming plant resistance by activation of redox-sensitive genes. *Free Radic. Biol. and Med.* 122, 171–180. doi: 10.1016/j.freeradbiomed.2017.12.028

Ji, Z., Wang, M., Wei, S., Zhang, J., and Wu, W. (2009). Isolation, structure elucidation and antibacterial activities of streptothricin acids. *J. Antibiot.* 62, 233–237. doi: 10.1038/ja.2009.16

Ji, Z., Wei, S., Zhang, J., Wu, W., and Wang, M. (2008). Identification of streptothricin class antibiotics in the earlystage of antibiotics screening by electrospray ionization mass spectrometry. *J. Antibiot.* 61, 660–667. doi: 10.1038/ja.2008.93

Kim, B. S., Moon, S. S., and Hwang, B. K. (1999). Isolation, identification, and antifungal activity of a macrolide antibiotic, oligomycin A, produced by *Streptomyces libani*. *Can. J. Bot.* 77, 850–858. doi: 10.1139/b99-044

Kim, J., Le, K. D., Yu, N. H., Kim, J. I., Kim, J. C., and Lee, C. W. (2020). Structure and antifungal activity of pelgipeptins from *Paenibacillus elgii* against phytopathogenic fungi. *Pestic. Biochem. Phys.* 163, 154–163. doi: 10.1016/j.pestbp.2019.11.009

Kondo, Y., Ito, T., Nakagami, H., Hirakawa, Y., Saito, M., Tamaki, T., et al. (2014). Plant GSK3 proteins regulate xylem cell differentiation downstream of TDIF–TDR signalling. *Nat. Commun.* 5:3504. doi: 10.1038/ncomms4504

Lazarovits, G., Turnbull, A., and Johnston-Monje, D. (2014). *Plant Health Management: Biological Control of Plant Pathogens*. Oxford: Academic Press.

Le, K. D., Kim, J., Yu, N. H., Kim, B., Lee, C. W., and Kim, J. C. (2020). Biological control of tomato bacterial wilt, Kimchi cabbage soft rot, and red pepper bacterial leaf spot using *Paenibacillus elgii* JCK-5075. *Front. Plant Sci.* 11:775. doi: 10.3389/fpls.2020.00775

Lee, I., Ouk Kim, Y., Park, S.-C., and Chun, J. (2016). OrthoANI: an improved algorithm and software for calculating average nucleotide identity. *Int. J. Syst. Evol. Microbiol.* 66, 1100–1103. doi: 10.1099/ijsem.0.000760

Lee, J. H., Kim, J.-C., Jang, K. S., Choi, Y. H., and Choi, G. J. (2014). Efficient screening method for resistance of cucumber cultivars to Fusarium oxysporum f. sp. cucumerinum. *Res. Plant Dis.* 20, 245–252. doi: 10.5423/RPD.2014.20.4.245

Li, N., Han, X., Feng, D., Yuan, D., and Huang, L.-J. (2019). Signaling crosstalk between salicylic acid and ethylene/jasmonate in plant defense: do we understand what they are whispering? *Int. J. Mol. Sci.* 20:671. doi: 10.3390/ijms20030671

Li, Y., Gu, Y., Li, J., Xu, M., Wei, Q., and Wang, Y. (2015). Biocontrol agent Bacillus amyloliquefaciens LJ02 induces systemic resistance against cucurbits powdery mildew. *Front. Microbiol.* 6:883. doi: 10.3389/fmicb.2015.00883

Lima, S. M., Melo, J. G., Militão, G. C., Lima, G. M., do Carmo, A. L. M., Aguiar, J. S., et al. (2017). Characterization of the biochemical, physiological, and medicinal properties of *Streptomyces hygroscopicus* ACTMS-9H isolated from the Amazon (Brazil). *Appl. Microbiol. Biotechnol.* 101, 711–723. doi: 10.1007/s00253-016-7886-9

Liu, Q., Liu, Y., Tang, Y., Chen, J., and Ding, W. (2017). Overexpression of NtWRKY50 increases resistance to *Ralstonia solanacearum* and alters salicylic acid and jasmonic acid production in tobacco. *Front. Plant. Sci.* 8:1710. doi: 10.3389/fpls.2017.01710

Molinari, S., Fanelli, E., and Leonetti, P. (2014). Expression of tomato salicylic acid (SA)-responsive pathogenesis-related genes in Mi-1-mediated and SA-induced resistance to root-knot nematodes. *Mol. Plant Pathol.* 15, 255–264. doi: 10.1111/mpp.12085

Mur, L. A. J., Kenton, P., Atzorn, R., Miersch, O., and Wasternack, C. (2006). The outcomes of concentration-specific interactions between salicylate and jasmonate signaling include synergy, antagonism, and oxidative stress leading to cell death. *Plant Physiol.* 140, 249. doi: 10.1104/pp.105.072348

Mwajita, M. R., Murage, H., Tani, A., and Kahangi, E. M. (2013). Evaluation of rhizosphere, rhizoplane and phyllosphere bacteria and fungi isolated from rice in Kenya for plant growth promoters. *SpringerPlus* 2:606. doi: 10.1186/2193-1801-2-606

Nasr-Eldin, M., Messiha, N., Othman, B., Megahed, A., and Elhalag, K. (2019). Induction of potato systemic resistance against the potato virus Y (PVYNTN), using crude filtrates of Streptomyces spp. under greenhouse conditions. *Egypt J. Biol. Pest Control* 29:62. doi: 10.1186/s41938-019-0165-1

Nishad, R., Ahmed, T., Rahman, V. J., and Kareem, A. (2020). Modulation of plant defense system in response to microbial interactions. *Front. Plant Sci.* 11:1298. doi: 10.3389/fmicb.2020.01298

Niu, D.-D., Liu, H.-X., Jiang, C.-H., Wang, Y.-P., Wang, Q.-Y., Jin, H.-L., et al. (2011). The plant growth–promoting rhizobacterium *Bacillus cereus* AR156 induces systemic resistance in *Arabidopsis thaliana* by simultaneously activating salicylate– and jasmonate/ethylene-dependent signaling pathways. *Mol. Plant Microb. Interact.* 24, 533–542. doi: 10.1094/mpmi-09-10-0213

Park, K. S., and Kloepper, J. W. (2000). Activation of PR-1a promoter by rhizobacteria that induce systemic resistance in tobacco against *Pseudomonas* syringae pv. tabaci. *Biol. Control* 18, 2–9. doi: 10.1006/bcon.2000.0815

Patil, H. J., Srivastava, A. K., Singh, D. P., Chaudhari, B. L., and Arora, D. K. (2011). Actinomycetes mediated biochemical responses in tomato (*Solanum lycopersicum*) enhances bioprotection against *Rhizoctonia solani*. *Crop Prot.* 30, 1269–1273. doi: 10.1016/j.cropro.2011.04.008

Suárez-Moreno, Z. R., Vinchira-Villarraga, D. M., Vergara-Morales, D. I., Castellanos, L., Ramos, F. A., Guarnaccia, C., et al. (2019). Plant-growth promotion and biocontrol properties of three *Streptomyces* spp. isolates to control bacterial rice pathogens. *Front. Microbiol.* 10:290. doi: 10.3389/fmicb.2019.00290

Ul Haq, I., Sarwar, M. K., Faraz, A., and Latif, M. Z. (2020). "Synthetic chemicals: major component of plant disease management," in *Plant Disease Management Strategies for Sustainable Agriculture Through Traditional and Modern Approaches*, eds I. Ul Haq and S. Ijaz (Cham: Springer International Publishing), 53–81.

Van Loon, L. C., and Van Strien, E. A. (1999). The families of pathogenesis-related proteins, their activities, and comparative analysis of PR-1 type proteins. *Physiol. Mol. Plant Pathol.* 55, 85–97. doi: 10.1006/pmpp.1999.0213

Van Wees, S. C., Van der Ent, S., and Pieterse, C. M. (2008). Plant immune responses triggered by beneficial microbes. *Curr. Opin. Plant Biol.* 11, 443–448. doi: 10.1016/j.pbi.2008.05.005

Vergnes, S., Gayrard, D., Veyssière, M., Toulotte, J., Martinez, Y., Dumont, V., et al. (2020). Phyllosphere colonization by a coil *Streptomyces* sp. promotes plant defense responses against fungal infection. *Mol. Plant Microb. Interact.* 33, 223–234. doi: 10.1094/mpmi-05-19-0142-r

Vurukonda, S., Giovanardi, D., and Stefani, E. (2018). Plant growth promoting and biocontrol activity of Streptomyces spp. as endophytes. *Int. J. Mol. Sci.* 19:952. doi: 10.3390/ijms19040952

Walters, D. R., Ratsep, J., and Havis, N. D. (2013). Controlling crop diseases using induced resistance: challenges for the future. *J. Exp. Bot.* 64, 1263–1280. doi: 10.1093/jxb/ert026

Conflict of Interest: The authors declare that the research was conducted in the absence of any commercial or financial relationships that could be construed as a potential conflict of interest. The authors also declare that they will apply for one patent using the results of this study.

Publisher's Note: All claims expressed in this article are solely those of the authors and do not necessarily represent those of their affiliated organizations, or those of the publisher, the editors and the reviewers. Any product that may be evaluated in this article, or claim that may be made by its manufacturer, is not guaranteed or endorsed by the publisher.

frontiers in Plant Science

ORIGINAL RESEARCH
published: 14 December 2021
doi: 10.3389/fpls.2021.767882

Comparative Transcriptome Profiling Reveals Defense-Related Genes Against *Ralstonia solanacearum* Infection in Tobacco

*Xiaoying Pan[1], Junbiao Chen[1], Aiguo Yang[2], Qinghua Yuan[1], Weicai Zhao[3], Tingyu Xu[1], Bowen Chen[1], Min Ren[2], Ruimei Geng[2], Zhaohui Zong[3], Zhuwen Ma[1], Zhenrui Huang[1] and Zhenchen Zhang[1]**

[1] Guangdong Provincial Engineering & Technology Research Center for Tobacco Breeding and Comprehensive Utilization, Guangdong Key Laboratory for Crops Genetic Improvement, Crops Research Institute, Guangdong Academy of Agricultural Sciences (GAAS), Guangzhou, China, [2] Key Laboratory of Tobacco Improvement and Biotechnology, Tobacco Research Institute of Chinese Academy of Agricultural Sciences, Qingdao, China, [3] Nanxiong Tobacco Science Institute of Guangdong, Nanxiong, China

OPEN ACCESS

Edited by:
Marc Valls,
University of Barcelona, Spain

Reviewed by:
Wei Ding,
Southwest University, China
Haibin Lu,
Northwest A&F University, China

***Correspondence:**
Zhenchen Zhang
zhangzhenchen163@163.com

Specialty section:
This article was submitted to Plant Pathogen Interactions, a section of the journal Frontiers in Plant Science

Received: 31 August 2021
Accepted: 17 November 2021
Published: 14 December 2021

Citation:
Pan X, Chen J, Yang A, Yuan Q, Zhao W, Xu T, Chen B, Ren M, Geng R, Zong Z, Ma Z, Huang Z and Zhang Z (2021) Comparative Transcriptome Profiling Reveals Defense-Related Genes Against Ralstonia solanacearum Infection in Tobacco. Front. Plant Sci. 12:767882. doi: 10.3389/fpls.2021.767882

Bacterial wilt (BW) caused by *Ralstonia solanacearum* (*R. solanacearum*), is a vascular disease affecting diverse solanaceous crops and causing tremendous damage to crop production. However, our knowledge of the mechanism underlying its resistance or susceptibility is very limited. In this study, we characterized the physiological differences and compared the defense-related transcriptomes of two tobacco varieties, 4411-3 (highly resistant, HR) and K326 (moderately resistant, MR), after *R. solanacearum* infection at 0, 10, and 17 days after inoculation (dpi). A total of 3967 differentially expressed genes (DEGs) were identified between the HR and MR genotypes under mock condition at three time points, including1395 up-regulated genes in the HR genotype and 2640 up-regulated genes in the MR genotype. Also, 6,233 and 21,541 DEGs were induced in the HR and MR genotypes after *R. solanacearum* infection, respectively. Furthermore, GO and KEGG analyses revealed that DEGs in the HR genotype were related to the cell wall, starch and sucrose metabolism, glutathione metabolism, ABC transporters, endocytosis, glycerolipid metabolism, and glycerophospholipid metabolism. The defense-related genes generally showed genotype-specific regulation and expression differences after *R. solanacearum* infection. In addition, genes related to auxin and ABA were dramatically up-regulated in the HR genotype. The contents of auxin and ABA in the MR genotype were significantly higher than those in the HR genotype after *R. solanacearum* infection, providing insight into the defense mechanisms of tobacco. Altogether, these results clarify the physiological and transcriptional regulation of *R. solanacearum* resistance infection in tobacco, and improve our understanding of the molecular mechanism underlying the plant-pathogen interaction.

Keywords: bacterial wilt, *Ralstonia solanacearum*, RNA sequencing, cell wall, hormone, tobacco

INTRODUCTION

Bacterial wilt (BW) is one of the most prevalent plant diseases, affecting hundreds of species, including agronomically important crops, such as tomato, chili pepper, sweet pepper, potato, eggplant, and tobacco belonging to the solanaceae family. The disease also affects non-solanaceous crops, like bananas, beans, and ornamental plants (Buddenhagen, 1986). BW is distributed worldwide in tropical and subtropical countries and is caused by the soilborne bacterial pathogen *R. solanacearum* (Hayward, 1991; Elphinstone et al., 2005). The mechanisms underlying natural resistance to *R. solanacearum* are related to the suppression of the growth and movement of the pathogen within the vascular system of their host (Xue et al., 2020). Histological analyses have revealed strengthened parenchyma cell walls and pit membranes in the xylem tissues and pathogen localization in the primary xylem tissues in the stems of a resistant tomato cultivar (Nakaho et al., 2000). In addition, the roles of cell wall proteins in defense against *R. solanacearum* in tomato have been discussed extensively (Wydra and Beri, 2006; Diogo and Wydra, 2007; Dahal et al., 2010; Schacht et al., 2011). Moreover, several recent studies have identified genes related to plant defense against *R. solanacearum*, including *StMKK1* in potato (Chen et al., 2021), *SlNAP1* and a bacterial effector protein RipAK in tomato (Wang et al., 2020; Wang Y. et al., 2021), and *CaNAC2c* in pepper (Cai et al., 2021).

Transcriptional profiling and analysis of gene function related to the host response to *R. solanacearum* are limited. Godiard et al. (1991) isolated cDNA clones corresponding to mRNAs that accumulate during the early phase of the hypersensitive response in suspension cultured tobacco cells challenged with a non-pathogenic strain of *R. solanacearum* (Godiard et al., 1991). Microarray analysis showed that R-response genes were related to xyloglucan biosynthesis and cell wall organization, while S-response genes were involved in response to stress and cell death in pepper (Hwang et al., 2011). A root transcriptome provided insight into the dynamic crosstalk between peanut and *R. solanacearum* (Chen et al., 2014). Several recent studies have evaluated root transcriptional responses during *R. solanacearum* infection in different plant species, including *Arabidopsis* (Zhao et al., 2019), tomato (French et al., 2018), and the wild potato *Solanum commersonii* (Zuluaga et al., 2015), revealing that auxin and ABA contribute to the infectivity of *R. solanacearum* and its ability to manipulate plant development.

Polygenic resistance patterns have been found in *Solanaceae* species, while monogenic inheritance was reported in *Arabidopsis thaliana* (Deslandes et al., 2002). The genetic basis of resistance to BW is similar in pepper and tomato. In tomato, several major QTL, particularly on chromosomes 4, 6, 8, and 12, are involved in the control of strain-specific resistance (Thoquet et al., 1996a,b; Wang et al., 2000; Carmeille et al., 2006). A quantitative character governed by oligogenic inheritance has also been reported to facilitate partial resistance to *R. solanacearum* in *Capsicum annuum* (Lafortune et al., 2005; Tran and Kim, 2010). Different modes of gene action among pathogen isolates with different levels of virulence have been reported in pepper, indicating the complex inheritance of BW resistance (Tran and Kim, 2010).

Several recent reports have provided a preliminary understanding of the molecular mechanism underlying the plant response to *R. solanacearum* by virus-induced gene silencing in tobacco. The suppression of DS1 (Disease suppression 1) function or *DS1* expression could rapidly activate plant defenses to achieve effective resistance against *R. solanacearum* in *Nicotiana benthamiana* (Nakano et al., 2013). NbPDKs played a crucial role in the regulation of hypersensitive cell death via plant hormone signaling and oxidative burst in the *NbPDK*-silenced plants challenged with *R. solanacearum* (Kiba et al., 2020). The *R. solanacearum* effector RipI induces a host defense reaction by interacting with the bHLH93 transcription factor in tobacco (Zhuo et al., 2020). The silencing of TOM20 (a marker of oxidative phosphorylation), PP1 (a protein phosphatase related to plant immune regulation), and HBP2 (a heme-binding protein related to the antioxidant pathway) in tobacco significantly altered resistance to *R. solanacearum* (Lee et al., 2012; Urvalek et al., 2015; Liu et al., 2019; Wang B. S. et al., 2021).

The mechanism underlying plant resistance to *R. solanacearum* is not clear. Moreover, BW is difficult to control due to its aggressiveness and the lack of resistant tobacco varieties in China. Tobacco cultivar GDSY-1, a Chinese domestic sun-cured tobacco variety, exhibits higher resistance to BW caused by *R. solanacearum* than other common tobacco cultivars (e.g., K326) carrying polygenic resistance derived from T.I.448A (Zhang et al., 2017). In this study, we measured physiological indexes in resistant (4411-3, carrying monogenic resistance derived from GDSY-1, referred to as HR) and moderately resistant (K326, referred to as MR) tobacco varieties. Further, we compared the defense transcriptomes and identified enriched GO and KEGG pathways, and hub genes associated with the tobacco response to *R. solanacearum* infection. Our results provide a valuable resource for understanding the interactions between tobacco and *R. solanacearum*.

MATERIALS AND METHODS

Plant Culture and Growth Conditions

Nicotiana tabacum L. cv. 4411-3 (carrying monogenic resistance derived from GDSY-1) and *N. tabacum* L. cv. K326 were used. To eliminate the effect of different genetic backgrounds between K326 and GDSY-1, we used K326 as the female parent and crossed it with the male parent GDSY-1. The F_1 plants were backcrossed to K326 (recurrent parent), and descendants were backcrossed to K326 four times to generate BC_4F_5 (4411-3), carrying monogenic resistance derived from GDSY-1, which was validated by BSA experiments. The final product, 4411-3 (K326-like type) was used for subsequent experiments.

Seeds were coated and germinated in a mixture of peat culture substrate, carbonized chaff, and perlite (3:2:1, V/V/V). The seedlings were grown in a naturally illuminated glasshouse for two months.

Treatments and Sampling

A moderately aggressive defoliating strain of *R. solanacearum*, B-2 (Xie et al., 2014), was used for the disease assay. Five-leaf-stage tobacco plants were infected with 300 mL *R. solanacearum* cell suspension (3×10^7 cell per mL) by irrigating roots in one pot. The roots of the control plants were irrigated with 300 mL distilled water. Tobacco seedlings of each variety were grown in five different pots, each containing 72 seedlings. Subsequently, the whole stem tissue of every plant was harvested. Tobacco stems from five individual seedlings taken from one pot were considered a biological replicate. Therefore, five biological replicates of each variety were harvested from five different pots at every time point. Three RNA samples from three biological replicates were used for RNA sequencing. Tobacco stems from five individual seedlings were taken from the inoculated and mock-inoculated plants at 0, 10, and 17 days post-inoculation (dpi). The samples were immediately frozen in liquid nitrogen and stored at −80°C for RNA exaction. Samples of five biological replicates were prepared.

The disease index was determined by GB/T 23224-2008 as described previously (Liu et al., 2017). The stems were weighed and ground using a mortar and pestle (with the addition of 10 mL sterile water) to measure their bacterial content. One mL supernatant was diluted five times after standing the ground samples 5 min. Next, 100 μL suspension was evenly spread on TTC plates and incubated at 30°C for 48 h. Finally, the bacterial colonies that formed were counted, and the bacterial content of the tobacco stems was calculated per unit gram.

Determination of Physiological Parameters

Leaf samples were harvested at 0, 10, and 17 dpi. Subsequently, the activities peroxidase (POD), superoxide dismutase (SOD), phenylalanine ammonia-lyase (PAL), polyphenol oxidase (PPO), ascorbate peroxidase (APX), and catalase (CAT) were assessed. Also, the contents of malonaldehyde (MDA), chlorophyll, exopolysaccharides, and soluble proteins were determined. These assays were performed using specific assay kits (Nanjing Jiancheng Bioengineering Institute, Nanjing, China), following the manufacturer's instructions. Mean values from five measurements were used for analyses. The results are presented as means ± SE of five biological and three technical replicates.

Endogenous Hormone Measurement

To examine the levels of auxin (IAA), gibberellins (GA3), trans-zeatin riboside (ZR), abscisic acid (ABA), and salicylic acid (SA) in HR and MR genotypes, the leaves were harvested and immediately frozen in liquid nitrogen until further use. Sample extraction and hormone measurements were performed using enzyme-linked immunosorbent assays as previously described (Yu et al., 2016). The level of SA was determined using LC-MS analysis as previously described but with slight modifications (Cui et al., 2015). Briefly, plant materials (50 mg fresh weight) were frozen in liquid nitrogen, ground into fine powder, and extracted with 1 mL of methanol/water/formic acid (15:4:1, V/V/V). The combined extracts were evaporated to dryness under a nitrogen gas stream, reconstituted in 100 μL of 80% methanol (V/V), and filtered through a 0.22 μm filter for further LC-MS analysis.

Standard IAA, ZR, GA3, ABA, and SA (Sangon Biotech Co., Ltd., Shanghai, China) were used for calibration. The results are presented as means ± SE of five biological and three technical replicates.

Transcriptomic Library Construction and Sequencing

Six samples (two genotypes × three biological replicates) were harvested at 0 dpi. Further, 24 samples (two genotypes × two treatments × two time points × three biological replicates) were harvested at 10 and 17 dpi. Finally, 30 samples were used for transcriptome sequencing. Total RNA was extracted from the stems of tobacco plants using TRIzol reagent (Invitrogen, Waltham, MA, United States). For RNA-seq library construction, 3 μg of total RNA was used and the library was sequenced on the Illumina HiSeq 2000 platform following the manufacturer's protocol to yield ∼8 Gb of PE150 raw data. Sequencing data have been deposited in the NCBI Sequence Read Archive under accession number PRJNA762496.

Bioinformatics Analysis of RNA-Seq Data

Clean reads were obtained by pre-processing raw reads to remove low-quality regions and adapter sequences. Clean reads were then mapped directly to the reference tobacco genome developed at the Yunnan Academy of Tobacco Agriculture Science (unpublished data) using HISAT2.0.5, and read counts of annotated genes were obtained. The expression level of each gene was measured in terms of FPKM (fragments per kilobase of transcript sequence per million base pairs sequenced). Using DESeq, transcripts with an adjusted *p*-value (padj) < 0.05 were identified as differentially expressed genes (DEGs) (Anders and Huber, 2010). Hierarchical clustering was conducted based on FPKM values. A Gene Ontology (GO) enrichment analysis of DEGs was conducted using the R package TopGO (Alexa et al., 2006) by an improved weighted scoring algorithm, using Fisher's test to determine significance. A heatmap was generated using the R package Complex Heatmap 3.5.0 (Sun et al., 2016). The Kyoto Encyclopedia of Genes and Genomes (KEGG) database was used for functional enrichment analyses using Cluster Profiler 3.4.4. Values of *p*-value < 0.05 indicated significantly enriched pathways.

Gene Expression Analysis

Total RNA was reverse-transcribed using the Prime Script™ RT Reagent Kit with gDNA Eraser (Perfect Real Time; Takara, Kusatsu, Japan) following the manufacturer's protocol. Fourteen genes were randomly selected for validation by RT-qPCR using primers listed in **Supplementary Table 1**, as described previously (Pan et al., 2015). The relative gene expression levels were calculated using the comparative C_T method (Livak and Schmittgen, 2001). The ubiquitin-conjugating enzyme gene

(*evm.TU.HIC_ASM_12.2258*) was used as the internal control for normalization of gene expression.

RESULTS

Characterization of the Two Tobacco Cultivars in Response to *Ralstonia solanacearum* Infection

We initially conducted disease assays to confirm the response of the two *N. tabacum* L. cultivars (4411-3:HR and K326:MR) to *R. solanacearum* infection. A significant difference in the disease response was observed between the HR and MR genotypes at 17 dpi. All MR seedlings exhibited intense disease symptoms and ultimately died, whereas most HR seedlings showed no obvious disease symptoms (**Figures 1A,B**). Notably, MR stems exhibited black colors (wilt symptoms) at 10 and 17 dpi (**Figures 1C,D**). However, no similar symptom was detected in the HR stems (**Figures 1C,D**). These results confirm that the K326 variety is moderately resistant while the 4411-3 variety is highly resistant to *R. solanacearum* infection (**Figure 1**; **Supplementary Figure 1** and **Supplementary Table 2**).

Physiological Changes in the Two Tobacco Cultivars in Response to *Ralstonia solanacearum* Infection

ROS burst is associated with enhanced activities of anti-oxidative enzymes (Dumanović et al., 2020). To test this possibility in this study, we measured the activities of six anti-oxidative enzymes, including POD, CAT, SOD, PPO, PAL, and APX, which are typically activated to remove elevated ROS under oxidative stresses (Miller et al., 2010). Unexpectedly, our results showed that POD activity was significantly higher in the MR genotype than in the HR genotype at 10 and 17 dpi (**Supplementary Figure 2A**). Besides, there were no considerable differences in CAT and SOD levels between HR and MR genotype after *R. solanacearum* infection (**Supplementary Figures 2B,C**). PPO activity was significantly lower in MR than in HR (**Supplementary Figure 2D**), with no considerable differences in PAL and APX between the HR and MR genotypes after *R. solanacearum* infection (**Supplementary Figures 2E,F**). The unexpected results could be because the experiment was performed within a short duration, thus the exposure time was not sufficient to allow the desired physiological response.

At the three time points, the levels of chlorophyll differed significantly between the HR and MR genotypes (**Supplementary Figure 3A**) following to *R. solanacearum* infection. The loss of photosynthetic pigments may be due to the reduced number of living cells containing chloroplasts, as evidenced by necrotic lesions. Furthermore, the level of MDA increased sharply after *R. solanacearum* infection but was higher in the MR than in the HR genotype (**Supplementary Figure 3B**). Moreover, no considerable differences in soluble proteins and exopolysaccharides were noted between the two genotypes (**Supplementary Figures 3C,D**).

Plant hormones play pivotal signaling roles in host-*R. solanacearum* interactions (Zuluaga et al., 2015; French et al., 2018; Zhao et al., 2019). Therefore, we determined the levels of various hormones in the leaves of plants with the two genotypes. The contents of IAA, GA, ZR, and ABA in the MR genotype were significantly higher than those in the HR genotype after *R. solanacearum* infection (**Figures 2A–D**). Furthermore, SA levels in HR were significantly higher than those in the MR genotype in response to *R. solanacearum* infection (**Figure 2E**). These results indicate that resistance to *R. solanacearum* potentially results from the activation of the phytohormone-mediated pathway.

Distinct Transcriptomes in 4411-3 and K326 Genotypes Under Mock Infection

We performed RNA-seq using RNA samples extracted from the stems of HR and MR genotypes at 0, 10, and17 dpi. In total, 1.80 billion clean reads (approximately 270.02 Gb of data) were obtained from 30 samples (**Supplementary Table 3**). Across all samples, the percentage of nucleotides with a quality score above 20 was over 97.86%, and the GC percentage ranged from 41.51% to 43.57% (**Supplementary Table 3**). After filtering and trimming, 84.74% to 95.32% of clean reads were uniquely mapped to the unpublished tobacco genome (**Supplementary Table 4**).

Furthermore, we performed RT-qPCR to compare the expression of 14 randomly selected genes with differential expression (DESeq2 padj $\leq$ 0.05 and fold change $>$ 2) between the HR and MR genotypes. The results were consistent with those obtained by RNA-seq (**Supplementary Table 5**), supporting the reliability of the RNA-sequencing results.

Using DESeq2 padj $\leq$ 0.05 and fold change $>$ 2 as thresholds, we found 3967 DEGs between the HR and MR genotypes at three time points. Among them, 1,395 and 2,640 had higher expression levels in the HR and MR genotypes, respectively (**Figure 3A**). These included 746 up-regulated genes in HR and 1981 up-regulated genes in MR at 0 dpi, 670 up-regulated genes in HR and 832 up-regulated genes in MR at 10 dpi, and 151 up-regulated genes in the HR genotype and 106 up-regulated genes in the MR genotype at 17 dpi (**Supplementary Figures 4A–C** and **Supplementary Table 6**). In addition, a hierarchical clustering algorithm revealed distinct expression profiles between the HR and MR genotypes (**Supplementary Figure 5**).

The DEGs between the HR and MR genotypes were further subjected to GO enrichment analysis. The up-regulated genes in the HR genotype were enriched in 26 biological processes (**Supplementary Table 7**). The terms cell wall macromolecule catabolic process, cell wall macromolecule metabolic process, and cell wall organization or biogenesis were over-represented (**Figure 4A**, **Supplementary Table 7**). The up-regulated genes in the MR genotype were enriched in 31 biological processes (**Supplementary Table 8**). Further, genes in the HR genotype were specifically enriched in the cellular component "cell wall" (**Figure 4A**, **Supplementary Table 7**). Within the molecular function category, three GO

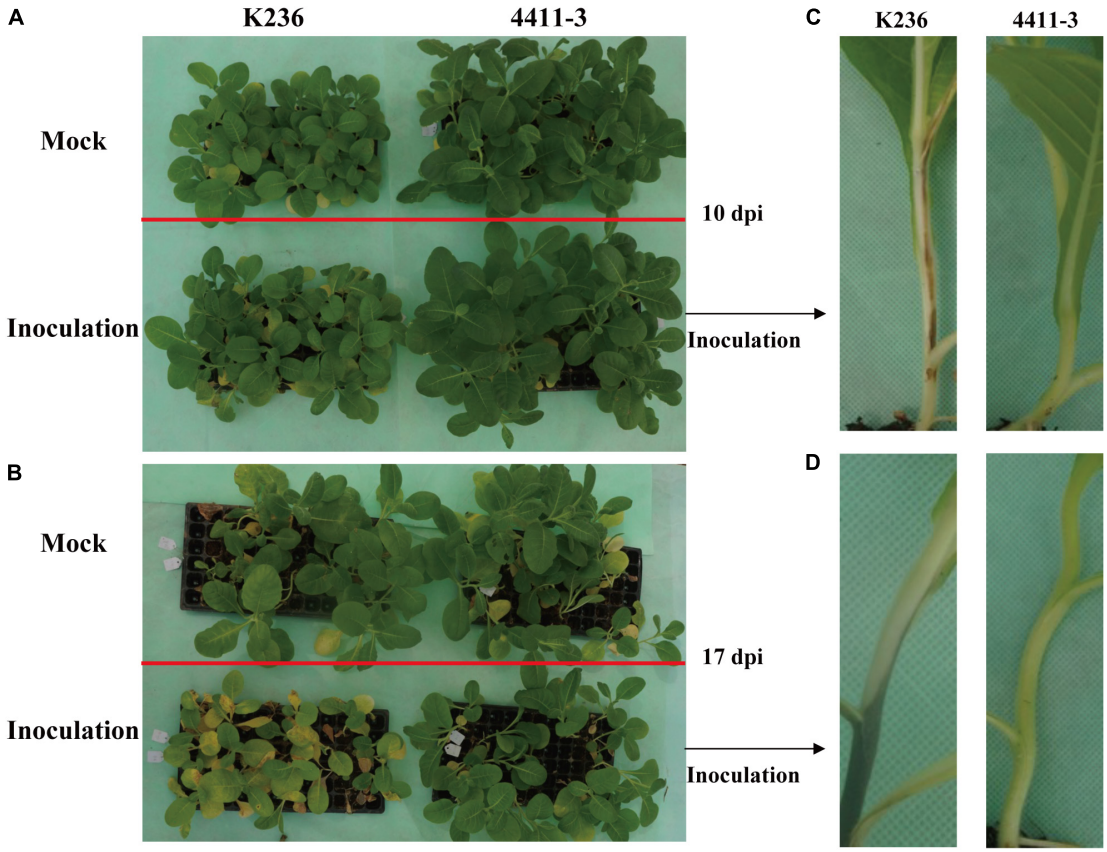

FIGURE 1 | Disease symptoms in 4411-3 and K326 plants after *Ralstonia solanacearum* inoculation. **(A,B)** Tobacco seedlings in the pot at 10 and 17 days post inoculation (dpi) with *Ralstonia solanacearum*. **(C,D)** Disease symptoms in stems of 4411-3 and K326 plants at 10 and 17 dpi with *Ralstonia solanacearum*.

terms were significantly enriched: "xyloglucosyl transferase activity," "glucosyltransferase activity," and "chitinase activity" (**Figure 4A**, **Supplementary Table 7**). Genes in the MR genotype were significantly enriched in five GO terms in the cellular component category, including "DNA packaging complex" and "nucleosome" (**Figure 4B**, **Supplementary Table 8**). Nineteen molecular function GO terms were overrepresented in the MR genotype, including "microtubule motor activity" and "microtubule binding" (**Figure 4B**, **Supplementary Table 8**).

Kyoto Encyclopedia of Genes and Genomes pathway analysis was performed to further predict the functions of these DEGs. Up-regulated genes in the HR genotype were significantly enriched in five KEGG pathways, including glutathione metabolism, ribosome, ABC transporters, plant hormone signal transduction, and phenylalanine metabolism (**Figure 5A**). Up-regulated genes in the MR genotype were involved in nine KEGG pathways, including linoleic acid metabolism, plant-pathogen interaction, homologous recombination, DNA replication, plant hormone signal transduction, fatty acid elongation, alpha-linolenic acid metabolism, diterpenoid biosynthesis and phenylalanine metabolism (**Figure 5B**). Notably, three pathways, including glutathione metabolism, ribosome, and ABC transporters, were only enriched in the HR genotype (**Figure 5**). Genes related to plant hormone signal transduction and phenylalanine metabolism pathways were enriched in both tobacco genotypes (**Figure 5**).

Identification of Differentially Expressed Genes Involved in the Response to *Ralstonia solanacearum* Infection

To examine transcriptome changes in both genotypes in response to *R. solanacearum* infection, we performed pairwise transcriptome comparisons between mock-treated and *R. solanacearum* inoculated plants at 10 and 17 dpi. In the HR genotype, 6,133 and 134 DEGs were identified in response to *R. solanacearum* infection at 10 and 17 dpi, respectively (**Supplementary Figures 6A,B**, **Supplementary Table 9**). In the MR genotype, 12,679 and 16,000 DEGs were identified at 10 and 17 dpi, respectively (**Supplementary Figures 6C,D**, **Supplementary Table 10**). In total, 6,233 and 21,541 non-redundant DEGs were identified in the HR and MR genotype, respectively, and 4,201 were common in both genotypes (**Figure 3B**).

Kyoto Encyclopedia of Genes and Genomes pathway analysis ($p < 0.05$) of 6,233 DEGs in the HR genotype under *R. solanacearum* infection revealed nine enriched pathways (**Figure 5C**). Meanwhile, 24 enriched pathways

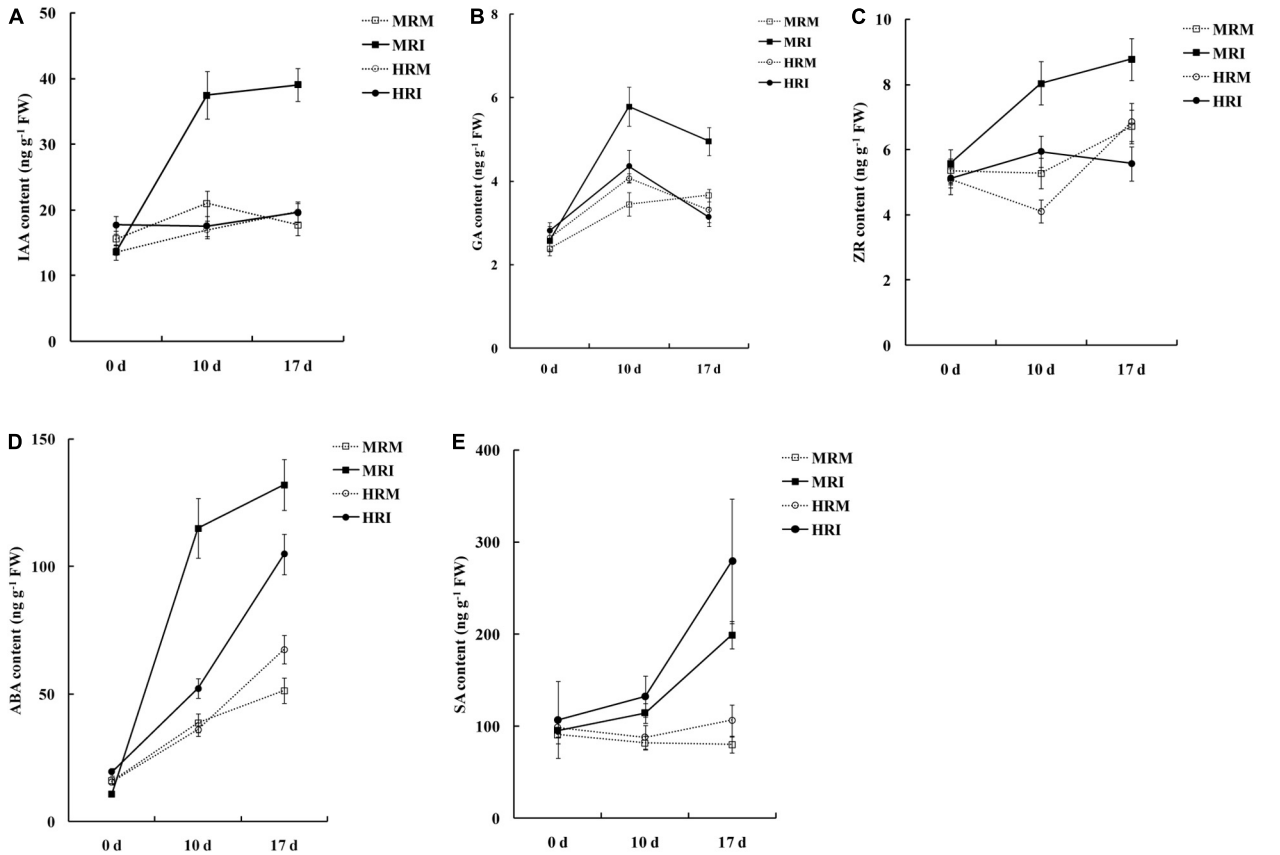

FIGURE 2 | Hormone accumulation in the 4411-3 and K326 genotypes at 0, 10, and 17 days post-inoculation with *Ralstonia solanacearum*. **(A)** Auxin (IAA). **(B)** Gibberellins (GA3). **(C)** Trans-zeatin riboside (ZR). **(D)** Abscisic (ABA). **(E)** salicylic acid (SA). Five independent experimental replicates were analyzed for each sample and data are presented as means ± SE (standard error).

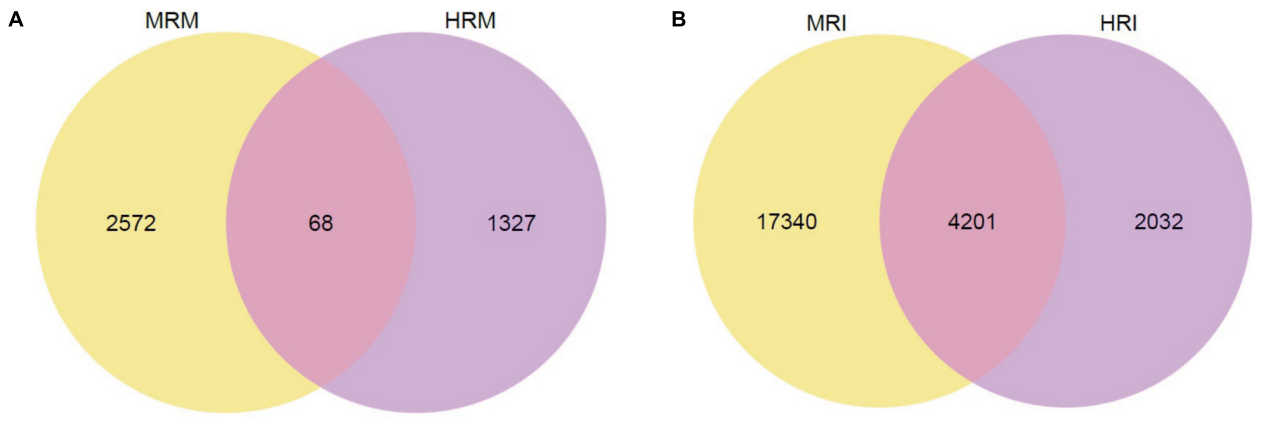

FIGURE 3 | Venn diagram of total DEGs between the 4411-3 and K326 genotypes at 0, 10 and 17 days post-inoculation. **(A)** Venn diagram of total DEGs between the 4411-3 and K326 genotypes at 0, 10 and 17 days post-inoculation (dpi) under mock conditions (HRM vs. MRM). **(B)** Venn diagram of total DEGs between the 4411-3 and K326 genotypes at 0, 10 and 17 dpi after *Ralstonia solanacearum* inoculation (HRI vs. MRI).

were detected among the 21,541 DEGs in the MR genotype following *R. solanacearum* infection (**Figure 5D**). Five pathways were enriched in both genotypes, including plant-pathogen interaction, alpha-linolenic acid metabolism, protein processing in endoplasmic reticulum, MAPK signaling pathway–plant, and amino sugar and nucleotide sugar metabolism (**Figures 5C,D**). Notably, four pathways were only enriched in the HR genotype, including endocytosis, starch and sucrose

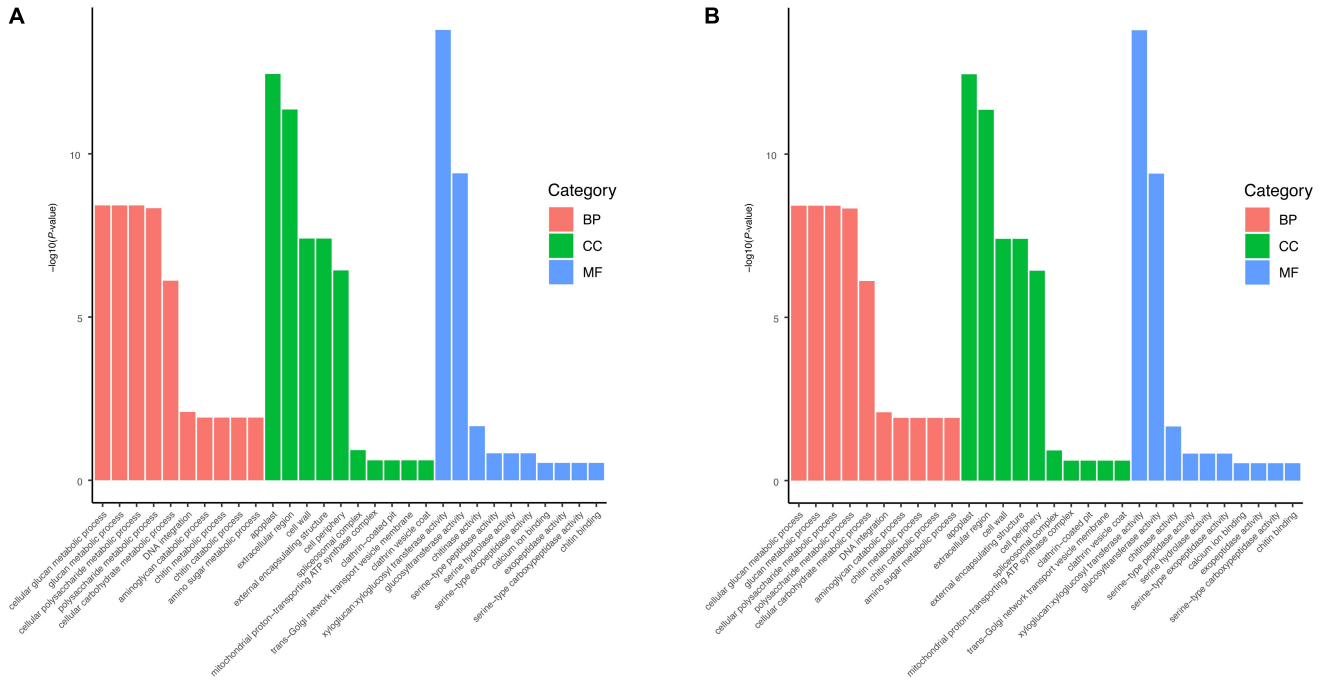

FIGURE 4 | Significantly enriched GO terms for up-regulated genes in **(A)** 4411-3 genotype vs. **(B)** K326 genotype under mock conditions.

metabolism, glycerolipid metabolism, and glycerophospholipid metabolism (**Figure 5C**).

Moreover, we found that the expression patterns of 4,201 common DEGs were very similar in both genotypes at 10 dpi (**Supplementary Figure 7A**). KEGG pathway analysis of the 4,201 DEGs revealed eleven enriched pathways (**Supplementary Figure 7B**), including plant-pathogen interaction, endocytosis, protein processing in endoplasmic reticulum, starch and sucrose metabolism, phosphatidylinositol signaling system, explaining the common resistance of 4411-3 and K326 genotypes against *R. solanacearum* infection.

Identification of Candidate Genes Related to *Ralstonia solanacearum* Resistance in Tobacco

According to the GO enrichment analysis, cell wall processing was over-represented in the up-regulated genes of the HR genotype but not in the MR genotype (**Figure 4**). The plant hormone signal transduction was selected according to KEGG pathway analysis and the physiological data obtained in this study (**Figures 2**, **5**). According to the KEGG analysis, certain processes were specifically enriched in the HR genotype compared with MR genotype under mock and inoculation conditions (**Figure 5**). The enriched processed included glutathione metabolism, ABC transporters, glycerolipid metabolism, glycerophospholipid metabolism, and endocytosis. Therefore, the DEGs in these pathways were chosen as the candidate genes for further analysis.

Next, we evaluated candidate genes associated *R. solanacearum* resistance, including those related to the cell wall, starch and sucrose metabolism, plant hormone signal transduction, glutathione metabolism, ABC transporters, glycerolipid metabolism, glycerophospholipid metabolism, and endocytosis (**Figure 6**).

A total of 28 genes involved in cell wall processing were identified (**Figure 6A**, **Supplementary Table 11**), including 18 genes encoding xyloglucan endotransglycosylase/hydrolase (XTH), five genes encoding pectinesterase inhibitor, and five genes encoding pectinesterase. Additionally, the expression of 21 genes involved in starch and sucrose metabolism was altered in response to *R. solanacearum* infection (**Figure 6B**, **Supplementary Table 11**).

Seven genes involved in plant hormone signal transduction were identified (**Figure 6C**, **Supplementary Table 11**), including one JA-related gene, four ABA-related genes, and two auxin-related genes. Strikingly, the levels of the auxin-related genes *SAUR21* (small auxin up RNA21, novel.5551) and *SAUR24* (evm.TU.HIC_ASM_2.116) were 4.1- and 55.5-fold higher, respectively, in the HR than in the MR genotype (**Figure 6C**, **Supplementary Table 11**).

Six genes involved in glutathione metabolism were identified. These genes (e.g., genes encoding glutathione *S*-transferase) exhibited higher expression in the HR genotype than in the MR genotype (**Figure 6D**, **Supplementary Table 11**). Only three genes encoding ABC transporters were detected (**Figure 6E**, **Supplementary Table 11**). Furthermore, 12 genes involved in glycerolipid metabolism, 15 genes involved in glycerophospholipid metabolism, and 32 genes involved

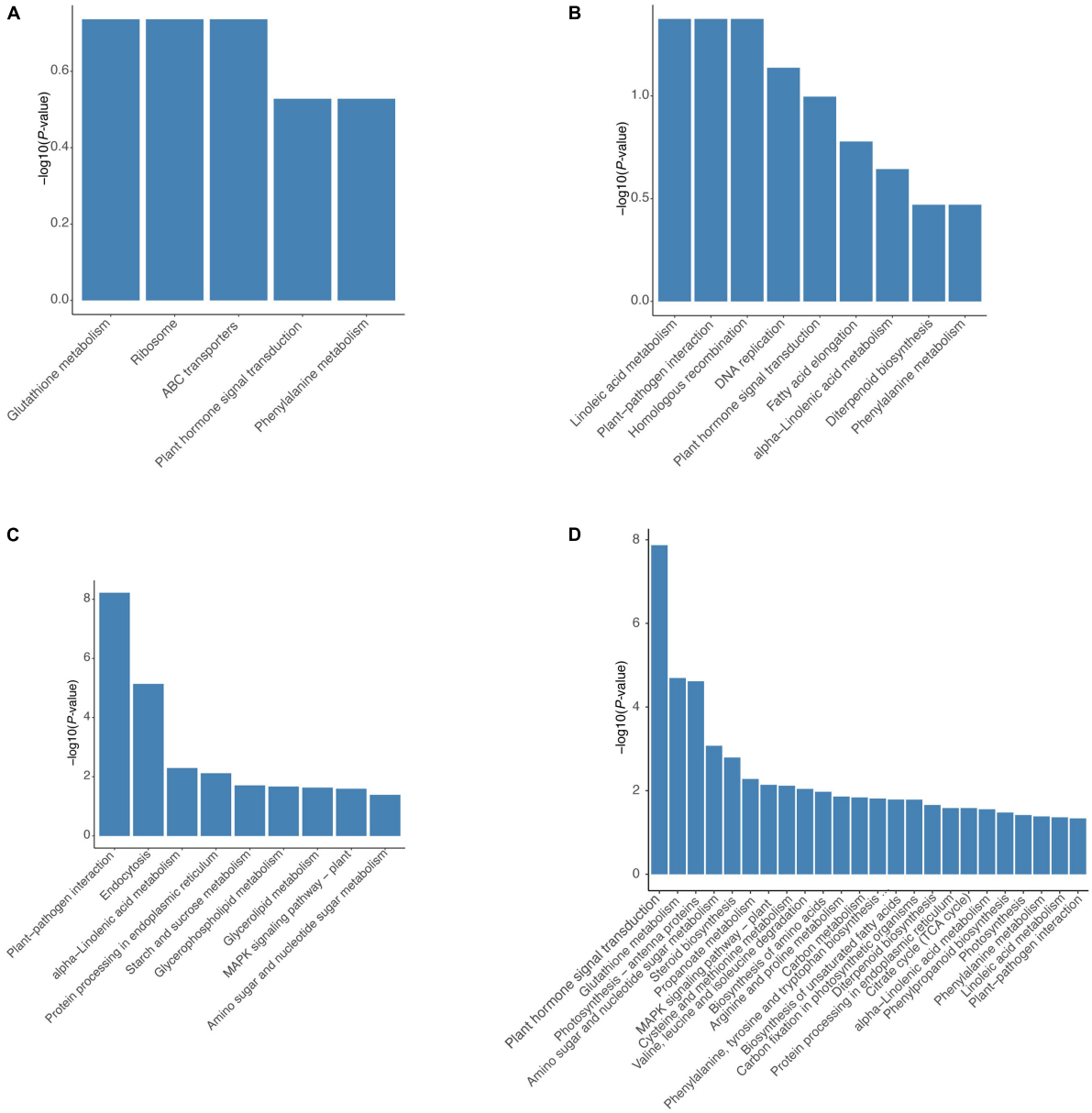

FIGURE 5 | Significantly enriched KEGG pathways for DEGs in both 4411-3 and K326 genotype. Significantly enriched KEGG pathways for up-regulated genes in **(A)** the 4411-3 genotype vs. **(B)** the K326 genotype under mock conditions. Significantly enriched KEGG pathways for DEGs in **(C)** the 4411-3 genotype versus **(D)** the K326 genotype in response to *R. solanacearum* infection.

in endocytosis (**Figures 6F–H**, **Supplementary Table 11**) were identified.

DISCUSSION

Common and Pathogen-Induced Transcriptomes Contribute to Tobacco Defense Against *Ralstonia solanacearum*

Few studies have characterized the interaction between tobacco and *R. solanacearum* at the molecular level (Nakano et al., 2013; Kiba et al., 2020; Zhuo et al., 2020; Wang Y. et al., 2021). In this study, a comparative transcriptomic analysis was performed to investigate the molecular mechanism underlying tobacco's pathogen-induced responses to *R. solanacearum*. In the HR genotype, DEGs represent both common and HR-gene mediated responses, while DEGs in the MR genotype reflect the common defense responses and pathogen-dependent reprogramming in the plant.

A total of 3967 DEGs were found between the HR and MR genotype at 0 dpi, of which 1,395 and 2,640 were more expressed in the HR and MR genotypes, respectively (**Figure 3A**). These

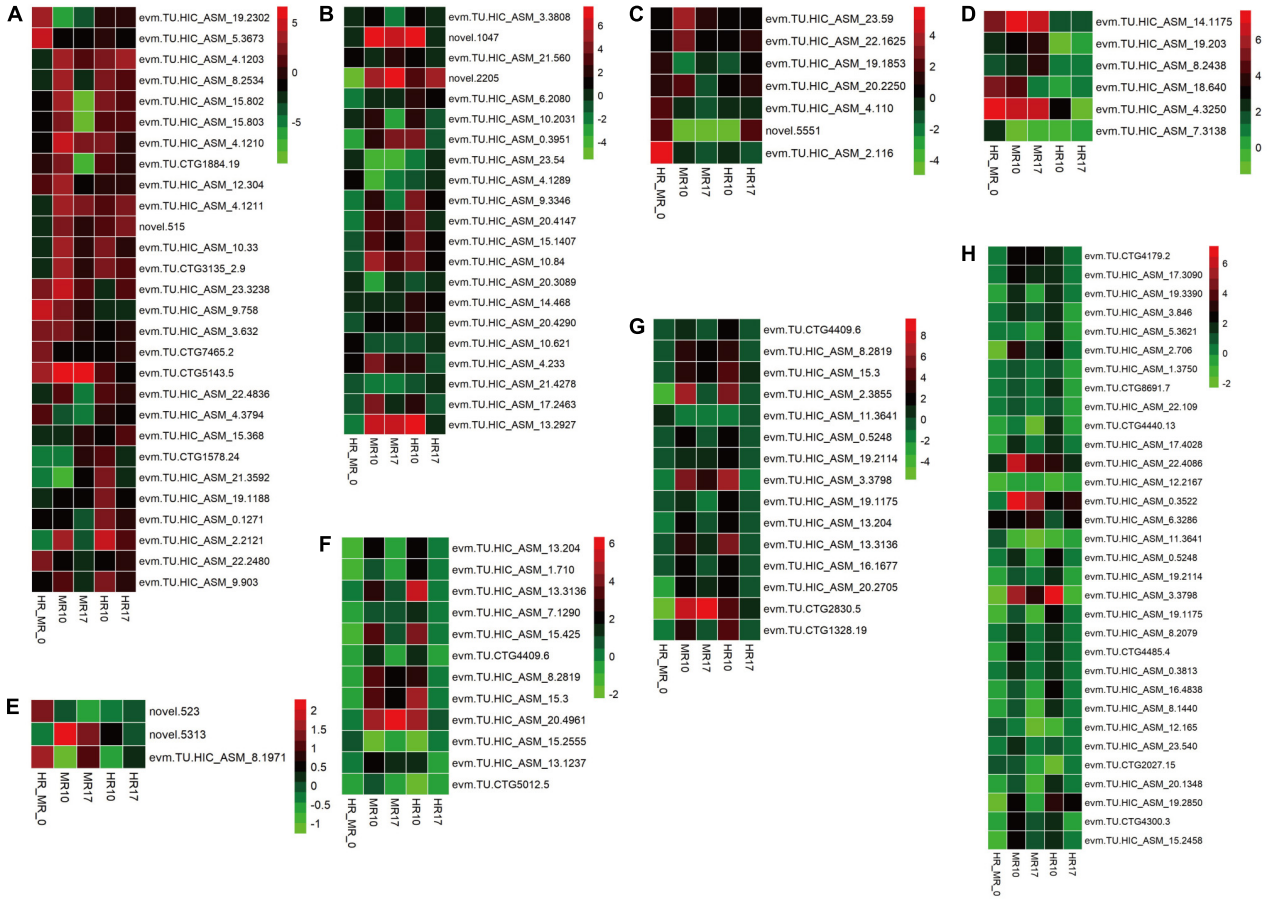

FIGURE 6 | Comparison of resistance-related genes expressed in the highly resistant (4411-3, HR) and moderately resistant (K326, MR) genotype in response to *R. solanacearum* infection using a heatmap. Colors represent the $\log_2$ fold change values. HR_MR_0 = HRM_0 vs. MRM_0; MR10 = MRI_10 vs. MRM_10; MR17 = MRI_17 vs. MRM_17; HR10 (=HRI_10 vs. HRM_10; HR17 (=HRI_17 vs. HRM_17.
(A) Cell wall-related genes. **(B)** Starch and sucrose metabolism-related genes. **(C)** Plant hormone signal transduction-related genes. **(D)** Glutathione metabolism-related genes. **(E)** ABC transporter-related genes. **(F)** Glycerolipid metabolism-related genes. **(G)** Glycerophospholipid metabolism-related genes. **(H)** Endocytosis-related genes.

DEGs potentially contributed to the resistance and susceptibility in the two tobacco genotypes. Further, we found 6,133 DEGs in the HR genotype in response to *R. solanacearum* infection at 10 dpi, which was 45.8-fold more than the number detected at 17 dpi (**Supplementary Figures 6A,B**, **Supplementary Table 9**), suggesting that the HR genotype developed *R. solanacearum* resistance at an early stage. Interestingly, 6,233 and 21,541 non-redundant DEGs were identified in the HR and MR genotype in response to *R. solanacearum* infection at 10 and 17 dpi, respectively (**Figure 3B**). Overall, the number of DEGs was significantly higher in the MR than HR genotype, including 4,201 common DEGs, indicating that the two genotypes mounted different defense responses against *R. solanacearum*. DEGs involved in the response to *R. solanacearum* infection may contribute to genotypic differences in disease symptoms. Analysis of 4021 shared DEGs and 5 KEGG pathways revealed common sets of genes involved in the general defense response (**Figures 3B**, **5**), indicating a complex and concerted response of the HR and MR genotypes to *R. solanacearum* infection. Notably, GO and KEGG analyses implicated seven specific pathways in the R genotype, including those associated with the cell wall, starch and sucrose metabolism, glutathione metabolism, ABC transporters, endocytosis, glycerolipid metabolism, and glycerophospholipid metabolism (**Figures 4**, **5**). Collectively, these findings provide important basis for understanding the defense process.

Cell Wall Biosynthesis May Be Linked to *Ralstonia solanacearum* Resistance in HR Tobacco Genotype

Cell wall is composed of hemicelluloses, cellulose microfibrils, and pectin. It provides a physical barrier to infection during pathogenic attack in plants (Molina et al., 2021). In this study, GO enrichment analysis indicated that many up-regulated genes in the HR genotype were involved in cell wall metabolism (**Figures 4**, **6A**, **Supplementary Table 11**), including the cell wall macromolecule catabolic process, cell wall macromolecule

metabolic process and cell wall organization or biogenesis. These findings are consistent with those of a previous study, which showed that genes associated with xyloglucan biosynthesis and cell wall organization were significantly enriched in response to *R. solanacearum* infection in pepper (Hwang et al., 2011). Also, cell wall-related genes showed genotype-specific expression differences between resistant and susceptible peanut (Chen et al., 2014).

In this study, some *XTH* genes were down-regulated in the MR genotype (**Figure 6A**, **Supplementary Table 11**). In addition, in terms of starch and sucrose metabolism, many genes involved in the biosynthesis of cell wall components exhibited different expression levels. For example, five of six enzymes (β-glucosidase) involved in cellulose hydrolysis were up-regulated in the HR genotype at 10 dpi (**Figures 5**, **6B**, **Supplementary Table 11**), which was the opposite expression pattern reported in *Brassica oleracea* in response to *Plasmodiophora brassicae* infection (Zhang et al., 2016). Moreover, the DEGs related to the cell wall were also inhibited in the MR genotype. These results suggest that cell wall-related genes may confer different functions in the two genotypes in response to *R. solanacearum* infection.

Plant Hormone Signal Transduction Pathways Participate in Tobacco-*Ralstonia solanacearum* Interactions and Initiate Defense Responses

Hormone crosstalk is crucial for plant defenses against pathogens (Robert-Seilaniantz et al., 2011). Auxin has also been implicated in the plant stress response but display complex plant-pathogen interactions patterns (Domingo et al., 2009; Kazan and Manners, 2009). In particular, root transcriptional analyses of *Arabidopsis*, tomato, and wild potato have demonstrated that hormone signaling pathways are altered upon contact with *R. solanacearum* (Zuluaga et al., 2015; French et al., 2018; Zhao et al., 2019), which may affect the root architecture and have direct or indirect effects on bacterial invasion.

Notably, SAUR may negatively regulate auxin biosynthesis and transport (Kant et al., 2009). In this study, the auxin-related genes *SAUR21* (*small auxin up RNA 21*, novel.5551) and *SAUR24* (evm.TU.HIC_ASM_2.116) were up-regulated 4.1- and 55.5-fold, respectively, in the HR genotype compared with the MR genotype. *SAUR21* and *SAUR24* were down-regulated 21.3- and 20.4-fold in MR genotype and R genotype at 10 dpi (**Figure 6C**, **Supplementary Table 11**). *SAUR24* was down-regulated 2.9- and 2.8-fold in MR and HR genotype at 17 dpi (**Figure 6C**, **Supplementary Table 11**). Consistently, we found that IAA accumulated in response to *R. solanacearum* infection, and this trend was stronger in the MR genotype than in the HR genotype (**Figure 2A**). These results indicate that an auxin signaling-mediated pathway may participate in the defense response of tobacco to *R. solanacearum*.

Transcriptomic analysis showed that *R. solanacearum* infection increased ABA-responsive gene expression in *Arabidopsis*, and several ABA receptor mutants with impaired ABA perception were more susceptible to *R. solanacearum* infection (Zhao et al., 2019). In this study, four ABA-related genes were highly expressed in the HR genotype in response to *R. solanacearum* infection. However, these genes showed expression changes in the MR genotype in response to *R. solanacearum* infection, in which two were up-regulated, while one was down-regulated (**Figure 6C**, **Supplementary Table 11**). These results show that ABA increases in response to *R. solanacearum* infection and this trend tends to be stronger in the MR genotype than in the HR genotype (**Figure 2D**).

Auxin was shown to be an important regulator of resistance to *R. solanacearum* infection in *Arabidopsis* (Zhao et al., 2019). Therefore, IAA and ABA may both participate in tobacco defense response against *R. solanacearum*. However, further studies are required to determine the precise role of these hormones in response to *R. solanacearum* infection in tobacco.

Additional Candidate Genes Associated With Resistance to *Ralstonia solanacearum* in Tobacco

Glutathione *S*-transferases (GSTs) regulates cellular metabolism and are involved in various stress responses (Marrs, 1996). For example, GST gene cluster plays an important role in *Verticillium wilt* resistance in cotton (Li et al., 2019). In this study, all genes encoding GST for glutathione metabolism were up-regulated in the HR genotype compared with the MR genotype; five were up-regulated in the MR genotype at 10 dpi (**Figure 6D**, **Supplementary Table 11**). Therefore, differential expression of *GST* genes may be vital for BW resistance in tobacco. However, further experiments are needed to characterize their functions.

Some ABC transporters contribute to resistance against pathogens. The ABC transporter Lr34 confers resistance to multiple fungal pathogens in wheat (Krattinger et al., 2009). ABC transporters were highly expressed in barley upon inoculation with barley yellow dwarf virus (Wang et al., 2013). Consistent with the previous findings, ABC transporters (novel.523 and evm.TU.HIC_ASM_8.1971) were more expressed in the HR genotype than in the MR genotype and were strongly repressed in the MR genotype at 10 dpi (**Figure 6E**, **Supplementary Table 11**), suggesting that a resistance mechanism involving ABC transporters contributes to *R. solanacearum* resistance in tobacco.

Here, we found three additional pathways enriched explicitly in the HR genotype in response to *R. solanacearum* infection, including endocytosis, glycerolipid metabolism, and glycerophospholipid metabolism (**Figures 6F–H**, **Supplementary Table 11**), providing new insights into BW resistance in plants.

Studies have shown that "cell wall and plant hormone signal transduction pathways" regulates *R. solanacearum* resistance in *Arabidopsis* (Zhao et al., 2019), tomato (Wang and Xie, 2012; French et al., 2018), potato (Zuluaga et al., 2015), pepper (Hwang et al., 2011), and peanut (Chen et al., 2014). Glutathione metabolism and ABC transporters were also found to mediate resistance to other phytopathogens but not *R. solanacearum* infection (Krattinger et al., 2009; Wang et al., 2013; **Supplementary Table 12**). However, endocytosis, glycerolipid metabolism, and glycerophospholipid metabolism

pathways have to been shown to regulate resistance against *R. solanacearum*, suggesting that these pathways may be specific to *R. solanacearum* resistance in tobacco. However, further studies are needed to verify these findings.

In conclusion, physiological indexes and transcriptomic analysis were performed to determine the mechanism underlying the response of tobacco to *R. solanacearum* infection. Numerous DEGs were detected in 4411-3 and K326 in response to *R. solanacearum* infection. The DEGs in the HR genotype were enriched in seven key pathways, including cell wall, starch and sucrose metabolism, glutathione metabolism, ABC transporters, endocytosis, glycerolipid metabolism, and glycerophospholipid metabolism. Notably, genes related to the cell wall, GST, and auxin synthesis potentially regulate complex resistance to *R. solanacearum* infection at the transcriptional level. Overall, these findings improve our understanding of the molecular mechanisms underlying the response of tobacco genotypes to *R. solanacearum* invasion and form the basis for identifying candidate genes involved in BW resistance in tobacco.

DATA AVAILABILITY STATEMENT

The original contributions presented in the study are publicly available. This data can be found here: National Center for Biotechnology Information (NCBI) BioProject database under accession number PRJNA762496.

AUTHOR CONTRIBUTIONS

ZeZ, XP, and JC designed the research. ZeZ, XP, JC, QY, WZ, TX, BC, MR, RG, ZaZ, ZM, and ZH performed the research. XP and ZeZ analyzed the data and wrote the manuscript. XP, ZeZ, and AY revised the manuscript. All authors approved the final manuscript.

FUNDING

This work was supported by Tobacco Genome Project of China National Tobacco Corporation [110201901015 (JY-02) and 110202001024 (JY-07)] and Science and Technology Project of Guangdong Tobacco Company [201544000024062 and 201744000020090].

ACKNOWLEDGMENTS

We thank He Xie at Yunnan Academy of Tobacco Agriculture Science for providing the reference tobacco genome.

SUPPLEMENTARY MATERIAL

The Supplementary Material for this article can be found online at: https://www.frontiersin.org/articles/10.3389/fpls.2021.767882/full#supplementary-material

Supplementary Figure 1 | The bacterial content of stem tissue for RNA sequencing.

Supplementary Figure 2 | Enzyme activities of POD **(A)**, CAT **(B)**, SOD **(C)**, PPO **(D)**, PAL **(E)**, and APX **(F)** in 4411-3 (HR) and K326 (MR) after *R. solanacearum* infection at 0, 10, and 17 days post-inoculation with *Ralstonia solanacearum*. Five independent experimental replicates were analyzed for each sample, and the data are presented as means ± SE (standard error). POD, peroxidase; CAT, catalase; SOD, superoxide dismutase; PPO, polyphenol oxidase; PAL, phenylalanine ammonia-lyase; APX, ascorbate peroxidase.

Supplementary Figure 3 | Contents of chlorophyll **(A)**, MDA **(B)**, soluble protein **(C)**, and exopolysaccharides **(D)** at 0, 10, and 17 days post-inoculation with *Ralstonia solanacearum*. Five independent experimental replicates were analyzed for each sample, and the data are presented as means ± SE (standard error). MDA, malondialdehyde.

Supplementary Figure 4 | Volcano plot of differentially expressed genes (DEGs) between 4411-3 (HR) genotype and K326 (MR) genotypes under mock conditions. **(A)** Volcano plot of differentially expressed genes (DEGs)between 4411-3 (HR) genotype and K326 (MR) genotypes at day 0 under mock conditions (HRM_0 vs. MRM_0). **(B)** Volcano plot of differentially expressed genes (DEGs)between the 4411-3 (HR) and K326 (MR) genotypes at day 10 under mock conditions(HRM_10 vs. MRM_10). **(C)** Volcano plot of differentially expressed genes (DEGs)between the 4411-3 (HR) and K326 (MR) genotypes at day 17 under mock conditions(HRM_17 vs. MRM_17).

Supplementary Figure 5 | Transcriptome profile analysis of both 4411-3 and K326 genotypes under mock conditions at 0, 10, and 17 days. Blue indicates low expression, white indicates intermediate expression, and red indicates high expression (FPKM > 1).

Supplementary Figure 6 | Volcano plot of differentially expressed genes (DEGs) in 4411-3 (HR) and K326 (MR) after *Ralstonia solanacearum* infection. **(A)** Volcano plot of differentially expressed genes (DEGs) in 4411-3 (HR) at 10 days post-inoculation with *Ralstonia solanacearum*. (HRI_10 vs. HRM_10). **(B)** Volcano plot of differentially expressed genes (DEGs) in 4411-3 (HR) at 17 days post-inoculation with *Ralstonia solanacearum*. (HRI_17 vs. HRM_17). **(C)** Volcano plot of differentially expressed genes (DEGs) in K326 (MR) at 10 days post-inoculation with *Ralstonia solanacearum*. (MRI_10 vs. MRM_10). **(D)** Volcano plot of differentially expressed genes (DEGs) in K326 (MR) at 17 days post-inoculation with *Ralstonia solanacearum*. (MRI_17 vs. MRM_17).

Supplementary Figure 7 | Transcriptome profile analysis and KEGG pathways of 4201 common genes in 4411-3 and K326 genotypes after *Ralstonia solanacearum* infection. **(A)** Transcriptome profile analysis of 4201 common genes in 4411-3 and K326 genotypes after *Ralstonia solanacearum* infection at 0, 10, and 17 days. Blue indicates low expression, white indicates intermediate expression, and red indicates high expression (FPKM > 1). **(B)** Significantly enriched KEGG pathways for 4201 common DEGs in the 4411-3 and K326 genotype in response to *Ralstonia solanacearum* infection.

Supplementary Table 1 | Sequences of primers used for RT-qPCR.

Supplementary Table 2 | Evaluation of disease resistance for experimental materials.

Supplementary Table 3 | Quality parameters for RNA-seq raw data.

Supplementary Table 4 | List of mapping results.

Supplementary Table 5 | List of genes validated by qRT-PCR to verify the reliability of RNA-seq data.

Supplementary Table 6 | List of differentially expressed genes (DEGs) in 4411-3 (HR) vs. K326 (MR) under mock conditions at 0, 10, and 17 days. HR_MR_0 = HRM_0 vs. MRM_0; HR_MR_10 = HRM_10 vs. MRM_10; HR_MR_17 = HRM_17 vs. MRM_17.

Supplementary Table 7 | List of significantly enriched GO terms for up-regulated genes in 4411-3 (HR) vs. K326 (MR) under mock conditions.

Supplementary Table 8 | List of significantly enriched GO terms for up-regulated genes in K326 (MR) vs. 4411-3 (HR) under mock conditions.

Supplementary Table 9 | List of differentially expressed genes (DEGs) in 4411-3 (HR) at 10 and 17 days post inoculation with *Ralstonia solanacearum*. HR10 = HRI_10 vs. HRM_10; HR17 = HRI_17 vs. HRM_17.

Supplementary Table 10 | List of differentially expressed genes (DEGs) in K326 (MR) at 10 and 17 days post inoculation with *Ralstonia solanacearum*. MR10 = MRI_10 vs. MRM_10; MR17 = MRI_17 vs. MRM_17.

Supplementary Table 11 | List of resistance-related genes expressed in 4411-3 (HR) and K326 (MR) in response to *Ralstonia solanacearum* infection.

Supplementary Table 12 | Significantly enriched GO terms after *Ralstonia solanacearum* infection in *Arabidopsis*, tomato, potato, pepper, and peanut.

REFERENCES

Alexa, A., Rahnenfuhrer, J., and Lengauer, T. (2006). Improved scoring of functional groups from gene expression data by de correlating GO graph structure. *Bioinformatics* 22, 1600–1607. doi: 10.1093/bioinformatics/btl140

Anders, S., and Huber, W. (2010). Differential expression analysis for sequence count data. *Genome Biol.* 11:R106. doi: 10.1186/gb-2010-11-10-r106

Buddenhagen, I. W. (1986). "Bacterial wilt revisited," in *Bacterial wilt in Asia and the South Pacific*, ed. G. J. Persley (Camberra: ACIAR), 126–139.

Cai, W. W., Yang, S., Wu, R. J., Cao, J. S., Shen, L., Guan, D. Y., et al. (2021). Pepper NAC-type transcription factor NAC2c balances the trade-off between growth and defense responses. *Plant Physiol.* 186, 2169–2189. doi: 10.1093/plphys/kiab190

Carmeille, A., Caranta, C., Dintinger, J., Prior, P., Luisetti, J., and Besse, P. (2006). Identification of QTLs for *Ralstonia solanacearum* race 3-phylotype resistance in tomato. *Theor. Appl. Genet.* 113, 110–121. doi: 10.1007/s00122-006-0277-3

Chen, X. K., Wang, W. B., Cai, P. P., Wang, Z. W., Li, T. T., and Du, Y. (2021). The role of the MAP kinase—kinase protein StMKK1 in potato immunity to different pathogens. *Hortic. Res.* 8, 1–9. doi: 10.1038/s41438-021-00556-5

Chen, Y. N., Ren, X. P., Zhou, X. J., Huang, L., Yan, L. Y., Lei, Y., et al. (2014). Dynamics in the resistant and susceptible peanut (*Arachis hypogaea* L.) root transcriptome on infection with the *Ralstonia solanacearum*. *BMC Genomics* 15:1078. doi: 10.1186/1471-2164-15-1078

Cui, K. Y., Lin, Y. Y., Zhou, X., Li, S. C., Liu, H., Zeng, F., et al. (2015). Comparison of sample pretreatment methods for the determination of multiple phytohormones in plant samples by liquid chromatography–electrospray ionization-tandem mass spectrometry. *Microchem. J.* 121, 25–31. doi: 10.1016/j.microc.2015.02.004

Dahal, D., Pich, A., Braun, H. P., and Wydra, K. (2010). Analysis of cell wall proteins regulated in stems of susceptible and resistant tomato species after inoculation with *Ralstonia solanacearum*: a proteomics approach. *Plant Mol. Biol.* 73, 643–658. doi: 10.1007/s11103-010-9646-z

Deslandes, L., Olivier, J., Theulieres, F., Hirsch, J., Feng, D. X., Bittner-Eddy, P., et al. (2002). Resistance to *Ralstonia Solanacearum* in *Arabidopsis Thaliana* is conferred by the recessive *RRS1-R* gene, a member of a novel family of resistance genes. *Proc. Natl. Acad. Sci. U S A.* 99, 2404–2409. doi: 10.1073/pnas.032485099

Diogo, R., and Wydra, K. (2007). Silicon-induced basal resistance in tomato against *Ralstonia solanacearum* is related to modification of pectic cell wall polysaccharide structure. *Physiol. Mol. Plant P* 70, 120–129. doi: 10.1016/j.pmpp.2007.07.008

Domingo, C., Andrés, F., Iglesias, D. J., and Talón, M. (2009). Constitutive expression of OsGH3.1 reduces auxin content and enhances defense response and resistance to a fungal pathogen in rice. *Mol. Plant Microbe In.* 22, 201–210. doi: 10.1094/MPMI-22-2-0201

Dumanović, J., Nepovimova, E., Natić, M., Kuča, K., and Jaćević, V. (2020). The significance of reactive oxygen species and antioxidant defense system in plants: a concise overview. *Front. Plant Sci.* 11:552969. doi: 10.3389/fpls.2020.552969

Elphinstone, J. G., Allen, C., Prior, P., and Hayward, A. C. (2005). "The current bacterial wilt situation: a global overview," in *bacterial wilt the disease and the Ralstonia Solanacearum species complex*, eds C. Allen, P. Prior, and A. C. Hayward (St. Paul: American Phytopathological Society), 9–18.

French, E., Kim, B. S., Rivera-Zuluaga, K., and Iyer-Pascuzzi, A. S. (2018). Whole root transcriptomic analysis suggests a role for auxin pathways in resistance to *Ralstonia solanacearum* in tomato. *Mol. Plant Microbe In.* 31, 432–444. doi: 10.1094/MPMI-08-17-0209-R

Godiard, L., Froissard, D., Fournier, J., Axelos, M., and Marco, Y. (1991). Differential regulation in tobacco cell suspensions of genes involved in plant-bacteria interactions by pathogen-related signals. *Plant Mol. Biol.* 17, 409–413. doi: 10.1007/BF00040635

Hayward, A. C. (1991). Biology and epidemiology of bacterial wilt caused by *Pseudomonas solanacearum*. *Ann. Rev. Phytopathol.* 29, 65–87. doi: 10.1146/annurev.phyto.29.1.65

Hwang, J. H., Choi, Y. M., Kang, J. S., Kim, S. T., Cho, M. C., Mihalte, L., et al. (2011). Microarray analysis of the transcriptome for bacterial wilt resistance in pepper (*Capsicum annuum* L.). *Not. Bot. Horti. Agrobo.* 39:49. doi: 10.15835/nbha3926820

Kant, S., Bi, Y. M., Zhu, T., and Rothstein, S. J. (2009). SAUR39, a small auxin-up RNA gene, acts as a negative regulator of auxin synthesis and transport in rice. *Plant Physiol.* 151, 691–701. doi: 10.1104/pp.109.143875

Kazan, K., and Manners, J. M. (2009). Linking development to defense: auxin in plant-pathogen interactions. *Trends Plant Sci.* 14, 373–382. doi: 10.1016/j.tplants.2009.04.005

Kiba, A., Fukui, K., Mitani, M., Galis, I., Hojo, Y., Shinya, T., et al. (2020). Silencing of phosphoinositide dependent protein kinase orthologs reduces hypersensitive cell death in *Nicotiana benthamiana*. *Plant Biotechnol NAR* 20:0511. doi: 10.5511/plantbiotechnology.20.0511b

Krattinger, S. G., Lagudah, E. S., Spielmeyer, W., Singh, R. P., McFadden, H., et al. (2009). A putative ABC transporter confers durable resistance to multiple fungal pathogens in wheat. *Science* 323, 1360–1363. doi: 10.1126/science.1166453

Lafortune, D., Beramis, M., Daubeze, A. M., Boissot, N., and Palloix, A. (2005). Partial resistance of pepper to bacterial wilt is oligogenic and stable under tropical conditions. *Plant Dis.* 89, 501–506. doi: 10.1094/PD-89-0501

Lee, H. J., Mochizuki, N., Masuda, T., and Buckhout, T. J. (2012). Disrupting the bimolecular binding of the haem-binding protein 5 (AtHBP5) to haem oxygenase 1 (HY1) leads to oxidative stress in Arabidopsis. *J. Exp. Bot.* 63, 5967–5978. doi: 10.1093/jxb/ers242

Li, Z. K., Chen, B., Li, X. X., Wang, J. P., Zhang, Y., Wang, X. F., et al. (2019). A newly identified cluster of glutathione *S*-transferase genes provides Verticillium wilt resistance in cotton. *Plant J.* 98, 213–227. doi: 10.1111/tpj.14206

Liu, Q. P., Liu, Y., Tang, Y. M., Chen, J. N., and Ding, W. (2017). Overexpression of NtWRKY50 increases resistance to *Ralstonia solanacearum* and alters salicylic acid and jasmonic acid production in tobacco. *Front. Plant Sci.* 8:1710. doi: 10.3389/fpls.2017.01710

Liu, Y. Q., Yan, J., Qin, Q. Q., Zhang, J., Chen, Y., Zhao, L. L., et al. (2019). Type one protein phosphatases (TOPPs) contribute to the plant defense response in Arabidopsis. *J. Integr. Plant Biol.* 62, 360–377. doi: 10.1111/jipb.12845

Livak, K. J., and Schmittgen, T. D. (2001). Analysis of relative gene expression data using real-time quantitative PCR and the $2^{-\Delta\Delta CT}$ method. *Methods* 25, 402–408. doi: 10.1006/meth.2001.1262

Marrs, K. A. (1996). The functions and regulation of glutathione S-transferases in plants. *Annu. Rev. Plant Biol.* 47, 127–158. doi: 10.1146/annurev.arplant.47.1.127

Miller, G., Suzuki, N., Ciftci-Yilmaz, S., and Mittler, R. (2010). Reactive oxygen species homeostasis and signaling during drought and salinity stresses. *Plant Cell Environ.* 33, 453–467. doi: 10.1111/j.1365-3040.2009.02041.x

Molina, A., Miedes, E., Bacete, L., Rodríguez, T., Mélida, H., Denancé, N., et al. (2021). Arabidopsis cell wall composition determines disease resistance specificity and fitness. *Proc. Natl. Acad. Sci. U S A.* 118:e2010243118. doi: 10.1101/2020.05.21.105650

Nakaho, K., Hibino, H., and Miyagawa, H. (2000). Possible mechanisms limiting movement of *Ralstonia solanacearum* in resistant tomato tissues. *Phytopathol* 148, 191–190. doi: 10.1046/j.1439-0434.2000.00476.x

Nakano, M., Nishihara, M., Yoshioka, H., Takahashi, H., Sawasaki, T., Ohnishi, K., et al. (2013). Suppression of DS1 phosphatidic acid phosphatase confirms resistance to *Ralstonia solanacearum* in *Nicotiana benthamiana*. *PLoS One* 8:e75124. doi: 10.1371/journal.pone.0075124

Pan, X. Y., Mahmudul, H. M., Li, Y. Q., Liao, C. S., Zheng, H., Liu, R., et al. (2015). Asymmetric transcriptomic signatures between the cob and florets in the maize ear under optimal- and low-nitrogen conditions at silking, and functional characterization of amino acid transporters ZmAAP4 and ZmVAAT3. *J. Exp. Bot.* 60:6149. doi: 10.1093/jxb/erv315

Robert-Seilaniantz, A., Grant, M., and Jones, J. D. (2011). Hormone crosstalk in plant disease and defense: more than just jasmonate-salicylate antagonism. *Annu. Rev. Phytopathol.* 49, 317–343. doi: 10.1146/annurev-phyto-073009-114447

Schacht, T., Unger, C., Pich, A., and Wydra, K. (2011). Endo- and exopolygalacturonases of *Ralstonia solanacearum* are inhibited by polygalacturonase-inhibiting protein (PGIP) activity in tomato stem extracts. *Plant Physiol. Bioch.* 49, 377–387. doi: 10.1016/j.plaphy.2011.02.001

Sun, C. Z., Li, Y. Q., Zhao, W. S., Song, X. F., Lu, M., Li, X. L., et al. (2016). Integration of hormonal and nutritional cues orchestrates progressive corolla opening. *Plant Physiol.* 171, 1209–1229. doi: 10.1104/pp.16.00209

Thoquet, P., Olivier, J., Sperisen, C., Rogowsky, P., Laterrot, H., and Grimsley, N. (1996a). Quantitative trait loci determining resistance to bacterial wilt in tomato cultivar Hawaii 7996. *Mol. Plant Microbe Interact.* 9, 826–836. doi: 10.1094/MPMI-9-0826

Thoquet, P., Olivier, J., Sperisen, C., Rogowsky, P., Prior, P., Anais, G., et al. (1996b). Polygenic resistance of tomato plants to bacterial wilt in the French West Indies. *Mol. Plant Microbe Interact.* 9, 837–842. doi: 10.1094/MPMI-9-0837

Tran, N. H., and Kim, B. S. (2010). Inheritance of resistance to bacterial wilt (*Ralstonia solancearum*) in pepper (*Capsicum annuum* L.). *Hort. Environ. Biotechnol.* 51, 431–439. doi: 10.1590/S0102-05362010000400020

Urvalek, A. M., Osei-Sarfo, K., Tang, X. H., Zhang, T., Scognamiglio, T., and Gudas, L. J. (2015). Identification of ethanol and 4-nitroquinoline-1-oxide induced epigenetic and oxidative stress markers during oral cavity carcinogenesis. *Alcohol. Clin. Exp. Res.* 39, 1360–1372. doi: 10.1111/acer.12772

Wang, B. S., He, T. J., Zheng, X. A., Song, B. T., and Chen, H. L. (2021). Proteomic Analysis of Potato Responding to the Invasion of *Ralstonia solanacearum* UW551 and Its Type III Secretion System Mutant. *Mol. Plant Microbe Interact.* 34, 337–350. doi: 10.1094/MPMI-06-20-0144-R

Wang, J. F., Olivier, J., Thoquet, P., Mangin, B., Sauviac, L., and Grimsley, N. H. (2000). Resistance of tomato line Hawaii7996 to *Ralstonia solanacearum* Pss4 in Taiwan is controlled mainly by a major strain-specific locus. *Mol. Plant Microbe Interact.* 13, 6–13. doi: 10.1094/MPMI.2000.13.1.6

Wang, J. G., and Xie, X. L. (2012). Induction of tomato jasmonate-resistant 1-like 1 gene expression can delay the colonization of *Ralstonia solanacearum* in transgenic tomato. *Bot. Stud.* 53, 75–84. doi: 10.1016/j.aquabot.2011.10.001

Wang, J., Zheng, C. F., Shao, X. Q., Hu, Z. J., Li, J. X., Wang, P., et al. (2020). Transcriptomic and genetic approaches reveal an essential role of the NAC transcription factor SlNAP1 in the growth and defense response of tomato. *Hortic. Res.* 7, 1–11. doi: 10.1038/s41438-020-00442-6

Wang, X. D., Liu, Y., Chen, L., Zhao, D., Wang, X. F., and Zhang, Z. Y. (2013). Wheat resistome in response to barley yellow dwarf virus infection. *Funct. Integr. Genomic* 13, 155–165. doi: 10.1007/s10142-013-0309-4

Wang, Y., Zhao, A., Morcillo, R. J., Yu, G., Xue, H., Rufian, J. S., et al. (2021). A bacterial effector protein uncovers a plant metabolic pathway involved in tolerance to bacterial wilt disease. *Mol. Plant* 2021, S1674–S2052. doi: 10.1016/j.molp.2021.04.014

Wydra, K., and Beri, H. (2006). Structural changes of homogalacturonan, rhamnogalacturonan I and arabinogalactan protein in xylem cell walls of tomato genotypes in reaction to *Ralstonia solanacearum*. *Physiol. Mol. Plant P* 68, 41–50. doi: 10.1016/j.pmpp.2006.06.001

Xie, R. H., Wu, S. X., Luo, Z. Y., Ma, Z. W., Li, J. Q., Zhang, Z. C., et al. (2014). Pathogenicity of *Ralstonia solanacearum* isolated from tobacco in Guangdong, Fujian and Guizhou province. *Microbiol. China* 41, 1800–1806. doi: 10.13344/j.microbiol.china.130652

Xue, H. R., Lozano-Durán, R., and Macho, A. P. (2020). Insights into the root invasion by the plant pathogenic bacterium *Ralstonia solanacearum*. *Plants* 9:lants9040516. doi: 10.3390/plants9040516

Yu, J. J., Han, J. N., Wang, R. F., and Li, X. X. (2016). Down-regulation of nitrogen/carbon metabolism coupled with coordinative hormone modulation contributes to developmental inhibition of the maize ear under nitrogen limitation. *Planta* 244, 111–124. doi: 10.1007/s00425-016-2499-1

Zhang, X. L., Liu, Y. M., Fang, Z. Y., Li, Z. S., Yang, L. M., Zhuang, M., et al. (2016). Comparative transcriptome analysis between broccoli (*Brassica oleracea var. italica*) and wild cabbage (*Brassica macrocarpa Guss.*) in response to *Plasmodiophora brassicae* during different infection stages. *Front. Plant Sci.* 7:1929. doi: 10.3389/fpls.2016.01929

Zhang, Z. C., Yuan, Q. H., Ma, Z. W., Guo, P. G., Li, J. Q., Qiu, M., et al. (2017). Inheritance of resistance to bacterial wilt in Chinese domestic tobacco cultivar GDSY-1. *Chin. Tobacco Sci.* 38, 9–16. doi: 10.13496/j.issn.1007-5119.2017.04.002

Zhao, C. Z., Wang, H. J., Lu, Y., Hu, J. X., Qu, L., Li, Z. Q., et al. (2019). Deep sequencing reveals early reprogramming of *Arabidopsis* root transcriptomes upon *Ralstonia solanacearum* infection. *Mol. Plant Microbe In.* 32, 813–827. doi: 10.1094/MPMI-10-18-0268-R

Zhuo, T., Wang, X., Chen, Z., Cui, H., Zeng, Y., Chen, Y., et al. (2020). The *Ralstonia solanacearum* effector RipI induces a defence reaction by interacting with the bHLH93 transcription factor in *Nicotiana benthamiana*. *Mol. Plant Pathol.* 21, 999–1004. doi: 10.1111/mpp.12937

Zuluaga, A. P., Solé, M., Lu, H. B., Góngora-Castillo, E., Vaillancourt, B., Coll, N., et al. (2015). Transcriptome responses to *Ralstonia solanacearum* infection in the roots of the wild potato *Solanum commersonii*. *BMC Genom.* 16:246. doi: 10.1186/s12864-015-1460-1

Conflict of Interest: The authors declare that the research was conducted in the absence of any commercial or financial relationships that could be construed as a potential conflict of interest.

Publisher's Note: All claims expressed in this article are solely those of the authors and do not necessarily represent those of their affiliated organizations, or those of the publisher, the editors and the reviewers. Any product that may be evaluated in this article, or claim that may be made by its manufacturer, is not guaranteed or endorsed by the publisher.

frontiers in Plant Science

ORIGINAL RESEARCH
published: 07 January 2022
doi: 10.3389/fpls.2021.780429

Metabolic Profiling of Resistant and Susceptible Tobaccos Response Incited by *Ralstonia pseudosolanacearum* Causing Bacterial Wilt

Liang Yang[1†], Zhouling Wei[1†], Marc Valls[2,3] and Wei Ding[1]*

[1]*Laboratory of Natural Products Pesticides, College of Plant Protection, Southwest University, Chongqing, China,* [2]*Centre for Research in Agricultural Genomics (CRAG), CSIC-IRTA-UAB-UB, Campus UAB, Barcelona, Spain,* [3]*Genetics Section, Facultat de Biologia, Universitat de Barcelona, Barcelona, Spain*

OPEN ACCESS

Edited by:
Sang-Wook Han,
Chung-Ang University, South Korea

Reviewed by:
Antonio Cellini,
University of Bologna, Italy
Tiffany Lowe-Power,
University of California, Davis, United States

***Correspondence:**
Wei Ding
dingw@swu.edu.cn

†These authors have contributed equally to this work

Specialty section:
This article was submitted to Plant Pathogen Interactions, a section of the journal Frontiers in Plant Science

Received: *21 September 2021*
Accepted: *24 November 2021*
Published: *07 January 2022*

Citation:
Yang L, Wei Z, Valls M and Ding W (2022) Metabolic Profiling of Resistant and Susceptible Tobaccos Response Incited by Ralstonia pseudosolanacearum Causing Bacterial Wilt. Front. Plant Sci. 12:780429. doi: 10.3389/fpls.2021.780429

The causal agent of bacterial wilt, *Ralstonia pseudosolanacearum*, can cause significant economic losses during tobacco production. Metabolic analyses are a useful tool for the comprehensive identification of plant defense response metabolites. In this study, a gas chromatography-mass spectrometry (GC-MS) approach was used to identify metabolites differences in tobacco xylem sap in response to *R. pseudosolanacearum* CQPS-1 in two tobacco cultivars: Yunyan87 (susceptible to *R. pseudosolanacearum*) and K326 (quantitatively resistant). Metabolite profiling 7 days post inoculation with *R. pseudosolanacearum* identified 88 known compounds, 42 of them enriched and 6 depleted in the susceptible cultivar Yunyan87, while almost no changes occurred in quantitatively resistant cultivar K326. Putrescine was the most enriched compound (12-fold) in infected susceptible tobacco xylem, followed by methyl-alpha-d-glucopyranoside (9-fold) and arabinitol (6-fold). Other sugars, amino acids, and organic acids were also enriched upon infection. Collectively, these metabolites can promote *R. pseudosolanacearum* growth, as shown by the increased growth of bacterial cultures supplemented with xylem sap from infected tobacco plants. Comparison with previous metabolic data showed that beta-alanine, phenylalanine, and leucine were enriched during bacterial wilt in both tobacco and tomato xylem.

Keywords: metabolomics, GC-MS, tobacco, *Ralstonia pseudosolanacearum*, amino acid

INTRODUCTION

Tobacco (*Nicotiana tabacum* L.) is the most important non-edible agricultural product worldwide (Reichert et al., 2019; Mirkarimi et al., 2021). China is the largest tobacco producer worldwide, growing 1,100,000 ha by almost 1,520,000 farmers that yield 2,610,000 tons of dried leaves every year (Shahbandeh, 2021). Bacterial wilt, a disease caused by the bacterium *Ralstonia solanacearum* species complex, affects tobacco production in numerous countries (Mansfield et al., 2012; Prior et al., 2016; Jiang et al., 2017). In the field, pathogen-infected tobacco

exhibits partial wilting symptoms and premature yellowing of leaves, and one side of the stem develops a brown discoloration. High disease incidence results in production losses, leading to serious damage to the tobacco industry. Bacterial wilt is currently widespread in the main tobacco production regions of Yunnan, Sichuan, Guizhou, Guangxi, Hunan, Hubei, Chongqing, and Guangdong provinces in China (Liu et al., 2017b).

Due to the bacterial aggressiveness, large host range, and broad geographical distribution, control of bacterial wilt has been challenging (Genin and Denny, 2012). Understanding the molecular mechanisms mediating interactions between pathogen and plants is fundamental to develop effective management strategies for disease control. Genomics, transcriptomics, proteomics, and metabolomics are currently applied to study the interaction between crops and pathogens (Planas-Marques et al., 2018; Gao et al., 2019; Gong et al., 2020; de Pedro-Jove et al., 2021). The complete genomic sequence of several *R. pseudosolanacearum* strains infecting tobacco in China have been recently published (Liu et al., 2017a). Global transcriptional gene expression of tomato and tobacco in response to *R. pseudosolanacearum* infection has been analyzed using comparative transcriptome analysis, showing the enrichment in two groups of gene ontology terms regarding glutathione and flavonoid metabolisms in resistant tobacco cultivars (Gao et al., 2019). Proteomic and transcriptomic results demonstrated that gamma-aminobutyric acid (GABA) biosynthesis pathway and methionine cycle (MTC) play a key role in pathogenic interaction between *R. solanacearum* and tomato plants (Wang et al., 2019). However, metabolite changes in tobacco after infection of *R. pseudosolanacearum* have not been addressed up to now.

Metabolomics is playing an important role in identification of the key metabolites in plant adaptation (Zhang et al., 2018; Lowe-Power et al., 2018b; Zeiss et al., 2019). GC-MS metabolic profiling has been widely used to detect metabolite changes in various tobacco cellular processes (Zhang et al., 2018; Tsaballa et al., 2020). Recent studies have investigated the metabolites changes of tobacco leaves from different geographical origins in China and demonstrated the key metabolic pathways related the environmental adaption (Liu et al., 2020). Certain metabolites such as phenolic amino acids, phenylpropanoids, linoleic acid, and hydroxycinnamic acid amides are changed after *Phytophthora parasitica* var. nicotianae inoculation in tobacco plants (Cho et al., 2012). This same approach applied to tomato plants challenged with *R. solanacearum* identified several enriched metabolites in the xylem sap, some of which can be carbon or nitrogen sources for *R. solanacearum* growth (Lowe-Power et al., 2018a). Glutamine and asparagine were identified as primary resources consumed by *R. solanacearum* during its colonization phase (Gerlin et al., 2021). Flavonoids and hydroxycinnamic acids are also of prime importance in the tomato defense response to *R. solanacearum* invasion (Lowe-Power et al., 2015; Zeiss et al., 2019). However, the metabolic profiles of different tobacco cultivars in response to *R. pseudosolanacearum* infection remain largely unknown.

In this work, metabolic profiling using GC-MS was performed to investigate the metabolites changes responses to *R. pseudosolanacearum* infection in two different tobacco cultivars (Yunyan87 and K326). On the basis of the functions of the identified metabolites, we studied the metabolic significance concerning the susceptibility of tobacco to *R. pseudosolanacearum*.

MATERIALS AND METHODS

Plant Growth Conditions and Bacterial Strain

Two tobacco cultivars (bacterial wilt-susceptible cv. Yunyan 87 and quantitatively resistant breeding line K326) were used in this experiment (Cai et al., 2021). Tobacco seeds were sown in plant growing mix soil in a 28°C climate chamber with a light/dark cycle of 14 h/10 h. Tobacco seedlings were transplanted 28 days post sowing into individual 12 cm pots containing mix soil. After 10 days post transplanted, tobacco plants were used for infection assay.

The highly aggressive *R. pseudosolanacearum* strain CQPS-1 (phylotype I, race 1, biovar 3) isolated from tobacco stems in China (Liu et al., 2017a) was used. The bacterial strain was grown in complete BG liquid medium supplemented with 0.5% glucose at 30°C and stored at −80°C in nutrient broth with 25% glycerol. Boucher's minimal medium (MM) pH 7.0 containing 20 mM glucose, 0.5 g/L $(NH_4)_2SO_4$, 3.4 g/L KH_2PO_4, 0.125 mg/L $FeSO_4{\cdot}7H_2O$, and 62.3 mg/L $MgSO_4$ was used for experiments.

Virulence Assay

Soil-drenching assays were performed to investigate the symptomatology of two different tobacco cultivars (Yunyan 87 and K326) after infection. To this end, 6-week-old tobacco plants were soil-soak inoculated by drenching with *R. pseudosolanacearum* bacterial suspension (1×10^8 colony forming units-CFU−/ml). Infected tobacco plants were moved into a growth chamber at 28°C with a 14/10 h light/dark cycle. Bacterial wilt symptoms were scored daily using a disease index scale from 0 to 4 (0 indicates no symptoms; 1: 1–25% of leaves wilted; 2: 26–50% of leaves wilted; 3: 51–75% of leaves wilted; 4: 76–100% of leaves wilted). Individual treatments contained 16 plants for each independent experiment, and the assay was repeated three times. The disease index was calculated as a weighted average.

Bacterial Density in Two Tobacco Cultivars

Bacterial populations were determined by harvesting 100 mg tobacco stem as previously described (Yang et al., 2018). Samples were disinfected and transferred into a 2.5-ml sterile centrifuge tube and ground with sterile glass beads using the MP Biomedicals FastPrep. Next, serially diluted homogenates were plated on SMSA medium, and colonies were counted after 2 days incubation at 28°C (Elphinstone et al., 1996). Each treatment contained 8 samples. The assay was repeated twice.

Collection of Xylem Saps From Tobacco Stems

For the untargeted metabolomics experiments, tobacco plants were used 7 days after soil-soak inoculation with *R. pseudosolanacearum* to collect xylem sap as described previously

with minor modifications (Siebrecht et al., 2003). Samples from healthy and infected tobacco stem tissues were harvested by centrifugation at 4,000 × *g* for 5 min at 4°C, and the supernatants were transferred into prechilled tubes. Samples were then sterilized with 0.22-μM filters and stored at −80°C until analysis. Each sample contains xylem sap from six tobacco plants.

Bacterial Growth Supplemented With Xylem Sap From Tobacco Cultivars

Xylem sap was harvested as described above. Xylem sap was collected from at least six healthy or infected tobacco plants and sterilized through a 0.22-μm filter. An overnight bacterial culture was washed and inoculated in MM, and 50 μl bacteria suspension were mixed with equal volume of xylem sap from healthy/infected plants and then transferred to a 96-well microplate. Fresh MM (50 μl) was added to control wells. The plate was returned into plate reader, and the bacterial OD600 was measured every 4 h during 40 h of cultivation. The experiment was repeated twice.

GC-MS Metabolomics Analysis

GC-MS analysis was performed for metabolite profiling by a GC-MS system (Agilent 7890A/5975C; Dunn et al., 2011). Briefly, 100 μl xylem sap was transferred into a 1.5-ml centrifuge tube with 400 μl of prechilled methanol and mixed for 60 s. Nonadecylic acid and d4-alanine were used as internal quantitative standard. After centrifugation for 10 min, supernatant was transferred into new tube. 60 μl methoxyamine pyridine solution and BSTFA reagent were added to the mixture and left to react for 90 min at 37°C. GC-MS was performed on a HP-5MS capillary column (Agilent J & w Scientific, Folsom, CA, United States), under a constant flow of 1 ml·min^{-1} helium. Samples were injected in split mode in a 20:1 split ratio by the auto-sampler. Column temperature was set at 60°C for 2 min, then ramped to 300°C by 10°C min^{-1}, and held constant for 5 min. Ions were generated with a −70 eV and 1800 V ionization energy, and masses (35–750 *m/z*) were acquired. Peak detection and deconvolution was performed in the Serveis Científicotècnics of the University of Barcelona. Metabolites were relatively quantified by peak area for the quantification ion.

Metabolomics Data Analysis

The GC-MS datasets were analyzed with XCMS online software (https://xcmsonline.scripps.edu/; Forsberg et al., 2018). The raw GC-MS data were processed with XCMS 3.5 software using an automated cloud-based method to process raw metabolomics data, generating a list of statistically significant features that could be used for biological interpretation. To extract potential differentially concentrated metabolites, the cutoff of *q*-value <0.01 and |fold change| > 2 was applied.

Statistical Analyses

The data were analyzed by SPSS software using Student's *t* test under significance levels of 0.05 and 0.01.

RESULTS

Phenotypic Observation After *R. pseudosolanacearum* Inoculation

Tobacco plants of cultivar Yunyan87 exhibited bacterial wilt on the leaf as early as 3 days post inoculation (dpi). On the contrary, the symptoms on the quantitatively resistant cultivar K326 started to appear at 5 dpi (**Figure 1A**). 7 days and 10 days after inoculation, the disease index of K326 was 0.65 and 1.65, which were significantly lower than disease index of Yunyan87 with 1.65 and 3.15 (**Figure 1A**). In agreement with the wilting symptoms, the bacterial population of R. pseudosolanacearum was significantly lower in K326 than in Yunyan87 both at 4, 7, and 10 days post inoculation (**Figure 1B**).

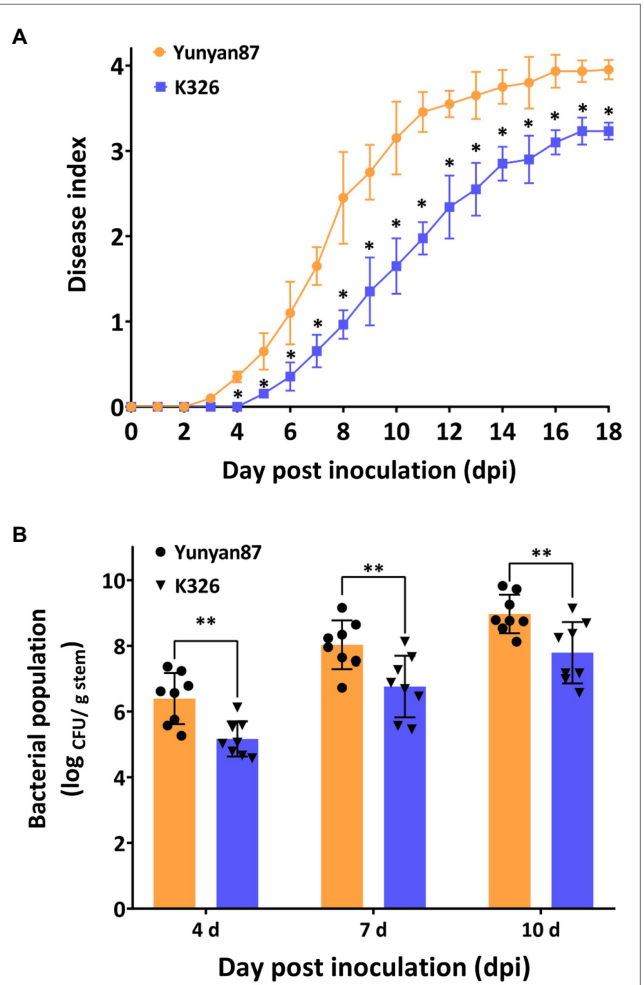

FIGURE 1 | Differential responses of tobacco cultivars Yunyan87 and K326 to *R. pseudosolanacearum* inoculation. **(A)** Bacterial wilt disease index of susceptible cultivar Yunyan87 and quantitatively resistant line K326 scored over time after soil-soak inoculation using a disease index scale from 0 to 4. **(B)** *R. pseudosolanacearum* bacterial populations in stem tissues of the two tobacco cultivars soil-soak inoculated with *R. pseudosolanacearum*. Each bar represents the mean ± standard error of eight experimental replicas. Asterisks indicate significant differences between tobacco cultivar Yunyan87 and K326 according to Student's *t* test (* indicates $p < 0.05$, ** indicates $p < 0.01$).

R. pseudosolanacearum Infection Significantly Alters the Metabolites in Xylem Sap of Tobacco Cultivars

The metabolite profiles of xylem sap of tobacco cultivars Yunyan87 and K326 were determined by untargeted metabolome analysis at 7 days post *R. pseudosolanacearum* inoculation (**Supplementary Figure S1**). The results displayed that *R. pseudosolanacearum* infection changes the chemical composition of tobacco xylem sap (**Figure 2**). Principal component analysis (PCA) of all samples indicated that the susceptible tobacco cultivar Yunyan87 showed dramatic metabolite changes after *R. pseudosolanacearum* infection, while the quantitatively resistant variety K326 showed few metabolite differences (**Supplementary Figure S1**). GC-MS analysis of the xylem sap samples detected 88 known compounds, including 48 metabolites identified as differentially concentrated (**Figure 2**). Interestingly, samples from the inoculated or non-inoculated K326 resistant variety showed few metabolite differences, sometimes hampering their differentiation by clustering (**Figure 2**).

Bacterial Wilt Infection Enriches Tobacco Xylem Sap to Favor *R. pseudosolanacearum* Growth

We focused on the influence of *R. pseudosolanacearum* infection on the metabolites in susceptible tobacco cultivar Yunyan87, whose profile was markedly different in infected compared to healthy plants, as shown by PCA (PC1 = 84.8%) and sample clustering (**Supplementary Figures S1, S2**). A total of 48 metabolites was identified as differentially abundant, 42 of which were enriched and 6 depleted. The enriched metabolites in xylem sap contained amino acids, organic acids, sugars, and others, suggesting that they could favor *R. pseudosolanacearum* growth *in planta* (**Figure 3A, 4**). Putrescine was the most enriched compound (12-fold) in infected tobacco xylem, followed by methyl-alpha-d-glucopyranoside (9-fold) and arabinitol (6-fold; **Figure 4D, Supplementary Table S2**). The enriched amino acids included aspartic acid, beta-alanine, glutamine, isoleucine, leucine, phenylalanine, proline, serine, threonine, and valine (**Figure 4A**). Among the organic acids were 3-hydroxybutyric acid, fumaric acid, galactonic acid, glucuronic acid, gulonic acid, mannonic acid, palmitic acid, pentenoic acid, propanoic acid, ribonic acid, and succinic acid (**Figure 4B**). Eleven sugars and polyols were also enriched upon infection: arabinitol, arabinose, fructose, galactose, glucopyranose, inositol, mannose, ribitol, ribose, xylitol, and xylose (**Figure 4C**). In order to evaluate the effect of xylem sap on *R. pseudosolanacearum* growth, tobacco xylem sap was collected following the same protocol used for metabolic analyses and used to supplement axenic bacterial cultures. As shown in **Figure 5**, supplementing minimal media with xylem sap significantly improved bacterial growth than mock treatment, and this effect was more apparent although not significantly when sap from *R. pseudosolanacearum*-infected plants was added.

Moderately Resistant Tobacco Cultivar K326 Displays Few Metabolite Changes in Response to Pathogen Infection

We tested the possibility that xylem sap from moderately resistant tobacco cultivar K326 contained concentrated chemicals that inhibited *R. pseudosolanacearum* growth, but supplementing minimal media with xylem sap from healthy or infected tobacco cultivar K326 improved *R. pseudosolanacearum* growth. As shown in **Supplementary Figure S2**, the metabolic profile of *R. pseudosolanacearum*-infected xylem sap was similar to that of healthy plants. Only one metabolite (beta-alanine) was identified more abundant in infected plants (**Figure 3B**). This suggested that sap from *R. pseudosolanacearum*-infected tobacco plants was enriched in nutrients rather than depleted in growth inhibitors.

R. pseudosolanacearum Infection Triggers Different Metabolite Responses in Tobacco and Tomato Plants

To identify key metabolites in the interaction between *R. pseudosolanacearum* and different plant hosts, we compared the metabolites changes of tobacco plant response to *R. pseudosolanacearum* infection to previously published metabolomic data on tomato (Lowe-Power et al., 2018a; **Supplementary Table S2**). Putrescine was the most enriched compound in xylem sap from both tobacco and tomato plants affected by bacterial wilt (12.97-fold and 75.68-fold, respectively). The concentration of 3-hydroxybutyric acid, galactonic acid, and amino acids beta-alanine, phenylalanine, leucine, and glycine was all enhanced in tobacco and tomato saps infected by *R. pseudosolanacearum* (**Supplementary Table S2**). However, additional amino acids increased in infected tobacco xylem, including proline, threonine, valine, serine, isoleucine, and glutamine. In turn, sugars and polyols were more enriched in tobacco than in tomato. In particular, methyl-alpha-d-glucopyranoside and arabinitol are major components of tobacco xylem metabolome, but they have not been found in tomato.

DISCUSSION

Metabolic Analysis of Two Tobacco Cultivars in Response to Infection by *R. pseudosolanacearum*

Metabolomics is a useful tool for investigation of plant adaptation to pathogen infection (Lowe-Power et al., 2018a). Recently, metabolite profiles of tobacco in response to different pathogens infection have been widely investigated (Lowe-Power et al., 2016; Wang et al., 2020; Zhang et al., 2020). In this study, a total of 88 known compounds were identified in two tobacco cultivars differing for resistance to bacterial wilt (moderately resistant cultivar K326 and susceptible cultivar Yunyan87). Seven days after inoculation, a higher number of differentially concentrated metabolites were identified in Yunyan87 (**Figure 2**), which could be due to the higher bacterial growth in this susceptible plant (**Figure 1B**). A recent study also proved that

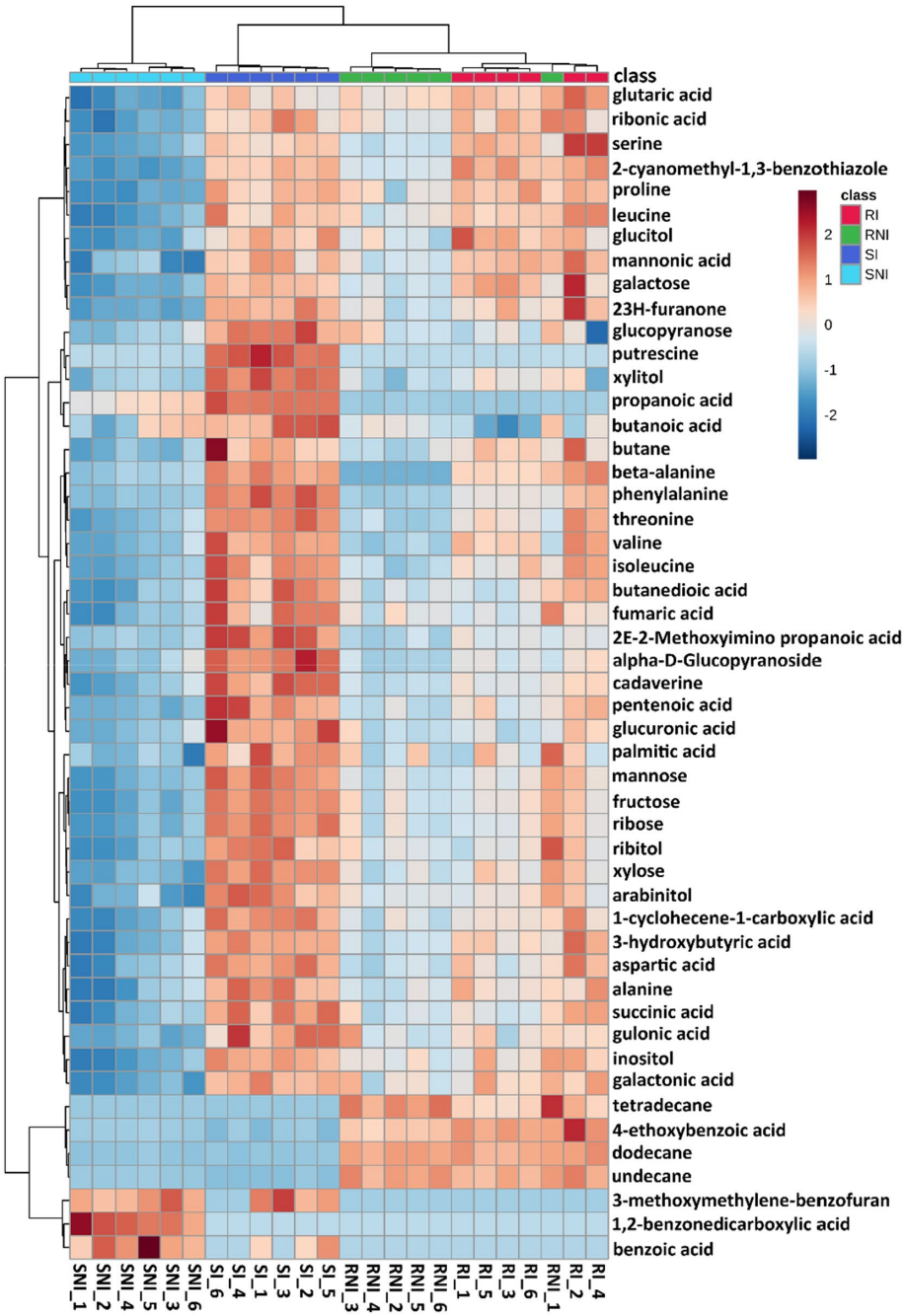

FIGURE 2 | Metabolome of tobacco (susceptible cultivar Yunyan87 and moderately resistant cultivar K326) in response to *R. pseudosolanacearum* infection. Heatmap of differentially expressed metabolites in tobacco cultivars (Yunyan87 and K326) in response to *R. pseudosolanacearum* invasion. Columns correspond to experimental replicas.

a larger number of enriched metabolites were secreted by susceptible tobacco cultivar Xinhuangjin 1,025 than by resistant Gexin 3 against tobacco black shank disease (Zhang et al., 2020). Unlike the extraction method of xylem sap from tomato plant infected by *R. solanacearum* through root pressure (Lowe-Power et al., 2018a), collection of xylem sap from tobacco stem tissue by centrifugation may have caused some damage to the tissue, leading to leaking of cellular metabolites.

Exploration of certain metabolites altered in the susceptible cultivar indicated a dramatic increase in methyl-alpha-D-glucopyranoside and arabinitol (**Figure 6**). These two compounds could be originated from glucose and xylose, respectively. Furthermore, infected sap also displayed increased levels of amino acids derived from glycerate (Ser), shikimate (Phe),

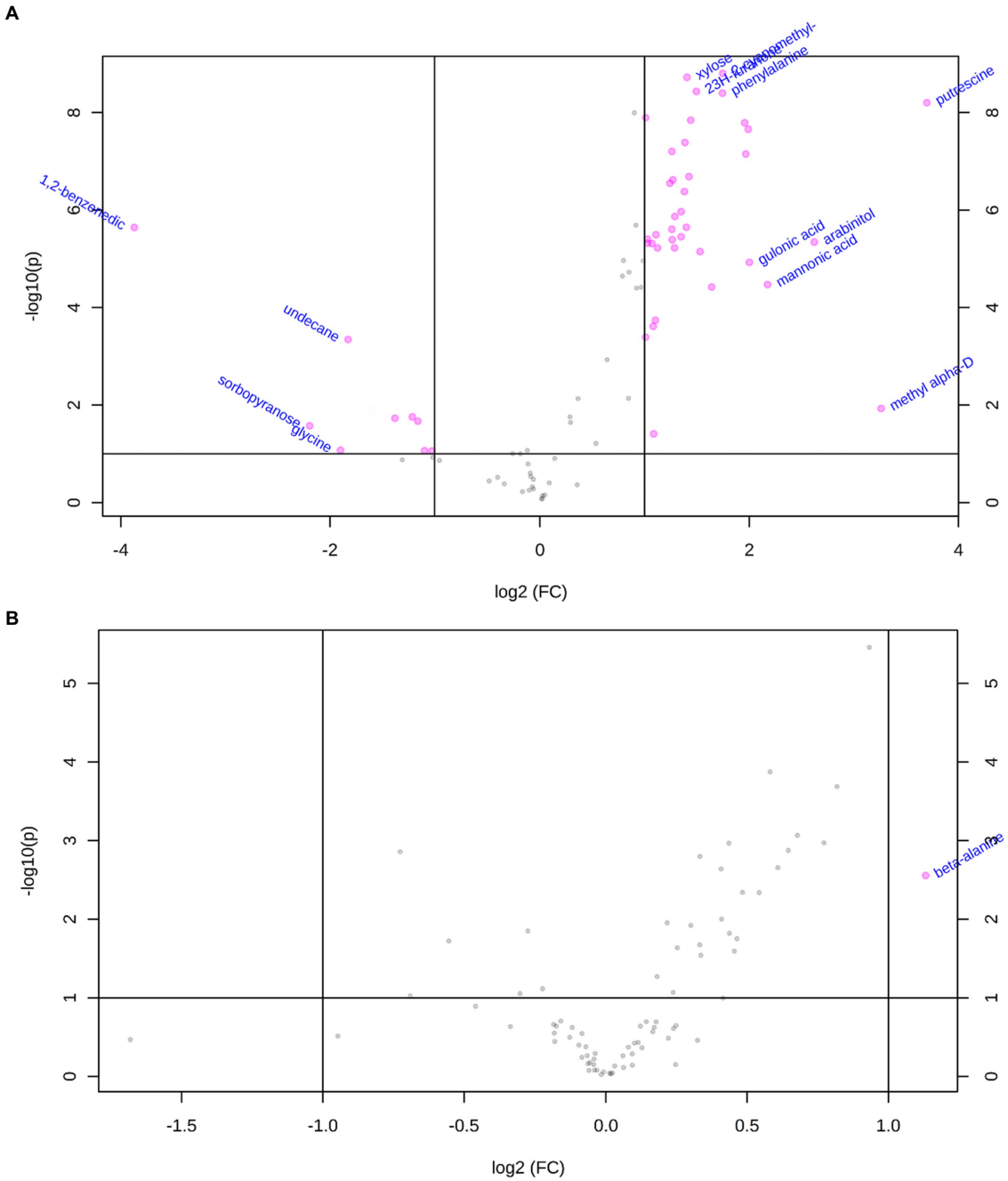

FIGURE 3 | Change of metabolome profile of tobacco in response to *R. pseudosolanacearum* infection. **(A)** Volcano plot showing differentially expressed (DE) metabolites and their value of *p* (p) in susceptible tobacco in response to *R. pseudosolanacearum* invasion. **(B)** Volcano plot showing differentially expressed (DE) metabolites and their value of *p* (p) in resistant tobacco in response to *R. pseudosolanacearum* invasion.

pyruvate (Val, Ile and Ala), 2-oxoglutarate (Glu and Pro) and malate (Asp, Thr, and beta-alanine). Derivatives from glutamic acid, glutamine, and putrescine were also enriched in infected plants. Alterations in the sugar metabolism also included accumulation of xylose, xylitol, galactose, inositol, fructose, mannose, and glucose. Finally, decreased levels of maltose, glycine, and shikimic acid in infected xylem sap were also observed (**Figure 6**). It is known that cell wall degrading enzymes of *R. solanacearum* could release cellulose-derived metabolites like cellobiose and gentiobiose during infection (Genin and Denny, 2012). In addition, it has been proposed that *R. solanacearum* may use type III secretion system to manipulate the host to release nutrients into the xylem (Deslandes and Genin, 2014). RipI promotes the biochemical activation

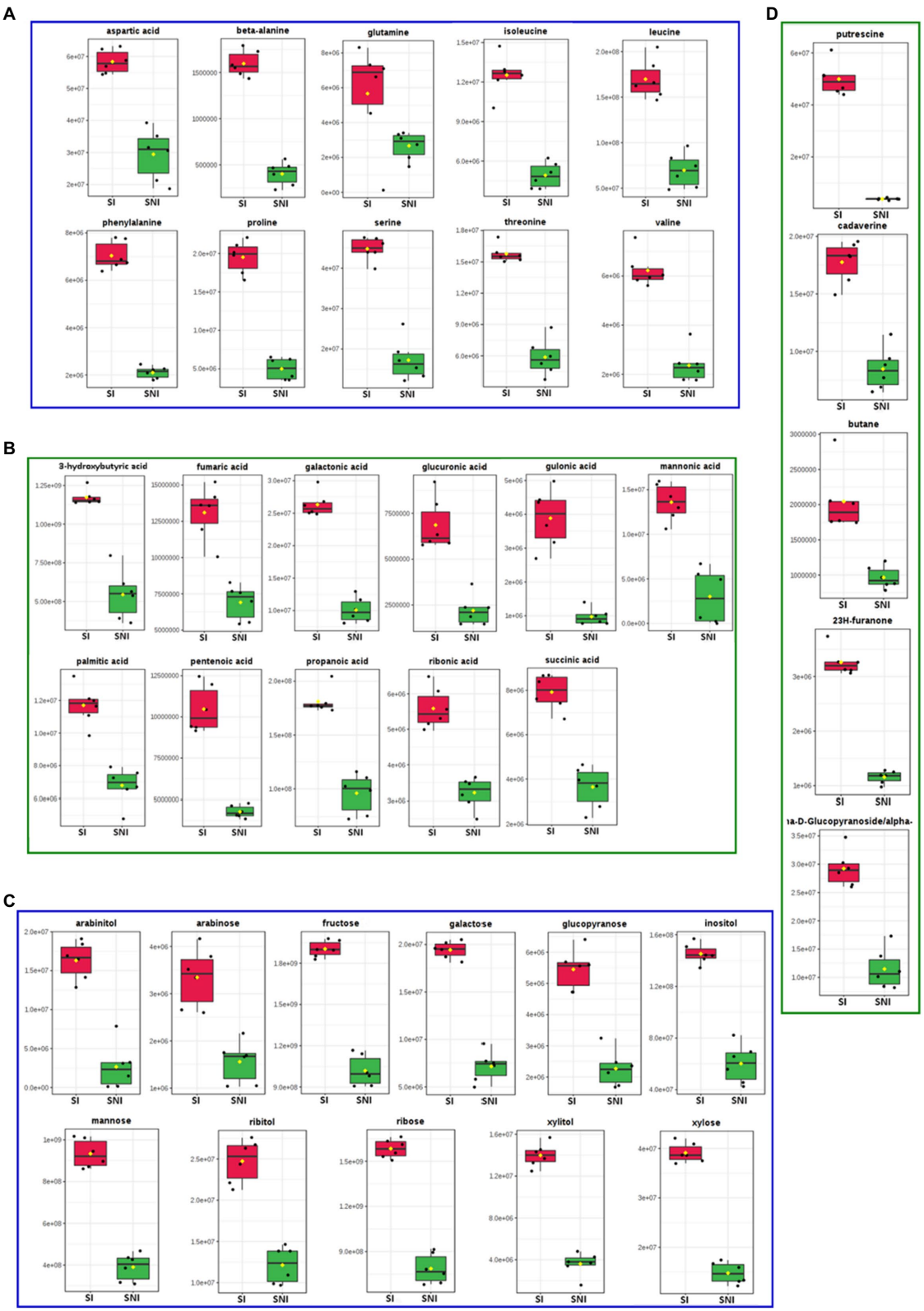

FIGURE 4 | The significantly enriched metabolites of susceptible tobacco cultivar Yunyan87 in response to *R. pseudosolanacearum* infection. **(A)** Enriched amino acids. **(B)** Enhanced organic acids. **(C)** Sugar and polyols compounds enriched. **(D)** Other enriched compounds after *R. pseudosolanacearum* infection. The red indicates the quantification peak area of metabolites from xylem sap of susceptible tobacco cultivar Yunyan87 infected with *R. pseudosolanacearum*, and green indicates quantification peak area of metabolites from xylem sap of healthy tobacco cultivar Yunyan87 plants.

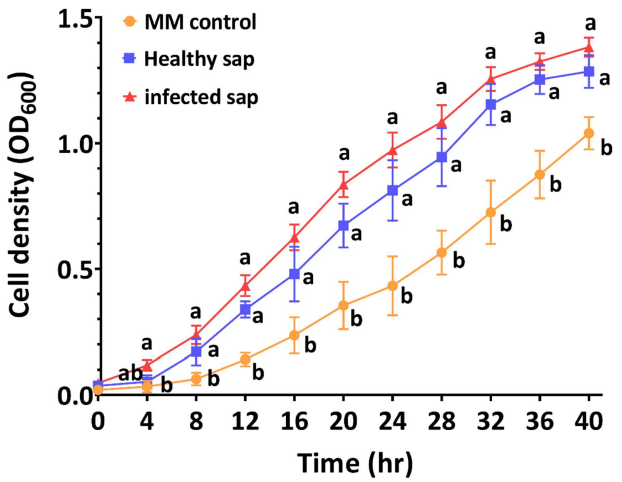

FIGURE 5 | Xylem sap from infected tobacco cultivar Yunyan87 improves *R. pseudosolanacearum* growth *in vitro*. *R. pseudosolanacearum* growth curves in minimal medium or minimal medium supplemented with xylem sap extracted from healthy/infected tobacco. Each bar represents the mean ± SE of three replicas. Different letters indicate xylem sap treatment and control treatment were significantly different ($p < 0.05$).

of glutamate decarboxylases (GADs) in plant cells, enhancing the production of gamma-aminobutyric acid (GABA) to support *R. solanacearum* nutrition during plant infection (Xian et al., 2020). However, most of metabolites were not enhanced during the interaction of this pathogen with resistant tobacco cultivar K326 (**Supplementary Table S2**).

Insights Into Pathogen Preferred Carbon Sources in Tobacco Plant

The fast proliferation of *R. solanacearum* in xylem sap should be sustained by nutrients that the pathogen takes up in this environment (Gerlin et al., 2021). The amino acids, organic acids, sugars, and other metabolites enriched in xylem sap might favor *R. pseudosolanacearum* growth *in planta*. Enriched amino acids included aspartic acid, beta-alanine, glutamine, isoleucine, leucine, phenylalanine, proline, serine, threonine, and valine (**Figures 3A, 4A**). Glutamine, asparagine, and gamma aminobutyric acid were identified as the major organic components of xylem sap in tomato (Zuluaga et al., 2013). Together with leucine, isoleucine and histidine decreased under *R. solanacearum* inoculation *in vitro* (Zuluaga et al., 2013; Gerlin et al., 2021). However, we did not detect any of these compounds decreasing

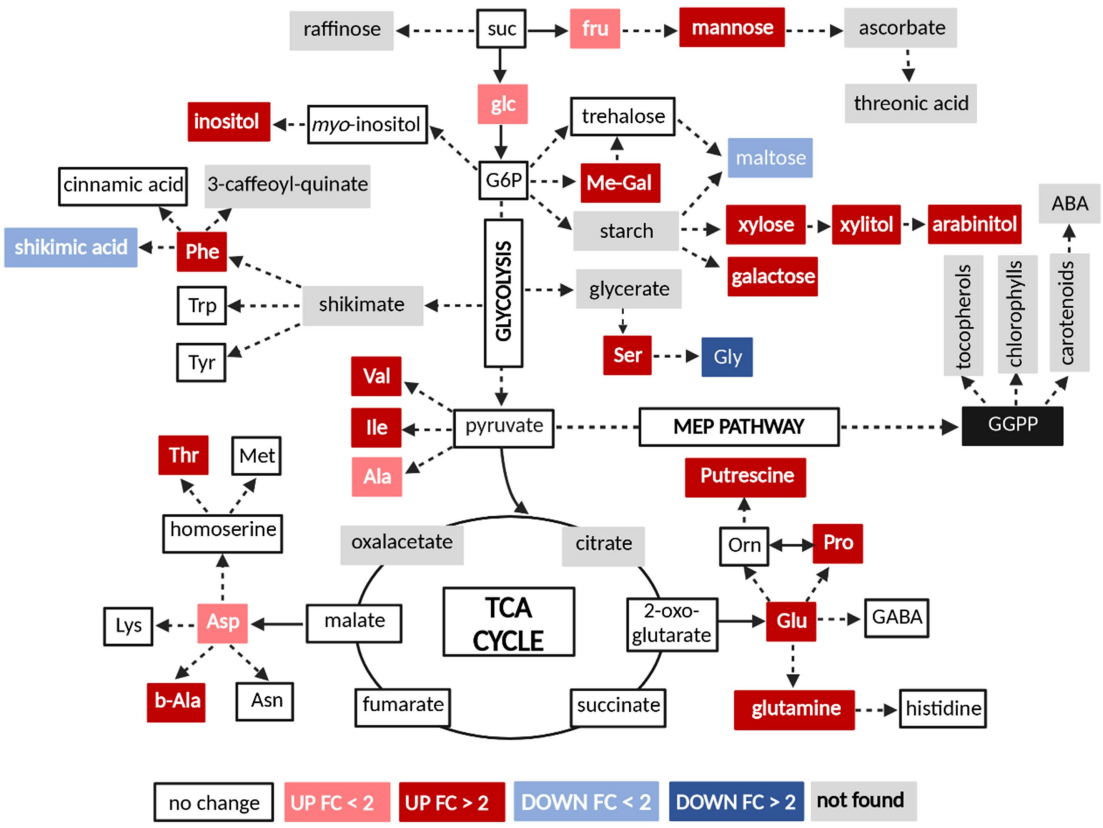

FIGURE 6 | Changes in the levels of selected differentially concentrated metabolites of susceptible cultivar Yunyan87 during *R. pseudosolanacearum* infection. Colors represent statistically significant fold-change (FC) values (*t* test, $p < 0.05$) of metabolite levels in xylem sap from infected tobacco plants relative to those in healthy plants controls. Suc, sucrose; Glc, glucose; Fru, fructose; Me-Gal, methyl-alpha-D-glucopyranoside; Ser, serine; Gly, glycine; Phe, phenylalanine; Trp, tryptophan; Tyr, tyrosine; Val, valine; Ile, isoleucine; Ala, alanine; Glu, glutamic acid; Orn, ornithine; Pro, proline; Asp, aspartic acid; Thr, threonine; Met, methionine; Lys, lysine; b-Ala, beta-alanine; Asn, asparagine. This figure was created by bio Render (https://biorender.com/).

in the tobacco xylem after infection and most of them even increased significantly. This correlates with previous findings in which glutamic acid, phenylalanine, beta-alanine, leucine, and glycine were enriched in xylem sap during *R. solanacearum* infection (Lowe-Power et al., 2018a; Zeiss et al., 2019). We thus hypothesize that *R. pseudosolanacearum* causes a deep plant metabolic reprogramming during infection to favor the production of compounds that can sustain its growth. In support of this theory is the recent finding that *R. solanacearum* effector protein RipI interacts with plant glutamate decarboxylases to alter plant metabolism, enhancing GABA production to support bacterial growth (Xian et al., 2020).

Metabolic Signatures of *Solanaceae* Plants in Response to Bacterial Wilt

In this study, we found that beta-alanine, phenylalanine, leucine, glycine, galactonic acid, 3-hydroxybutyric acid, shikimic acid, ribose, and putrescine were both enriched in tomato and tobacco plants in response to *R. pseudosolanacearum* infection, putrescine being the most enriched in both plant xylems (**Supplementary Table S2**). Putrescine cannot be used as a carbon source or nutrient by *R. solanacearum* and is copiously produced by this bacterium. Thus, this molecule would be mostly derived from the pathogen and it would act as a virulence metabolite by inducing the wilting symptoms (Lowe-Power et al., 2018a; Gerlin et al., 2021). A recent study showed that putrescine could be produced by tomato cells hijacked by a *R. solanacearum* effector (Wu et al., 2019).

Certain studies have demonstrated that 3-hydroxybutyric acid was identified as a storage compound in *R. solanacearum* and phylogenetically close β-proteobacteria, precursor of polyhydroxybutyrate (Terpolilli et al., 2016; Gerlin et al., 2021). As previously reported, 3-hydroxybutyric acid increased in the xylem sap of *R. solanacearum* infected plants, and this metabolite could be excreted by *R. solanacearum*, and consumed before returning to the soil (Lowe-Power et al., 2018a; Gerlin et al., 2021). This is in agreement with our finding that 3-hydroxybutyric acid was enriched in the xylem of infected tobacco plant. However, whether this metabolite produced by plants or bacteria is still unclear, as the biosynthetic pathway of the metabolite is present in both organisms (Yuan et al., 2016).

Certain Metabolic Pathways Are Involved in Plant Defense in Response to *R. pseudosolanacearum* Attack

Several amino acid pathways contribute to defense responses of plants exposed to infection by *R. solanacearum*. Proteomic and transcriptomic analysis revealed that the methionine cycle (MTC) and γ-aminobutyric acid (GABA) play a key role in plant defense against *R. solanacearum*. Silencing of MTC-associated genes *SAHH1* and *MS1* and GABA biosynthesis gene *GAD2* in tomato leads to decreased resistance against *R. solanacearum* (Wang et al., 2019). Certain studies have proven that GABA levels were rapidly increased in plants in response to various biotic stresses (Park et al., 2010; Ramesh et al., 2017). Arabidopsis wat1 (walls are thin1)-mediated resistance to *R. solanacearum* is mediated by cross-regulation of salicylic acid and tryptophan metabolism (Denance et al., 2013). Plant metabolic pathways mediated by pyruvate decarboxylases (PDCs) also contribute to plant tolerance to bacterial wilt. And an effector protein secreted by *R. solanacearum*, RipAK, interacts with PDCs and is involved in plant resistance to biotic and abiotic stresses (Wang et al., 2021). Moreover, application of pyruvic acid and acetic acid (substrate and product of the PDC pathway) enhanced plant tolerance to bacterial wilt. In this study, we found that certain amino acids such as alanine, phenylalanine, leucine, and glycine were enriched in tobacco and tomato after *R. pseudosolanacearum* infection (**Figure 6**; **Supplementary Table S2**). The role of these amino acids in plant defense against bacterial wilt needs further investigation.

CONCLUSION

In conclusion, GC-MS-based metabolomic analysis revealed relatively metabolic profiling in two tobacco cultivars that are quantitatively resistant (K326) or susceptible (Yunyan87) to initial infection by *R. pseudosolanacearum*. A total of 48 different concentrated metabolites were identified in tobacco cultivar Yunyan87. The contents of metabolites related to amino acid metabolism, sugar metabolism, and organic acid metabolism were enriched in infected tobacco xylem sap. Certain amino acids such as alanine, phenylalanine, leucine, and glycine were enriched in tobacco and tomato after *R. pseudosolanacearum* infection. The role of certain amino acids needs further and more detailed investigation.

DATA AVAILABILITY STATEMENT

The datasets presented in this study can be found in online repositories. The names of the repository/repositories and accession number(s) can be found in the article/**Supplementary Material**.

AUTHOR CONTRIBUTIONS

WD and LY conceived and designed the experiments. LY and MV performed the experiments. LY, ZW, and MV analyzed the data. LY, WD, and MV wrote and revised the paper. All authors contributed to the article and approved the submitted version.

FUNDING

The research was supported by the key project of the China National Tobacco Corporation (110201901042), the National Natural Science Foundation of China (31972288), the Chongqing Special Postdoctoral Science Foundation, PID2019-108595RB-I00/AEI/10.13039/501100011033 and CEX2019-000902-S from the Spanish Ministry of Science and Innovation, and the CERCA Program from the Catalan Government (Generalitat de Catalunya) and China Postdoctoral Science Foundation (2021M702707).

SUPPLEMENTARY MATERIAL

The Supplementary Material for this article can be found online at: https://www.frontiersin.org/articles/10.3389/fpls.2021.780429/full#supplementary-material

Supplementary Figure S1 | Metabolome analysis of tobacco cultivar in response to *R. pseudosolanacearum* infection. **(A)** Tobacco plants were soil-soak inoculated with *R. pseudosolanacearum* CQPS-1, after inoculation for 7 days, xylem sap was harvested from infected and healthy plants. **(B)** PCA analysis of metabolites change of infected tobacco plant and healthy plant. SI means susceptible tobacco cultivar infected with *R. pseudosolanacearum*, SNI indicates susceptible cultivar without pathogen infection. RI means moderately resistant tobacco cultivar K326 inoculated with *R. pseudosolanacearum*, RNI means K326 tobacco plants without inoculated with *R. pseudosolanacearum*. **(C)** The clustering tree of changed metabolites of tobacco xylem sap under *R. pseudosolanacearum* infection.

Supplementary Figure S2 | Different effect of tobacco metabolome of two tobacco cultivars in response to *R. pseudosolanacearum* infection. **(A)** PCA analysis of metabolite changes in infected and healthy tobacco plants. SI means susceptible tobacco cultivar infected with *R. pseudosolanacearum*, SNI indicates susceptible cultivar without pathogen infection. **(B)** The clustering tree of changed metabolites of tobacco Yunyan87 xylem sap under *R. pseudosolanacearum* infection. **(C)** PCA analysis of metabolites change of infected and healthy tobacco plants. RI means moderately resistant tobacco cultivar infected with *R. pseudosolanacearum*, RNI indicates moderately resistant cultivar without pathogen infection. **(D)** The clustering tree of changed metabolites in tobacco K326 xylem sap during *R. pseudosolanacearum* infection.

Supplementary Table S1 | Relative quantification of metabolites in tobacco cultivars xylem sap.

Supplementary Table S2 | Xylem sap metabolites altered by bacterial wilt disease in tobacco and tomato plants.

REFERENCES

Cai, Q. H., Zhou, G. S., Ahmed, W., Cao, Y. Y., Zhao, M. W., Li, Z. H., et al. (2021). Study on the relationship between bacterial wilt and rhizospheric microbial diversity of flue-cured tobacco cultivars. *Eur. J. Plant Pathol.* 160, 265–276. doi: 10.1007/s10658-021-02237-4

Cho, K., Kim, Y., Wi, S. J., Seo, J. B., Kwon, J., Chung, J. H., et al. (2012). Nontargeted metabolite profiling in compatible pathogen-inoculated tobacco (*Nicotiana tabacum* L. cv. Wisconsin 38) using UPLC-Q-TOF/MS. *J. Agric. Food Chem.* 60, 11647–11648. doi: 10.1021/jf304735b

de Pedro-Jove, R., Puigvert, M., Sebastia, P., Macho, A. P., Monteiro, J. S., Coll, N. S., et al. (2021). Dynamic expression of *Ralstonia solanacearum* virulence factors and metabolism-controlling genes during plant infection. *BMC Genomics* 22:170. doi: 10.1186/s12864-021-07457-w

Denance, N., Ranocha, P., Oria, N., Barlet, X., Riviere, M. P., Yadeta, K. A., et al. (2013). Arabidopsis wat1 (walls are thin1)-mediated resistance to the bacterial vascular pathogen, *Ralstonia solanacearum*, is accompanied by cross-regulation of salicylic acid and tryptophan metabolism. *Plant J.* 73, 225–239. doi: 10.1111/tpj.12027

Deslandes, L., and Genin, S. (2014). Opening the *Ralstonia solanacearum* type III effector tool box: insights into host cell subversion mechanisms. *Curr. Opin. Plant Biol.* 20, 110–117. doi: 10.1016/j.pbi.2014.05.002

Dunn, W. B., Broadhurst, D., Begley, P., Zelena, E., Francis-McIntyre, S., Anderson, N., et al. (2011). Procedures for large-scale metabolic profiling of serum and plasma using gas chromatography and liquid chromatography coupled to mass spectrometry. *Nat. Protoc.* 6, 1060–1083. doi: 10.1038/nprot.2011.335

Elphinstone, J. G., Hennessy, J., Wilson, J. K., and Stead, D. E. (1996). Sensitivity of different methods for the detection of *Ralstonia solanacearum* in potato tuber extracts. *EPPO Bull.* 26, 663–678. doi: 10.1111/j.1365-2338.1996.tb01511.x

Forsberg, E. M., Huan, T., Rinehart, D., Benton, H. P., Warth, B., Hilmers, B., et al. (2018). Data processing, multi-omic pathway mapping, and metabolite activity analysis using XCMS online. *Nat. Protoc.* 13, 633–651. doi: 10.1038/nprot.2017.151

Gao, W. X., Chen, R. J., Pan, M. M., Tang, W. Q., Lan, T., Huang, L. K., et al. (2019). Early transcriptional response of seedling roots to *Ralstonia solanacearum* in tobacco (*Nicotiana tabacum* L.). *Eur. J. Plant Pathol.* 155, 527–536. doi: 10.1007/s10658-019-01788-x

Genin, S., and Denny, T. P. (2012). Pathogenomics of the *Ralstonia solanacearum* species complex. *Annu. Rev. Phytopathol.* 50, 67–89. doi: 10.1146/annurev-phyto-081211-173000

Gerlin, L., Escourrou, A., Cassan, C., Macia, F. M., Peeters, N., Genin, S., et al. (2021). Unravelling physiological signatures of tomato bacterial wilt and xylem metabolites exploited by *Ralstonia solanacearum*. *Environ. Microbiol.* 23, 5962–5978. doi: 10.1111/1462-2920.15535

Gong, L., Gao, J., Xu, T. S., Qu, J. L., Wang, Z. B., Yang, Z. M., et al. (2020). Transcriptome analysis of field-grown Asian ginseng provides clues to environmental conditions and developmental mechanisms related to red skin root syndrome. *Ind. Crop. Prod.* 153:112486. doi: 10.1016/j.indcrop.2020.112486

Jiang, G. F., Wei, Z., Xu, J., Chen, H. L., Zhang, Y., She, X. M., et al. (2017). Bacterial wilt in China: history, current status, and future perspectives. *Front. Plant Sci.* 8:1549. doi: 10.3389/fpls.2017.01549

Liu, P. P., Luo, J., Zheng, Q. X., Chen, Q. S., Zhai, N., Xu, S. C., et al. (2020). Integrating transcriptome and metabolome reveals molecular networks involved in genetic and environmental variation in tobacco. *DNA Res.* 27:dsaa006. doi: 10.1093/dnares/dsaa006

Liu, Y., Tang, Y. M., Qin, X. Y., Yang, L., Jiang, G. F., Li, S. L., et al. (2017a). Genome sequencing of *Ralstonia solanacearum* CQPS-1, a phylotype I strain collected from a highland area with continuous cropping of tobacco. *Front. Microbiol.* 8:974. doi: 10.3389/fmicb.2017.00974

Liu, Y., Wu, D. S., Liu, Q. P., Zhang, S. T., Tang, Y. M., Jiang, G. F., et al. (2017b). The sequevar distribution of *Ralstonia solanacearum* in tobacco-growing zones of China is structured by elevation. *Eur. J. Plant Pathol.* 147, 541–551. doi: 10.1007/s10658-016-1023-6

Lowe-Power, T. M., Ailloud, F., and Allen, C. (2015). Hydroxycinnamic acid degradation, a broadly conserved trait, protects *Ralstonia solanacearum* from chemical plant defenses and contributes to root colonization and virulence. *Mol. Plant-Microbe Interact.* 28, 286–297. doi: 10.1094/MPMI-09-14-0292-FI

Lowe-Power, T. M., Hendrich, C. G., von Roepenack-Lahaye, E., Li, B., Wu, D., Mitra, R., et al. (2018a). Metabolomics of tomato xylem sap during bacterial wilt reveals *Ralstonia solanacearum* produces abundant putrescine, a metabolite that accelerates wilt disease. *Environ. Microbiol.* 20, 1330–1349. doi: 10.1111/1462-2920.14020

Lowe-Power, T. M., Jacobs, J. M., Ailloud, F., Fochs, B., Prior, P., and Allen, C. (2016). Degradation of the plant defense signal salicylic acid protects *Ralstonia solanacearum* from toxicity and enhances virulence on tobacco. *MBio* 7, e00656–e00616. doi: 10.1128/mBio.00656-16

Lowe-Power, T. M., Khokhani, D., and Allen, C. (2018b). How *Ralstonia solanacearum* exploits and thrives in the flowing plant xylem environment. *Trends Microbiol.* 26, 929–942. doi: 10.1016/j.tim.2018.06.002

Mansfield, J., Genin, S., Magori, S., Citovsky, V., Sriariyanum, M., Ronald, P., et al. (2012). Top 10 plant pathogenic bacteria in molecular plant pathology. *Mol. Plant Pathol.* 13, 614–629. doi: 10.1111/j.1364-3703.2012.00804.x

Mirkarimi, S. R., Ardakani, Z., and Rostamian, R. (2021). Economic and environmental assessment of tobacco production in Northern Iran. *Ind. Crop. Prod.* 161:113171. doi: 10.1016/j.indcrop.2020.113171

Park, D. H., Mirabella, R., Bronstein, P. A., Preston, G. M., Haring, M. A., Lim, C. K., et al. (2010). Mutations in gamma-aminobutyric acid (GABA) transaminase genes in plants or *Pseudomonas syringae* reduce bacterial virulence. *Plant J.* 64, 318–330. doi: 10.1111/j.1365-313X.2010.04327.x

Planas-Marques, M., Bernardo-Faura, M., Paulus, J., Kaschani, F., Kaiser, M., Valls, M., et al. (2018). Protease activities triggered by *Ralstonia solanacearum* infection in susceptible and tolerant tomato lines. *Mol. Cell. Proteomics* 17, 1112–1125. doi: 10.1074/mcp.RA117.000052

Prior, P., Ailloud, F., Dalsing, B. L., Remenant, B., Sanchez, B., and Allen, C. (2016). Genomic and proteomic evidence supporting the division of the plant pathogen Ralstonia solanacearum into three species. *BMC Genomics* 17:90. doi: 10.1186/s12864-016-2413-z

Ramesh, S. A., Tyerman, S. D., Gilliham, M., and Xu, B. (2017). Gamma-aminobutyric acid (GABA) signalling in plants. *Cell. Mol. Life Sci.* 74, 1577–1603. doi: 10.1007/s00018-016-2415-7

Reichert, J. M., Pellegrini, A., and Rodrigues, M. F. (2019). Tobacco growth, yield and quality affected by soil constraints on steeplands. *Ind. Crop. Prod.* 128, 512–526. doi: 10.1016/j.indcrop.2018.11.037

Shahbandeh, M. (2021). World tabacco production by country. Available at: https://www.statista.com/statistics/261173/leading-countries-in-tobacco-production/ (Accessed January 13, 2021).

Siebrecht, S., Herdel, K., Schurr, U., and Tischner, R. (2003). Nutrient translocation in the xylem of poplar - diurnal variations and spatial distribution along the shoot axis. *Planta* 217, 783–793. doi: 10.1007/s00425-003-1041-4

Terpolilli, J. J., Masakapalli, S. K., Karunakaran, R., Webb, I. U. C., Green, R., Watmough, N. J., et al. (2016). Lipogenesis and redox balance in nitrogen-fixing pea bacteroids. *J. Bacteriol.* 198, 2864–2875. doi: 10.1128/JB.00451-16

Tsaballa, A., Sarrou, E., Xanthopoulou, A., Tsaliki, E., Kissoudis, C., Karagiannis, E., et al. (2020). Comprehensive approaches reveal key transcripts and metabolites highlighting metabolic diversity among three oriental tobacco varieties. *Ind. Crop. Prod.* 143:111933. doi: 10.1016/j.indcrop.2019.111933

Wang, G. P., Kong, J., Cui, D. D., Zhao, H. B., Niu, Y., Xu, M. Y., et al. (2019). Resistance against *Ralstonia solanacearum* in tomato depends on the methionine cycle and the gamma-aminobutyric acid metabolic pathway. *Plant J.* 97, 1032–1047. doi: 10.1111/tpj.14175

Wang, Y., Zhao, A., Morcillo, R. J. L., Yu, G., Xue, H., Rufian, J. S., et al. (2021). A bacterial effector protein uncovers a plant metabolic pathway involved in tolerance to bacterial wilt disease. *Mol. Plant* 14, 1281–1296. doi: 10.1016/j.molp.2021.04.014

Wang, Y. C., Liu, M. H., Han, X. B., Zheng, Y. F., Chao, J. M., and Zhang, C. S. (2020). Prickly ash seed kernel: a new bio-fumigation material against tobacco black shank. *Agronomy* 10:770. doi: 10.3390/agronomy10060770

Wu, D. S., von Roepenack-Lahaye, E., Buntru, M., de Lange, O., Schandry, N., Perez-Quintero, A. L., et al. (2019). A plant pathogen type III effector protein subverts translational regulation to boost host polyamine levels. *Cell Host Microbe* 26, 638–649. doi: 10.1016/j.chom.2019.09.014

Xian, L., Yu, G., Wei, Y. L., Rufian, J. S., Li, Y. S., Zhuang, H. Y., et al. (2020). A bacterial effector protein hijacks plant metabolism to support pathogen nutrition. *Cell Host Microbe* 28, 548–557. doi: 10.1016/j.chom.2020.07.003

Yang, L., Wu, L. T., Yao, X. Y., Zhao, S. Y., Wang, J., Li, S. L., et al. (2018). Hydroxycoumarins: new, effective plant-derived compounds reduce *Ralstonia pseudosolanacearum* populations and control tobacco bacterial wilt. *Microbiol. Res.* 215, 15–21. doi: 10.1016/j.micres.2018.05.011

Yuan, H. L., Cheung, C. Y. M., Poolman, M. G., Hilbers, P. A. J., and van Riel, N. A. W. (2016). A genome-scale metabolic network reconstruction of tomato (*Solanum lycopersicum* L.) and its application to photorespiratory metabolism. *Plant J.* 85, 289–304. doi: 10.1111/tpj.13075

Zeiss, D. R., Mhlongo, M. I., Tugizimana, F., Steenkamp, P. A., and Dubery, I. A. (2019). Metabolomic profiling of the host response of tomato (*Solanum lycopersicum*) following infection by *Ralstonia solanacearum*. *Int. J. Mol. Sci.* 20:3945. doi: 10.3390/ijms20163945

Zhang, C. S., Feng, C., Zheng, Y. F., Wang, J., and Wang, F. L. (2020). Root exudates metabolic profiling suggests distinct defense mechanisms between resistant and susceptible tobacco cultivars against black shank disease. *Front. Plant Sci.* 11:559775. doi: 10.3389/fpls.2020.616977

Zhang, L., Zhang, X. T., Ji, H. W., Wang, W. W., Liu, J., Wang, F., et al. (2018). Metabolic profiling of tobacco leaves at different growth stages or different stalk positions by gas chromatography-mass spectrometry. *Ind. Crop. Prod.* 116, 46–55. doi: 10.1016/j.indcrop.2018.02.041

Zuluaga, A. P., Puigvert, M., and Valls, M. (2013). Novel plant inputs influencing *Ralstonia solanacearum* during infection. *Front. Microbiol.* 4:349. doi: 10.3389/fmicb.2013.00349

Conflict of Interest: The authors declare that the research was conducted in the absence of any commercial or financial relationships that could be construed as a potential conflict of interest.

Publisher's Note: All claims expressed in this article are solely those of the authors and do not necessarily represent those of their affiliated organizations, or those of the publisher, the editors and the reviewers. Any product that may be evaluated in this article, or claim that may be made by its manufacturer, is not guaranteed or endorsed by the publisher.

frontiers in Microbiology

ORIGINAL RESEARCH
published: 23 February 2022
doi: 10.3389/fmicb.2022.830900

Complete Genome Sequence Analysis of *Ralstonia solanacearum* Strain PeaFJ1 Provides Insights Into Its Strong Virulence in Peanut Plants

Xiaodan Tan[1], Xiaoqiu Dai[1], Ting Chen[1], Yushuang Wu[1], Dong Yang[1], Yixiong Zheng[1], Huilan Chen[2], Xiaorong Wan[1] and Yong Yang[1]**

[1] *Guangzhou Key Laboratory for Research and Development of Crop Germplasm Resources, Zhongkai University of Agriculture and Engineering, Guangzhou, China,* [2] *Key Laboratory of Horticultural Plant Biology (HZAU), Ministry of Education, Key Laboratory of Potato Biology and Biotechnology (HZAU), Ministry of Agriculture and Rural Affairs, Huazhong Agricultural University, Wuhan, China*

The bacterial wilt of peanut (*Arachis hypogaea* L.) caused by *Ralstonia solanacearum* is a devastating soil-borne disease that seriously restricted the world peanut production. However, the molecular mechanism of *R. solanacearum*–peanut interaction remains largely unknown. We found that *R. solanacearum* HA4-1 and PeaFJ1 isolated from peanut plants showed different pathogenicity by inoculating more than 110 cultivated peanuts. Phylogenetic tree analysis demonstrated that HA4-1 and PeaFJ1 both belonged to phylotype I and sequevar 14M, which indicates a high degree of genomic homology between them. Genomic sequencing and comparative genomic analysis of PeaFJ1 revealed 153 strain-specific genes compared with HA4-1. The PeaFJ1 strain-specific genes consisted of diverse virulence-related genes including LysR-type transcriptional regulators, two-component system-related genes, and genes contributing to motility and adhesion. In addition, the repertoire of the type III effectors of PeaFJ1 was bioinformatically compared with that of HA4-1 to find the candidate effectors responsible for their different virulences. There are 79 effectors in the PeaFJ1 genome, only 4 of which are different effectors compared with HA4-1, including RipS4, RipBB, RipBS, and RS_T3E_Hyp6. Based on the virulence profiles of the two strains against peanuts, we speculated that RipS4 and RipBB are candidate virulence effectors in PeaFJ1 while RipBS and RS_T3E_Hyp6 are avirulence effectors in HA4-1. In general, our research greatly reduced the scope of virulence-related genes and made it easier to find out the candidates that caused the difference in pathogenicity between the two strains. These results will help to reveal the molecular mechanism of peanut–*R. solanacearum* interaction and develop targeted control strategies in the future.

Keywords: ***Ralstonia solanacearum*, peanut, genome sequencing, comparative genomic analysis, pathogenicity**

OPEN ACCESS

Edited by:
Stephane Genin,
Institut National de la Recherche Agronomique (INRA), France

Reviewed by:
Gang Yu,
Center for Excellence in Molecular Plant Sciences, Chinese Academy of Sciences (CAS), China
Jeffrey K. Schachterle,
Beltsville Agricultural Research Center, Agricultural Research Service, United States Department of Agriculture (USDA), United States

****Correspondence:***
Xiaorong Wan
bioxrwan@hotmail.com
Yong Yang
yangyong@zhku.edu.cn

Specialty section:
This article was submitted to Microbe and Virus Interactions with Plants, a section of the journal Frontiers in Microbiology

Received: *07 December 2021*
Accepted: *12 January 2022*
Published: *23 February 2022*

Citation:
Tan X, Dai X, Chen T, Wu Y, Yang D, Zheng Y, Chen H, Wan X and Yang Y (2022) Complete Genome Sequence Analysis of Ralstonia solanacearum Strain PeaFJ1 Provides Insights Into Its Strong Virulence in Peanut Plants. Front. Microbiol. 13:830900. doi: 10.3389/fmicb.2022.830900

INTRODUCTION

Cultivated peanut (*Arachis hypoaea* L.), also known as groundnut, is a major oilseed legume crop grown in more than 100 countries around the world. It is often consumed in different forms of high-quality edible oil, edible nuts, peanut jelly, and sweets (Pandey et al., 2012). Approximately 44 million tons of peanuts are produced and consumed annually all over the world (FAOSTAT, 2016[1]). China is the largest peanut producer in total annual production, accounting for about 40.26% in the world. However, bacterial wilt, a destructive disease caused by *Ralstonia solanacearum*, always seriously blocks the peanut production all over the world. It outbreaks in the 13 main peanut-producing provinces of China and causes up to 50–100% yield losses (Jiang et al., 2017). Although bacterial wilt has been well studied in other plants, there are few studies in peanut, and current research mainly focused on transcriptome change after *R. solanacearum* inoculation and resistance marker screening (Chen et al., 2014; Luo et al., 2019). Up to now, some quantitative trait locus (QTLs) and resistance genes (e.g., *AhRLK1*, *AhRRS5*, and *AhGLKb*) against bacterial wilt have been identified in peanut (Zhang et al., 2017, 2019; Ali et al., 2020), but the molecular mechanism of peanut–*R. solanacearum* interaction is still poorly understood. The main reasons for this are that the peanut plant itself is not easy to conduct molecular experiments with, and it is the lack of specialized and in-depth research on the pathogenic bacteria causing peanut bacterial wilt.

R. solanacearum strains, by sensing root exudates, move to host roots using chemotaxis and flagellar movement (Yao and Allen, 2006; Hida et al., 2015). They enter the root through wounds, root tips, and secondary root emerging points; move to the vascular bundle; and reach the vascular tissue. Once inside the vascular system, the bacteria will quickly spread throughout the host's body. Some bacteria are planktonic in the vascular fluid stream, while others use twitching motility to move along the vascular wall (Liu et al., 2001). These isolated cells eventually grow into biofilm-dependent aggregates that fill the entire vascular system and block water flow (Tran et al., 2016; Caldwell et al., 2017). In summary, the bacteria can break through the root system of the plant, enter the vascular system, multiply in the host body, and cause irreversible wilting of the plant.

The pathogenicity of *R. solanacearum* is the result of the cooperation and coordination of various pathogenic factors, mainly including extracellular polysaccharide (EPS), type II secretion system (T2SS), and type III secretion system (T3SS). After *R. solanacearum* enters the vascular system of plants, it will secrete a large number of EPS to block the vascular bundle and eventually cause the wilting of plants. T2SS can secrete cell wall degradation enzymes, cellulose, and pectin enzymes and produce motion and attachment elements and chemotaxis, which play key roles in the pathogenicity of *R. solanacearum* (Genin and Denny, 2012). T3SS can secrete type III effectors (T3Es), which play an important role in the pathogenesis of susceptible plants and the hypersensitive response of resistant plants. At present, the total number of T3Es identified in *R. solanacearum* complex species is about 120 (each strain varies greatly), which is significantly more than other plant-pathogenic bacteria (such as Pseudomonas and Xanthomonas) (Peeters et al., 2013). There is a large degree of polymorphism and functional redundancy in the T3Es of *R. solanacearum*, which is an important reason for its wide host range and host specificity (Macho et al., 2010). T3Es can help pathogens infecting the host as virulence proteins to inhibit the immune system. On the other hand, some T3Es can be recognized by the resistant proteins of the host as avirulence proteins to activate downstream immune signaling pathways and trigger defense response (Coll and Valls, 2013).

Since the first *R. solanacearum* GMI1000 was sequenced (Salanoubat et al., 2002), more and more *R. solanacearum* genome information has been released. However, only two *R. solanacearum* strains from peanut have been sequenced (Tan et al., 2019; Chen et al., 2021). With the development of sequencing technology and discovery of new *R. solanacearum* isolates, comparative genome analysis played an important role in discovering the virulence and avirulence factors of many pathogens. Previously, several genomics comparison studies were performed in order to identify differences in the gene content of *R. solanacearum* corresponding to low or high virulence in different hosts. A deletion of 33.7 kb was found in the megaplasmid of strain UY043 isolated from soil by comparative genomics hybridization analysis (Cruz et al., 2014). This region contains a cluster of six genes involved in type IV pili synthesis, which contributes to early bacterial wilt pathogenesis and the colonization fitness of potato roots. Another case of *R. solanacearum* was reported for two sequenced phylotype IIB-1 strains IPO1609 and UW551. The two strains are closely related but differ significantly in the virulence in their host plants. The research revealed that IPO1609 carries a 77 kb genomic deletion, which is responsible for almost complete loss of pathogenicity of the strain (Gonzalez et al., 2011). Recently, the *R. solanacearum* avirulence effectors RipJ and RipAZ1 were identified by the comparative genomic analysis of two strains with different virulence against *Solanum pimpinellifolium* and *S. Americanum*, respectively (Moon et al., 2021; Pandey and Moon, 2021). In the current study, we performed a comprehensive comparative analysis of the genome sequences of *R. solanacearum* strain PeaFJ1 and other strains, especially HA4-1. PeaFJ1 and HA4-1 were isolated from peanut, and PeaFJ1 showed more aggressiveness in many cultivated peanut varieties than HA4-1. The genes that may be responsible for the hypervirulence of *R. solanacearum* strain PeaFJ1 were revealed and analyzed in this study.

MATERIALS AND METHODS

Strain Information and Cultivation

R. solanacearum strain PeaFJ1 was isolated from wilt peanut plant in Fuzhou City, Fujian Province of China and was identified as phylotype I, sequevar 14M, biovar 3 (Wang et al., 2017). *R. solanacearum* stored in an ultra-cold storage freezer was revived by incubating on a casamino acid-peptone-glucose (CPG) solid medium containing triphenyltetrazolium chloride (TTC) (10 g/L peptone, 2.5 g/L glucose, 1 g/L casamino acids, 50 mg/L TTC, 15 g/L agar) at 28°C for 48–72 h. The pearly

[1]https://www.fao.org/faostat/en/#home

cream-white but displaying pink in the center, irregular shaped and fluidal colonies are typical *R. solanacearum* colonies. The typical *R. solanacearum* colonies were streaked on new CPG medium plates containing TTC and incubated at 28°C for 48 h. These colonies were further inoculated into conical flasks containing CPG liquid medium and grown overnight at 28°C with shaking at 200 rpm. The freshly prepared bacterial suspension culture was expandingly propagated for inoculation assay or genome DNA extraction.

Peanut Planting and Inoculation

Peanut seeds were soaked in tap water for 4 h and then placed in glass culture dishes with wet filter paper. They were grown at 28 ± 1°C in a greenhouse with cycles of 16 h light/8 h night. After 2 days, germinated seeds were transferred into pots containing soil mix. Two weeks later, the seedlings with seven-to-eight full-grown leaves were used for inoculation experiments. The freshly prepared 20 μl bacterial suspension was added into a conical flask with CPG liquid medium and cultivated overnight to an $OD_{600\ nm}$ of approximately 1.0. Then, the cultured bacteria were centrifuged at 4,000 rpm for 10–15 min, and the pellet was re-suspended in water to $OD_{600\ nm}$ of 0.1. Two diagonal leaflets from the inverted third and fourth leaves were perpendicularly cut away (one-third of the leaflets was cut) by sterile scissors dipped the bacterial suspension. The control was inoculated with sterile water. The disease score of each plant was recorded every day after inoculation. The bacterial wilt severity of infected plants was divided into five grades: grade 1–few leaves wilt; grade 2–no more than 1/3 leaves wilt; grade 3–all leaves except the tip are wilt; grade 4–the whole plant wilts and dies. The disease index (DI) is calculated by the following formula: $DI = 100\Sigma ni/4N$, where, i is the disease score of the plants; n is the number of plants showing the disease score of i; and N is the total number of the plants inoculated. The evaluation criteria of bacterial wilt resistance are divided into four levels: resistance (R), moderate resistance (MR), moderate susceptibility (MS), and susceptibility (S). The corresponding DIs were $0 \leq DI < 25$, $25 \leq DI < 50$, $50 \leq DI < 75$, and $75 \leq DI < 100$, respectively. A total of 72 peanut plants were inoculated for each strain. Three biological replicates were set with 24 plants per replicate. To calculate the survival ratio of the infected peanut plants, the disease grade was transformed into binary data according to the following criteria: a disease grade lower than 2 was defined as "0," while a disease grade equal to or higher than 2 was defined as "1" for each specific time point (Remigi et al., 2011).

Extraction of the Genomic DNA, Sequencing and Assembly

The genomic DNA of *R. solanacearum* strain PeaFJ1 was extracted using the HiPure Bacterial DNA Kit (Magen Bio, Guangzhou, China) according to the manufacturer's protocols. The quality of the extracted DNA was evaluated using Qubit 2.0 Flurometer (Life Technologies, Carlsbad, CA, United States) and NanoDrop (Thermo Fisher Scientific, Wilmington, DE, United States). The qualified genomic DNA were used for complete genome sequencing through the PacBio long-read sequencer. The genomic DNA was fragmented and end-repaired to construct SMRTbell libraries (fragment sizes of > 10 Kb were selected by Blue Pippin system) according to the manufacturer's specification (Pacific Biosciences, Menlo Park, CA, United States). The library quality was determined by Qubit 2.0 Flurometer (Life Technologies, Carlsbad, CA, United States) and its average fragment size was estimated at the Bioanalyzer 2100 (Agilent Technologies, Santa Clara, CA, United States). The single molecule real time (SMRT) sequencing was accomplished on the PacBio Sequel system (Pacific Biosciences, Menlo Park, CA, United States) according to standard protocols. The *de novo* assembly of the PacBio long-reads was performed using the program Falcon (version 0.3.0) with default parameters.

Functional Annotation

The program Prokka (version 1.11), combined with National Center for Biotechnology Information (NCBI) prokaryotic genome annotation pipeline, was used to predict the open reading frames (ORFs) (Seemann, 2014; Tatusova et al., 2016). The predicted genes of *R. solanacearum* strain PeaFJ1 were annotated by BLASTN (*E*-value < 1e-5) using NCBI non-redundant protein (Nr) database, Swissport, Cluster of Orthologous Groups of proteins (COG), Kyoto Encyclopedia of Genes and Genomes (KEGG), and Gene Ontology (GO) databases based on sequence homology. The rRNAs, tRNA, and sRNA were identified using the program rRNAmmer (version 1.2), tRNAscan (version 1.3.1), and cmscan (version 1.1.2), respectively (Lagesen et al., 2007; Nawrocki and Eddy, 2013; Lowe and Chan, 2016). Genomic islands (GIs) were analyzed using the Island Viewer online tool (version 4.0)[2] (Bertelli et al., 2017). Prophages were identified using the program Phage Finder (version 2.0) (Fouts, 2006). Protein family annotation was performed with Pfam_Scan (version 1.6) based on the Pfam database (version 32.0) (Finn et al., 2014). Blastp and Blastn with default parameters were used to compare annotations to the Pathogen Host Interactions (PHI) and Virulence Factors of Pathogenic Bacteria (VFDB) databases. Two-component systems (TCSs) were predicted based on their structure characteristics (Cheung and Hendrickson, 2010). Type III effectors were identified according to the Ralsto T3E database (Sabbagh et al., 2019) and the gene functional annotation. All analyses were carried out using the default parameters.

Comparative Genomic Analysis

MUMmer software was used to compare the target genome with the reference genome to determine the large range of collinearity between genomes (Kurtz et al., 2004). Then, SyRI was used to make comparison between regions, confirm local location arrangement relationship, and find translocation and inversion regions (Goel et al., 2019). The *R. solanacearum* PeaFJ1 and HA4-1 genome alignments were carried out in an all-against-all comparison using the MUMmer 3 package (version 3.2.2) with default parameters (Kurtz et al., 2004). Orthologous gene clusters in the genomes of PeaFJ1 and other strains were identified consecutively through combining the program DIAMOND and the program OrthoMCL (version 2.0)

[2]http://www.pathogenomics.sfu.ca/islandviewer/upload/

(Silva-Pereira et al., 2019). Then, all the putative proteins of the PeaFJ1 and core orthologs were aligned using BLASTP (Hirsh and Fraser, 2001). In addition, the strain-specific genes of PeaFJ1 compared with HA4-1 were analyzed for screening the candidates for the difference pathogenicity to peanut. GO and KEGG enrichment analyses were performed using the functional annotation tool DAVID (version 6.8) with default parameters (Dennis et al., 2003; Sherman et al., 2007).

Statistical Analysis

Statistical analyses and graphs were generated by using the GraphPad Prism 8.0 software. The *p*-values less than 0.05 indicate significant differences among the survival ratio of HA4-1 and PeaFJ1.

RESULTS AND DISCUSSION

PeaFJ1 Strain Shows More Aggressive to Most Peanut Varieties

To screen bacterial wilt-resistant and -susceptible sources, we evaluated 303 cultivated peanut varieties for disease susceptibility to two *R. solanacearum* strains PeaFJ1 and HA4-1. We found that PeaFJ1 was more aggressive to most varieties than HA4-1 according to the wilting symptoms and DI. To confirm this result, we randomly selected 113 varieties to repeat the inoculation assay. Of the 113 varieties, 85 were susceptible to PeaFJ1 and 62 were susceptible to HA4-1. The susceptibility rates were 75% (85/113) and 55% (62/113), respectively (**Supplementary Figure 1A**). In addition, in the DI of most varieties, inoculated PeaFJ1 was higher than that of inoculated HA4-1. For some peanut varieties, the pathogenicity of the two strains was significantly different (**Supplementary Figure 1B**). For example, PeaFJ1 showed reproducible and robust hypervirulence phenotypes, while HA4-1 showed hypovirulent phenotypes, in peanut variety A184. However, for a few varieties, the DI was equal or higher after inoculation with HA4-1 than with PeaFJ1. For example, HA4-1 could cause strong disease symptoms in another peanut variety A281, which indicates that it retains its intrinsic pathogenicity as a pathogen (**Figure 1**). These results indicated that PeaFJ1 and HA4-1 had different virulence profiles, and PeaFJ1 was more virulent to most peanut varieties than HA4-1. The hypovirulence of HA4-1 to certain peanut varieties is probably owed to host specificity at genotype levels, which is closely related to the type III effectors, since T3Es always narrow the host range when certain effectors are specifically recognized as avirulence factors by the host (Jones and Dangl, 2006; Chiesa et al., 2019; Cho et al., 2019; Tan et al., 2019). These data suggest that HA4-1 may contain an avirulence T3E(s) that induces bacterial wilt disease resistance in A184. Further phylogenetic trees analysis based on the similarity of endoglucanase gene sequence revealed that PeaFJ1 and HA4-1 were close phylogenetically and both belonged to phylotype I sequevar 14 (**Supplementary Figure 2A**), indicating that the genome differences between the two strains will be relatively small. This is a great advantage for us to use comparative genomic analysis to find the key genes that determine PeaFJ1 stronger pathogenicity in most peanut varieties. In addition, considering the A184-specific avirulence phenotype of HA4-1, we can also screen some candidate avirulence T3Es for further analysis by screening the absent T3Es in the PeaFJ1 genome.

Sequencing, Assembly and Overview of the PeaFJ1 Genome

The genome of *R. solanacearum* PeaFJ1 was sequenced using the PacBio Sequel platform. As a result, a total of 1.4 Gb polymerase reads from a 20 kb library were generated by SMRT sequencing. After removing adapters and low-quality or ambiguous reads, we obtained 1.4 GB (∼241 ×) subreads for complete genome assembly of PeaFJ1. The PeaFJ1 genome consists of a circle chromosome contig of 3,800,378 bp with 66.78% GC content and a circle megaplasmid contig of 2,008,534 bp with 66.97% GC content (**Figures 2A,B** and **Table 1**). No small plasmid was found in PeaFJ1. The full length of PeaFJ1 chromosome is relatively smaller than that of HA4-1 (3,800,378 bp vs. 3,890,347 bp) while the megaplasmid is larger than that of HA4-1 (2,008,534 bp vs. 1,947,245 bp). As a whole, the genome size of PeaFJ1 is slightly smaller than that of HA4-1 (5,808,912 bp vs. 5,837,592 bp) (Tan et al., 2019). In order to compare the genome of PeaFJ1 with other sequenced phylotype I *R. solanacearum* genomes, the synteny blocks between PeaFJ1 and other representative sequenced *R. solanacearum* strains such as HA4-1, Rs-P.362200, HZAU091, GMI1000, and CQPS-1 were identified using the program C-Sibelia (Minkin et al., 2013; **Figure 3A**). The results revealed that the PeaFJ1 genome situates a higher syntenic relationship with HA4-1, Rs-P.362200, and HZAU091. The number of collinear blocks are 20, 26, and 24, respectively. The proportion of the total base length of collinear blocks accounts for more than 97% of the PeaFJ1 genome, whereas 80 and 82 collinear blocks were identified in PeaFJ1 when compared with GMI1000 and CQPS-1. The full length of collinear blocks accounts for 91.9 and 93.34% in the genome of PeaFJ1, respectively. It suggests that the genome of PeaFJ1 is more similar with HA4-1, Rs-P.362200, and HZAU091. *R. solanacearum* strains HA4-1 and HZAU091 both belonged to phylotype I and sequevar 14M and isolated from peanut and potato, respectively (Wang et al., 2017; Tan et al., 2019). The *R. solanacearum* strain Rs-P.362200 was isolated from peanut and belonged to phylotype I (Chen et al., 2021). The GMI1000 is most widely used as a standard strain, isolated from the tomato and belonged to phylotype I, sequevar 18, while the CQPS-1 is isolated from the tobacco (Liu et al., 2017). The result of synteny analysis indicates that the genomic similarity of *R. solanacearum* strains could be preliminarily estimated by the sequevar identification or their host. Structural variation (SV) is the insertion, deletion, inversion, and translocation of the long sequence fragments whose length is more than 50 bp. Here, we detected 5 translocated regions, 15 duplicated regions, and 2 inverted regions between the genome of PeaFJ1 and HA4-1 (**Figure 3B**). In addition, four inverted duplicated regions and one inverted translocated region were also identified. The difference in virulence between PeaFJ1 and HA4-1 may be closely related to these variations.

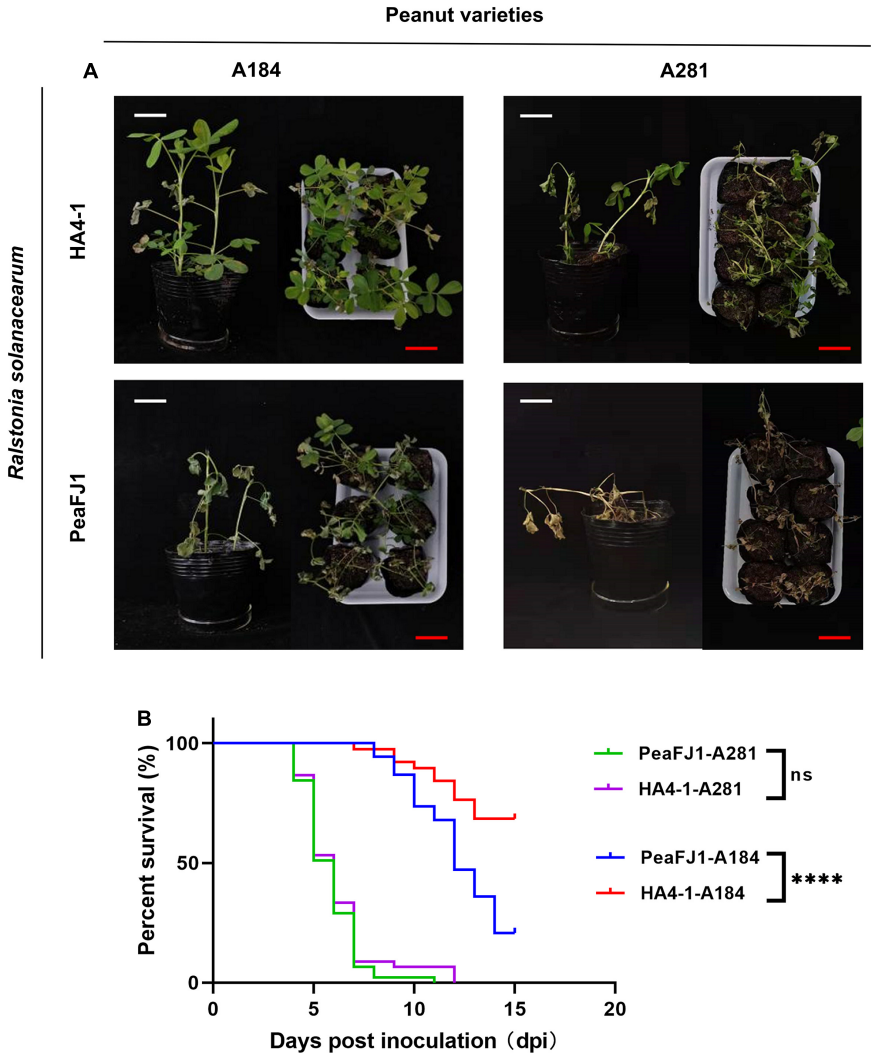

FIGURE 1 | *R. solanacearum* PeaFJ1 shows different virulent profiles compared with HA4-1 in peanut varieties. Bacterial wilt symptoms **(A)** and survival ratio **(B)** of the peanut varieties A184 and A281 infected with *R. solanacearum* PeaFJ1 and HA4-1, respectively. **(A)** Photographs from representative plants were taken at 10 days post- inoculation. White scale bars = 5 cm, red scale bars = 10 cm. **(B)** The percentage of surviving peanuts was recorded for 15 days. The data used for the survival ratio were collected from three independent experiments. Gehan–Breslow–Wilcoxon test *p*-values are < 0.0001 and 0.6471 in A184 and A281, respectively. ****indicates $p < 0.0001$, (ns) means no significantly different.

Functional Annotation of the PeaFJ1 Genome

The general characteristics of the PeaFJ1 genome are listed in **Table 1**. There are 5,098 ORFs identified (3,502 in the chromosome and 1,596 in the megaplasmid) in the genome of *R. solanacearum* PeaFJ1. By searching several databases, 3,342 and 1,527 coding genes were predicted in the chromosome and the megaplasmid, respectively. Of all the 4,869 genes, 4,865 (99.92%), 2,886 (59.27%), 3,686 (75.7%), and 2,579 (52.97%) genes were annotated according to NCBI Nr, SwissProt, COG, and KEGG databases, respectively (**Supplementary Table 1**). In addition, 155 pseudogenes were identified in the whole genome. Functional annotation successfully classified 2,640 chromosome genes into 22 COG categories and 1,647 megaplasmid genes into 21 COG categories (**Figures 2C,D**). Although more genes are in the chromosome, there are more genes related to cell motility in the megaplasmid. The PeaFJ1 genome contains 12 rRNAs, 59 tRNAs, and 8 sRNAs (**Table 1**). The full length of ncRNAs is 23,714 bp, accounting for 0.75% of the PeaFJ1 whole genome sequence. Virulence factor is an important basis of bacterial virulence, which plays a major role in the pathogenesis of the pathogen. The biological function analysis of virulence factor has become the primary task of the pathogenic mechanism study. There are 351 genes in PeaFJ1 having homologs in the VFDB database (**Supplementary Table 2**), which is a pathogen virulence factor database.[3] These genes are highly homologous with those genes in other pathogens that have been shown to contribute to their virulence. There are 1,085 genes having homologs in the PHI database (**Supplementary Table 2**), which collects sequences

[3]http://www.mgc.ac.cn/VFs/main.htm

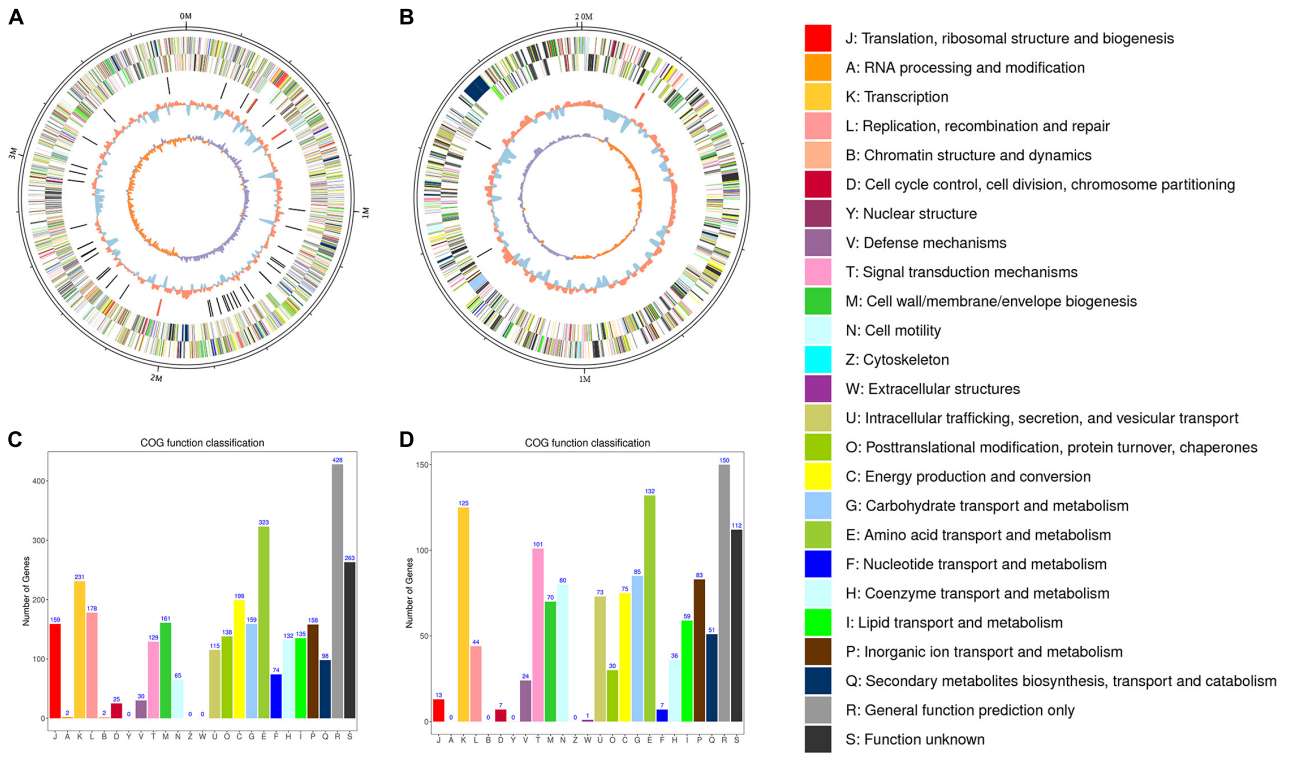

FIGURE 2 | Circos plot of the genome of *R. solanacearum* strain PeaFJ1. The genome of strain PeaFJ1 consists of a chromosome contig with a full length of 3,800,378 bp **(A)** and a megaplasmid contig with a full length of 2,008,534 bp **(B)**. From the outer circle to the inner circle, it represents the length of chromosomes, CDS, tRNAs, GC content, and GC skew curve, respectively. **(C,D)** The distribution of genes with COG functional categories in the chromosome **(C)** and the megaplasmid **(D)** of PeaFJ1. Different colors represent different COG functional classifications that were explained in the right side.

of experimentally validated pathogenic and effector genes from the literature.[4] The homologous genes of these genes have been experimentally confirmed to cause certain diseases in certain hosts and to interact with certain genes in the host. These predictions could help us quickly identify the key genes that cause PeaFJ1 to be more virulent to most peanut varieties.

[4]http://www.phi-base.org/

TABLE 1 | General features of the *R. solanacearum* PeaFJ1 genome.

Features	Values
Genome size (bp)	5,808,912
Chromosome (bp)	3,800,378
Megaplasmid (bp)	2,008,534
G + C content (%)	66.88
ORFs	5,098
Predicted genes	4,869
Pseudogenes	155
rRNA	12
tRNA	59
sRNA	8
Genomic islands	21
Prophages	2

Genomic Islands and Prophage Elements

Horizontal gene transfer (HGT) can enhance the adaptability of bacteria to the environments. Genomic islands and prophages are the most important mobile elements in HGT (Fouts, 2006). The coding regions of genomic islands usually contain large numbers of virulence gene clusters, which encode the virulence factors in many pathogenic bacteria (Tatusova et al., 2016). In total, 21 genomic islands (GIs) were predicted in the whole genome (16 located in the chromosome and 5 located in the megaplasmid) of PeaFJ1 (**Figure 4** and **Supplementary Table 3**). The total length of the GIs is 475,829 bp, which accounts for 8.2% of the PeaFJ1 genome. There are three type III effectors located in the GIs, which are RipP1, RipAX2, and RipG2. There are five GIs longer than 35 kb, and each containing more than 30 genes. The prophage sequences may confer some bacteria antibiotic resistance, improve bacterial adaptability to the environments, strengthen bacterial adhesion, or cause the bacteria to be more pathogenic (Bertelli et al., 2017). There are two prophages predicted in the chromosome, whose sizes are 13,278 and 32,359 bp (**Supplementary Table 4**). There are 15 and 42 genes in the two prophage regions, respectively. The GC content of the prophages is lower than that of the chromosome (64.34%). The bacteriophages best matched to the two prophages are NC_004821 and NC_009382. One of the prophage regions partially overlaps with the GIs. HGT plays

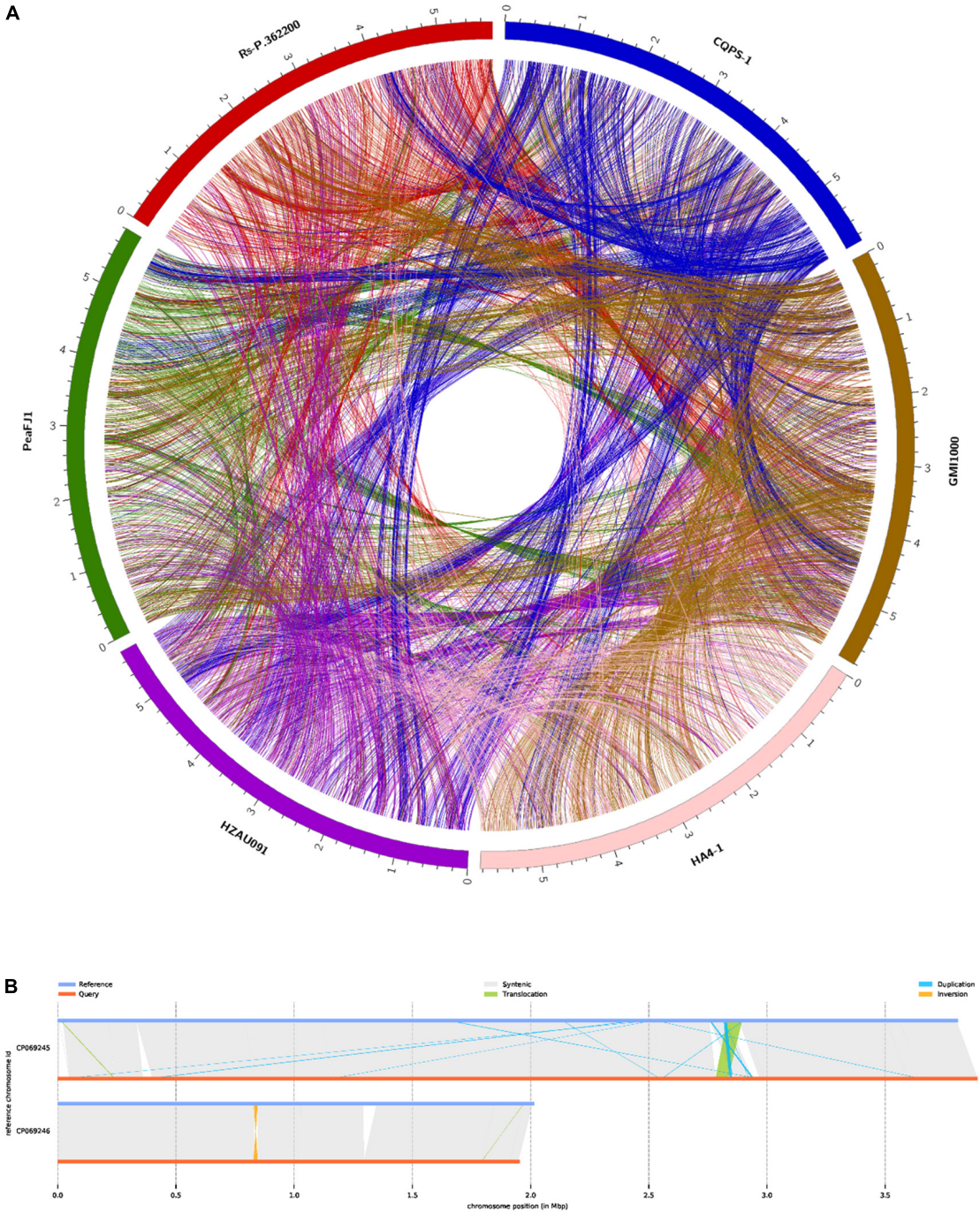

FIGURE 3 | Comparison of *R. solanacearum* PeaFJ1 with other representative sequenced *R. solanacearum* strains. **(A)** Synteny blocks identified in PeaFJ1 across HA4-1, Rs-P.362200, HZAU091, GMI1000, and CQPS-1. **(B)** Illustration of structural variation types between PeaFJ1 and HA4-1. Reference is HA4-1, and query is PeaFJ1.

an important role in *R. solanacearum* genetic and pathogenic diversity by contributing to the rapid acquisition of novel adaptive functions and pathogenic factors and is thus crucial for the adaptation and the emergence of pathogenic variants. Therefore, the HGT-related genes of PeaFJ1 are worthy of attention in the future study.

Specific Genes Analysis of PeaFJ1

The genomic comparison of the PeaFJ1 with the other five sequenced *R. solanacearum* strains was carried out using the genomic protein sequences, and the unique gene families of PeaFJ1 were identified (**Figure 5A**). Gene family analysis showed that there were 4,869 gene clusters in the genome

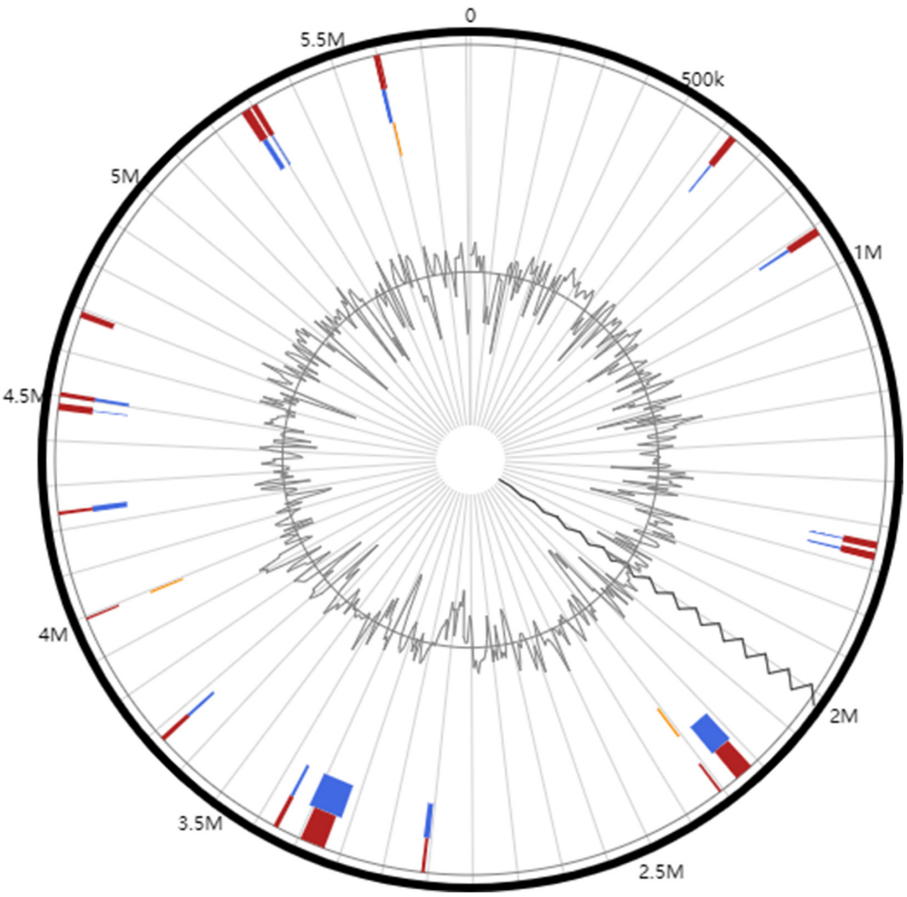

FIGURE 4 | Circular plots of genomic islands identified in *R. solanacearum* PeaFJ1 genome. The orange- and blue-colored shapes determine the predicted genomic islands as identified by SIGI-HMM (orange) and IslandPath-DIMOB (blue), and red shows the integrated genomic island search results.

of the PeaFJ1 strain, which could be classified into 4,744 gene families, among which 34 gene families were unique to PeaFJ1 (**Supplementary Table 5**). By analyzing the specific gene families of PeaFJ1 compared with other strains, there were 4,619, 4,639, and 4,450 common gene families, 148, 138, and 299 unique gene families in PeaFJ1 compared with strains HA4-1, Rs-P.362200, and HZAU091, respectively (**Figure 5B**). While compared with CQPS-1 and GMI1000, there were 4,251 and 4,354 common gene families and 526 and 423 specific gene families in PeaFJ1. It indicated that PeaFJ1 was more closely related to the three strains HA4-1, Rs-P.362200, and HZAU091, consistent with the ANI (average nucleotide identity) analysis results (**Supplementary Figure 2B**).

Because *R. solanacearum* PeaFJ1 is more pathogenic than HA4-1, the specific genes in PeaFJ1 compared with HA4-1 could be the determinants. By comparative genomic analysis, we identified 153 (in 148 gene families) and 161 (in 160 gene families) specific genes in PeaFJ1 and HA4-1 genomes, respectively (**Figure 5C** and **Supplementary Table 6**). To further reveal the gene ontology and functional classification of these PeaFJ1-specific genes, we performed the GO and KEGG enrichment analysis. Among the strain-specific genes of PeaFJ1, 49 (59.04%), 29 (34.94%), and 5 (6.02%) GO terms were enriched in the three categories of biological process, molecular function, and cellular component, respectively (**Supplementary Table 7**). KEGG enrichment analysis demonstrated that PeaFJ1-specific genes are mainly enriched in microbial metabolism in diverse environments (ko01120), carbon metabolism (ko01200), and the biosynthesis of amino acids (ko01230) (**Figure 5D**). Further analysis of these strain- specific genes showed that most of the specific genes (114 genes) are located in six gene clusters (**Supplementary Table 6**). The largest gene cluster consists of 38 genes (from JNO62_20500 to JNO62_20690). Four of the gene clusters almost overlap with the GIs. There are a total of 58 PeaFJ1-specific genes located on the GIs, accounting for 38% of the specific genes. One of the gene clusters consisting of 14 genes (from JNO62_05980 to JNO62_06045) is located on the prophage region. The above data suggested that many specific genes of PeaFJ1 are located on the mobile elements and related to HGT. The genes matched to the VFDB database and PHI database are important for the pathogenicity and host interaction for the pathogens. Here, we found that there were 7 and 20 specific genes, respectively, which were homologous with genes in the two databases (**Supplementary Table 2**).

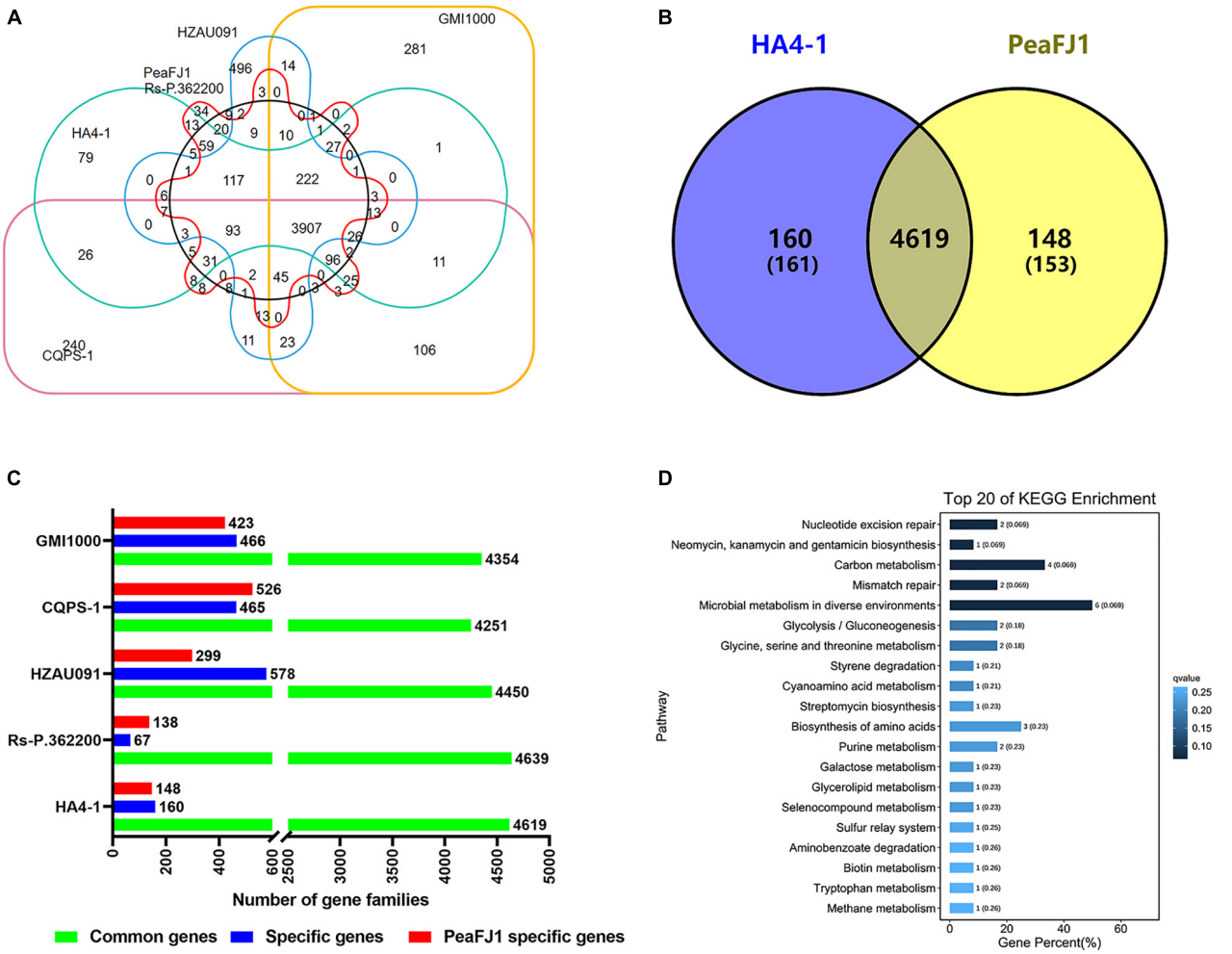

FIGURE 5 | Comparison of orthologs of strain PeaFJ1 with other *R. solanacearum* strains. **(A)** A big Venn diagram of orthologs for PeaFJ1, HA4-1, Rs-P.362200, HZAU091, GMI1000, and CQPS-1. **(B)** Statistical analysis of common/specific orthologs between PeaFJ1 and the other five strains. The *x*-axis indicates the number of gene families; the *y*-axis means the different *R. solanacearum* strains. Green bar, blue bar, and red bar mean common gene families, specific gene families, and PeaFJ1- specific gene families when PeaFJ1 is compared with the other five strains, respectively. **(C)** A Venn diagram of the common/specific genes between PeaFJ1 and HA4-1. **(D)** Top 20 enriched KEGG pathways of strain-specific genes in PeaFJ1 whole genome. The *q*-value results from the *p*-value *via* multi-test correction. The ranges of *q*-value are from 0 to 1, and a higher enrichment is achieved when the *q*-value reaches to 0.

Swimming Motility-Related Genes

R. solanacearum has evolved with different movement strategies to reach different plant tissues and get inside the vascular system, of which swimming motility is an individual cell movement produced in aqueous environments and powered by rotating flagella (Corral et al., 2020). In *R. solanacearum*, swimming motility is mediated by one to four polar flagella (Tans-Kersten et al., 2001). The flagellum comprises three functional parts: a thin helical flagellar filament that acts as a propeller, a reversible rotary molecular motor embedded on the envelope, and a hook that acts as a universal connection joint between the motor and the flagellar filament (Macnab, 2003). Among the PeaFJ1 strain-specific genes, one gene was functionally annotated to be the *fliK* gene (JNO62_02405), which encodes a protein with a flagellar hook length control motif (**Supplementary Table 6**). The bacterial flagellum is a complex organelle of the cell. The *fliK* gene is required for flagellar filament assembly and function (Evans et al., 2014). A mutant of the *fliK* gene in *Bacillus thuringiensis* completely failed to produce detectable flagellar filaments, and its biofilm formation is highly compromised as well. Both flagellar assembly and swimming motility are restored by the functional complementation of the mutant strains by the *fliK* ORF (Attieh et al., 2020). These results confirm the essential function of the FliK protein in the flagellar assembly, motility, and biofilm formation in *B. thuringiensis*. Compared with HA4-1, the predicted *fliK* gene is unique in PeaFJ1, indicating that it is probably responsible for the more aggressiveness of PeaFJ1 strain. In the future, systematic experiments including mutant construction were needed to verify the function of the *fliK* gene of *R. solanacearum* both *in vitro* and *in vivo* and especially in peanuts.

LysR-Type Transcriptional Regulators

The LysR-type transcriptional regulators represent the most abundant type of transcriptional regulators in the prokaryotic kingdom. By affecting the efficiency of transcription initiation, the LysR-type transcriptional regulators regulate a diverse set of genes, including those involved in virulence, metabolism, quorum sensing, and motility (Hernández-Lucas et al., 2008; Maddocks and Oyston, 2008). To date, many LysR-type transcriptional regulators have been identified to be important for the virulence of many pathogenic bacteria (Huang et al., 1998; Habdas et al., 2010; Rashid et al., 2016). In the *R. solanacearum*, a quorum-sensing-dependent LysR-type transcriptional regulator PhcA has been well characterized as a global regulator that controls the expression of diverse virulence-related genes, including those involved in plant cell wall degradation, motility, synthesis of EPS, and the T3SS (Brumbley et al., 1993; Huang et al., 1995; Genin et al., 2005). Among the PeaFJ1 strain-specific genes, three genes were functionally annotated to be LysR-type transcriptional regulators (JNO62_02440, JNO62_02445, and JNO62_20640) (**Supplementary Table 6**). Relative to HA4-1, the strong virulence of PeaFJ1 may be due to the presence of these three genes.

Adhesion- and Invasion-Related Genes

Lipoproteins, as an important part of outer membrane proteins that are widely distributed in Gram-negative bacteria, have been shown to perform a variety of roles in bacterial physiological and pathogenic processes (Kovacs-Simon et al., 2011; Sutcliffe et al., 2012). VacJ protein is a recently discovered outer membrane lipoprotein that relates to virulence in several pathogens. It plays an essential role in maintaining outer membrane integrity, stress tolerance, biofilm formation, adherence to, and invasion in host cells related to the pathogen (Zhao et al., 2017). Adherence to the host cell surface is an essential process for bacterial colonization and cellular invasion, which contribute to the breaching of the cell barrier, staying inside the host and ultimately leading to systemic disease (Vahle et al., 1997). Adhesion and invasion of host cells are also considered as important factors for pathogenesis in *R. solanacearum*. Among the PeaFJ1 strain-specific genes, one gene was functionally annotated to be the *VacJ* gene (JNO62_18020) (**Supplementary Table 6**). As a plant bacterial pathogen that colonizes in the vascular system, *R. solanacearum* infecting the host also depends on the adhesion and invasion of host cells. Thus, the *VacJ* gene in the PeaFJ1 but not in HA4-1 may be responsible for their different pathogenicity to peanuts. The definite function of *VacJ* gene in PeaFJ1 is to be studied by constructing the mutant strain in the following research.

Two-Component Systems-Related Genes

Bacteria alter their gene expression in response to environment changes through a variety of mechanisms including signal transduction systems. These signal transduction systems use kinase with extracellular or periplasmic sensing domains to transfer phosphate groups to DNA-binding molecules and consequently induce the gene expression change. Bacterial signal-transduction systems often involve only two proteins (a sensing protein and a transcription factor), and are thus called TCSs (Stock et al., 2000; Groisman, 2016). In the PeaFJ1 genome, there are 32 TCSs (19 located in the chromosome and 13 located in the megaplasmid) (**Supplementary Figure 3** and **Supplementary Table 8**). Among the PeaFJ1 strain-specific genes, four genes were functionally annotated to be TCS-related genes. The four genes are JNO62_20595, JNO62_20600, JNO62_20655, and JNO62_20660 (**Supplementary Tables 6, 8**), among which, JNO62_20595 and JNO62_20655 were predicted to encode sensor kinases while JNO62_20600 and JNO62_20660 were predicted to encode response regulators. The four genes make up two TCSs located in the megaplasmid. So far, no studies on TCS have been reported in *R. solanacearum*. TCSs are known to play important roles in bacterial motility and chemotaxis, physiological responses to osmotic changes, biofilm formation, and the regulation of virulence in many bacteria (Stock et al., 2000; Freeman et al., 2013; Groisman, 2016). Whether these two PeaFJ1-specific TCSs are responsible for the different virulence between PeaFJ1 and HA4-1 needs further research.

Type III Effector Genes

The secretory systems and their secreted components are always important for the virulence of pathogens, among which, the T3SS and its effectors especially attracted more attention of the researchers. T3Es are secreted by the "molecular syringe-like" T3SS and translocated into the cell to play versatile functions when interacting with the host. Many studies have showed that *R. solanacearum* effectors can regulate the host metabolism, suppress plant defense responses, or avoid bacterial recognition through various molecular mechanisms. For example, the effector RipG belonging to the GAxALA (GALA) effector protein family can inhibit the ubiquitination signal in the host and then promote the infection response of *R. solanacearum* (Angot et al., 2006; Remigi et al., 2011). RipAY can be selectively activated by thioredoxin to degrade glutathione in the host, providing a suitable environment for *R. solanacearum* infection (Wei et al., 2017; Sang et al., 2018). RipN acts as a nudix hydrolase, alters the nicotinamide adenine dinucleotide (NADH)/nicotinamide adenine dinucleotide (NAD^+) ratio of the plant, and contributes to virulence by suppression of PAMP-triggered immunity (PTI) of the host (Sun et al., 2018). RipAB inhibits the calcium-signaling pathway, which in turn decreases the accumulation of reactive oxygen species mediated by Pathogen-associated molecular patterns (PAMPs), thus making the transgenic potatoes of *RipAB* more susceptible to *R. solanacearum* (Zheng et al., 2018). RipV2 has the activity of E3 ubiquitin ligase, which can cause cell necrosis in tobacco leaves and inhibit the PTI immune defense response in plants (Cheng et al., 2021). RipI interacts with plant glutamate decarboxylases to alter plant metabolism and support bacterial growth (Xian et al., 2020). On the other hand, *R. solanacearum* T3Es can be perceived by the plant and activate the defense response in the host. RipP2, an effector protein of YopJ family, has acetyltransferase activity. It can acetylate the WRKY domain of nucleotide-binding leucine-rich repeat receptor (NLR)-resistant proteins and stimulate immune resistance to *Arabidopsis thaliana*. RipP1, which also belongs to the YopJ family with acetyltransferase activity, can induce an immune response in petunias (Poueymiro et al., 2009). RipB induced bacterial wilt resistance in tobacco by the recognition of Roq1 (Nakano and Mukaihara, 2019). RipAX2 elicited immune

responses in wild and cultivated eggplants, which were dependent on the Zn-finger domain in wild eggplants but not in cultivated eggplants (Nahar et al., 2014; Morel et al., 2018). Although every *R. solanacearum* has more than 50 effectors, different strains have different repertoire of effectors. In order to reveal the effector repertoire of *R. solanacearum* PeaFJ1, we identified the effectors according to the Ralsto T3E database (Sabbagh et al., 2019) and the gene functional annotation. As a result, 79 type III effectors were identified, among which 11 are pseudogenes (**Supplementary Table 9**).

In order to quickly identify the key effectors related to pathogenicity of pathogens from numerous effectors, a lot of strategies have been performed by researchers. Some T3Es with important functions are selected out largely depending on the comparative analysis of the effectors. For instance, the recently reported *R. solanacearum* avirulence effectors RipJ and RipAZ1 are identified by the comparative genomic analysis of two strains with different virulence against *S. pimpinellifolium* and *S. americanum*, respectively (Moon et al., 2021; Pandey and Moon, 2021). Similarly, by comparing all the effectors of PeaFJ1 and HA4-1, we found that most of the effectors are exactly identical with the counterparts of *R. solanacearum* HA4-1. Only a few effectors are discrepant in the two strains (**Supplementary Table 9**). RipS4 is present in both stains, whereas it is prematurely terminated due to a base pair deletion in HA4-1. As the C-terminal of a protein always plays an important role in its function, the difference of RipS4 may be responsible for the difference of virulence between the two strains. A single copy of *RipBR* gene was identified in the megaplasmid of PeaFJ1, while two copies of *RipBR* gene were located in the megaplasmid and small plasmid of HA4-1, respectively, although the latter was inserted by a transposon (Tan et al., 2019). There are three copies of *RipBS* gene existing in the genome and small plasmid of HA4-1, while no *RipBS* gene was found in the genome of PeaFJ1. In addition, RS_T3E_Hyp6 is absent in PeaFJ1, while it is present in HA4-1. On the contrary, RipBB is present in PeaFJ1 but not HA4-1 (**Supplementary Table 9**). According to the general function of effectors, RipBB may be responsible for the higher pathogenicity of PeaFJ1 against peanuts. That is to say, RipS4 and RipBB are virulence effectors. The hypovirulence of HA4-1 to certain peanut varieties may be due to the presence of RipBS and RS_T3E_Hyp6. That is to say, RipBS and RS_T3E_Hyp6 may be avirulence effectors. The specific roles of these four effectors acting on peanuts need to be explored by systematic experiments in the following study. There is a minor difference in RipG5 and RipH1 genes between PeaFJ1 and HA4-1. However, it cannot be ruled out that one or two amino acid differences may cause differences in effector functions. The above-mentioned T3Es will be an important direction for the mechanism research of *R. solanacearum*–peanut interaction, so a series of experiments are required to explore the particular roles of these effectors in the future.

CONCLUSION

In this study, we completed a high-quality sequencing and analysis of a strong virulent *R. solanacearum* strain PeaFJ1 isolated from peanut. In view of the pathogen research of peanut bacterial wilt still being scarce, the results of the genome analysis and the pathogenicity of PeaFJ1 to various peanut varieties will provide strong support for the study of the interaction between *R. solanacearum* and peanut. Through a detailed comparative analysis of the genomes between PeaFJ1 and another *R. solanacearum* strain HA4-1 from peanut, we screened out the strain-specific genes of PeaFJ1, which may be the key factors causing different virulence profiles between the two strains. It is the first time to explore the key genes of *R. solanacearum* pathogenicity by doing a comparative genomic analysis of two different virulence strains from peanut. Our study enriches the information of the *R. solanacearum* species complex genomes and contributes to gain a deeper insight into the pathogenic factors of *R. solanacearum* against peanut as well. These results will greatly promote the study of interaction mechanism between peanut and *R. solanacearum* and will also be beneficial to the development of peanut bacterial wilt control agents.

DATA AVAILABILITY STATEMENT

The datasets presented in this study can be found in online repositories. The names of the repository/repositories and accession number(s) can be found in the article/ **Supplementary Material**.

AUTHOR CONTRIBUTIONS

XT and YY designed the research, analyzed the data, and wrote the manuscript with contributions of all the authors. XD and TC performed the experiments and analyzed the data. DY, YW, and YY provided technical assistance to XT. YZ and HC supervised the experiments. XW supervised and complemented the writing. All authors contributed to the article and approved the submitted version.

FUNDING

This work was supported by the Guangdong University Scientific Research Platform and Research Project (Young Innovative Talents) (Grant No. 2021KQNCX033), the Starting Research Fund from Zhongkai University of Agriculture and Engineering (Grant Nos. KA210319277 and KA210319256), the grants (Nos. 31770652 and 32071737) from the National Natural Science Foundation of China, the grant (No. 202002010010) from the Guangzhou Key Laboratory for Research and Development of Crop Germplasm Resources and a grant (to XW) from the Department of Education of Guangdong Province. HC was supported by the National Natural Science Foundation of China (No. 31871686).

ACKNOWLEDGMENTS

We would like to thank other members of Guangzhou Key Laboratory for Research and Development of Crop Germplasm

Resources and the Peanut Group for their kind help during the preparation of this article.

SUPPLEMENTARY MATERIAL

The Supplementary Material for this article can be found online at: https://www.frontiersin.org/articles/10.3389/fmicb.2022.830900/full#supplementary-material

Supplementary Figure 1 | PeaFJ1 have different virulence profiles with HA4-1 on different peanut varieties. **(A)** The heatmap of disease grade of 113 peanut varieties after 10 days inoculated with *R. solanacearum* HA4-1 and PeaFJ1, respectively. The column is *R. solanacearum* HA4-1 and PeaFJ1, and the row is the different peanut varieties. R, Resistance, $0 \leq DI < 25$; MR, Medium Resistance, $25 \leq DI < 50$; MS, Medium Susceptible, $50 \leq DI < 75$; S, Susceptible, $75 \leq DI < 100$. **(B)** The DI of 113 peanut varieties after 10 days inoculated with *R. solanacearum* HA4-1 and PeaFJ1, respectively. Significant differences were assessed by ANOVA and indicated by asterisks; single asterisk (*) indicates $P < 0.05$, and double asterisk (**) indicates $P < 0.01$. Values are means of three biological replicates, with error bars indicating the SD.

Supplementary Figure 2 | Genetic relationship analysis of PeaFJ1 with other *R. solanacearum* strains. **(A)** Phylogenetic tree constructed with different *R. solanacearum* strains including HA4-1- and PeaFJ1-based *egl* gene sequences. The result confirms that HA4-1 and PeaFJ1 are closely phylogenetical and belong to phylotype I sequevar 14. HA4-1 and PeaFJ1 is indicated by a red box. Alignments were conducted in ClustalW, and the phylogenetic tree was constructed by the neighbor-joining algorithm in MEGA 6 software. Bootstrap values (1,000 replicates) are shown as percentages at the branch nodes. **(B)** The heatmap of ANI percentage identity for PeaFJ1 with other *R. solanacearum* strains. The number in the heatmap indicates different ANI percentage.

Supplementary Figure 3 | Schematic diagram of two-component systems in *R. solanacearum* PeaFJ1. **(A)** The 19 TCSs in the chromosome. **(B)** The 13 TCSs in the megaplasmid. HisKA (blue): Phosphate receptor domain containing an H-box of conserved histidine sites capable of autophosphorylation. HATPase_c (red) is the intracellular catalytic domain of histidine kinase, responsible for the transfer of ATP phosphate groups to histidine. Response_reg (green): Response regulator (RR), response regulator protein. Black module: transmembrane helix. Numbers at both ends: gene ID.

Supplementary Table 1 | Basic annotation of PeaFJ1 chromosome and megaplasmid.

Supplementary Table 2 | PeaFJ1 genes annotated in VFDB and PHI database.

Supplementary Table 3 | General features of genomic islands of PeaFJ1 genome.

Supplementary Table 4 | General features of genomic prophages of PeaFJ1 genome.

Supplementary Table 5 | The gene family of PeaFJ1 compared with other five sequenced strains.

Supplementary Table 6 | *R. solanacearum* PeaFJ strain-specific genes compared with HA4-1.

Supplementary Table 7 | GO enrichment analysis of PeaFJ1-specific genes compared with HA4-1.

Supplementary Table 8 | TCS prediction results in *R. solanacearum* PeaFJ1.

Supplementary Table 9 | Comparison analysis of type III effector genes of strain PeaFJ1 with strain HA4-1.

REFERENCES

Ali, N., Chen, H., Zhang, C., Khan, S. A., Gandeka, M., Xie, D., et al. (2020). Ectopic Expression of *AhGLK1b* (GOLDEN2-like Transcription Factor) in *Arabidopsis* Confers Dual Resistance to Fungal and Bacterial Pathogens. *Genes* 11:343. doi: 10.3390/genes11030343

Angot, A., Peeters, N., Lechner, E., Vailleau, F., Baud, C., Gentzbittel, L., et al. (2006). *Ralstonia solanacearum* requires F-box-like domain-containing type III effectors to promote disease on several host plants. *Proc. Natl. Acad. Sci. U.S.A.* 103, 14620–14625. doi: 10.1073/pnas.0509393103

Attieh, Z., Mouawad, C., Rejasse, A., Jehanno, I., Perchat, S. I, Hegna, K., et al. (2020). The *fliK* Gene Is Required for the Resistance of *Bacillus thuringiensis* to Antimicrobial Peptides and Virulence in *Drosophila melanogaster*. *Front. Microbiol.* 11:611220. doi: 10.3389/fmicb.2020.611220

Bertelli, C., Laird, M. R., Williams, K. P., Simon Fraser University Research Computing Group, Lau, B. Y., Hoad, G., et al. (2017). IslandViewer 4: expanded prediction of genomic islands for larger-scale datasets. *Nucleic Acids Res.* 45, W30–W35. doi: 10.1093/nar/gkx343

Brumbley, S. M., Carney, B. F., and Denny, T. P. (1993). Phenotype conversion in *Pseudomonas solanacearum* due to spontaneous inactivation of PhcA, a putative LysR transcriptional regulator. *J. Bacteriol.* 175, 5477–5487. doi: 10.1128/jb.175.17.5477-5487.1993

Caldwell, D., Kim, B. S., and Iyer-Pascuzzi, A. S. (2017). *Ralstonia solanacearum* Differentially Colonizes Roots of Resistant and Susceptible Tomato Plants. *Phytopathology* 107, 528–536. doi: 10.1094/PHYTO-09-16-0353-R

Chen, K., Wang, L., Chen, H., Zhang, C., Wang, S., Chu, P., et al. (2021). Complete genome sequence analysis of the peanut pathogen *Ralstonia solanacearum* strain Rs-P.362200. *BMC Microbiol.* 21:118. doi: 10.1186/s12866-021-02157-7

Chen, Y., Ren, X., Zhou, X., Huang, L., Yan, L., Lei, Y., et al. (2014). Dynamics in the resistant and susceptible peanut (*Arachis hypogaea* L.) root transcriptome on infection with the *Ralstonia solanacearum*. *BMC Genom.* 15:1078. doi: 10.1186/1471-2164-15-1078

Cheng, D., Zhou, D., Wang, Y., Wang, B., He, Q., Song, B., et al. (2021). *Ralstonia solanacearum* type III effector RipV2 encoding a novel E3 ubiquitin ligase (NEL) is required for full virulence by suppressing plant PAMP-triggered immunity. *Biochem. Biophys. Res. Commun.* 550, 120–126. doi: 10.1016/j.bbrc.2021.02.082

Cheung, J., and Hendrickson, W. A. (2010). Sensor domains of two-component regulatory systems. *Curr. Opin. Microbiol.* 13, 116–123. doi: 10.1016/j.mib.2010.01.016

Chiesa, M. A., Roeschlin, R. A., Favaro, M. A., Uviedo, F., Campos-Beneyto, L., D'Andrea, R., et al. (2019). Plant responses underlying nonhost resistance of *Citrus limon* against *Xanthomonas campestris* pv. *campestris*. *Mol. Plant Pathol.* 20, 254–269. doi: 10.1111/mpp.12752

Cho, H., Song, E. S., Heu, S., Baek, J., Lee, Y. K., Lee, S., et al. (2019). Prediction of Host-Specific Genes by Pan-Genome Analyses of the Korean *Ralstonia solanacearum* Species Complex. *Front. Microbiol.* 10:506. doi: 10.3389/fmicb.2019.00506

Coll, N. S., and Valls, M. (2013). Current knowledge on the *Ralstonia solanacearum* type III secretion system. *Microb. Biotechnol.* 6, 614–620. doi: 10.1111/1751-7915.12056

Corral, J., Sebastià, P., Coll, N. S., Barbé, J., Aranda, J., and Valls, M. (2020). Twitching and Swimming Motility Play a Role in *Ralstonia solanacearum* Pathogenicity. *mSphere* 5, e719–e740. doi: 10.1128/mSphere.00740-19

Cruz, A. P. Z., Ferreira, V., Pianzzola, M. J., Siri, M. I., Coll, N. S., and Valls, M. (2014). A Novel, Sensitive Method to Evaluate Potato Germplasm for Bacterial Wilt Resistance Using a Luminescent *Ralstonia solanacearum* Reporter Strain. *Mol. Plant Microbe Interact.* 27, 277–285. doi: 10.1094/MPMI-10-13-0303-FI

Dennis, G. Jr., Sherman, B. T., Hosack, D. A., Yang, J., Gao, W., Lane, H. C., et al. (2003). DAVID: database for Annotation, Visualization, and Integrated Discovery. *Genom. Biol.* 4:3.

Evans, L. D., Hughes, C., and Fraser, G. M. (2014). Building a flagellum outside the bacterial cell. *Trends Microbiol.* 22, 566–572. doi: 10.1016/j.tim.2014.05.009

Finn, R. D., Bateman, A., Clements, J., Coggill, P., Eberhardt, R. Y., Eddy, S. R., et al. (2014). Pfam: the protein families database. *Nucleic Acids Res.* 42, D222–D230. doi: 10.1093/nar/gkt1223

Fouts, D. E. (2006). Phage_Finder: automated identification and classification of prophage regions in complete bacterial genome sequences. *Nucleic Acids Res.* 34, 5839–5851. doi: 10.1093/nar/gkl732

Freeman, Z. N., Dorus, S., and Waterfield, N. R. (2013). The KdpD/KdpE two-component system: integrating K^+ homeostasis and virulence. *PLoS Pathog.* 9:e1003201. doi: 10.1371/journal.ppat.1003201

Genin, S., Brito, B., Denny, T. P., and Boucher, C. (2005). Control of the *Ralstonia solanacearum* Type III secretion system (Hrp) genes by the global virulence regulator PhcA. *FEBS Lett.* 579, 2077–2081. doi: 10.1016/j.febslet.2005.02.058

Genin, S., and Denny, T. P. (2012). Pathogenomics of the *Ralstonia solanacearum* species complex. *Annu. Rev. Phytopathol.* 50, 67–89. doi: 10.1146/annurev-phyto-081211-173000

Goel, M., Sun, H., Jiao, W. B., and Schneeberger, K. (2019). SyRI: finding genomic rearrangements and local sequence differences from whole-genome assemblies. *Genom. Biol.* 20:277. doi: 10.1186/s13059-019-1911-0

Gonzalez, A., Plener, L., Restrepo, S., Boucher, C., and Genin, S. (2011). Detection and functional characterization of a large genomic deletion resulting in decreased pathogenicity in *Ralstonia solanacearum* race 3 biovar 2 strains. *Environ. Microbiol.* 13, 3172–3185. doi: 10.1111/j.1462-2920.2011.02636.x

Groisman, E. A. (2016). Feedback Control of Two-Component Regulatory Systems. *Annu. Rev. Microbiol.* 70, 103–124. doi: 10.1146/annurev-micro-102215-095331

Habdas, B. J., Smart, J., Kaper, J. B., and Sperandio, V. (2010). The LysR-type transcriptional regulator QseD alters type three secretion in enterohemorrhagic *Escherichia coli* and motility in K-12 *Escherichia coli*. *J. Bacteriol.* 192, 3699–3712. doi: 10.1128/JB.00382-10

Hernández-Lucas, I., Gallego-Hernández, A. L., Encarnación, S., Fernández-Mora, M., Martínez-Batallar, A. G., Salgado, H., et al. (2008). The LysR-type transcriptional regulator LeuO controls expression of several genes in *Salmonella enterica* serovar Typhi. *J. Bacteriol.* 190, 1658–1670. doi: 10.1128/JB.01649-07

Hida, A., Oku, S., Kawasaki, T., and Nakashimada, Y. (2015). Identification of the *mcpA* and *mcpM* genes, encoding methyl-accepting proteins involved in amino acid and l-malate chemotaxis, and involvement of McpM-mediated chemotaxis in plant infection by *Ralstonia pseudosolanacearum* (formerly *Ralstonia solanacearum* phylotypes I and III). *Appl. Environ. Microbiol.* 81, 7420–7430. doi: 10.1128/AEM.01870-15

Hirsh, A. E., and Fraser, H. B. (2001). Protein dispensability and rate of evolution. *Nature* 411, 1046–1049. doi: 10.1038/35082561

Huang, J., Carney, B. F., Denny, T. P., Weissinger, A. K., and Schell, M. A. (1995). A complex network regulates expression of eps and other virulence genes of *Pseudomonas solanacearum*. *J. Bacteriol.* 177, 1259–1267. doi: 10.1128/jb.177.5.1259-1267.1995

Huang, J., Yindeeyoungyeon, W., Garg, R. P., Denny, T. P., and Schell, M. A. (1998). Joint transcriptional control of xpsR, the unusual signal integrator of the *Ralstonia solanacearum* virulence gene regulatory network, by a response regulator and a LysR-type transcriptional activator. *J. Bacteriol.* 180, 2736–2743. doi: 10.1128/jb.180.10.2736-2743.1998

Jiang, G., Wei, Z., Xu, J., Chen, H., Zhang, Y., She, X., et al. (2017). Bacterial Wilt in China: history, Current Status, and Future Perspectives. *Front. Plant Sci.* 8:1549. doi: 10.3389/fpls.2017.01549

Jones, J., and Dangl, J. (2006). The plant immune system. *Nature* 444, 323–329. doi: 10.1038/nature05286

Kovacs-Simon, A., Titball, R. W., and Michell, S. L. (2011). Lipoproteins of bacterial pathogens. *Infect. Immun.* 79, 548–561. doi: 10.1128/IAI.00682-10

Kurtz, S., Phillippy, A., Delcher, A. L., Smoot, M., Shumway, M., Antonescu, C., et al. (2004). Versatile and open software for comparing large genomes. *Genom. Biol.* 5:R12. doi: 10.1186/gb-2004-5-2-r12

Lagesen, K., Hallin, P., Rødland, E. A., Stærfeldt, H.-H., Rognes, T., and Ussery, D. W. (2007). RNAmmer: consistent and rapid annotation of ribosomal RNA genes. *Nucleic Acids Res.* 35, 3100–3108. doi: 10.1093/nar/gkm160

Liu, H., Kang, Y., Genin, S., Schell, M. A., and Denny, T. P. (2001). Twitching motility of *Ralstonia solanacearum* requires a type IV pilus system. *Microbiology* 147, 3215–3229. doi: 10.1099/00221287-147-12-3215

Liu, Y., Tang, Y., Qin, X., Yang, L., Jiang, G., Li, S., et al. (2017). Genome Sequencing of *Ralstonia solanacearum* CQPS-1, a Phylotype I Strain Collected from a Highland Area with Continuous Cropping of Tobacco. *Front. Microbiol.* 8:974. doi: 10.3389/fmicb.2017.00974

Lowe, T. M., and Chan, P. P. (2016). tRNAscan-SE On-line: integrating search and context for analysis of transfer RNA genes. *Nucleic Acids Res.* 44, W54–W57. doi: 10.1093/nar/gkw413

Luo, H., Pandey, M. K., Khan, A. W., Wu, B., Guo, J., Ren, X., et al. (2019). Next-generation sequencing identified genomic region and diagnostic markers for resistance to bacterial wilt on chromosome B02 in peanut (*Arachis hypogaea* L.). *Plant Biotechnol. J.* 17, 2356–2369. doi: 10.1111/pbi.13153

Macho, A. P., Guidot, A., Barberis, P., Beuzon, C. R., and Genin, S. (2010). A Competitive Index Assay Identifies Several *Ralstonia solanacearum* Type III Effector Mutant Strains with Reduced Fitness in Host Plants. *Mol. Plant Microbe Interact.* 23, 1197–1205. doi: 10.1094/MPMI-23-9-1197

Macnab, R. M. (2003). How bacteria assemble flagella. *Annu. Rev. Microbiol.* 57, 77–100. doi: 10.1146/annurev.micro.57.030502.090832

Maddocks, S. E., and Oyston, P. C. F. (2008). Structure and function of the LysR-type transcriptional regulator (LTTR) family proteins. *Microbiology* 154, 3609–3623. doi: 10.1099/mic.0.2008/022772-0

Minkin, I., Pham, H., Starostina, E., Vyahhi, N., and Pham, S. (2013). C-Sibelia: an easy-to-use and highly accurate tool for bacterial genome comparison. *F1000Res* 2:258. doi: 10.12688/f1000research.2-258.v1

Moon, H., Pandey, A., Yoon, H., Choi, S., Jeon, H., Prokchorchik, M., et al. (2021). Identification of RipAZ1 as an avirulence determinant of *Ralstonia solanacearum* in *Solanum americanum*. *Mol. Plant Pathol.* 22, 317–333. doi: 10.1111/mpp.13030

Morel, A., Guinard, J., Lonjon, F., Sujeeun, L., Barberis, P., Genin, S., et al. (2018). The eggplant AG91-25 recognizes the Type III-secreted effector RipAX2 to trigger resistance to bacterial wilt (*Ralstonia solanacearum* species complex). *Mol. Plant Pathol.* 19, 2459–2472. doi: 10.1111/mpp.12724

Nahar, K., Matsumoto, I., Taguchi, F., Inagaki, Y., Yamamoto, M., Toyoda, K., et al. (2014). Ralstonia solanacearum type III secretion system effector Rip36 induces a hypersensitive response in the nonhost wild eggplant *Solanum torvum*. *Mol. Plant Pathol.* 15, 297–303. doi: 10.1111/mpp.12079

Nakano, M., and Mukaihara, T. (2019). The type III effector RipB from *Ralstonia solanacearum* RS1000 acts as a major avirulence factor in *Nicotiana benthamiana* and other *Nicotiana* species. *Mol. Plant Pathol.* 20, 1237–1251. doi: 10.1111/mpp.12824

Nawrocki, E. P., and Eddy, S. R. (2013). Infernal 1.1: 100-fold faster RNA homology searches. *Bioinformatics* 29, 2933–2935. doi: 10.1093/bioinformatics/btt509

Pandey, A., and Moon, H. (2021). Ralstonia solanacearum type III Effector RipJ Triggers Bacterial Wilt Resistance in *Solanum pimpinellifolium*. *Mol. Plant Microbe Interact.* 34, 962–972. doi: 10.1094/MPMI-09-20-0256-R

Pandey, M. K., Monyo, E., Ozias-Akins, P., Liang, X., Guimarães, P., Nigam, S. N., et al. (2012). Advances in Arachis genomics for peanut improvement. *Biotechnol. Adv.* 30, 639–651. doi: 10.1016/j.biotechadv.2011.11.001

Peeters, N., Carrere, S., Anisimova, M., Plener, L., Cazale, A. C., and Genin, S. (2013). Repertoire, unified nomenclature and evolution of the Type III effector gene set in the *Ralstonia solanacearum* species complex. *BMC Genom.* 14:859. doi: 10.1186/1471-2164-14-859

Poueymiro, M., Cunnac, S., Barberis, P., Deslandes, L., Peeters, N., Cazale-Noel, A. C., et al. (2009). Two type III secretion system effectors from *Ralstonia solanacearum* GMI1000 determine host-range specificity on tobacco. *Mol. Plant Microbe Interact.* 22, 538–550. doi: 10.1094/MPMI-22-5-0538

Rashid, M. M., Ikawa, Y., and Tsuge, S. (2016). GamR, the LysR-Type Galactose Metabolism Regulator, Regulates hrp Gene Expression via Transcriptional Activation of Two Key hrp Regulators, HrpG and HrpX, in *Xanthomonas oryzae* pv. *oryzae*. *Appl. Environ. Microbiol.* 82, 3947–3958. doi: 10.1128/AEM.00513-16

Remigi, P., Anisimova, M., Guidot, A., Genin, S., and Peeters, N. (2011). Functional diversification of the GALA type III effector family contributes to *Ralstonia solanacearum* adaptation on different plant hosts. *New Phytol.* 192, 976–987. doi: 10.1111/j.1469-8137.2011.03854.x

Sabbagh, C. R. R., Carrère, S., Lonjon, F., Vailleau, F., Macho, A. P., Genin, S., et al. (2019). Pangenomic type III effector database of the plant pathogenic *Ralstonia spp*. *PeerJ* 7:e7346. doi: 10.7717/peerj.7346

Salanoubat, M., Genin, S., Artiguenave, F., Gouzy, J., Mangenot, S., Arlat, M., et al. (2002). Genome sequence of the plant pathogen *Ralstonia solanacearum*. *Nature* 415, 497–502. doi: 10.1038/415497a

Sang, Y., Wang, Y., Ni, H., Cazale, A. C., She, Y. M., Peeters, N., et al. (2018). The *Ralstonia solanacearum* type III effector RipAY targets plant redox regulators to suppress immune responses. *Mol. Plant Pathol.* 19, 129–142. doi: 10.1111/mpp.12504

Seemann, T. (2014). Prokka: rapid prokaryotic genome annotation. *Bioinformatics* 30, 2068–2069. doi: 10.1093/bioinformatics/btu153

Sherman, B. T., Huang da, W., Tan, Q., Guo, Y., Bour, S., Liu, D., et al. (2007). DAVID Knowledgebase: a gene-centered database integrating heterogeneous gene annotation resources to facilitate high-throughput gene functional analysis. *BMC Bioinform.* 8:426. doi: 10.1186/1471-2105-8-426

Silva-Pereira, T. T., Ikuta, C. Y., Zimpel, C. K., Camargo, N. C. S., de Souza Filho, A. F., Ferreira Neto, J. S., et al. (2019). Genome sequencing of *Mycobacterium pinnipedii* strains: genetic characterization and evidence of superinfection in a South American sea lion (*Otaria flavescens*). *BMC Genom.* 20:1030. doi: 10.1186/s12864-019-6407-5

Stock, A. M., Robinson, V. L., and Goudreau, P. N. (2000). Two-component signal transduction. *Annu. Rev. Biochem.* 69, 183–215. doi: 10.1146/annurev.biochem.69.1.183

Sun, Y., Li, P., Shen, D., Wei, Q., He, J., and Lu, Y. (2018). The *Ralstonia solanacearum* effector RipN suppresses plant PAMP-triggered immunity, localizes to the endoplasmic reticulum and nucleus, and alters the NADH/NAD^+ ratio in *Arabidopsis*. *Mol. Plant Pathol.* 20, 533–546. doi: 10.1111/mpp.12773

Sutcliffe, I. C., Harrington, D. J., and Hutchings, M. I. (2012). A phylum level analysis reveals lipoprotein biosynthesis to be a fundamental property of bacteria. *Protein Cell* 3, 163–170. doi: 10.1007/s13238-012-2023-8

Tan, X., Qiu, H., Li, F., Cheng, D., Zheng, X., Wang, B., et al. (2019). Complete Genome Sequence of Sequevar 14M *Ralstonia solanacearum* Strain HA4-1 Reveals Novel Type III Effectors Acquired Through Horizontal Gene Transfer. *Front. Microbiol.* 10:1893. doi: 10.3389/fmicb.2019.01893

Tans-Kersten, J., Huang, H., and Allen, C. (2001). *Ralstonia solanacearum* needs motility for invasive virulence on tomato. *J. Bacteriol.* 183, 3597–3605. doi: 10.1128/JB.183.12.3597-3605.2001

Tatusova, T., DiCuccio, M., Badretdin, A., Chetvernin, V., Nawrocki, E. P., Zaslavsky, L., et al. (2016). NCBI prokaryotic genome annotation pipeline. *Nucleic Acids Res.* 44, 6614–6624. doi: 10.1093/nar/gkw569

Tran, T. M., MacIntyre, A., Hawes, M., and Allen, C. (2016). Escaping Underground Nets: extracellular DNases Degrade Plant Extracellular Traps and Contribute to Virulence of the Plant Pathogenic Bacterium *Ralstonia solanacearum*. *PLoS Pathog.* 12:e1005686. doi: 10.1371/journal.ppat.1005686

Vahle, J. L., Haynes, J. S., and Andrews, J. J. (1997). Interaction of Haemophilus parasuis with nasal and tracheal mucosa following intranasal inoculation of cesarean derived colostrum deprived (CDCD) swine. *Can. J. Vet. Res.* 61, 200–206.

Wang, L., Wang, B., Zhao, G., Cai, X., Jabaji, S., Seguin, P., et al. (2017). Genetic and Pathogenic Diversity of *Ralstonia solanacearum* Causing Potato Brown Rot in China. *Am. J. Potato Res.* 94, 403–416. doi: 10.1007/s12230-017-9576-2

Wei, Y., Sang, Y., and Macho, A. P. (2017). The *Ralstonia solanacearum* Type III Effector RipAY Is Phosphorylated in Plant Cells to Modulate Its Enzymatic Activity. *Front. Plant Sci.* 8:1899. doi: 10.3389/fpls.2017.01899

Xian, L., Yu, G., Wei, Y., Rufian, J. S., Li, Y., Zhuang, H., et al. (2020). A Bacterial Effector Protein Hijacks Plant Metabolism to Support Pathogen Nutrition. *Cell Host Microbe* 28:e7. doi: 10.1016/j.chom.2020.07.003

Yao, J., and Allen, C. (2006). Chemotaxis is required for virulence and competitive fitness of the bacterial wilt pathogen *Ralstonia solanacearum*. *J. Bacteriol.* 188, 3697–3708. doi: 10.1128/JB.188.10.3697-3708.2006

Zhang, C., Chen, H., Cai, T., Deng, Y., Zhuang, R., Zhang, N., et al. (2017). Overexpression of a novel peanut NBS-LRR gene *AhRRS5* enhances disease resistance to *Ralstonia solanacearum* in tobacco. *Plant Biotechnol. J.* 15, 39–55. doi: 10.1111/pbi.12589

Zhang, C., Chen, H., Zhuang, R. R., Chen, Y. T., Deng, Y., Cai, T. C., et al. (2019). Overexpression of the peanut *CLAVATA1*-like leucine-rich repeat receptor-like kinase *AhRLK1*, confers increased resistance to bacterial wilt in tobacco. *J. Exp. Bot.* 70, 5407–5421. doi: 10.1093/jxb/erz274

Zhao, L., Gao, X., Liu, C., Lv, X., Jiang, N., and Zheng, S. (2017). Deletion of the *vacJ* gene affects the biology and virulence in Haemophilus parasuis serovar 5. *Gene* 603, 42–53. doi: 10.1016/j.gene.2016.12.009

Zheng, X., Li, X., Wang, B., Cheng, D., Li, Y., Li, W., et al. (2018). A systematic screen of conserved *Ralstonia solanacearum* effectors reveals the role of RipAB, a nuclear-localized effector that suppresses immune responses in potato. *Mol. Plant Pathol.* 20, 547–561. doi: 10.1111/mpp.12774

Conflict of Interest: The authors declare that the research was conducted in the absence of any commercial or financial relationships that could be construed as a potential conflict of interest.

Publisher's Note: All claims expressed in this article are solely those of the authors and do not necessarily represent those of their affiliated organizations, or those of the publisher, the editors and the reviewers. Any product that may be evaluated in this article, or claim that may be made by its manufacturer, is not guaranteed or endorsed by the publisher.

Advantages of publishing in Frontiers

OPEN ACCESS
Articles are free to read for greatest visibility and readership

FAST PUBLICATION
Around 90 days from submission to decision

HIGH QUALITY PEER-REVIEW
Rigorous, collaborative, and constructive peer-review

TRANSPARENT PEER-REVIEW
Editors and reviewers acknowledged by name on published articles

Frontiers
Avenue du Tribunal-Fédéral 34
1005 Lausanne | Switzerland

Visit us: www.frontiersin.org
Contact us: frontiersin.org/about/contact

REPRODUCIBILITY OF RESEARCH
Support open data and methods to enhance research reproducibility

DIGITAL PUBLISHING
Articles designed for optimal readership across devices

FOLLOW US
@frontiersin

IMPACT METRICS
Advanced article metrics track visibility across digital media

EXTENSIVE PROMOTION
Marketing and promotion of impactful research

LOOP RESEARCH NETWORK
Our network increases your article's readership